

AD-A102 747

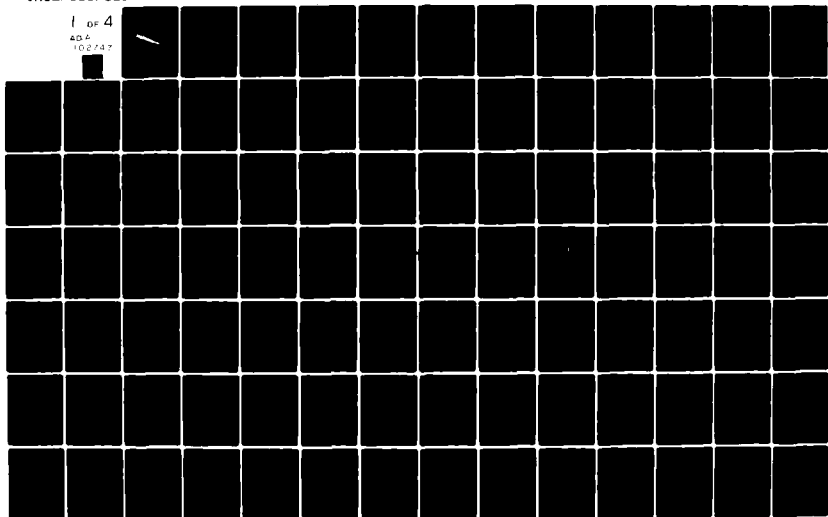
SCIENCE APPLICATIONS INC HUNTSVILLE AL  
NUCLEAR ANALYSIS AND TECHNOLOGY ASSESSMENT OF RADAR CONCEPTS, V--ETC(U)  
MAY 81 J P SWIRCZYNSKI, C S CHEEK  
DASG60-78-C-0029

NL

UNCLASSIFIED

SAI-82-604-HU

1 OF 4  
ADA  
102747



REPORT DOCUMENTATION PAGE		READ INSTRUCTIONS BEFORE COMPLETING FORM	
1. REPORT NUMBER	2. GOVT ACCESSION NO.	3. RECIPIENT'S CATALOG NUMBER	
AD-AJ02747			
4. TITLE (and Subtitle) Nuclear Analysis and Technology Assessment of Radar Concepts. Vol. II. Radiation Vulnerability Assessment of Radar Components		5. TYPE OF REPORT & PERIOD COVERED Final Report	
7. AUTHOR(s) John P. Swirczynski Curtis S. Cheek		6. PERFORMING ORG. REPORT NUMBER 144 SAI-82-604-HU	
9. PERFORMING ORGANIZATION NAME AND ADDRESS Science Applications Inc. 2103 W. Clinton Ave. Huntsville, Alabama 35805		10. PROGRAM ELEMENT, PROJECT, TASK AREA & WORK UNIT NUMBERS DASG60-78-C-0029	
11. CONTROLLING OFFICE NAME AND ADDRESS Ballistic Missile Defense Advanced Technology Center, ATTN: ATC-R P. O. Box 1500, Huntsville, AL 35807		12. REPORT DATE May 1981	
14. MONITORING AGENCY NAME & ADDRESS (if different from Controlling Office)		13. NUMBER OF PAGES 330	
16. DISTRIBUTION STATEMENT (for this report)		15. SECURITY CLASS. (of this report) Unclassified	
Ballistic Missile Defense Advanced Technology Center ATTN: BMDATC-R (5) BMDATC-T (1) BMDATC-M (1) P.O. Box 1500 BMDATC-O (1) Huntsville, AL 35807		Approved for public release. Distribution Unlimited DACS-BMT (1) AMC Building, 7th Floor 5001 Eisenhower Avenue Alexandria, VA 22333 (cont. on pageii)	
17. DISTRIBUTION STATEMENT (of the abstract entered in Block 20, if different from Report)		12 AUG 1981	
18. SUPPLEMENTARY NOTES			
19. KEY WORDS (Continue on reverse side if necessary and identify by block number) Nuclear Vulnerability Transient Radiation Effects on Materials and Electronic Components Transient Radiation Effects on Microwave Components Transient Radiation Effects on Electronics			
20. ABSTRACT (Continue on reverse side if necessary and identify by block number) This document assesses the vulnerability to transient nuclear radiation of classes of materials and devices that could be found in BMDATC-radars. Since the system is not defined, the study was based on damage thresholds and focussed on technologies rather than on specific generic types of components. The goals were to develop a set of design guidelines that could be used to mitigate the effects of nuclear radiation, to identify those technologies which must be avoided, and to identify those areas which require a development program so that survivable components are available when they are needed to field a survivable system.(cont. on pageii)			

## 16. DISTRIBUTION STATEMENT

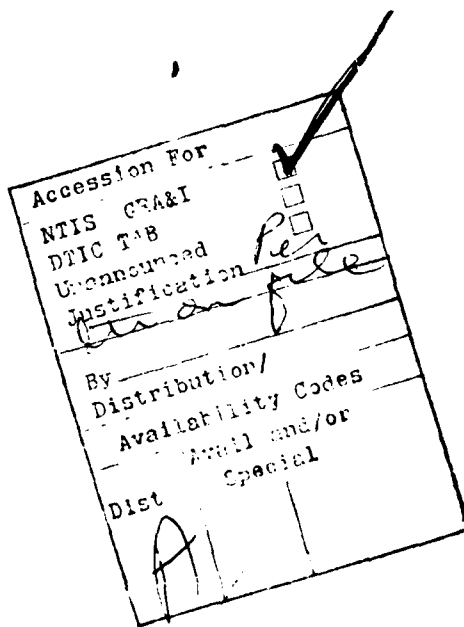
BMDSC-HW (1)  
ATTN: N. Hurst  
P.O. Box 1500  
Huntsville, AL 35807

Defense Technical (2)  
Information Center  
Cameron Station  
Alexander, VA 22314

## 20. ABSTRACT

The study has produced a three volume set. Volume I lists the nuclear requirements and the methodology that was used to produce them. Volume II contains vulnerability data, damage mechanisms, recommendations, and design guidelines. An Executive Summary summarizes Volume II. A deliberate effort was made to keep both Volume II and the Executive Summary unclassified to facilitate its distribution. However, Volume I, by its very nature, must be classified.

The topics covered in this volume were: 1) materials; 2) nonsemiconductor components; 3) RF semiconductor components; and 4) microwave and millimeter wave components. In addition, this volume contains a brief description of the interaction of transient nuclear radiation with material. Besides the problems associated with electronic components, one important result of this study was that quartz crystal oscillators emerged as one of the most vulnerable and critical components in any radar system. An appropriate solution is not reported in the literature. However, a possible solution to this problem is proposed in this volume.



Unclassified

## TABLE OF CONTENTS

<u>SECTION</u>	<u>PAGE</u>
1 INTRODUCTION . . . . .	1
2 GENERAL DISCUSSION OF NUCLEAR RADIATION EFFECTS. . . . .	3
3 MATERIALS. . . . .	9
3.1 INSULATORS. . . . .	9
3.2 ADHESIVES . . . . .	17
3.3 SEALS . . . . .	22
3.4 LAMINATES . . . . .	25
3.5 ENCAPSULANTS. . . . .	32
4 NONSEMICONDUCTOR COMPONENTS. . . . .	43
4.1 RESISTORS AND CAPACITORS. . . . .	43
4.2 QUARTZ CRYSTAL OSCILLATORS. . . . .	48
5 RADIO FREQUENCY SEMICONDUCTOR DEVICES. . . . .	76
5.1 DISCRETE RF SEMICONDUCTOR DEVICES . . . . .	76
5.2 INTEGRATED CIRCUITS . . . . .	155
6 MICROWAVE AND MILLIMETER WAVE DEVICES. . . . .	202
6.1 IMPATT-LIKE DEVICES . . . . .	202
6.2 GUNN DIODES . . . . .	228
6.3 PIN DIODES. . . . .	260
6.4 FERRITES. . . . .	270
6.5 MICROWAVE TRANSISTORS . . . . .	274
7 CONCLUDING REMARKS . . . . .	280
REFERENCES . . . . .	282
APPENDIX A. RECOMMENDATIONS AND DESIGN GUIDELINES. . .	301

## LIST OF FIGURES

<u>Figure</u>		<u>Page</u>
1	Production of a Defect Cluster . . . . .	4
2	Volume Resistivity of 4 mil TFE Teflon . . . . .	11
3	Neutron Effects on Inorganic Insulating Materials . . .	19
4	Effect of Total Dose on Cellulose . . . . .	28
5	Radiation Data for a Polystyrene Foam (Styrofoam 22) . .	36
6	Radiation-Induced Pressure in 3M-241 Epoxy . . . . .	39
7	Internal Stress as a Function of Radiation in H2E-011 Epoxy . . . . .	40
8	Equivalent Circuit of a Resistor Under Irradiation . .	43
9	Neutron Effects on Commonly Used Resistors . . . . .	45
10	Relative Neutron-Radiation Sensitivity of Capacitors . . . . .	47
11	Idealized Behavior of Frequency versus Time for Quartz Resonators Following an X-Ray Exposure Pulse . .	50
12	Steady-State Frequency Offset of Unswept Natural Quartz as a Function of Absorbed Dose . . . . .	51
13	Radiation Response of 5 MHz Premium-Q Resonators . . .	52
14	Radiation Response of 5 MHz SARP Premium-Q Quartz Resonators . . . . .	53
15	Dose Response of Premium-Q 5 MHz Resonators . . . . .	54
16	Dose Response of Premium-Q 5 MHz Resonators . . . . .	54
17	Steady-State Radiation Response of 5 MHz Premium-Q Quartz Crystal Oscillators . . . . .	55
18	Steady-State Radiation Response of 5 MHz Quartz Oscillators . . . . .	55
19	Steady-State Offset Oscillator Frequency as a Function of Dose for 5 MHz Resonators . . . . .	56
20	Steady-State Frequency Offsets of 5 MHz Resonators . .	58
21	Steady-State Frequency Offsets of Premium-Q 5 MHz Resonators . . . . .	59
22	Steady-State Response of Three Crystals from the Same Bar of Premium-Q Quartz . . . . .	60



LIST OF FIGURES (continued)

Figure		Page
23	Steady-State Frequency Offset for 5 MHz Resonators Fabricated from Electronic-Grade Quartz Crystals Cut from the Same Bar . . . . .	60
24	Typical Curves of f versus Time for 32 MHz Resonators Fabricated from Natural, Unswept Synthetic, and Swept Synthetic Quartz . . . . .	62
25	Transient Response of 32 MHz Quartz Resonators at 25°C .	62
26	Transient Offset Frequency versus Time for 125 MHz Natural, Swept Synthetic, and Unswept Synthetic Quartz Resonators . . . . .	63
27	Typical Curves for Log Annealable Frequency Offset versus Log Time for both 32- and 125-MHz Quartz Oscillators . . . . .	63
28	Radiation-Induced Prompt and Delayed Photoconductivity for Natural, Swept, and Unswept Synthetic Quartz . . . .	65
29	Radiation-Induced Change in the Series Resonance Resistance for 32 MHz Quartz Crystal Oscillators . . . .	65
30	Radiation-Induced Change in the Series Resonance Resistance for a 5 MHz Natural Quartz Oscillator . . . .	66
31	Comparison of the Changes in R <sub>s</sub> in a 32 MHz Natural Quartz Oscillator with that of a 5 MHz Oscillator after an Exposure of $1 \times 10^4$ rad(Si) . . . .	67
32	$\text{Al}^{+3}$ -Hole Center ESR Spectra for Unswept Premium-Q Quartz after Irradiation at a) 77°K, b) Room Temperature and again at c) 77°K . . . . .	69
33	$\text{Al}^{+3}$ -Hole Center ESR Spectra for Swept Premium-Q Quartz after Irradiation at a) 77°K, b) Room Temperature and again at c) 77°K . . . . .	69
34	Frequency Shift as a Function of Neutron Fluence (>10KeV Fission Spectrum) . . . . .	73
35	Frequency Offset versus Neutron Fluence Showing the Effect of the Correction for Gamma Radiation . . . .	74
36	Potential Energy Diagrams and I-V Characteristics for a p-n Junction . . . . .	78
37	The Volt-Ampere Characteristic of a p-n Diode . . . .	79
38	Forward Voltage at Constant Current versus Neutron Fluence . . . . .	81



LIST OF FIGURES (continued)

Figure		Page
39	Effects of Neutron Fluence on Si Diodes . . . . .	83
40	Change in Zener Voltage as a Function of Neutron Fluence . . . . .	84
41	Change in Forward Voltage as a Function of Neutron Fluence for Reference Diodes . . . . .	84
42	Effects of Neutron Fluence on Silicon Tunnel Diodes . .	86
43	Carrier Generation through a Defect . . . . .	88
44	Typical Shape of a Primary Photocurrent Induced by a Square Ionization Pulse with Width of $t_p - t$ . . . . .	90
45	Diode Photocurrent versus Reverse Voltage for Various Radiation Dose Rates . . . . .	91
46	Diode Photocurrent versus Reverse Bias for Three Values of Breakdown Voltage . . . . .	92
47	Peak Photocurrent versus Bias Current for Various Diode Breakdown Voltages . . . . .	95
48	Zener Impedance versus Zener Voltage for Different Bias Currents . . . . .	95
49	Composite Change in Diode Characteristics versus Total Dose . . . . .	96
50	Physical Structure of a Silicon Controlled Rectifier. .	99
51	Schematic of the Two Transistor Model . . . . .	100
52	SCR Switching Failure Probability as a Function of Neutron Fluence . . . . .	102
53	Simplified Picture of Transistor Operation for the External Circuit . . . . .	104
54	Current Gain versus $I_C$ for a Family of Neutron Fluences	108
55	Silicon Transistor Nomograph for Determining Neutron-Induced Gain Degradation . . . . .	112
56	Silicon Transistor Nomograph Treating the Neutron Damage Constant as a Random Variable . . . . .	115
57	Change in Saturation Voltage with Neutron Irradiation .	124
58	Saturation Voltage versus Neutron Fluence for a 2N2907A Transistor and a Forced $\beta$ of 10 with a $I_C$ of 500 mA . . . . .	125



LIST OF FIGURES (continued)

Figure		Page
59	Leakage Current as a Function of Neutron Fluence for a 2N1613 Transistor . . . . .	128
60	Avalanche Breakdown for a p-n Silicon Junction . . . . .	129
61	Dose Effects on npn Transistor . . . . .	130
62	The Creation of a Channel in the Base Region Due to the Migration of Positive Charge to the Silicon- Silicon Dioxide Interface . . . . .	131
63	The Emitter-Base Junction after the Channel has Receded	132
64	$V_{CEsat}$ versus Dose for the 2N3752 . . . . .	135
65	Variations in $I_{CBO}$ for Two 2N1613 Transistors as a Function of Total Dose Exposure . . . . .	136
66	The Flow of Minority Carriers Producing Primary Photocurrents in a npn Transistor . . . . .	137
67	Predicted versus Measured Primary Photocurrents in Silicon Switching and Amplifier Transistors at $10^{10}$ rad(Si)/sec . . . . .	142
68	Characteristics of Primary Photocurrent versus $\gamma$ . . . . .	140
69	The Response of a 2N915 Transistor With an Open Emitter	144
70	Photocurrent Compensation . . . . .	145
71	Photocurrent Compensation . . . . .	146
72	Second Breakdown for Typical Forward-Biased Transistor .	147
73	Relationship Between $t_p$ and $t_{sr}$ . . . . .	149
74	Typical Transistor Primary Photocurrent Response to a Step Radiation Pulse with a Pulse Width of $t_p$ . . . . .	150
75	Fundamental Boolean Operations . . . . .	156
76	NAND and NOR Operations . . . . .	156
77	Logic Gate Symbols . . . . .	157
78	RTL Gate . . . . .	157
79	DTL NOR Gate . . . . .	158
80	Simple TTL Gate . . . . .	159
81	Measurement of Propagation Delay and Rise and Fall Times	160
82	TTL NAND Gate with Active Pull-Up . . . . .	161
83	TTL Gate with N-Gate Fan-Out . . . . .	162



LIST OF FIGURES (continued)

Figure		Page
84	Voltage Transfer Characteristic for Typical SN54/74 NAND Gate . . . . .	163
85	Schottky TTL Structure and Symbol . . . . .	164
86	Neutron-Induced Gain Degradation and Decreased Fan-Out Capability . . . . .	167
87	Neutron-Induced Increase of Output Low-Level Voltage . .	168
88	TTL Neutron Failure Levels . . . . .	170
89	Effects of Total Dose on IC Transistors . . . . .	171
90	TTL Total Dose Failure Levels . . . . .	174
91	Photocurrent Compensation . . . . .	176
92	Junction Isolation versus Dielectric Isolation . . . . .	179
93	Lapback Technique of Dielectric Isolation . . . . .	180
94	Cross Section After Lapping When Using an Epitaxial n+ Layer on an n Substrate . . . . .	180
95	TTL Dose rate-Induced Transient Upset Failure Levels. .	183
96	TTL Pulse-Width Dependence of Transient Vulnerability .	184
97	The Difference Amplifier . . . . .	186
98	Motorola MECL III Gate . . . . .	187
99	Reference Supply Circuit for ECL Gates . . . . .	187
100	ECL Transfer Characteristic . . . . .	188
101	NMOS Total Dose Failure Levels . . . . .	200
102	NMOS Dose Rate-Induced Transient Upset Failure Levels .	201
103	Idealized Abrupt pn Junction. . . . .	203
104	Ideal Abrupt PIN Junction . . . . .	204
105	Idealized Plot of the Velocity of Free Electrons in Semiconductors versus Electric Field . . . . .	206
106	Electric Field Distribution Through a Read Diode . . . .	207
107	Time Displacement of a Square Voltage Pulse Applied to an Impatt Diode and Its Resultant Square Current Pulse . . . . .	208
108	RF Power from an Impatt . . . . .	210



LIST OF FIGURES (continued)

Figure		Page
109	Threshold Current and Output Power for X-Band, Silicon Oscillators as a Function of Neutron Fluence .	210
110	RF Power From a 10 GHZ Impatt Oscillator For Various Dose Rates . . . . .	212
111	Dose Rate-Induced Frequency Shifts in a 10 GHz Impatt Oscillator . . . . .	213
112	Effects of Neutron Fluence on the Breakdown Voltage of Impatts and Trapatts . . . . .	214
113	Calculated and Measured Temperature Coefficient at 30 A/cm <sup>2</sup> versus Neutron Fluence . . . . .	216
114	Average RF Output Power Normalized to Pre-Irradiation Values versus Neutron Fluence for 500 nsec. Bias Pulses	217
115	Plot of Trapatt Frequency of Operation versus Neutron Fluence . . . . .	218
116	RF Output Power From a 2.5 Ghz Trapatt Oscillator as a Function of Dose Rate . . . . .	219
117	A Comparison of the Theoretical and Experimental Performance of Trapatt Oscillators as a Function of Dose Rate . . . . .	220
118	Typical Structure of Baritt Diode and the Electric Field Profile . . . . .	221
119	V-I Characteristic of a Baritt Diode . . . . .	222
120	V-I Characteristic of MSM Baritt Diodes Before and After Neutron Exposure . . . . .	223
121	Output Power From a 4.5 GHZ Metal-Semiconductor- Metal Baritt Oscillator as a Function of Neutron Fluence . . . . .	224
122	Normalized RF Output Power as a Function of Normalized Dose Rate for Five Types of Baritt Diodes . . . . .	227
123	Current versus Time in n-Type GaAs . . . . .	229
124	Electric Field-Dependent Average Drift Velocity of Electrons in n-Type GaAs . . . . .	230
125	Idealized Energy Band Structure for Semiconductors . .	230
126	Band Structure of GaAs . . . . .	231
127	Numerical Simulation of the Generation and Propagation of a Dipole Domain Through n-Type GaAs . . . . .	233



LIST OF FIGURES (continued)

Figure		Page
128	Typical Waveforms for Transit-Time Mode Operation of a Gunn Oscillator . . . . .	234
129	Typical Waveforms for Delayed-Domain Mode Operation of a Gunn Oscillator . . . . .	235
130	Typical Waveforms for Quench-Domain Mode Operation of a Gunn Oscillator . . . . .	236
131	Carrier Concentration versus Fluence for a Typical Gunn Device . . . . .	239
132	Degradation Parameters a and b for Bulk GaAs versus Initial Carrier Concentration . . . . .	240
133	Mobility Degradation Parameter versus Donor Density .	241
134	Carrier Removal Rate versus Initial Carrier Concentration . . . . .	241
135	Donor Impurity Concentration versus Depth Before and After Exposure to a Fluence of $1.5 \times 10^{17}$ n/cm <sup>2</sup> . .	244
136	Neutron Fluence at Device Power Failure versus Initial Carrier Concentration . . . . .	245
137	Maximum Efficiency of Gunn Diodes versus Neutron Fluence . . . . .	246
138	V-I Characteristics of a Gunn Diode After Various Levels of Neutron Irradiation . . . . .	248
139	Effect of Neutron Irradiation on the Frequency of Gunn Diodes . . . . .	250
140	Peak Photocurrent of Gunn Diodes versus Dose . . . .	251
141	Radiation-Induced Transients in Three Gunn Diodes' Output Power for a Dose Rate of $3 \times 10^8$ rads(Si)/sec .	253
142	Recovery Time versus Dose for Pulsed Gunn Diodes . .	254
143	Recovery Time and Normalized Output Power versus Dose Rate . . . . .	256
144	Peak Photocurrents in Gunn Amplifiers versus Dose Rate . . . . .	257
145	Electric Field Distribution Across a Gunn Amplifier .	258
146	Gunn Amplifier Gain versus Dose Rate . . . . .	258
147	Degradation of PIN diode to 14 MeV Neutrons. . . . .	261
148	Lifetime Degradation of PIN Diodes versus 1 MeV Neutron Fluence . . . . .	262



LIST OF FIGURES (continued)

Figure		Page
149	Lifetime versus Neutron Fluence for PIN Diodes Irradiated with 1 MeV Neutrons . . . . .	263
150	Typical V-I Characteristics of a PIN Diode for Various 1 MeV Fluences . . . . .	263
151	$R_i$ versus Neutron Fluence . . . . .	264
152	1 MeV Neutron Fluence Required to Increase $R_i$ to 10 versus Width of the Intrinsic Region . . . . .	266
153	Decrease of PIN Diode Lifetime After Exposure to $^{60}\text{Co}$ Gamma Rays. . . . .	267
154	Crystal Structure of the Mineral Spinel $\text{MgAl}_2\text{O}_4$ . .	270
155	The Magnetization Curve or Hysterisis Loop . . . . .	271
156	Magnetization versus Temperature of Microwave Ferrites Ferrites . . . . .	273
157	Effect of a Thermal Gradient on the Hysterisis Loop of a Microwave Garnet Toroid . . . . .	274
158	Radiation-Induced Transient $I_{DS}$ Response of GaAs MESFET . . . . .	276
159	Two Basic GaAs FET Configurations . . . . .	276
160	Pulsed Radiation Response Characteristics of GaAs MESFET's at Various $I_{DS}$ Levels. . . . .	277
161	Recovery Time Constant versus Reciprocal Temperature for GaAs FET's . . . . .	278



## LIST OF TABLES

Table		Page
1	Particle Conversion for Si and C . . . . .	8
2	Doses for Mechanical Damage Thresholds and 25% Mechanical Damage . . . . .	13
3	Damage Thresholds and Typical Uses of Common Electrical Insulators . . . . .	14
4	Ranking of Organic Insulators . . . . .	15
5	Total Dose Damage Thresholds of Material . . . . .	18
6	Effects of Radiation on Tensile Shear Strength of Adhesives at Room Temperature . . . . .	21
7	Radiation Vulnerability of Adhesives . . . . .	22
8	Dose Damage Thresholds for Elastomer Seals . . . . .	24
9	Radiation Vulnerability of Elastomers Suitable for Seals . . . . .	25
10	Plastics Used for Seals and Retainers . . . . .	27
11	Ranking of Plastics Applicable for Seals . . . . .	26
12	Effect of Total Dose Radiation on the Tensile Strength of Cotton and Rayon . . . . .	29
13	Response of Fibers to a Total Dose of $10^6$ rad(C) . . . .	30
14	Effects of Total Dose on Laminates Composed of Various Fillers and Phenol Formaldehyde Resin . . . .	32
15	Twenty Five Percent Total Dose Damage Point for Common Laminates . . . . .	33
16	Effects of Total Dose Radiation on Unfilled Epoxy Resins . . . . .	34
17	Dose Effects on Polyester-Styrene Resin . . . . .	34
18	Total Dose Effects on Common Encapsulants . . . . .	37
19	Radiation-Induced Evolution of Gas . . . . .	38
20	Ranking of Encapsulants . . . . .	41
21	Neutron Damage Thresholds of Resistors . . . . .	44
22	Resistor Proportionality Factor . . . . .	46
23	Representative Radiation-Induced Frequency Offsets . . .	57
24	Relative Concentrations of $\text{Al}^{+3}$ -Hole Centers as Determined by ESR. . . . .	70



LIST OF TABLES (continued)

Table		Page
25	Neutron Response of Typical Diodes . . . . .	32
26	Response of Reference Diodes to Neutron Irradiation . . . . .	35
27	Dose Rate Response of Typical Diodes . . . . .	34
28	Dose Response of Typical Diodes . . . . .	37
29	Effects of Total Dose Exposure on the Breakdown Voltage of Diodes . . . . .	38
30	Total Dose Data for the 2N2323 SCR . . . . .	102
31	Effects of Neutron Irradiation on Transistor's Gain . . . . .	110
32	Effects of Neutron Irradiation on Transistor's Saturation Voltage and Leakage Current . . . . .	125
33	Total Dose-Induced Gain Degradation (Average) in Irradiated Transistors with $V_{CE} = 2V$ ; Sample Size = 10 . . . . .	133
34	Effects of Total Dose Exposure on Transistor's Saturation Voltage and Leakage Current . . . . .	134
35	Dose Rate Response of Typical Transistors . . . . .	139
36	Defining Equations . . . . .	141
37	DDT&E Costs for Hardening Against Neutrons . . . . .	153
38	Speed/Power Characteristics of Standard TTL, Schottky TTL, Advanced Schottky TTL . . . . .	165
39	Average Low State Output Voltage of Surviving Devices After Neutron Irradiation to Specified Fluences . . . . .	169
40	Flip-Flop Transient Radiation Failure Levels . . . . .	182
41	Effects of Fan-Out on MECL II . . . . .	189
42	ECL Radiation Vulnerability . . . . .	191
43	ECL IC Pulse-Width Failure Level Dependence . . . . .	192
44	Typical Radar System Parts List . . . . .	193
45	Effects of Dose Rate on Baritt Diodes . . . . .	226
46	Baritt Diode Characteristics in a Benign Environment . . . . .	226
47	Comparison of TE Oscillators (TEO) and Reflection-Type Amplifiers (TEA) with Other Microwave Devices . . . . .	238
48	Transport Properties of Epitaxially Grown GaAs versus Fluence . . . . .	243
49	I-V Gunn Characteristics versus Neutron Fluence . . . . .	247



LIST OF TABLES (continued)

Table		Page
50	Factors for Determining the Recovery Time . . . . .	254
51	Summary of Radiation Effects on Gunn Devices . . . . .	259
52	Increase in Insertion Loss of Microwave Circuits versus 14 MeV Neutron Fluences. . . . .	265
53	Average Insertion Losses for Mesa PIN Diodes Exposed to Neutrons. . . . .	265
54	Damage Constants for PIN Diodes Exposed to Neutrons and Gammas . . . . .	268
55	Radiation Test Data on Epi-Layer Power MESFET's . . . . .	273

## INTRODUCTION

This report is concerned with the vulnerability of BMDATC-radars to nuclear radiation. Since the system has not been completely characterized the assessment was based on technologies rather than specific devices and materials. Rather than determining the survivability of the system the goals were to identify technologies or technology classes to be avoided, rank the technologies according to their sensitivities, wherever possible develop design guidelines which can be used to mitigate the effects of radiation, and identify technology gaps which require technology advancements so that hardened components are available when it comes time to build a survivable system.

The lack of a complete system definition required that the assessment be based on damage thresholds. The damage threshold of a material or device is that level or value of the threat constituent required to produce a measurable change in the properties of the material or device. It is more appropriate to use damage thresholds rather than failure thresholds since failure depends on the particular application of the material or device and, as such, is system dependent.

This report actually consists of a two volume set. Volume I is confined to the threat environment and a discussion of the methodology, scenario, and the deployment configuration that was used to generate the environments. Basically these correspond to the environmental requirements which have been placed on LoADs. The major difference is that Volume I does include the dose time history while the LoAD's documentation does not. The authors do feel that this is a serious oversight since the occurrence of transient upset in integrated circuits is very sensitive to pulse width with the dose rate level required to produce this upset varying as much as two to three orders of magnitude as the pulse width is lengthened.

Since the threat levels are quite high, as indicated in Volume I, it seemed appropriate to assemble some vulnerability data on components not normally considered in a vulnerability assessment. Primarily this meant including materials rather than confining the assessment to devices.



Based on interactions with BMD personnel it would seem beneficial to include in this report a very brief and as simple as possible summary of the interactions of nuclear radiation with material. Hopefully this will serve not only as a tutorial but also as an introduction to enough of the jargon, terminology, and concepts to give meaning to the subsequent discussions on the vulnerability of materials and classes of devices.

This volume as well as the project itself has been divided into appropriate and natural subsections. The division that was used was: (1) general discussion of nuclear radiation effects, (2) materials, (3) nonsemiconductor components, (4) general semiconductor components (including integrated circuits (IC's)), and (5) microwave components. It is hoped that this division will facilitate the reading and future referencing of the report.



## 2.0 GENERAL DISCUSSION OF NUCLEAR RADIATION EFFECTS

The label transient radiation effects (TRE) is commonly associated with the effects of the interaction of nuclear radiation with material. The adjective "transient" applies to the radiation and not to the effects caused by the radiation since the effects can be both permanent such as the neutron-induced gain degradation of a bipolar transistor or transient such as the dose rate-induced primary photocurrent in a discrete transistor. The primary components of the nuclear radiation environment are neutrons, electrons, alpha particles, gamma radiation, and x-radiation. For endoatmospheric applications such as those envisioned for BMDATC-radars, electrons and alpha particles are absorbed in very short distances in the atmosphere. Thus, for this study, neutrons are the primary particulate radiation capable of damaging or degrading radar systems. The weapon's x-radiation is absorbed in the atmosphere and the distance they travel before they are absorbed is dependent on their energy. As x-rays are absorbed the air becomes very hot and in turn re-radiates energy in the infrared, visible, and ultraviolet region of the spectrum. This appears as the light and heat associated with the fireball.

Two atomic changes can result from the interaction of nuclear radiation with matter: atomic displacement effects and ionization effects. For displacement, atoms must receive sufficient energy to be dislodged from their normal sites. There are two general classes of radiation-induced displacement defects in crystals. If only a few atoms are displaced from their normal lattice sites, the defect is called a simple defect. Simple defects are caused by electrons or gamma rays. Usually the effect of simple defects is not serious. The other type of defect is a cluster which involves a few hundred atoms and, as such, can have a more serious impact than simple defects.

It is relatively easy to visualize how a simple defect can be formed. The lattice atom is simply displaced from its normal position in the lattice resulting in a vacancy in the lattice and an interstitial atom. The production of a defect cluster is somewhat more difficult to visualize.

Because of their kinetic energy and momentum, heavy particles, such as neutrons, are efficient producers of defects in general and defect clusters



in particular. Neutrons lose their energy in crystals primarily through elastic collisions or scattering with lattice atoms. Some of the energy of the neutron is transferred to the lattice atom and appears as kinetic energy of the atom resulting in a recoil atom. In a series of these elastic collisions the neutron will lose more and more of its energy until it moves very slowly, and has approximately the same kinetic energy as the molecules of the medium through which it is moving. At this point it is called a thermal neutron.

The recoil atom will collide with neighboring atoms with the end result being a cascade or trail of displaced or recoil atoms. This process will continue until all the atoms involved are reduced to energies below the displacement energy (i.e., the minimum or threshold energy required to displace an atom in lattice). The simplified illustration in Figure 1 depicts the situation.

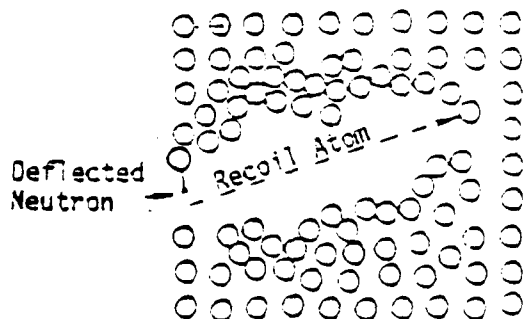


Figure 1. Production of a Defect Cluster

Several hundred atoms are usually involved with the situation being somewhat analogous to the impact or collision of a cue ball (the neutron) with a billiard ball on a pool table filled with billiard balls. The recoil atom produces as much or more lattice distortion as the neutron. In any case, the core of the

defect cluster contains a large number of vacancies and is surrounded, initially at least, by a large number of interstitial atoms. Some annealing of the initial damage occurs almost immediately at room temperature. The interstitial atoms drift or diffuse back to fill a vacancy. The bulk of the annealing in silicon at room temperature is completed in less than a second and the cluster assumes a stable form.<sup>1</sup> Both the total amount and the rate of annealing depend on the thermal energy of the lattice atoms and thus on the temperature of the crystal.

Displacement is particularly important to crystal materials. These include quartz whose physical properties are often dependent on the perfection of the crystal lattice. They also include semiconductor material because the defects contain many energy levels in the forbidden band or energy gap of a semiconductor and some of these serve as recombination centers. In addition, neutron irradiation also introduces trapping centers which remove majority carriers. In any case the presence or introduction of defects in semiconductor material can have a serious impact on the electrical properties of the device.

To briefly digress, it should be noted that there is a great similarity between the effect of the neutron-induced recoil atom and the implantation of an ion. Ion implantation, of course, is a technique that is being used to dope silicon. The process is attractive because the number of implanted ions and their depth distribution can be controlled externally (i.e., by the system voltage and beam current) rather than by the physical properties of the substrate as in the case of thermal diffusion. However, with this manufacturing process, it must be remembered that this technique produces defect clusters in the same manner as neutron irradiation since the ion performs the same role as the recoil atom from a radiation damage standpoint. The implanted ion eventually comes to rest but it leaves a region of heavy disorders in its wake--in effect it has generated a defect cluster. A heavy ion with an energy of 40 KeV implanted at room temperature will permanently displace a few thousand silicon or germanium atoms.<sup>2</sup> There are, of course, differences (e.g., the required annealing temperature for ion implantation are higher than that required by fast-neutron irradiation<sup>2</sup>) but the damage mechanism is the same.



In addition to atomic displacement, nuclear radiation can also produce ionization effects. Ionization occurs through the interaction of gamma rays, x-rays, energetic electrons, and high-energy neutrons. It results in the formation of electron-ion pairs in a material. The free carriers thus produced undergo random motion, diffuse to regions of lower carrier concentration, drift with applied electric fields, are trapped at impurity atom sites, or eventually recombine into their normal nonionized state. The results of ionization include trapped charges, covalent bond breakage, formation of new molecules, charge transfer, increased bulk conductivity, and excessive minority carriers. For semiconductor devices these, in turn, may be further characterized as surface effects, increased junction leakage current, and parameter (such as the current gain) degradation. Since covalent bands are broken, ionization can induce cross linking and scission of polymers which can result in new polymers, free radicals, and liberation of free molecules. In fact ionization radiation is one of the techniques used to produce polymers since it eliminates the need for a catalyst and the application of extreme heat.

Gamma rays can also affect materials by excitation. The atoms of a material can acquire additional energy from the gamma rays and be raised to an excited energy state. This can result in discoloration and luminescence which may be important in optical components such as filters, lens, and fiber optic cables.

Another effect associated with total dose is the heating of material when exposed to radiation. A portion of the energy of the gamma rays is transferred or converted to thermal energy of the atoms of the crystal resulting in an increase in the ambient temperature of the material. This can result in a temperature higher than the component or the system was designed to withstand. The resulting temperature rise will depend not only on the total amount of energy that is transferred to the material but also on the rate at which this transfer occurs. A prompt-gamma dose of  $10^7$  rads (Si) delivered in less than a microsecond will increase the temperature of silicon by more than  $100^{\circ}$  C.<sup>2</sup>

Besides heating, dose-rate has an effect on semiconductor devices



based on the fact that ionizing radiation generates electron-hole pairs. In silicon, 1 rad absorbed can produce more than  $10^{13}$  electron-hole pairs /cm<sup>3</sup>.<sup>3</sup> The current, which is produced in a pn junction by ionizing radiation, is called the primary photocurrent. This primary photocurrent can be multiplied within transistors due to their inherent current gain, multiplied still further by the rest of the circuitry, and appear as an amplified or a secondary photocurrent.

The ionizing dose-rate effects include transient false signals, device burnout, semiconductor logic upset, and reversible and irreversible changes of state. Perhaps one of the most serious effects is latch up. This effect is initiated in any four-layer semiconductor junction (pnpn). This, of course, corresponds to any SCR type structure - either intentional or unintentional. The dose-rate induced photocurrent fires the SCR and latch-up occurs. During latch-up, larger than normal currents flow through the latched device until primary power is removed. In some cases, continuance of latch-up can cause device burnout. In any case, there is an operational problem since a latched device cannot respond to input signals.

To quantify displacement and ionization effects, one must relate the effects to a description of the radiation environment. The description appropriate to displacement (caused primarily by neutrons) effects is different from that for ionization effects. For displacement effects, the description requires that the number density and the energies of the incoming neutrons be related to the cross section versus energy for displacements in the material. Neutrons are produced in both fission and fusion reactions and can have a range of energies. The neutrons of interest are those with energies from 10 KeV to 14 MeV. Damage caused by a spectrum of such neutrons can be normalized by a suitable correction factor to that caused by a fluence composed only of 1 MeV neutrons. This is the usual procedure although sometime the spectrum is normalized to 14 MeV neutrons.

For ionization effects, the description that is appropriate will specify the radiation that is absorbed in terms of the energy deposited in the material in units of rad (material). The unit rad is an acronym that stands



for roentgen absorbed dose. The roentgen is that quantity of radiation required to produce  $2.08 \times 10^3$  ion pairs per cubic centimeter of air at standard temperature and pressure.<sup>4</sup> The rad corresponds to an absorbed dose of energy of 100 ergs per gram of absorbing material. It is important to specify the material when rad is used because this unit specifies the amount of radiant energy absorption of any form (particle or electromagnetic) in any material and the extent of energy deposition and absorption depends to a great extent on the nature of the material. For carbon and silicon the relationship between the unit rad and fluence is given in Table 1 which was taken from references 2 and 5.

Table 1. Particle Conversion for Si and C

1 rad (C, Si) = 100 ergs/g (C, Si)
1 rad (Si) = $5 \times 10^{10}$ neutrons/cm <sup>2</sup> (1 MeV)
1 rad (C) = $3 \times 10^6$ neutrons/cm <sup>2</sup> (1 MeV)
1 rad (Si) = $2.25 \times 10^3$ protons/cm <sup>2</sup> (1 MeV)
1 rad (C) = $1 \times 10^6$ protons/cm <sup>2</sup> (1 MeV)
1 rad (C) = $2.2 \times 10^3$ photons/cm <sup>2</sup> (1 MeV)
1 rad (Si) = $2.4 \times 10^3$ photons/cm <sup>2</sup> (1 MeV)

This brings to an end the general discussion on transient radiation interactions on materials. It is acknowledged that this discussion can only serve as a very brief--perhaps too brief--introduction to the subject. Hopefully it will familiarize the reader with some of the jargon and terminology. The specific impact and effects will be elaborated on as they come up during the report. To enter into such a detailed discussion would not be appropriate at this time and would have less meaning to the reader unless the discussion was accompanied by specific examples in which the reader had interest. Therefore, the report will now continue on in a more normal fashion.



### 3.0 MATERIALS

Obviously, it is not possible or necessary to cover all classes and applications of materials that could occur in a radar system. The only viable method was to divide materials into classes according to their application or use in the system. The division that seemed to be most appropriate was: (1) insulators, (2) adhesives, (3) seals, (4) laminates, and (5) encapsulants. There is some overlap in this division, e.g., between encapsulants and adhesives but this is bound to occur and the above division would appear to include material applications that are necessary for any system, i.e., they are system independent.

#### 3.1 INSULATORS

In general insulators are composed of either organic or inorganic materials. The organic materials that are used are polymers. These are characterized by repeating chemical structural units called "monomer units" which are joined by chemical bonds into long chains. Radiation affects organic materials by removing (ionizing) valence electrons. This breaks the covalent bonds and portions of the chain or even individual atoms that were formerly bonded together move apart. The main effects of organic materials being exposed to radiation are cross linking and chain cleavage or scission.

Cross linking occurs when two or more intermediate chains or free radicals bind together to form a new molecule. The new bonds formed in polymers by radiation-induced crosslinking are very stable and cannot be annealed by heating. The crosslinking is similar to polymerization because it does link molecules together. However, it is different in the sense that crosslink binding is more random than in polymerization. The result is the formation of a three dimensional structure rather than the long chain which is typical of polymerization. The impacts of cross linkage are to increase the tensile strength, melting point, and Young's modulus. Quite often these are beneficial changes and, in general, if a polymer predominately cross-links then it will have good radiation resistance.



Chain cleavage or scission simply means that polymer chain is broken into smaller short lived intermediate molecules. These free radicals are very reactive toward oxygen and there is a tendency for any free radical formed during irradiation to form peroxides rather than crosslink. In many cases the breakdown is accelerated because crosslinking is impaired while scission or cleavage continues. The breakdown is often accompanied by a significant formation of hydroxyl and carbonyl groups. This simply indicates the effect of the surrounding atmosphere (e.g., oxygen content) on the radiation response of organic materials and does give an indication of the complexity and competing nature of the chemical reactions induced by radiation. In fact, at the present time, it is not possible to predict, exactly, from first principles if crosslinking or scission will dominate for a given polymer.

In any case chain cleavage results in brittleness, a decrease in strength, the formation of different bonds, and the formation of gas. This gas formation occurs in polyethylene where the C-H bond is more easily broken and the material outgasses hydrogen. Halogenated polymers (e.g., Teflon or polyvinyl chloride) outgas the halogen or even yield the acid (e.g., with Teflon, HF, or hydrofluoric acid). In some fluorinated polymers if they are irradiated in a glass container  $\text{SiF}_4$  is eventually formed<sup>6</sup> due to the etching of the glass by HF. In other words, halogenated polymers when they are irradiated outgas acid vapors which are quite corrosive to any exposed material including metal.

Since Teflon is so popular due to its excellent insulating properties, some comments on it should be made. Teflon undergoes a change caused by total dose radiation in which the polymer chains are broken and fluorine and other decomposition products are involved. It suffers less degradation in a vacuum than in air. Oxygen probably contributes to the degradation. In fact, it has been established that both TFE and FEP Teflon resins are very sensitive to total dose radiation in the presence of oxygen but are quite stable in the absence of oxygen.

Figure 2 indicates the change in resistive characteristics of Teflon as a function of total dose.<sup>2</sup> As this figure indicates exposure to total dose beyond roughly  $10^5$  rads(C) does not degrade the volume resistivity further than  $10^{12} \Omega\text{-cm}$ . However, the damage threshold of  $10^4$  rads(C) would preclude its use in BMDATC radars.



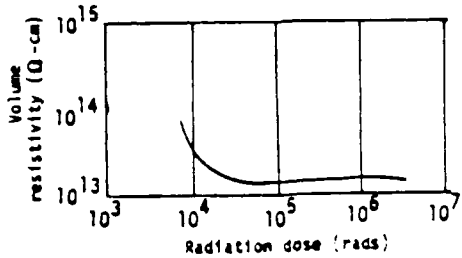


Figure 2. Volume Resistivity of 4 mil TFE Teflon

Another halogenated material that sees wide use is polyvinylchloride (PVC). PVC exhibits mild to moderate damage from  $10^5$  rads(C) to approximately  $10^7$  rads(C).<sup>1</sup> Above this point PVC loses its tensile strength. In addition and perhaps even more important is the fact that hydrogen chloride is released which, in some cases, may prohibit its use. Like Teflon the use of PVC should be avoided.

Polystyrene is another common organic material that finds application as an electrical insulator. The physical properties of this material have a damage threshold of approximately  $10^8$  rad(C) with 25% degradation occurring above  $4 \times 10^9$  rad(C). Some authors take this to mean that polystyrene is acceptable.<sup>2,5</sup> However, the electrical properties, specifically the volume resistivity and insulation resistance, are affected by much lower levels of radiation. An order of magnitude decrease in these parameters has been noted for doses as low as  $4.5 \times 10^6$  rad(C). This damage threshold is high enough to allow the use of polystyrene in BMDATC-radars but better materials do exist.

One of the better and more popular materials is Mylar or polyethylene terephthalate. Irradiation of Mylar does not cause crosslinkage but it does result in scission or chain cleavage. The mechanical properties are unchanged up to a dosage of  $3 \times 10^7$  rad(C).<sup>7</sup> No significant change in electrical properties occurs up to approximately  $10^8$  rad(C) and, as such, Mylar can be safely used in any application.



Table 2 is a list of some of the more common insulating plastics. This table lists the mechanical damage threshold and the dose required to produce 25% mechanical damage.<sup>8</sup> Both the chemical and the common commercial name are listed. It is hoped that the inclusion of the 25% degradation points will yield some insight concerning the rate of degradation as a function of the dose. Teflon, vinylite, and polyester with no filler all degrade to the 25% point within roughly an increase of 2.5 times the dose damage threshold and this fact coupled with the lower damage threshold make these materials unacceptable. However, Kel-F, Saran, Styron 475, and Lucite could find some application even though the damage threshold is relatively low since the rate of degradation is slow.

The impact of fillers should be noted. Polyester with no filler has a mechanical damage threshold of  $3.9 \times 10^5$  rad(C) while with a mineral filler the material has a damage threshold of  $1.0 \times 10^6$  rad(C). However, polystyrene with no filler has a damage threshold of  $3.7 \times 10^5$  rad(C) while with a black pigment filler the material has a damage threshold of  $4.1 \times 10^5$  rad(C). Thus, the addition of a filler does not always decrease the vulnerability of a material. In addition, it should be remembered that these are the doses required to produce mechanical degradation and not that required to produce degradation of electrical parameters or outgassing.

Besides only containing mechanical damage thresholds, Table 2 also fails to give any indication of the appropriate use of the material. Table 3<sup>9</sup> is an attempt to rectify this shortcoming but the 25% damage points were not available. It should be mentioned that these listings should not be considered with the same degree of inflexibility as specification but rather as guidelines. This in part is due to uncertainties with the test conditions such as temperature, the accuracy of the tolerance data, and the applicability of the tolerance data. As best as possible the data in these tables represent the damage thresholds of a class of materials. However, there may be specific examples within a material class with radiation properties exceeding those listed. The spread in damage thresholds for a particular class in Table 3 gives some indication of this. As is evident from this table the classification of

Table 2. Doses for Mechanical Damage Thresholds and  
25% Mechanical Damage

Material	Damage Threshold rad(C)	25% Damage Dose rad(C)	Material	Damage Threshold rad(C)	25% Damage Dose (rad(C))
Cellulose Acetate (Plastacete)	$3 \times 10^6$	$2.1 \times 10^7$	polystyrene, black pigment filler (Styron 475)	$4.4 \times 10^5$	$4.9 \times 10^6$
Methyl Methacrylate (Lucite or Plexiglas)	$8.9 \times 10^5$	$1.2 \times 10^7$	polystyrene (Ampiphenol)	$8.7 \times 10^8^*$	$> 4.4 \times 10^9$
Phenol Formaldehyde asbestos fiber filler (Bakelite)	$8.7 \times 10^7$	$1.0 \times 10^9$	Polytetrafluoroethylene (Teflon)	$2.0 \times 10^4$	$4.5 \times 10^4$
Polyamide (Nylon, FM10001, FM-1)	$9.2 \times 10^5$	$5.0 \times 10^6$	Polyvinyl butyral (Butacite)	$5.0 \times 10^6$	$2.0 \times 10^7$
Polyester, no filler (Slectron 5036)	$3.9 \times 10^5$	$1.0 \times 10^6$	Polyvinyl Chloride (Geon 2046)	$2.2 \times 10^7$	$1.3 \times 10^8$
Polyester, mineral filler (Plaskon Alkyd)	$1.0 \times 10^8$	$4.4 \times 10^9$	Polyvinyl formal (Formvar)	$1.7 \times 10^7$	$8.9 \times 10^7$
Polyethylene (Polythene)	$2.0 \times 10^7$	$9.6 \times 10^7$	Vinyl-vinylidene Chloride (Saran)	$4.8 \times 10^6$	$5.2 \times 10^7$
Polyethylene Terephthalate (Mylar)	$3.4 \times 10^7$	$1.4 \times 10^8$	Vinyl Chloride Acetate (Vinylite)	$1.6 \times 10^6$	$2.8 \times 10^6$
Monochlorotrifluoro- ethylene (Fluorothene or Kel-F)	$1.6 \times 10^6$	$2.4 \times 10^7$			

Note: ( ) is the commercial name of the compound.

\*Electrical parameter damage threshold  $\sim 10^6$  rad(C)

Table 3. Damage Thresholds and Typical Uses of Common Electrical Insulators

Materials	Damage Threshold rad(C)	Remarks and Typical Use
Polyethylene Expanded Tubing, heat shrinkable Types 1, 2, and 3	$2 \times 10^7$ to $10^8$	Type 1: Heat shrinkable jacket insulation for equipment wiring. Type 2: Repair material for jacket uses. Type 3: Dual-wall shrinkable material for splicing parts. Material has excellent electrical properties for wire connector insulation and membrane insulation.
Modified Neoprene Rubber Tubing, heat shrinkable, flexible	$3 \times 10^5$ to $10^3$	For repair of jackets where oil resistance is needed; will soften in benzene group solvents and in ketones
Teflon coated, tape, glass braid lacing	$10^5$	Teflon coating limits radiation resistance, threshold probably does not include evolution of fluorine
Vinyl coated tape, glass braid lacing and tubing	$2 \times 10^7$ to $5 \times 10^3$	Excellent electrical and radiation properties; thermal stability may be a question.
Irradiated polyalkene insulation with irradiated polyvinylidene fluoride jacket (Kynar)	$2 \times 10^3$	One of the preferred cable or wire insulation for space applications. Generally used in preference to polyethylene insulation. Note the presence of pre-irradiated material.
Irradiated modified polyethylene	$5 \times 10^3$	Same use in space applications.
Polyamide (Nylon)	$5 \times 10^5$ to $10^3$	Electrical insulation.
Polyester (Tylan), glass filled	$2 \times 10^3$ to $5 \times 10^3$	Electrical insulation.
Polychloroprene Rubber (Neoprene)	$3 \times 10^5$ to $2 \times 10^3$	Electromeric cable sheathing, belted parts, bumpers, shock absorbers, jacketing, and stretching. The material should not be used as an insulator.
Surel Rubber	$10^5$ to $10^7$	
Polyvinyl Formal (Formvar)	$2 \times 10^7$ to $3 \times 10^3$	Used as magnetic wire insulation.
Polyethylene	$2 \times 10^7$ to $2 \times 10^3$	Material does become embrittled in ultraviolet radiation.
Polyvinyl Fluoride (Federan)	$10^3$	Electrical insulation that is used in the manufacture of wire and cables. Material has better ultraviolet stability than vinyl.
Polymerized Acrylates	$10^4$	Magnetic wire insulation; thin coating.

materials is not absolute since this listing contains not only organic insulators and elastomers but also include some combinations of inorganic and organic materials (e.g., vinyl coated tape with glass braid lacing and typing).

A ranking of organic materials commonly used for insulators based on radiation data is shown in Table 4.

Table 4. Ranking of Organic Insulators

Preferred Class:	Polyester with mineral filler (Plaskon Alkyd), preirradiated Kynar, preirradiated polyolefin, glass filled polyester, polyvinyl fluoride (Tedlar)
Recommended Class:	Bakelite, polyethylene, polyvinyl formal (Formvar) some forms of nylon, polymethyl methacrylates, polystyrene no filler
Not Recommended	
Class:	Teflon, polyvinyl chloride, Lucite, polyester with no filler, Kel-F, polystyrene with black pigment (Styron 475), butyl rubber, Neoprene

The definitions of the various classes in this table are given by: (1) Preferred Class: These are the first choices and the most radiation resistant of the insulators with damage thresholds of greater than  $10^8$  rad(C). (2) Recommended Class: These materials should be used only if all members of the Preferred class have been found to be unsuitable for nonradiation considerations. The damage thresholds for these materials are between  $10^6$  rad(C) and  $10^8$  rad(C). (3) Not Recommended Class: These materials should be avoided if possible. They should never be used unless test data indicates an acceptable radiation response. Their damage thresholds are all below  $10^6$  rad(C).

It should be noted that some of the materials in Table 3 and 4 will be discussed more fully in other subsections. This particularly applies to butyl rubber and Neoprene which are elastomers and will be discussed in the section on seals.



The use of inorganics deserves a bit more elaboration. In general, inorganic materials are more radiation resistant than organic materials. This is reflected in Table 5 with the dose damage threshold of inorganic materials usually being an order of magnitude above that of organics. The reason is that inorganics are not altered chemically by radiation in that no bonds are broken or made. Atomic displacements produce most of the damage in inorganic material. However, the effects are not always in the same direction. The densities of crystalline insulators decrease under neutron irradiation while the density of amorphous insulators such as glass increase with neutron irradiation. DC resistivity is the primary electrical parameter affected by radiation but the ac resistivity is not significantly affected. The vulnerability of various inorganic insulating materials to neutron damage is shown in Figure 3.

All the materials represented in this figure are certainly acceptable with quartz being the most radiation resistant of the group. The damage threshold of quartz is approximately  $8 \times 10^{20}$  n/cm. Using the conversion factors of Table 1 this corresponds to  $1.6 \times 10^{10}$  rad(Si). However, some quartz crystal oscillators which will be discussed in the section on nonsemiconductor components have ceased operating after an exposure of roughly  $10^4$  rad(Si). This serves to illustrate the impact of the application of the material or device and the damage mechanism. In the case of the oscillator the mechanism is thermal-mechanical strain while for the insulating application the mechanism is displacement. Quartz used for an insulator is quite acceptable while for the oscillator it is quite vulnerable. In any case, the use of inorganics should be maximized.

This concludes the portion of the report dealing with insulators. The next subsection deals with adhesives.

### 3.2 ADHESIVES

Adhesives, of course, are used for bonding materials and, as such, are found in every system. They are organic polymers and have the same problems as the organic insulators. Thus the discussion on the damage mechanisms for insulators also applies to adhesives.

One of the more common materials used as an adhesive is epoxy. The damage threshold for epoxies in general must be taken as  $10^4$  rad(C).<sup>2</sup> This would seem to exclude this material from use. However, the term "epoxy"



Table 5. Total Dose Damage Thresholds of Materials

Material	Damage Threshold rads(C)	Material	Damage Threshold rads(C)
<b>Organic Material</b>			
Silicone treated mica	$10^7$	Polystyrene	$10^8$
Silicone, varnished	$10^7$	Bakelite	$10^8$
glass fiber		Epoxy resin	
Polyethylene	$10^7$	Curing Agent	
Mylar	$10^7$	Dicyandiamide	$10^4$
Teflon	$10^4$	Pyromelhtic Dianhydride	$10^8$
Polyurethane glass fiber	$10^8$	Glass-bonded mica	$10^8$
Polyvinylchloride	$10^5$	Diallyl Phthalate	$10^8$
		Nylon	$10^5$
<b>Inorganic Materials</b>			
Metals	$>10^{12}$	Spinel	$10^{12}$
Fused glass	$10^9$	Silicon	$10^{11}$
Alumina	$10^{12}$	Porcelain	$10^{11}$
Mica	$10^9$	Fosterite	$10^{12}$
Barium Oxide	$10^{12}$	Germanium	$10^9$
Steatite	$10^{12}$	Carbon	$10^{12}$
Boron Nitride	$10^8$		
Ceramic	$10^{12}$		
<b>Elastomers</b>			
Natural rubber	$10^6$	Viton A	$10^7$
Butyl rubber	$10^6$	Silicon rubber	$10^6$
Neoprene	$10^6$	Buna-N	$10^5$



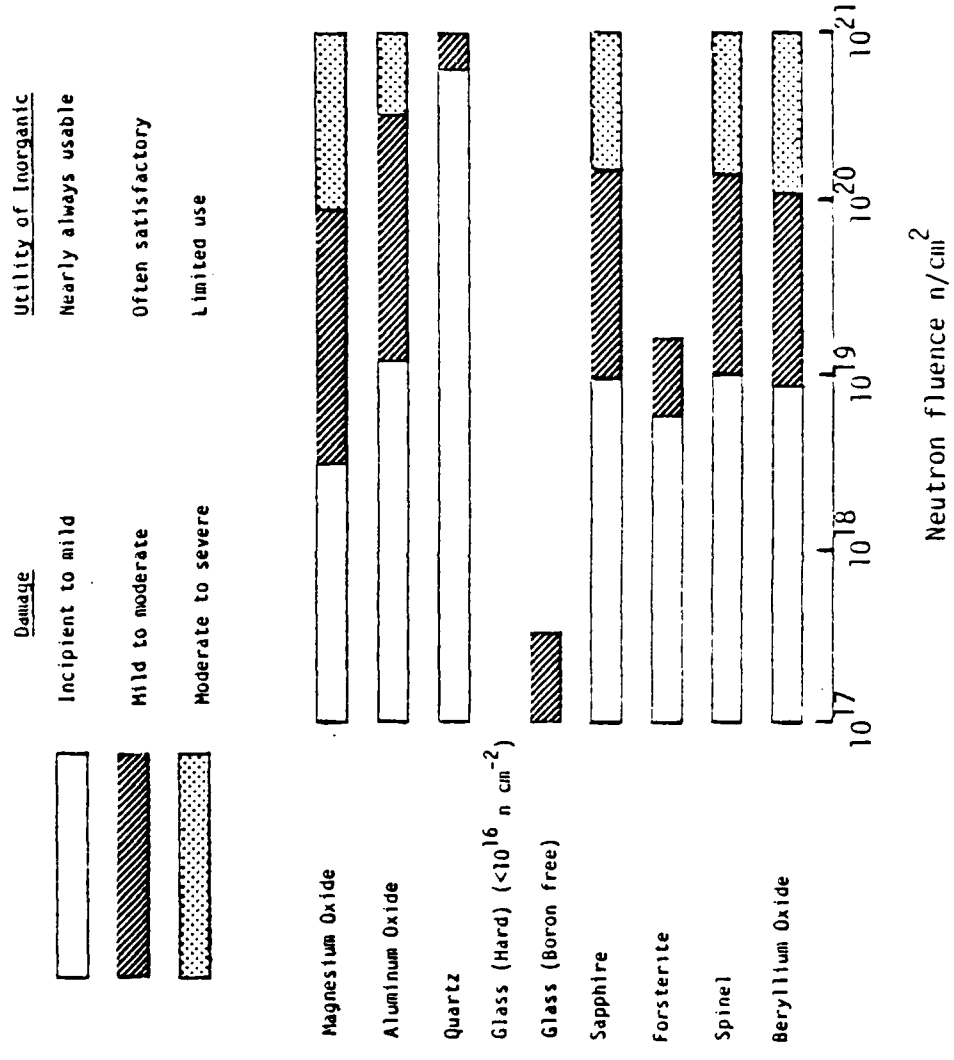


Figure 3. Neutron Effect on Inorganic Insulating Materials

covers a broad class of compounds and many of these have quite acceptable radiation characteristics. Since these compounds do have such wide applications not only as adhesive or bonding materials but also as structural plastics the class of epoxies does deserve some further discussion.

The curing agent for epoxies constitutes a significant portion of the resin and, as such, has a great impact on the radiation vulnerability of a particular epoxy resin. Dicyandiamide is the only common curing agent found to be deleterious to the radiation resistance of epoxies and resulted in the  $10^4$  rad(C) damage threshold.<sup>10</sup> The best (hardest) radiation characteristics are obtained with aromatic amine and aromatic anhydride curing agents such as m-phenylene-diamine and pyromellitic dianhydride. Such systems are unaffected by dose levels up to at least  $10^8$  rad(C) and, of course, can be safely used in any application.

Epoxies, of course, are not the only candidates for adhesives. The most common members of adhesives are organic polymers which have been modified by various compounding agents. Organic resins which are used to form adhesives are either straight chain or cross-linked polymers. The radiation vulnerability will depend primarily on the basic chemical structure of the polymer and, in particular, on the inter-molecular bonding system. Adhesive resins may be classified into four major types: (1) thermosetting; (2) thermoplastic; (3) elastomeric; and (4) blended. Thermosetting resins are characterized by a three-dimensional cross-linked network. Thermoplastic resins have little or no cross-linking and are usually weaker than thermosetting resins. Elastomers consist of repeating chemical structural units called "monomer units" which are joined by chemical bonds into long chains and quite often possess a double bond between adjacent carbon atoms. These three groups can be inter-blended to tailor the properties of the adhesive to a particular application. Classification of adhesives and their radiation characteristics is further complicated by the multitude of agents, fillers, and catalysts that can be added to modify the properties of the adhesive.

Table 6 lists the effects of a radiation environment on several types of common adhesives.<sup>11,12</sup> The radiation levels do not represent the damage thresholds but only the levels that were used for the test. However, the table

Table 6. Effects of Radiation of Tensile Shear Strength of Adhesives at Room Temperature

Name	Class	Tensile Shear Strength (psi)	Dose Level In Air (rad/C.)	Tensile Shear Strength in Air (psi)	Dose Level in Vacuum (psi)	Tensile Shear Strength in Vacuum (psi)	Percent Change
Epon 929	Epoxy	2264	3.9 x 10 <sup>0</sup>	2310	+ 11	2.9 x 10 <sup>0</sup>	+ 12
Epon 934	Epoxy	2662	3.9 x 10 <sup>0</sup>	2640	+ 10	2.9 x 10 <sup>0</sup>	- 9
Epon B	Epoxy	2461	--	--	--	1.7 x 10 <sup>0</sup>	- 12
FM 6000	Epoxy-polyamide (nylon)	6005	3.9 x 10 <sup>0</sup>	6006	- 3	1.7 x 10 <sup>0</sup>	Negligible
Petibond 402	Epoxy-polyamide (nylon)	4023	1.1 x 10 <sup>0</sup>	5940	+ 23	6121	Negligible
III 424	Epoxy-phenolic	3605	4.9 x 10 <sup>0</sup>	352	- 94	6117	Negligible
Epon 4223	Epoxy-phenolic	2362	3.9 x 10 <sup>0</sup>	2399	- 28	2.9 x 10 <sup>0</sup>	- 0
Narco A	Modified epoxy	4157	3.9 x 10 <sup>0</sup>	1614	- 13	2.9 x 10 <sup>0</sup>	+ 16
Petibond 4000	Vinyl epoxy-nylon	4003	--	--	--	4.9 x 10 <sup>0</sup>	- 70
FM 47	Vinyl-phenolic	4115	3.9 x 10 <sup>0</sup>	3116	- 14	2.9 x 10 <sup>0</sup>	- 42
Petibond 4021	Nitro-phenolic	4910	3.9 x 10 <sup>0</sup>	3234	- 26	3.9 x 10 <sup>0</sup>	- 40
At-6	Nitro-phenolic	2570	11 x 10 <sup>0</sup>	3094	+ 40	3.9 x 10 <sup>0</sup>	- 25
APC 1252	Polyurethane	2743	3.9 x 10 <sup>0</sup>	3262	+ 19	2.9 x 10 <sup>0</sup>	+ 12
Narco C	Polyurethane	III	6 x 10 <sup>0</sup>	5020	+ 83	2.9 x 10 <sup>0</sup>	-
			3.9 x 10 <sup>0</sup>	20 0	- 90	454	- 40

does list three epoxies which exhibit only slight changes after an exposure of between  $1.7$  to  $3.9 \times 10^8$  rad(C). This slight change indicates that these dose levels must be very close to the damage thresholds for these materials. This, of course, implies that these epoxies are certainly acceptable for BMDATC-radar applications. Unfortunately the data did not indicate the curing agent but it was probably promellitic dianhydride.

The table also serves to indicate the effect of the surrounding atmosphere on the radiation response of adhesives. As mentioned in the discussion on insulators the free radicals resulting from radiation exposure are very reactive toward oxygen which tends to compete with cross-linking. Thus, in general, there is more degradation of the material in air than in vacuum.

A ranking of the polymers usually used for adhesives based on radiation vulnerability is shown in Table 7.

Table 7. Radiation Vulnerability of Adhesives

Preferred Class:	General class of phenolics, epoxy-phenolics, and epoxies excluding those epoxies using dicyandiamide
Recommended Class:	Neoprene <sup>R</sup> -phenolics
Not Recommended Class:	Neoprene <sup>R</sup> -Nylon <sup>R</sup> -phenolics, cellulose adhesives and epoxies using dicyandiamide

The classes in this table have the same definition as those in Table 4 except for the damage thresholds. For this table, Table 7, the preferred class have damage thresholds between  $5 \times 10^8$  and  $10^9$  rad(C), the recommended class have damage thresholds between  $10^7$  and  $5 \times 10^8$  rad(C), and the not recommended class have damage thresholds between  $10^4$  and  $10$  rad (C). It should be mentioned that it is always a good rule to use the most radiation resistant material or device possible. However, in this case, there is very little distinction between the preferred and the recommended class in that both will easily survive threat level environments in any scenario but the not recommended class should be avoided.



This brings to an end the discussion of the vulnerability of adhesives to nuclear radiation. The next general area to be covered will be materials that find applications as seals such as O rings and gaskets.

### 3.3 SEALS

Seals, of course, are found in almost any system including radars. Like the rest of material applications they are sometimes overlooked but very few systems can be built without O rings and gaskets. The polymer materials commonly used for seals are plastics and elastomers. Metals and combinations of polymers and metals occasionally are also used. However, elastomers are usually chosen because of their high degree of resilience and conformability, relatively low cost, and ease of integrating them into an acceptable seal design (i.e., they generally produce no harmful reaction on the mating surfaces). Elastomers are defined by the American Society for Testing and Materials as: (1) capable of being stretched 100%; and (2) after being stretched 100%, held for five minutes and then released, the material is capable of retracting to within 10% of its original length within 5 minutes after release. In other words these materials are rubber. Of course, all seals do not require a rubber-like substance. This is especially true for a permanent or semi-permanent seal where a gasket of soft metal, plastic, or a combination of plastic and metal is used. Elastomeric sealants or caulking compounds which are applied in a resinous uncured form are sometimes used for permanent seals.

The metals which are appropriate include lead, indium, aluminum, copper (including alloys like brass), and even stainless steel. Compared to polymers the metals are invulnerable to radiation. However, due to their relatively poor compressibility and elasticity, their use in seals is limited.

As stated previously more seals are made out of elastomers than any other class of material. Much of what has already been said applies to this application of elastomers. Particulate radiation such as neutrons have almost no effect on this class of materials. The cause of damage is ionization and not atomic displacement. Total dose effects manifest themselves in this material as a decrease in elongation. The tensile strength may increase or decrease in response to threshold levels of total dose but as the dose level increases the tensile strength eventually decreases to unstable levels.<sup>11</sup>



Table 8. Dose Damage Thresholds for Elastomers Seals

Material	Application	Operating Temp. Range (°F)	Damage Threshold (rad(2))	Remarks
<u>Elastomeric Seals</u>				
Butadiene-Acrylonitrile (Buna-N)	Bearings, gaskets, and vacuum seals	-40 to 250	$10^5$	25% change in useful seal properties at $1 \times 10^6$ rad(2) and become brittle at higher dose levels. Some indications in literature threshold can be as low as $10^3$ .
Nedoprene	Pneumatic and vacuum seals	-65 to 250	$10^7$ to $10^8$ $2 \times 10^3$	Stability is very dependent on the precise composition and the presence of additives.
Natural Rubber	Low pressure pneumatic seals	-40 to 125	$10^6$ to $10^8$ $1 \times 10^4$	Heat rays can increase radiation resistance about a factor of 5. Has the highest radiation resistance in the absence of oxygen.
Butyl Rubber	Pneumatic and vacuum seals	-65 to 225	$10^6$ to $10^7$	Least radiation resistant solid elastomer. Gradually softens and at $5 \times 10^4$ rad(2) becomes a tacky fluid.
Fluorosilicone Rubber	Low pressure pneumatic seals and vacuum seals	-100 to 400	$10^5$	
Styrene-Butadiene Rubber (Buna-S; SBR)	Bearings, gaskets, and vacuum seals	-40 to 150	$5 \times 10^5$ to $5 \times 10^8$	
Silicone Rubber	High temp. pneumatic seals and vacuum seals	-70 to 480	$5 \times 10^5$ to $5 \times 10^7$	Poor radiation stability. Becomes brittle and crumbly at $5 \times 10^4$ rad.
Viton (Fluoro-carbon rubber)	High temp. pneumatic and hydraulic seals and vacuum seals	-65 to 450	$5 \times 10^5$ to $5 \times 10^7$	Some indication in the literature that the damage thresholds may be as low as $5 \times 10^4$ rad(2). Very poor radiation stability when irradiated in air above 150°C.
<u>Elastomeric Sealants</u>				
Polysulfide Rubber (RTV)	Sealant applied as caulking, permanent seal	-65 to 135	$5 \times 10^5$ to $5 \times 10^8$	Poor vacuum and temperature resistance. Low radiation stability and gradually softens to tacky substance.
Silicone Rubber (RTV or RT)	Sealing pneumatic lines	-70 to 480	$5 \times 10^5$ to $5 \times 10^8$	
Thread Sealant	Thread sealant and retainer for bolts	-75 to 250	$10^3$ (estimated)	Commercial name "Locite 4"

Table 8 indicates the damage threshold for elastomers commonly used for seals.<sup>9</sup> This table also includes the usual application of each compound and the temperature range over which the materials may be used. In addition, sealant materials applied in the form of a caulking compound or uncured resin have been included. The term "antirad" is used in this table. These are additives to high polymers which inhibit radiation-induced degradation. These include antioxidants and antiozonants which prevent oxidation or the reaction of free radicals with oxygen and ozone. In addition, the group includes additives which function by preferentially absorbing the energy induced in the polymer by radiation and releasing it in a less damaging form such as heat. Phenyl or aromatic compounds because of their ring structure act as an energy sink and are used as antirads.<sup>13</sup> Two examples of these compounds are hydroxyquinoline and naphthaline.

In any case, Table 9 is a listing of common classes of elastomers broken into three groups based on radiation resistance.

Table 9. Radiation Vulnerability of Elastomers Suitable for Seals

Preferred Class: Neoprene (chloroprenes), natural rubber containing antirads, and threat sealant.

Recommended Class: Natural rubber without antirads, silicone, and styrene-butadiene (Buna-S).

Not Recommended Class: Butyl, fluorosilicone, fluorocarbon (Vitron), butadiene-acrylonitrile (Buna-N), and polysulfide.

The classes in this table have the same definition as those in Table 4, except for the damage thresholds. For this table, Table 8, the preferred class has a damage threshold of  $10^7$  rad(C) or greater, the recommended class has a damage threshold of  $5 \times 10^6$  rad(C) or greater, and the not recommended class has a damage threshold of  $10^6$  rad(C) or less. As was the case with insulators and adhesives, the preferred and recommended classes will survive in any scenario but the not recommended class should be avoided.



It should also be noted that the polyurethanes have not been included. This class of elastomers are quite radiation resistant with a damage threshold of approximately  $5 \times 10^7$  rad(C).<sup>5</sup> However, they are usually used as foams for vibration damping and, therefore, it was thought not to be appropriate to include them in the list of seals and sealants.

The other class of materials that finds some application as seals either by themselves or in composite seals with metals is plastics. They are not used as often as elastomers because of their lack of resilience and conformability. However, they do have good low temperature properties and chemical inertness so they do have some applications. Table 10 lists some of the more common plastics along with their usual applications.<sup>9</sup> Most of these materials were discussed in the section on insulators and, therefore, will not be repeated here. Table 11 is ranking of these plastics according to radiation properties.

Table 11. Ranking of Plastics Applicable for Seals

Preferred Class: Kynar and Polyethylene

Recommended Class: Nylon and Kel-F

Not Recommended Class: Teflon (TFE and FEP), and polyvinyl chloride

The definitions of the classes in this table are the same as those used previously except for the damage thresholds. For Table 11, the preferred class has a damage threshold of  $10^7$  rad(C) or greater, the recommended class has a damage threshold of  $10^6$  rad(C) or greater, and the not recommended class has a damage threshold of  $10^6$  rad(C) or less. The not recommended class should be avoided while the preferred and recommended classes should survive the threat.

This finishes the discussion of the work that was performed on the project concerning the vulnerability of seals.

### 3.4 LAMINATES

Laminates are another class of materials found in almost every system. One common application is printed circuit boards. This material consists of a filler which is usually an inorganic compound such as glass cloth, mica, or



Table 10, Plastics Used for Seals and Retainers

Material	Application	Operating Temp. <sup>(°F)</sup>	Damage Threshold (rad(C))	Remarks
Nylon	Backup rings, low pressure moving seals and gaskets	-100 to 300	$10^6$	Loses its crystallinity, becomes more transparent, will yield hydrogen. Retains moisture which can outgas under vacuum.
Teflon (PTFE) (Polytetrafluoroethylene)	Retainers and Seals	-400 to 500	$2 \times 10^4$ to $10^6$	Outgasses fluorine. Fillers improve radiation resistance slightly. Filled Teflon hold seal better than solids. Crumbles at $10^7$ rad(C).
Teflon (TTFP) Fluorinated ethylene propylene	Retainers and Seals	-400 to 450	$10^5$ to $10^6$	Similar to Teflon (PTFE) but slightly higher radiation properties and slightly lower temperature properties.
Kel-F (Polytrifluoro-chloroethylene)	Retainers and Seals	-400 to 350	$10^6$ to $10^7$	Slightly higher radiation properties than Teflon. Becomes very brittle above $10^8$ rad(C).
Kynar (Polyvinylidene fluoride)	Retainers and Seals	-80 to 300	$10^7$	More abrasion resistant than Teflon. Perhaps, the most radiation resistant commercial fluorocarbon.
Polyethylene	Retainers and Seals	-100 to 180	$2 \times 10^7$	
Polyvinyl Chloride	Retainers and Seals	-100 to 200	$10^5$	Outgasses chlorine. Damage threshold for sealant properties is $2 \times 10^7$ .

asbestos coupled with an organic binder. For such a combination the radiation response is, of course, dominated by the organic binder. In these cases, organic material such as paper, natural fibers (cellulose), or synthetic fibers (e.g., nylon) are sometimes used as fillers and the response of the filler may be significant.

When an organic filler is used, the behavior of the fiber is not significantly different from the base polymers in some other form. The chemical structure dominates the radiation response of the fiber.<sup>13,14,15</sup> Much of what has been said about organic polymers in the previous sections applies here. Exposure to radiation can induce cross linkage, scission, and evolution of gas. Polymers which are used in fibers that contain only hydrogen and carbon are the most resistant to radiation.<sup>13</sup> Among the most vulnerable polymers to radiation are cellulose and halogenated polymers, both of which have very little resistance to chain cleavage.

Up to this point in the report very little has been said about cellulose materials. Scission in these materials is induced by radiation exposure. Figure 4 is a typical curve of scission versus total dose.<sup>16</sup>

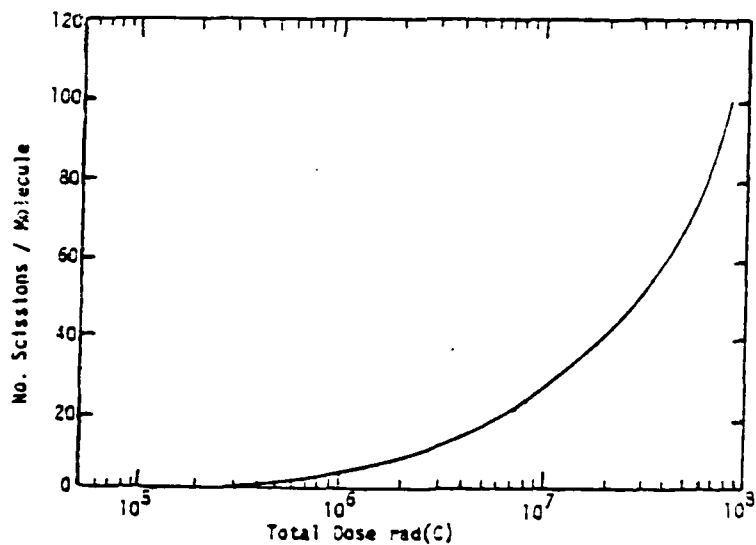


Figure 4. Effect of Total Dose on Cellulose



The effect of radiation on these materials is not limited to just scission but also includes the formation of carbonyl and carboxyl groups. Curves for carbonyl and carboxyl formation have essentially the same shape<sup>3</sup> as Figure 4. Referring to Figure 4, this means that the cellulose chain is not significantly affected chemically for total dose exposures of  $10^6$  rad(C) or less. It should be noted that some authors list the damage threshold for cellulose as  $10^5$  rad(C).<sup>17,18,19,20</sup> This is not in disagreement with Figure 4 since the changes at this dose level in the figure are measurable even though they are very small.

In any case, irradiation of cellulose materials always produces losses in tensile strength, elongation, and Young's modulus. This is indicated in Table 12 for cotton and rayon.<sup>3</sup>

Table 12. Effects of Total Dose Radiation on the Tensile Strength on Cotton and Rayon

Material	Dose $10^6$ rad(C)	Condition of Exposure	% Loss in Strength
30/1 Cotton Yarn	4.2	Air	27
		Vacuum	29
Cotton Fiber <sup>3</sup>	4.4	O <sub>2</sub>	23
		N <sub>2</sub>	24
HT Rayon Cord <sup>20</sup>	8.5	Air	40
		Vacuum	37

The effects of radiation on cellulose fibers are a function of only the total dose and are independent of the dose rate.<sup>21</sup> The order of resistance to scission is given by<sup>15,22</sup> acetates > rayons > cottons.

As a general rule, cellulose materials, even the acetates, are not recommended for radiation resistant applications. To illustrate this, Table 13 is a comparison between cellulose fibers and polyamide (Nylon), polyester (Dacron), and polyacrylic (Orlon) fibers.<sup>3</sup> Viscosity is included in this table because it gives an indication of the first significant change in fiber structures



Table 13. Response of Fibers to a Total Dose of  $10^6$  Rad(C)

Material	Significant Loss in Tensile Strength	Significant Change in Viscosity	Complete Destruction of Fibrous Properties
Cotton	0.1	0.055	30
Rayon	0.8	0.5	80
Acetate	1.0	1.3	100
Nylon 6 or 56	2.0	1.1	100
Orlon	8.0	--	1,000
Dacron	15.0	--	10,000

which, in turn, impacts the macroscopic properties of the material. In general, the cellulose materials (the first three in Table 13) are degraded no matter what property or criteria is used. The synthetic fibers (the last three in the table) are more resistant to radiation and at low doses may show an increase in modulus which would indicate cross linking.

Laminates are composite materials consisting of a binder and a filler. Table 14<sup>17</sup> indicates the results of irradiating several laminates consisting of the same binder (phenol formaldehyde) but different fillers. This table indicates that laminates with inorganic fillers are more radiation resistant than both those with cellulose fillers and also the unfilled resin itself. This illustrates the general rule that filled or reinforced plastics have better radiation resistance than the same plastic when it is unfilled.<sup>5</sup>

As mentioned previously, generally the filler of a laminate is an inorganic compound and the binder is an organic. In these cases the radiation response of the laminates is dominated by the binder since most inorganic fibrous materials are not affected by doses up to  $10^{12}$  rad(C). Table 15 lists some common laminates along with the 25% damage points and operating temperature ranges.<sup>9,23,24,25</sup> The actual damage thresholds are roughly a decade below the levels in the table.

The table pertains to changes in the materials which compose the



Table 14. Effect of Total Dose Composed of Various Fillers and Phenol Formaldehyde Resin

Filler	Dose rad (C)	Tensile Strength psi $\times 10^{-3}$	% Change	Elastic Modulus psi $\times 10^{-6}$	% Change	Impact Strength ft-lb/in	% Change
None	0	10.0	0.0	0.6	0.0	0.53	0.0
	$8 \times 10^7$	7.8	22.0	0.56	6.67	-	-
	$4 \times 10^8$	5.0	50.0	0.36	40.0	0.32	39.6
	$1 \times 10^9$	All properties are very poor					
Asbestos Fabric	0	11.0	0.0	1.8	0.0	5.2	0.0
	$5 \times 10^8$	-	-	-	-	3.6	30.8
	$8 \times 10^8$	8.8	20.0	1.8	0.0	3.6	30.8
	$1 \times 10^9$	11.0	0.0	-	-	-	-
Graphite	0	2.1	0.0	1.8	0.0	0.27	0.0
	$2 \times 10^9$	2.4	14.3	2.2	18.2	0.24	11.1
	$4 \times 10^9$	2.8	33.3	2.4	33.3	0.27	0.0
Linen Fabric	0	11.1	0.0	1.1	0.0	2.75	0.0
	$5 \times 10^7$	7.2	35.1	1.0	9.1	0.45	83.6
	$2 \times 10^8$	3.7	66.7	0.88	20.0	0.25	90.9
Paper	0	10.3	0.0	1.04	0.0	0.66	0.0
	$5 \times 10^7$	7.1	31.1	1.14	9.6	0.33	50.0
	$2 \times 10^8$	5.2	49.5	1.04	0.0	0.22	66.7

laminates. All organic materials will evolve some gas when irradiated. As long as the materials involved contain only carbon, hydrogen, oxygen, and nitrogen, the gases which are evolved will not be detrimental to the laminate. However, as mentioned in previous sections, halogenated polymers will evolve acidic vapors which can be very corrosive. In this regard, the point should be made that many fire-retardant systems employ highly halogenated components and, as such, must be employed with caution. In any case, the evolution of gas, corrosive or not, can cause blistering, warping, and distortion to metallic foil runs. This constitutes one of the main mechanical damage mechanisms for printed circuit boards.

Another major radiation effect on circuit boards is increased leakage current. It has been postulated<sup>9,26</sup> that this is due to radiation-induced ionization in the air which establishes conductive paths between exposed copper conductors. Another form of electrical degradation has been observed in the form of metal oxide deposits on the surface of the copper foil strips as well as discontinuities in the foil itself.<sup>26</sup> Coatings improve the radiation resistance by offsetting the ionization effects. However, there is some ambiguity concerning the relative efficiency of the different types of coatings. Reference 9 states that "the most efficient one seems to be silicone varnish," while reference 26 states that "a polyester coating appears superior to epoxy-polyamide and to a silicone varnish in preserving the electrical characteristics of the boards." Regardless of these differences there is agreement on the improvement in the radiation resistance which results from the use of a coating.

A preferred list of laminates has not been compiled since this entails combinations of the fillers and binders and this would be quite extensive. Regardless any of the laminates in Table 15, except the last entry, can be safely used. In addition, some guidelines can be formulated. These are listed below. For fillers:

- (1) Use inorganics
- (2) If organics must be used, then choose synthetic materials
- (3) Avoid using cellulose materials.



Table 15. Twenty Five Percent Total Dose Damage Point for Common Laminates

Material	Temp. Range (°F)	Damage Threshold rad (C)	Remarks
Copper-clad epoxy glass laminate	-65 to 300	$5 \times 10^9$	Printed circuit board
Epoxy resin, glass fabric laminate (low pressure) and sheet (high pressure)	-300 to 250	$2 \times 10^9$ to $5 \times 10^9$	Preferred structural plastic. This is a thermosetting material. It is undamaged in most mechanical and electrical properties at doses of $10^9$ rad(C) except impact strength which decreases roughly 30%.
Silicon glass laminate	-65 to 500	$3 \times 10^8$ to $5 \times 10^9$	Good electrical properties and temperature resistance.
Phenolic resin, glass fabric laminate	-300 to 500	$8 \times 10^8$ to $8 \times 10^9$	Preferred structural plastic. This is a thermosetting material. Has excellent mechanical properties throughout its temperature range if properly postcured.
Polyester resin, glass fiber laminate	-100 to 200	$2 \times 10^9$ to $5 \times 10^9$	General purpose laminate. This is a thermosetting material.
Phenolic resin, glass fiber molding	-300 to 450	$8 \times 10^8$ to $8 \times 10^9$	General purpose molding compound. Not for primary structural applications.
Melamine resin, glass fiber molding	-65 to 350	$10^8$ to $10^9$	This is a thermosetting compound. Not for primary structural applications.
Diallyl phthalate	-100 to 400	$10^8$	Used for molded potting containers.
Copper-clad Teflon glass laminate	-65 to 400	$10^5$ to $10^6$	Restricted use. Vulnerability dominated by Teflon.



Binders:

- (1) Avoid halogenated polymers
- (2) Be guided by the recommended list for insulators in section 3.1 of this report

Laminated printed circuit boards:

- (1) Use a coating of either polyester or a silicone varnish.

However, as indicated by the data in Table 13, laminates should be able to withstand threat levels of the environment. The exception to this is copper-clad Teflon glass laminate which has a damage threshold of approximately  $10^4$  rad(C). In any case it is good design practice to follow the above guidelines whenever possible.

3.5 - Encapsulants

The last application of organics that will be considered in this study is encapsulation or potting. There are a wide variety of reasons for potting including mechanical shock insulation, thermal insulation, and environmental (such as moisture and oxidation) protection. Because of this, mechanical properties are more important than electrical for this application. It should also be noted that coating and impregnating a component with a compound to provide moisture and oxidation protection is very similar to potting and some of the materials that were included can be used for these applications.

The compounds used for encapsulation invariably consist of highly crosslinked resins and, as such, the discussion on the organic binders of laminates also applies here. The resins, of course, require a curing agent which can have a significant impact on the radiation vulnerability of the compound. This was illustrated in the discussion on adhesives in section 3.2, by epoxies and the difference in the damage threshold for compounds cured by dicyandiamide (threshold of  $10^4$  rad(C)) and by pyromellitic dianhydride (threshold of  $10^8$  rad(C)). Table 16 lists the effects of dose on various properties of epoxy resins cured by different agents.<sup>27</sup> In this table, hardness means the resistance that a material has to abrasions and indentations. Barcol hardness simply refers to a specific method of measuring hardness.



Table 16. Effects of Total Dose Radiation on Unfilled Epoxy Resins

Curing Agent	Total Dose rad(C)	Barcol Hardness	Heat Distortion Temp. (°F)	Compression Strength (psi)
p-p' methylenedianiline	0	20	295	2750
	$10^6$	27	295	2860
	$10^7$	29	295	2900
	$10^8$	31	275	2880
Pyromellitic dianhydride	0	39	575	-
	$10^6$	39	570	-
	$10^7$	39	575	-
	$10^8$	39	575	-
m-phenylenediamine	0	33	290	3015
	$10^6$	31	280	3050
	$10^7$	31	280	3250
	$10^8$	30	255	2905

Table 17. Dose Effects on Polyester-Styrene Resin

Total Dose rad(C)	Tensile Strength (psi)	Elongation (percent)	Elastic Modulus (psi)	Shear Strength (psi)	Impact Strength ft-lb/in <sup>2</sup>
0	2000	20	.58 x 10 <sup>5</sup>	3100	.73
$4 \times 10^6$	4000	16	$1.7 \times 10^5$	6200	.62
$7 \times 10^7$	8600	6	$3.0 \times 10^5$	6500	.58
$7 \times 10^8$	5900	3	$3.1 \times 10^5$	5600	.44
$1.5 \times 10^9$	2000	-	-	4000	.22

Some of the properties of the compounds in Table 16 show an increase with radiation. This is due to radiation-induced cross linking. This effect is more clearly indicated in Table 17.<sup>17</sup> This data is for a polyester-styrene resin. Compounds of this type are also commonly used for potting. They are formed by dissolving the polyester in styrene or some other vinyl monomer.<sup>3</sup> In any case, the data in Table 17 does indicate that radiation-induced cross linkage can result in a desirable increase in the mechanical properties of a material. The Young's modulus, the tensile strength, and yield strength are increased.<sup>3</sup> Cross linkage also causes an improvement in heat distortion<sup>28</sup> and resistance to solvent action. However, all the effects are not desirable. The impact strength is decreased, the compound becomes brittle, and the elongation before break may be significantly reduced.<sup>3</sup> Thus, radiation-induced cross linking can be helpful or harmful depending on the particular application.

Table 18<sup>9</sup> is a list of the damage thresholds of some common commercially available potting compounds along with their operating temperature range. The list includes polyurethane encapsulants. These materials have some of the best radiation response characteristics of any polymer. They are recommended for use whenever there is a requirement for shock insulation or vibrational damping. The list also contains some compounds which are suitable for coatings and impregnating components. It contains the commercial name along with the manufacturer. The list is not intended to be all inclusive but simply representative.

Damage threshold data for a particular example of polystyrenes and of phenolics was not available. However, some data shown in Figure 5 on Styrofoam 22 (a polystyrene foam)<sup>27</sup> was obtained. This foam had a density of 2 lb/ft<sup>3</sup>. Irradiation in air at room temperature produced degradation at doses as low as  $5 \times 10^7$  rad(C). This contradicts the damage threshold listed in Table 18. One possible explanation for this low damage level is the fact that most foams are produced by mixing into the polymer a thermally unstable compound, or blowing agent, which decomposes and gasifies upon heating. Small quantities of the residual blowing agent or its degradation product may degrade further and attack the polymer when irradiated. A typical blowing agent,



methyl chloride, decomposes when irradiated to form an acid which attacks polystyrene.

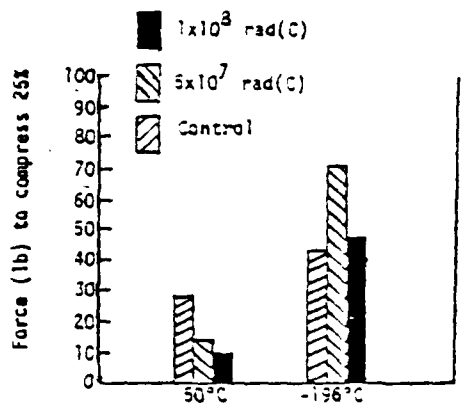


Figure 5. Radiation Data for a Polystyrene  
Foam (Styrofoam 22)

This same phenomena has been reported for Stafoam AA-402 (a poly-ether-resin urethane foam).<sup>29</sup> The same explanation applies. The blowing agent when irradiated evolves chlorine which forms the acid which degrades the foam itself. The data did not include a damage threshold, but the foam did exhibit degradation at  $5 \times 10^7$  rad(C) at room temperature. This does not contradict the damage thresholds in Table 18 since this was for a specific example of polyurethane.

This illustrates the impact that additives can have on the radiation response of organic polymers. Care must be exercised in choosing curing or blowing agents that will not experience radiation-induced degradation whose products will attack the polymer. For these two examples, polyurethane and polystyrene, the use of methyl chloride lowers the damage threshold by an order of magnitude.

An important consideration associated with irradiated potting compounds is gas evolution. This may cause significant effects for hermetically sealed potting systems. This effect has been reported impacting transformers, capacitors, and inductors. For capacitors, the problem is further aggravated



Table 18, Total Dose Effects on Common Encapsulants

Material	Application	Temp. Range (°F)	Damage Threshold (rad(C))	
<u>Polyurethane Encapsulants</u>				
Eccofoam FP (Class A, B, and C), Emerson and Cummings, Inc.; Hitco R (Class A, B, and C), H.I. Thompson Co.	Foam-in-place Type I	-65 to 165	$10^4$	Rigid foam encapsulant for mechanical shock and vibration damping; type is determined by the maximum temperature of use.
	Type II	-65 to 250	$10^5$	Class is determined by density: Class A: 2 lb/ft <sup>3</sup> ; Class B: 10 lb/ft <sup>3</sup> ; Class C: 20 lb/ft <sup>3</sup>
	Type III	-65 to 350°	$10^6$	Ultraviolet radiation results in some discoloration
<u>Silicone Rubber</u>				
Dow-Corning Corporation 0-9-0031-1/2 0-9-3003-1/2 0-9-0006-1/2 RTV-503	Potting	-85 to 500	$5 \times 10^6$	Requires a rigid mold for mechanical shock and vibration; should not be used at 400 to 500° F unless given a progressive cure in 100° F steps to 500° F.
Products Research Co. PR-1930-1/2 PR-1920-1/2 PR-1910-1/2				
<u>Silicone Rubber Primer</u>				
General Electric Co. SS-4004 Products Research Co. 1902	Primer to RTV rubber	-85 to 500	$5 \times 10^6$	1 hour cure at room temperature
<u>Polysulfide</u>				
JC-737, Class A JC-747T, Class B Churchill Chemical Co.	Potting	-70 to 300	$10^4$	Used primarily for cable connectors; not recommended for general purpose potting
<u>Epoxy Encapsulants</u>				
Insulating Lacquer 1162 Dennis Chemical Company	Moisture resistant coating (thin)	-65 to 200	$10^7$	Spray or dip coat (< .005 in.) printed wiring board coating

since these devices quite often employ solid or liquid organic dielectrics which can also undergo radiation-induced gas evolution. Table 19 lists data on

Table 19. Radiation-induced Evolution of Gas

Material	Gas Evolution* ml/g per $10^6$ rad(C)
Triallyl cyanurate	.0013
Aniline formaldehyde	.00064
Casein plastic	.006
Phenol formaldehyde	.0032
Allyl diglycol carbonate	.057
Polyester-styrene (mineral filler)	.0031
Melamine formaldehyde with cellulose filler	.0054
Urea formaldehyde with cellulose filler	.010
Epoxy cured with aliphatic amine, mineral filled	≈.015 (based on weight of resin)

\* This is for standard temperature, and pressure.

the evolution of gas from various irradiated potting compounds. The table indicates that gas evolution may be a problem for allyl diglycol carbonate, cellulose filled urea formaldehyde, and mineral filled epoxy. Referring to the discussion on laminates, it must be remembered that cellulose decomposes readily and results in physical degradation and gas evolution. Thus, the gas evolution for cellulose filled compounds is expected to be greater than the unfilled version. Viewed in this light the gas evolution of unfilled urea formaldehyde may be quite acceptable.

In any case, the evolution of gas can result in distortion and internal stresses within the potting compound. This internal stress within a potting material cannot only damage the embedded component but in certain cases can also affect the operation of the devices. Examples of devices whose operation is modified can be found among the ferrites which can be particularly sensitive to stresses. In fact, this property or effect has been used to



develop a strain gauge to measure the stresses inside epoxies as a function of dose.<sup>30</sup> The device was used to measure the internal stress within two epoxies: a semirigid epoxy (Scotchcast 3M-241) and a rigid epoxy (Epocast H2E-001). The 3M-241 response is shown in Figure 6. It is interesting to note that in the

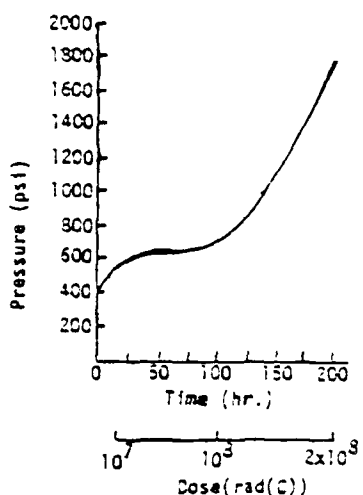


Figure 6. Radiation-induced Pressure in 3M-241 Epoxy

absence of radiation the stress internal to the epoxy is 400 psi. The radiation-induced increase in stress is due to either cross-linking or gas formation.

The response can vary from epoxy to epoxy. Figure 7 depicts the response of the H2E-011 epoxy which is markedly different from that shown in Figure 6. Initially the pressure is fairly stable with radiation. However, after roughly 15 hours of irradiation, spikes did occur. Although not apparent from the figure because of the scale, the spikes have a magnitude of 1500 psi. In addition, the nonradiated value of 33,000 psi would appear to be potentially damaging to any compound embedded in the material.



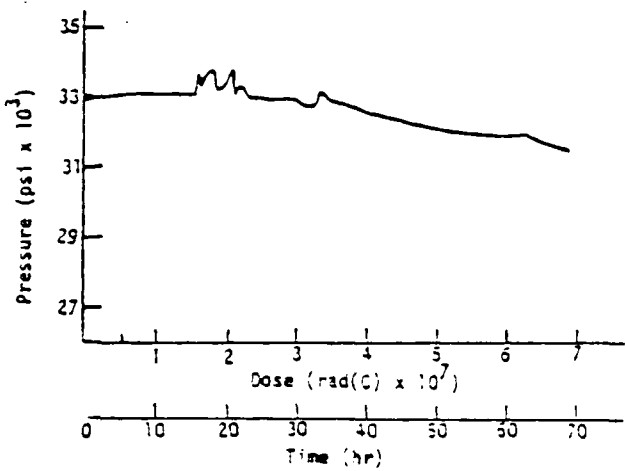


Figure 7. Internal Stress as a Function of Radiation in H2E-011 Epoxy

The difference in the responses shown in the two figures is due to differences between the chemical structure of the two epoxies. H2E-011 is a fully cross-linked three dimensional structure while the 3M-241 is not. With a fully cross-linked structure like the H2E-011 the predominate radiation degradation process is probably cleavage of the carbon-to-carbon bonds in both the main chain and the cross links. In any case, this does illustrate the possibility of the existence of high internal stresses in the potting compound.

The data on the materials suitable for encapsulants contained in this report was used to form the ranking shown in Table 20. This ranking does not include gas evolution but is based solely on the damage thresholds for mechanical properties. It also assumes that a nonhalogenated blowing agent is used to form the foams. In this table the preferred class has a damage threshold of  $10^8$  rad(C) or greater, the recommended class is  $10^7$  rad(C), and the not recommended class is  $10^6$  rad(C). Of course this is not an all inclusive list and the list should not be regarded as specifications but rather as guidelines. However, as indicated by the damage thresholds all of the listed materials should be able to withstand the threat with little or no effect.



Table 20, Ranking of Encapsulants

Preferred material: Polyurethane (Eccofoam FP and Hitco R), polystyrene, phenolic, epoxy (Epocast H2E-011, H2E-012, H2E-037; Scotchcast No. 3)
Recommended Material: Epoxy (insulating lacquer 1162; Epocast 202/9615, 202/9647, 202-11/9615A)
Not Recommended Material: Polysulfide (3C-737, Class A; 3C-747T, Class B); silicon rubber (Q-9-0031-1/2, Q-9-3003-1/2, Q-9-006-1/2, RTV-503, PR-1930-1/2, PR-1920-1/2, PR-1910-1/2); silicon rubber primer (General Electric Co. SS-4004; Products Research Co. 1902)

There is an additional area associated with binders which could present potential problems. This is associated with the propellants for the interceptor. Even though this is not a subject of concern to this project, it was thought that this information could be of use and should at least be mentioned.

Modern propellants are composites of an oxidizer, a fuel binder, and a powdered metal. The binder is typically an elastomer or plastic such as polyvinyl chloride, polysulfide, or carboxyl-terminated polybutadiene. One of the requirements for the binder is to provide sufficient strength so that the composite propellant will retain structural integrity during the high acceleration phases of the flight. Another requirement for the binder is that its burning rate must be sufficiently high so that the burn rate of the composite fuel is high enough to accelerate the missile at its required value.<sup>31</sup> The purpose of the oxidizer, of course, is to promote oxidation. From the discussions on polymers in this report it would appear that, in view of the requirements on the binder and the oxidizer, scission of the binder will occur in the presence of radiation. This could easily lead to the evolution of gas and loss of strength in the binder. As mentioned previously, this is not an area that is pertinent to this study. However, it certainly can have serious consequences on the performance of the interceptor.

This finishes the work that was done on the radiation response of materials. It has been mentioned previously but it must be restated that the



listings in this report should not be considere with the same degree of inflexibility as a specification but rather as guidelines. As best as possible the data in these sections represent damage thresholds of a class of materials. However, there will be specific examples within a class with radiation properties exceeding those listed.



## 4.0 NONSEMICONDUCTOR COMPONENTS

The nonsemiconductor components that were covered consist of three classes: resistors, capacitors, and quartz crystal oscillators. These classes of components are usually ignored. However, with the high threat levels that are expected it was felt that these classes could exhibit some susceptibility to radiation-induced degradation or disruption. This section has been divided into two subsections; one dealing with resistors and capacitors and one covering quartz crystal oscillators.

### 4.1 RESISTORS AND CAPACITORS

Resistors are affected by neutrons and dose-rate. Neutrons cause permanent or long term resistance changes due to displacement effects. The dose rate effects are momentary and last only a few microseconds. These transient effects exhibit themselves as a shunt leak resistance and a Compton replacement current. The shunt resistance is due to ionization resulting in a shunt leakage resistance. The replacement current is caused by Compton scattering of electrons from the resistor's atom. Figure 8 is the equivalent circuit of a resistor which has been irradiated.

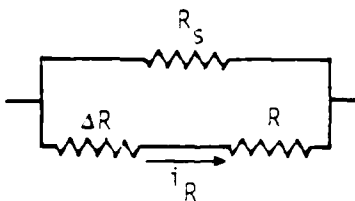


Figure 8. Equivalent Circuit of a Resistor Under Irradiation.  
R is Preirradiated Resistance

The  $\Delta R$  is the change in the resistance due to neutrons. The wire-wound resistors are the least sensitive to neutron irradiation. Their neutron damage threshold is approximately  $10^{15}$  to  $10^{16}$  n/cm<sup>2</sup>. Oxide film resistors are the most sensitive



to neutrons. Their damage threshold is only  $10^{12}$  n/cm<sup>2</sup>. The damage threshold for carbon composition is approximately  $10^{13}$  n/cm<sup>2</sup> and an exposure to a fluence of  $10^{14}$  n/cm<sup>2</sup> causes a 2% reduction in resistance.<sup>32</sup> The magnitude of the neutron-induced degradation is dependent on the size of the resistor. In general, the larger the resistor the greater will be its percentage change in resistance when exposed to a neutron fluence. The change in a one megohm resistor is about a factor of 3 to 4 times that experienced by a 100 ohm resistor. The effects of neutron irradiation on some common types of resistors are summarized in Table 21<sup>2</sup> and Figure 9.<sup>33</sup>

TABLE 21. NEUTRON DAMAGE THRESHOLDS OF RESISTORS

Resistor Type	Damage Thresholds (n/cm <sup>2</sup> )
Carbon composition	$10^{13}$
Metal film	$3 \times 10^{16}$
Carbon film	$10^{15}$
Oxide film	$2 \times 10^{12}$
Precision wirewound	
Ceramic	$5 \times 10^{17}$
Epoxy	$10^{15}$

Besides neutron-induced degradation, resistors are also subjected to dose-rate effects. The impacts are the generation of a replacement or Compton current which is  $i_R$  in Figure 8 and a reduction of the element's effective resistance due to leakage in the resistance material and its surroundings. This last effect is equivalent to the transient shunt leakage resistance represented by  $R_s$  in Figure 8. This leakage shunt resistance is inversely proportional to the dose rate while the Compton replacement current is directly proportional to the dose rate. Two very simple equations provide first order approximations to the leakage resistance and the replacement current:

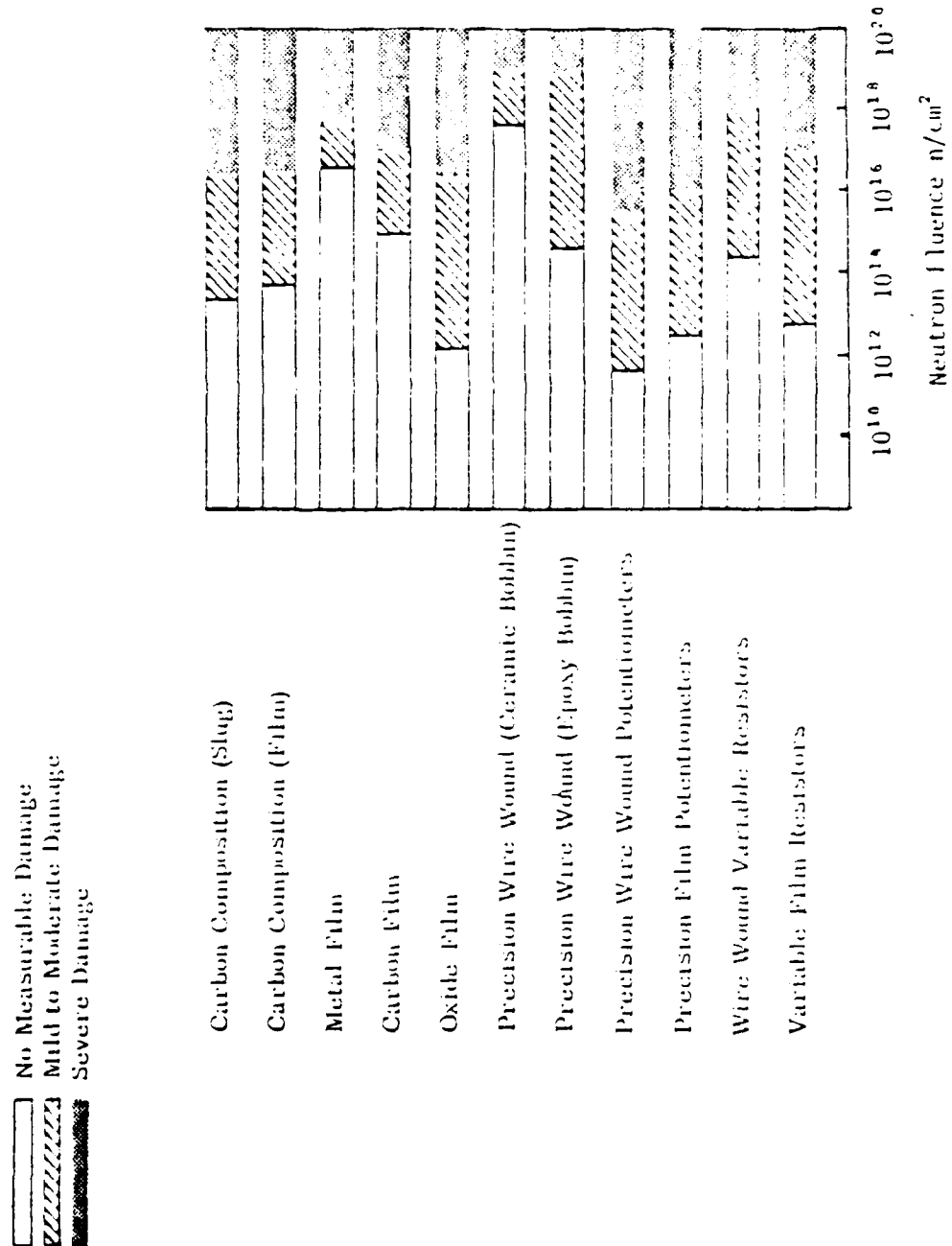


figure 9. Neutron Effects on Commonly Used Resistors

$$R_s \approx \frac{B_1}{\gamma}$$

and

$$i_R \approx B_2$$

The proportionality constants vary with the wattage and potting material of the resistor. There is some disagreement on the value of these constants in the literature but the best agreement seems to be for the values shown in Table 2.32  
22.

Table 22. Resistor Proportionality Factor

Resistor Type	Potting Compound	$B_1 \times 10^{13}$ (kohms-Rad(C)/sec)	$B_2 \times 10^{-12}$ (amps/Rad(C)/sec)
Carbon Composition (watts)			
1	Air (630 mm Hg)	2.1	0.78
1	Silastic	> 4.3	0.5
1/8	Dow-Corning 200	> 1.7	3.0
Ceramic encased	Paraffin	>170.0	0.045
Metal film 1/8 watt	Paraffin	> 40.0	0.041

Therefore, at threat levels, it should be anticipated that the leakage resistance and the replacement current will experience an increase governed by the above equations.

Similar to resistors very little recent work has been reported in the literature on capacitors. Normally the environments are not high enough to create significant problems. However, in our case the radiation effects can be significant. The parameters of a capacitor that are affected by radiation are the capacitance, the dissipation factor, and the leakage resistance. The changes in capacitance may be either positive or negative, the dissipation factor nearly always increases, and the leakage resistance nearly always decreases.

Capacitors using Teflon as a dielectric exposed to  $10^{14}$  n/cm<sup>2</sup> have an increase in capacitance of approximately 10% while the leakage resistance drops from  $6 \times 10^{11}$  to  $6 \times 10^8$  ohms. Capacitors using Mylar film show essentially no degradation in electrical properties up to  $10^8$  rad(C) and in mechanical properties up to  $10^9$  rad(C). However, the dielectric constant does exhibit some changes but recovers after irradiation. Mica used in capacitors seems to be unaffected by neutron fluences up to  $5 \times 10^{18}$  n/cm<sup>2</sup>.<sup>2</sup> The relative effects of neutron fluence on various capacitors is shown in Figure 10.<sup>34</sup>

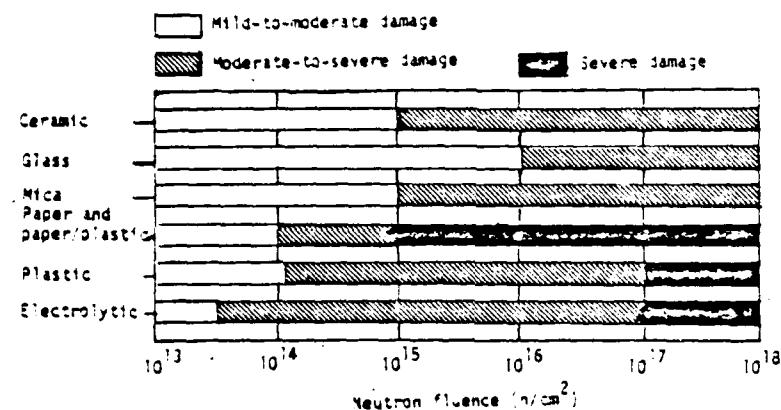


Figure 10. Relative Neutron-Radiation Sensitivity of Capacitors

It should be noted that some of the most sensitive capacitors are those which used impregnated paper for a dielectric. The impregnants that are commonly used are mineral oil, wax, castor oil, petroleum jelly, and chlorinated compounds. The damage to these type capacitors is due primarily to gas being evolved from these impregnants which results in pressure buildup, bursting, and eventually open circuiting of the capacitor. The damage threshold for this type capacitor is approximately  $10^{13}$  n/cm<sup>2</sup>.

As evidenced by Figure 10, types of capacitors can be chosen which will survive the threat. Some guidelines can be stated that will aid in such a choice. These are:

- 1) Avoid organic dielectric materials if possible.
- 2) Paper dielectric units must not be impregnated with hydrocarbons.
- 3) The preferred types of capacitors are glass, ceramic, and tantalum in that order.

#### 4.2 QUARTZ CRYSTAL OSCILLATORS

Quartz crystal oscillators are used for precision master clocks in many systems. Often this class of components is overlooked in a radiation vulnerability assessment. However, radiation will affect the frequency of these oscillators. They will suffer a transient and a permanent effect and in the extreme will cease to oscillate.

It is fairly well established that a significant increase in the radiation hardness of quartz oscillators is achieved by electrodiffusing or sweeping the quartz prior to fabrication of the resonators.<sup>35-41</sup> This process consists of applying an electric field parallel to the crystal's c-axis while maintaining the sample temperature in the 400 to 500° C range.<sup>42</sup> Electrodes are applied to the face of the bar of the quartz and impurities (generally Li<sup>+</sup> and Na<sup>+</sup> interstitial ions) are swept out. The process is carried out at high temperatures to increase the mobility of the impurities. It should be noted that the alkali interstitials are always present in as-grown crystal since they are deliberately introduced during the growth process to act as charge compensators for the ubiquitous silicon-substituted aluminum ions.

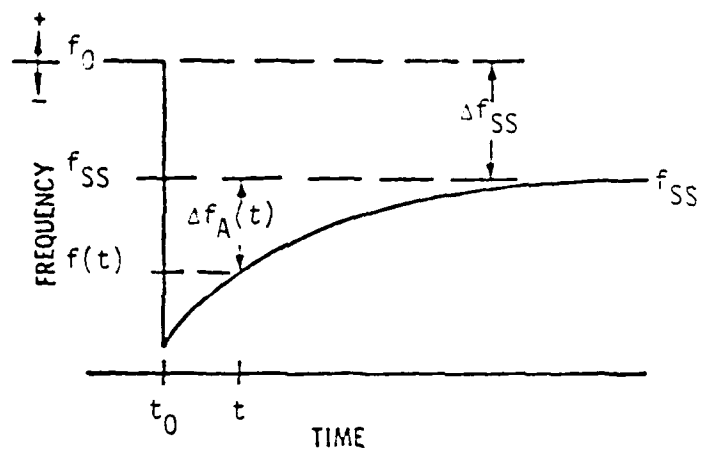
In unirradiated crystals, aluminum is located in the quartz lattice as a substitute for silicon. The concentration of Al in the lattice depends on the growth conditions but it does tend to be the dominant lattice impurity with the concentration generally having an upper limit of 3000 ppm (i.e., per number of silicon atoms).<sup>43</sup> From an ionic viewpoint, aluminum is a +3 entity in the +4 silicon site and there is a general tendency to achieve charge compensation by the location of a +1 ion (H<sup>+</sup>, Li<sup>+</sup>, or Na<sup>+</sup>) at a nearby interstitial site.



Synthetic quartz suffers from a low value of Q (acoustic losses, internal friction, or figure of merit). The initial reason for sweeping was to improve the Q value and not to demonstrate that swept synthetic quartz is more tolerant to radiation.<sup>44</sup> Therefore, little work has been done to optimize the sweeping process for radiation hardness and sweeping is critical to the radiation hardness of synthetic quartz crystals at room temperature. Eernisse<sup>45</sup> indicates that unless electrolysis is carried out with care more impurities can be introduced than are removed. The situation is further complicated by the fact that the sweeping process has not been standardized (e.g., sweeping is performed in vacuum, air, hydrogen, or inert atmospheres). Variations in the sweeping process cause variations in the kinds, locations, and amounts of imperfections within the quartz lattice structure which are, in turn, reflected in the variations in the radiation response of the oscillators.

Following a pulse of radiation, the frequency and Q of the oscillator change. These changes do partially anneal toward preirradiation values for about 20 minutes after the cessation of radiation, after which the changes in Q and frequency are fairly stable. The situation is illustrated in an idealized form<sup>41</sup> in Figure 11. Changes which anneal within roughly 20 minutes after the cessation of radiation are called transient shifts. All those changes which persist for longer than 20 minutes are called steady-state shifts,  $f_{ss}$ . The annealable portion of the frequency offset in Figure 11 is designated by  $\Delta f_A$ . It should be noted that the steady-state shifts are not permanent but will anneal out. However, the annealing of the steady-state shifts is very slow and will continue for days until the preirradiation value of frequency is obtained.





$f_0$  = original, preirradiation frequency

$f_{SS}$  = steady-state frequency (approximately 15 minutes after exposure)

$f(t)$  = instantaneous frequency at any time,  $t$

$\Delta f_A$  = annealable portion of the frequency change

Figure 11. Idealized Behavior of Frequency versus Time for Quartz Resonators Following an X-Ray Exposure Pulse

There are two ranges of dose in which the resonators exhibit different steady-state behavior. The response in one region can not be inferred or extrapolated from the behavior in the other, which probably indicates different mechanisms for the radiation response in the two regions. In the low dose range ( $\lesssim 10^3$  to  $10^4$  rads (Si)), the frequency change is usually positive, small (typically 1-10 pp  $10^8$ ), and shows little dose dependence. With larger doses, it increases strongly with dose and can reach high negative values.

The early work was concentrated on steady-state changes and principally in the high dose region. However, some low dose data does exist. For swept synthetic quartz, both positive and negative shifts have been observed. Shifts of the order of 1 pp  $10^8$  can occur for doses as low as 100 rads. In some cases the change in frequency has been observed to reach a plateau for exposures as low as 400 rads (Si). Once the response has saturated no further frequency shifts will occur until the absorbed dose exceeds 3000 rads (Si). This low dose offset is indicated in Figure 12<sup>46</sup>, 13<sup>47</sup> and 14.<sup>37</sup> The data in Figure 12 is on

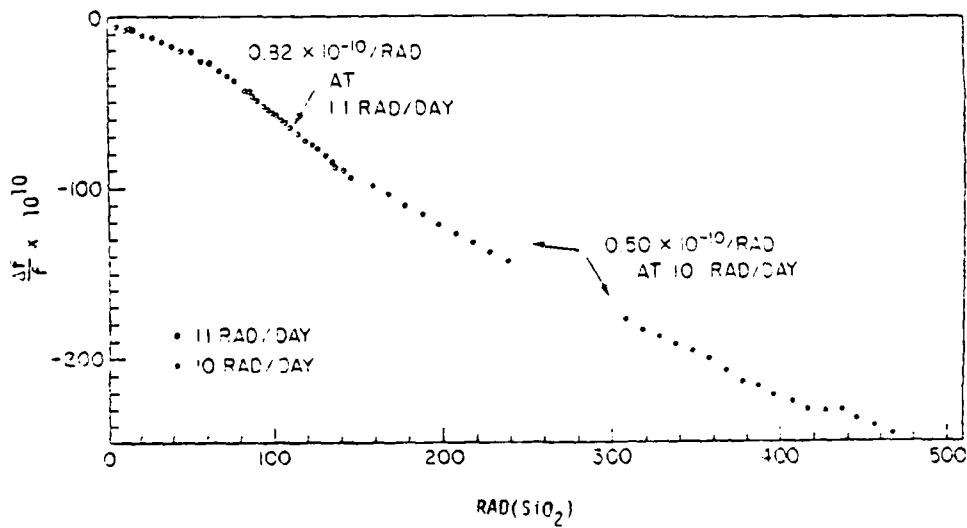


Figure 12. Steady State Frequency Offset of Unswept Natural Quartz as a Function of Absorbed Dose

SRI

a 5 MHz unswept natural quartz oscillator. This figure seems to indicate that increasing the dose rate changes the rate of frequency offset per rad (Si). However, even at a constant dose rate the rate of frequency offset appears to be changing as indicated by the tailing of the curve above 400 rad (Si). This indicates that the slope is a function of the accumulated dose rather than dose rate.

Figure 13 indicates the response of swept and unswept Premium-Q synthetic quartz<sup>47</sup>. This figure gives some indication of the transition region between

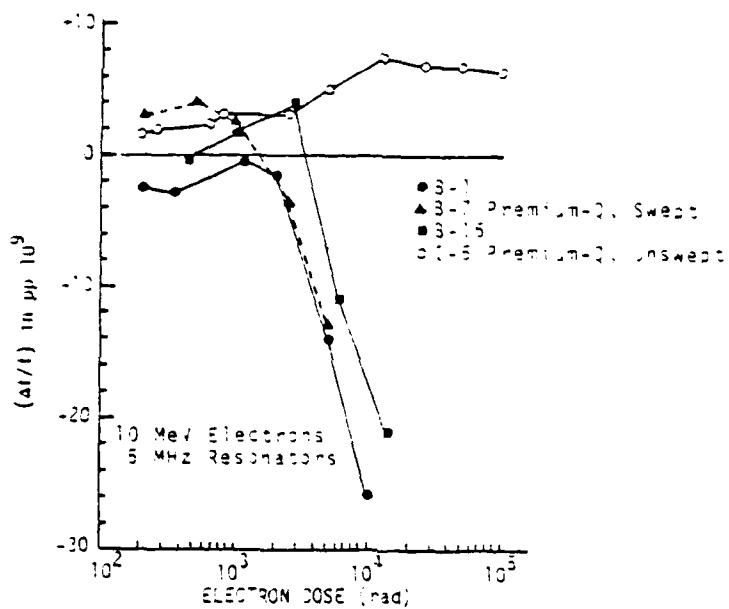


Figure 13. Radiation Response of 5 MHz Premium-Q Resonators

the low and high dose regimes. The transition region is further expanded in Figure 14.<sup>37</sup> The data in Figure 14 is for 5 MHz Sawyer Research Products (SARP) Premium-Q quartz resonators. Unfortunately the scales in Figures 13 and 14 are different which makes a comparison of the two figures difficult. However, they

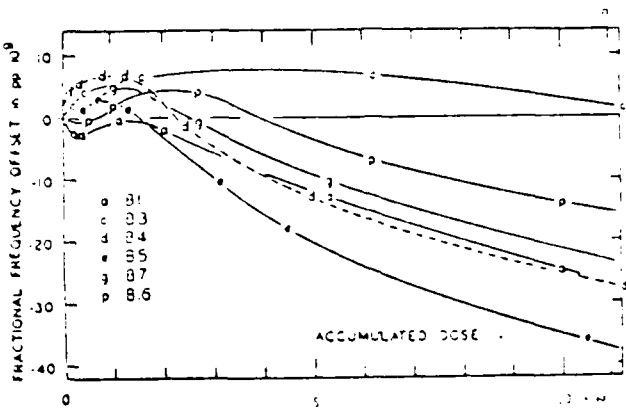


Figure 14. Radiation Response of 5 MHz SARP Premium-Q Quartz Resonators

are essentially in agreement with one another and indicate that at  $10^3$  rad (Si) the offset for swept synthetic crystals will usually be small and positive. As the absorbed dose is increased the offset will decrease sharply with dose. In any case the offset below a dose of  $10^4$  rad (Si) will be less than  $4 \times 10^{-8}$  and in all likelihood will be too small to have much of an impact on the performance of the radar.

The early work on quartz crystals was concentrated on the steady-state changes in the high dose regions ( $\geq 10^4$  rad (Si)). However, there are some

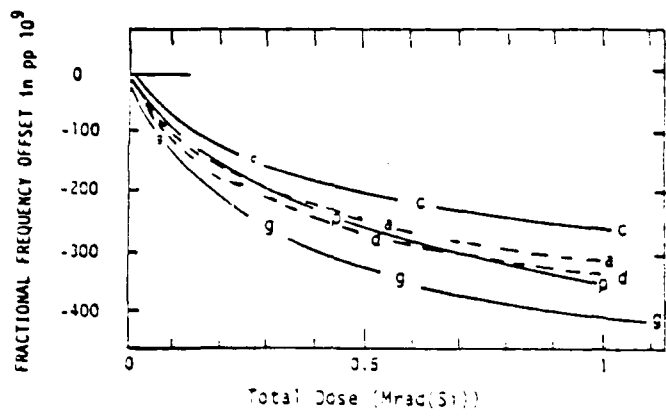


Figure 15. Steady-State Fractional Frequency as a Function of Accumulated Dose on 6 SARP Swept Premium-Q Quartz Resonators

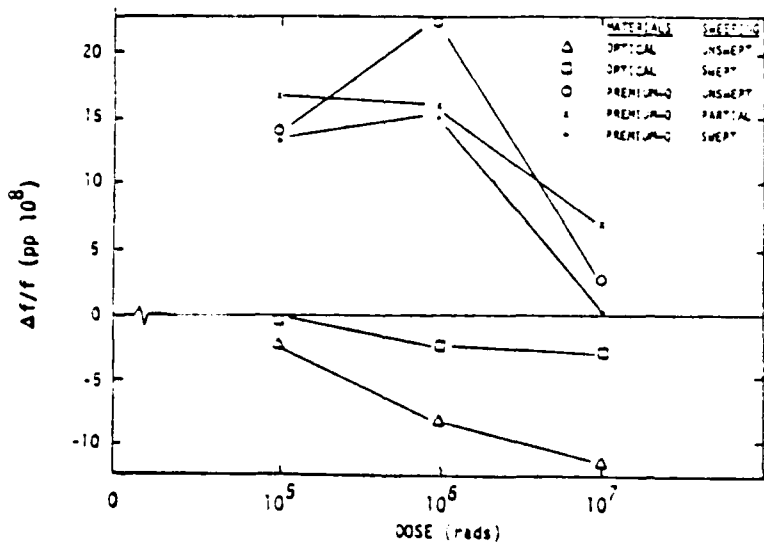


Figure 16. Steady-State Fractional Function as a Function of Accumulated Dose

ambiguities and irreproducible results in the literature.<sup>37,42</sup> Figures 15<sup>37</sup> and 16<sup>48</sup> are among the latest reported data and are indicative of the variation in the literature. For essentially the same type of material, SARP Premium-Q quartz in 5 MHz AT-cut resonators the change in frequency at 1 Mrad (Si) in Figure 15 can be as low as -400 pp  $10^9$  while in Figure 16 it can be as high as +150 pp  $10^9$ . A variety of factors could have caused these discrepancies including the sweeping process, the fabrication process, and the resonant circuit itself. As mentioned previously apparently little effort has been made to standardize the experiments or the manufacturing process so correlating data from different experiments is difficult. Differences such as those between Figure 15 and 16 are the rule rather than the exception.

Another example of some of the latest data is presented in Figure 17<sup>47</sup>. The curve for unswept quartz is really in contradiction to work reported earlier<sup>40</sup>

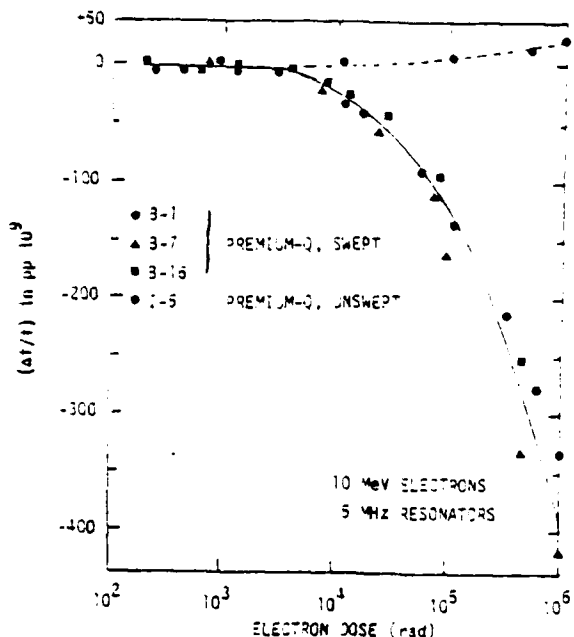


Figure 17. Steady-State Radiation Response of 5 MHz Premium-Q Quartz Crystal Oscillators

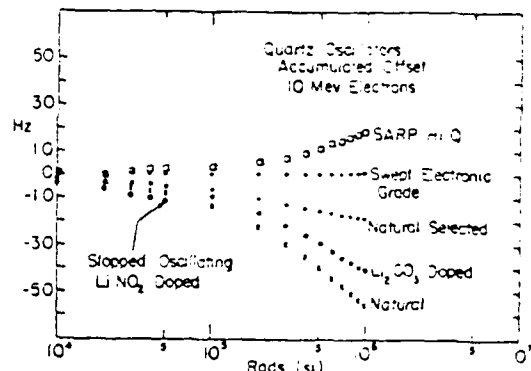


Figure 18. Steady-State Radiation Response of 5 MHz Quartz Oscillators

represented in Figure 18. The consensus in the literature indicates that the relative behavior of swept quartz depicted in Figure 18 is more typical of this type of crystal. Once again the scales are different but to facilitate a comparison between the two figures the following conversion factors can be used: 1 Hz in Figure 18 = 200 pp  $10^9$ ; 10 Hz = 2000 pp  $10^9$ ; and 50 Hz = 10,000 pp  $10^9$ . These conversion factors indicate that data presented in the form of Figure 18 creates the false impression concerning the magnitude of the problem. Figure 19 is a repict of Figure 13 using the  $\Delta f/f \times 10^9$  format. This indicates that unswept

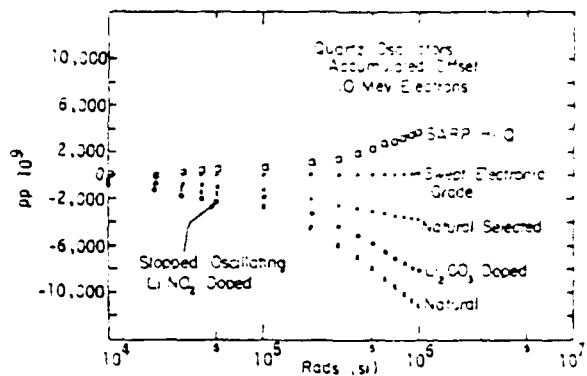


Figure 19. Steady-State Offset Oscillator Frequency as a Function of Dose for 5 MHz Resonators

natural quartz must never be used in a radiation environment since at 1 Mrad (Si) it will experience an offset in excess of 10,000 pp  $10^9$ . This is brought out even clearer in Table 23<sup>46</sup> which lists representative radiation-induced frequency

Table 23  
Representative Radiation-Induced Frequency Offsets

Crystal	Type	Frequency Changes	Ref.
N-1	Natural, 5th overtone, 5 MHz	$1 \times 10^6$ rad(SI) -	740 pp $10^8$ 38
N-2	Natural, 5th overtone, 5 MHz	$1 \times 10^6$ rad(SI) -	780 pp $10^8$ 38
N-3	Natural, 5th overtone, 5 MHz	$5 \times 10^4$ rad(SI) -	60 pp $10^8$ 38
N-4	Natural, fundamental, 5 MHz	$5 \times 10^4$ rad(SI) -	78 pp $10^8$ 38
S-1	Swept synthetic, 5th overtone, 5 MHz	$1 \times 10^6$ rad(SI) +	2.8 pp $10^8$ 38
S-2	Swept synthetic, 5th overtone 5 MHz	$1 \times 10^6$ rad(SI) +	9.4 pp $10^8$ 38
C-1	Unswept synthetic, electronic grade	$3 \times 10^4$ rad(SI) -	20 pp $10^8$ 41
C-6			
A23-8	Unswept synthetic, electronic grade	$1 \times 10^6$ rad(SI) - 3300 pp $10^8$	46



offsets for various levels in the high dose region. As indicated in this table the offset in unswept natural quartz is generally at least an order of magnitude greater than that in swept synthetic quartz.

The variation in the radiation response of natural quartz exhibited in Table 21 is also present in other types of quartz. This is indicated in Figure 20<sup>39</sup> for 5 MHz oscillators made from swept synthetic electronic-grade quartz. These crystals were cut from four different bars (i.e., L-4, L-5, R-3,

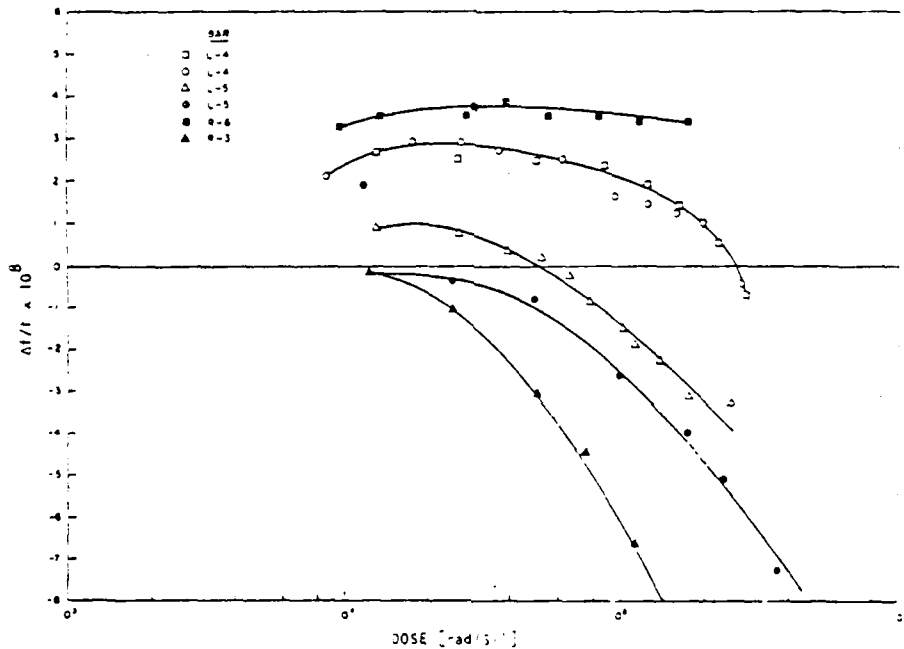


Figure 20. Steady-State Frequency Offsets of 5 MHz Resonators

and R-6). The radiation-induced steady-state offset does vary considerably between different bars and can be either positive or negative.

The same type of behavior is also exhibited by Premium-Q grade quartz as indicated by Figure 21.<sup>49</sup> In this figure the bars A11 and A13 are Premium-Q and E1 is electronic grade quartz. As indicated by this figure both grades of material exhibit the same type of steady-state behavior.



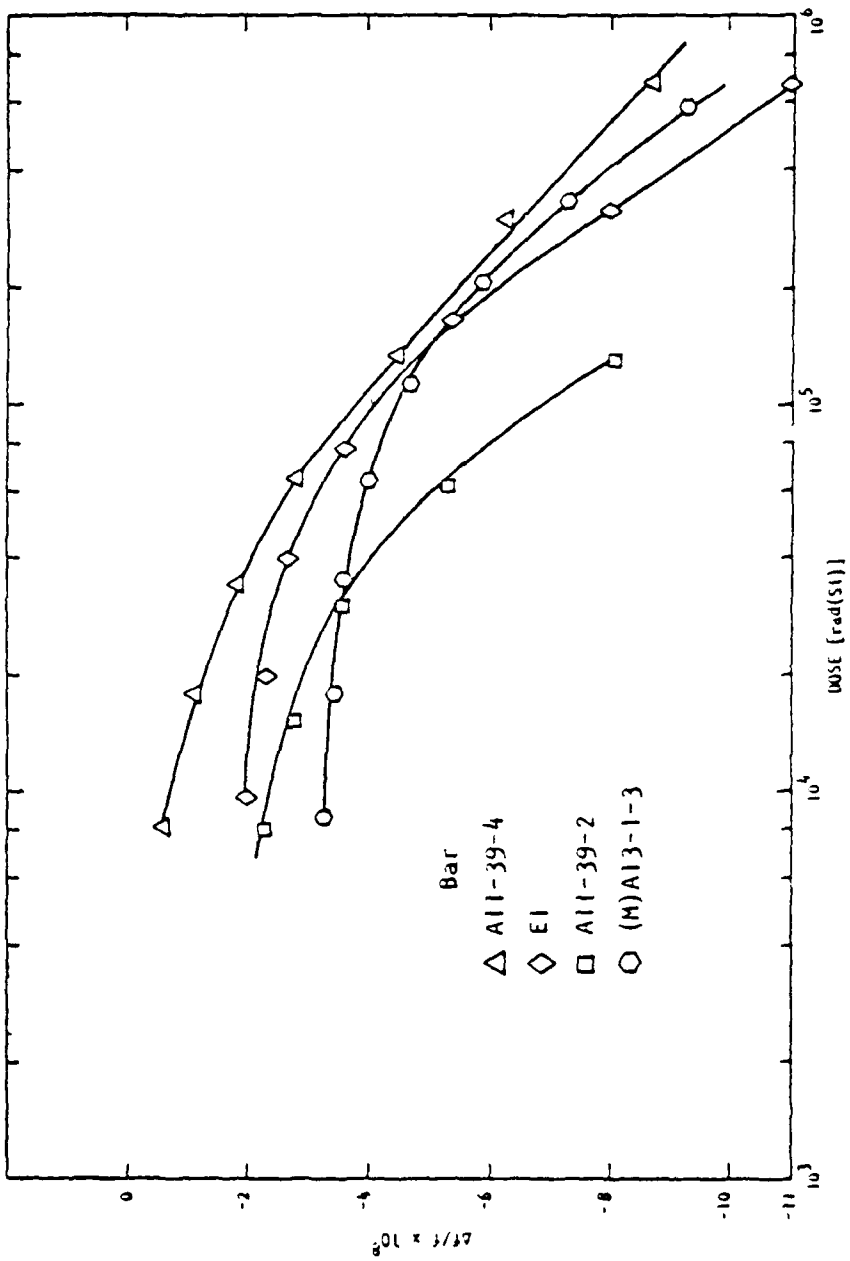


Figure 21. Premium-Q (Al1 and Al3) and electronic-grade (EI)  $\gamma$ -MHz resonators frequency offset versus dose from 37-MeV electrons. Sweeping was performed with platinum electrodes.

There is some indication in Figure 20 that the variation in the offset between crystals cut from the same bar can be quite small. This fact is more clearly illustrated in Figures 22<sup>49</sup> and 23<sup>39</sup>. Figure 22 depicts data on

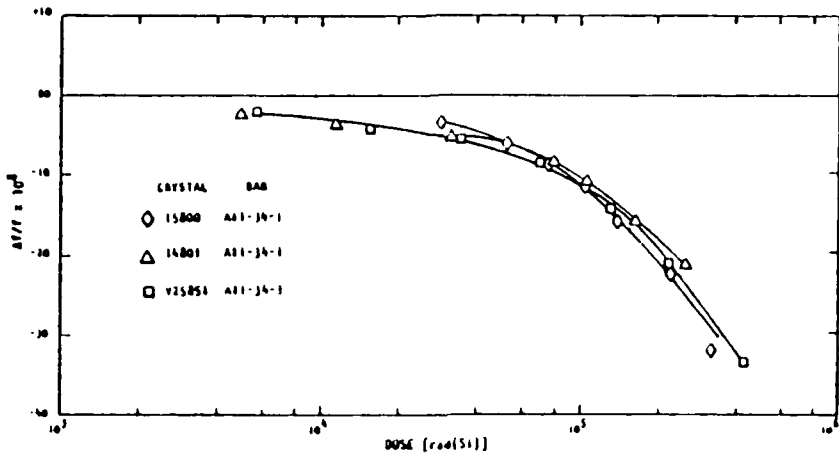


Figure 22. Steady-State Response of Three Crystals  
from the Same Bar of Premium-Q Quartz

three crystals cut from the same bar of Premium-Q quartz while Figure 23 indicates the steady-state response of two sets of three crystals with each set coming

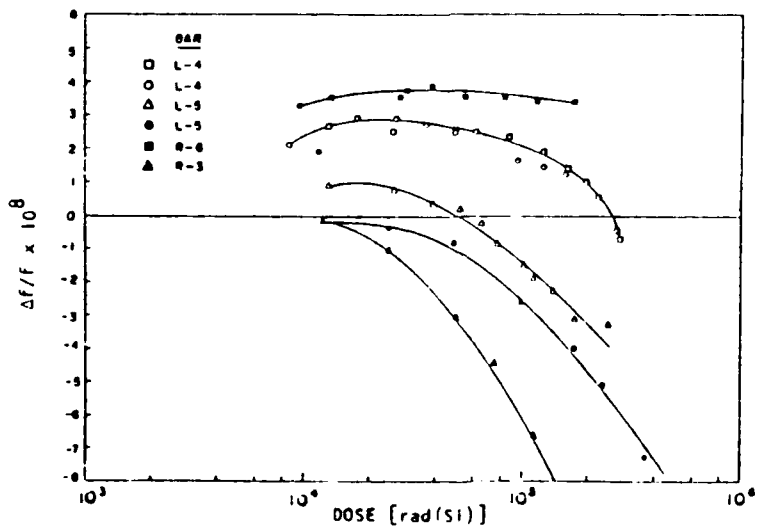


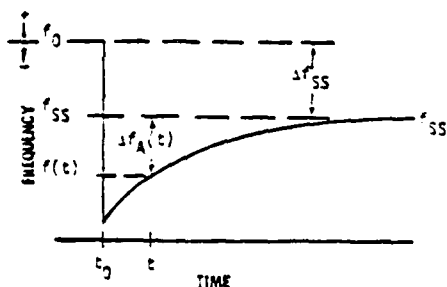
Figure 23. Steady-State Frequency Offset for 5 MHz Resonators  
Fabricated from Electronic-Grade Quartz Crystals  
Cut from the Same Bar



from the same bar of electronic-grade quartz. After  $10^5$  rad (Si) none of the units from the same bar have offsets which differ by more than 1 pp  $10^8$ .<sup>39,49</sup> This would indicate that hardness assurance considerations could be satisfied by testing one crystal from a bar and use these results to characterize all crystals cut from that bar.

However, a note of caution must be raised. It has been reported that one experimenter received two units, supposedly cut from the same bar of swept synthetic quartz which exhibited steady-state offsets larger than in natural quartz.<sup>48</sup> This would suggest improper sweeping which is probably a major source of the ambiguities in the literature. In general, very little information concerning the sweeping process is included in the literature and certainly constitutes one of the difficulties associated with assessing the vulnerability of quartz crystals.

Up to this point the discussion has focussed on the steady-state response of quartz oscillators. However, this is only part of the problem. The transient frequency offset is much more serious because it is an order of magnitude larger than the steady-state offset. The situation that was depicted in Figure 11 has been repeated below to refresh the reader's memory.



$f_0$  = original, preirradiation frequency  
 $f_{ss}$  = steady-state frequency (approximately 15 minutes after exposure)  
 $f(t)$  = instantaneous frequency at any time,  $t$   
 $\Delta f_A$  = annealable portion of the frequency change

Figure 11. Idealized Plot of Frequency versus Time for a Quartz Crystal Oscillator



The transient response consists of a rather sharp negative shift or spike in frequency immediately after exposure. This is depicted in Figure 24<sup>41</sup> for natural (N-4, N-3), unswept synthetic (C-7) and swept synthetic (S-25 and S-26)

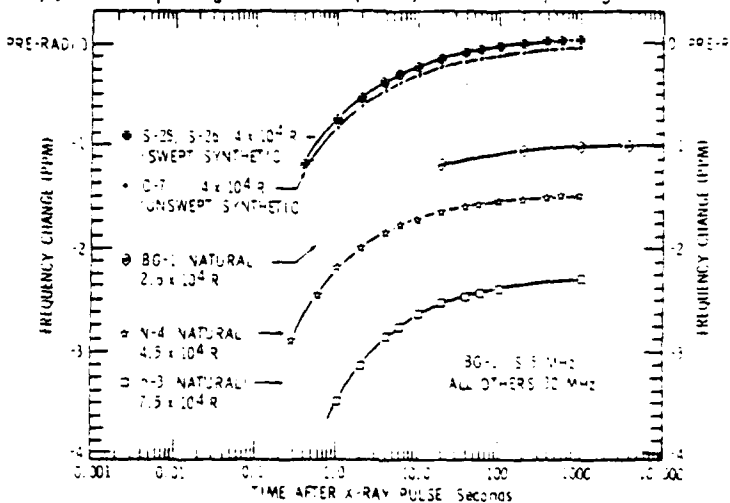


Figure 24. Typical Curves of  $\Delta f$  Versus Time For 32 MHz Resonators Fabricated From Natural, Unswept Synthetic, and Swept Synthetic Quartz

quartz crystals used in 32 MHz resonators. The response of a natural quartz crystal (BG-1) used in a 5 MHz resonator is also shown in this figure. Additional data is shown in Figure 25<sup>44</sup> for 32 MHz natural quartz resonators

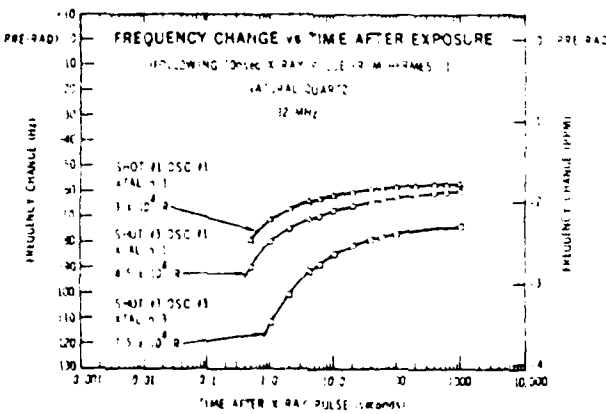


Figure 25. Transient Response of 32 MHz Natural Quartz Resonators at 25°C



at  $15^{\circ}\text{C}$ . The increase in the transient offset for a repeat exposure of crystal n-1 at  $4.5 \times 10^4$  rad(Si) in comparison with the initial exposure of  $4.0 \times 10^4$  rad(Si) should be noted. Essentially the same type of behavior is exhibited by 125 MHz resonators as depicted in Figure 26.<sup>35</sup>

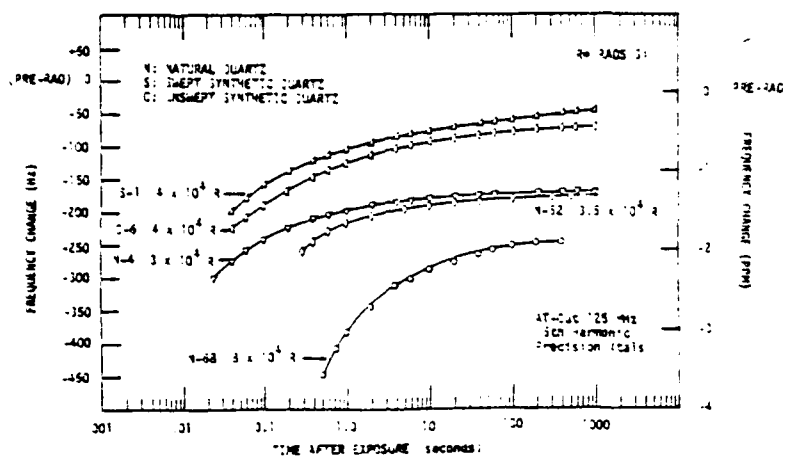
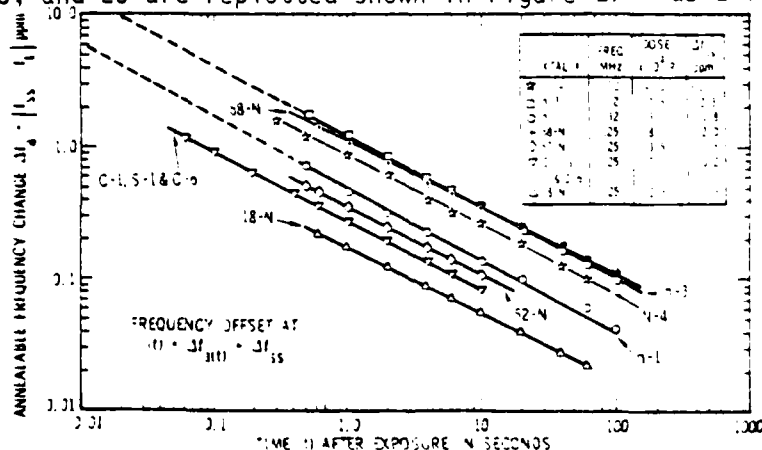


Figure 26. Transient Offset Frequency Versus Time for 125 MHz Natural, Swept Synthetic, and Unswept Synthetic Quartz Resonators

The similarity between the transient response of the resonators shown in Figure 24 and 26 has led some workers<sup>41,46</sup> to conclude that between 1 and 125 MHz the transient frequency offset is, to the first approximation, independent of frequency.

Some remarkable features are revealed when data such as that in Figures 24, 25, and 26 are replotted shown in Figure 27<sup>44</sup> as a function of the



log of the annealable frequency offset versus the log of time after exposure. In this plot the annealable frequency shift  $\Delta f$  is equal to the difference between the steady-state value of frequency,  $f_{ss}$ , and the frequency,  $f_t$ , at time,  $t$ . The data for a particular resonator falls on a straight line and the lines for different types of crystals, with the exception of SP-15, are nearly parallel with a slope of  $-1/2$ . This, of course, implies that the transient frequency offset anneals as a function of  $t^{-1/2}$  and, as shown in Figure 27, this behavior continues over four decades of time. The kinetics of this behavior has been examined in Reference 50 and found to result from a one dimensional diffusion and trapping of  $H^+$  by the  $Al^{+3}$  centers in order to achieve charge compensation.<sup>41</sup>

The SP-15 crystal is a vacuum swept synthetic 32 MHz crystal. Basically this unit was swept in a hydrogen-free atmosphere and is one of the few oscillators reported to have a negligibly small transient frequency offset. It has been postulated that vacuum electrolysis either removes the hydrogen responsible for the frequency offset or stabilizes the hydrogen in OH centers. For the SP-15 unit there was a permanent offset of roughly 1 ppm for a dose of  $3 \times 10^4$  rad(Si).<sup>41</sup> However, it should be pointed out that this data was published in 1973 and the results have not been duplicated in any further work to date. Therefore, the authors view the data on the SP-15 with a great deal of caution.

There is some indication that natural quartz will cease to oscillate for a short period of time (10 to 15 usec) following exposure. This short-duration failure is attributed to prompt photoconductivity due to the diffusion of ions along the optical axis of the crystal. The induced photoconductivity during the radiation pulse effectively shunts the crystal unit with a low value of resistance which stops oscillation. Actually there is a prompt and delayed component of the photoconductivity and as shown in Figure 28 this phenomenon is not confined to natural quartz but also exists for swept and unswept synthetic quartz. Figure 28 depicts the log of the conductivity during and after a  $10^4$  rad(Si) pulse as a function of the log of the time after the pulse. The conductivity of the swept synthetic quartz decays rather rapidly after the radiation pulse and essentially vanishes  $10^{-7}$  sec. after the pulse. In natural



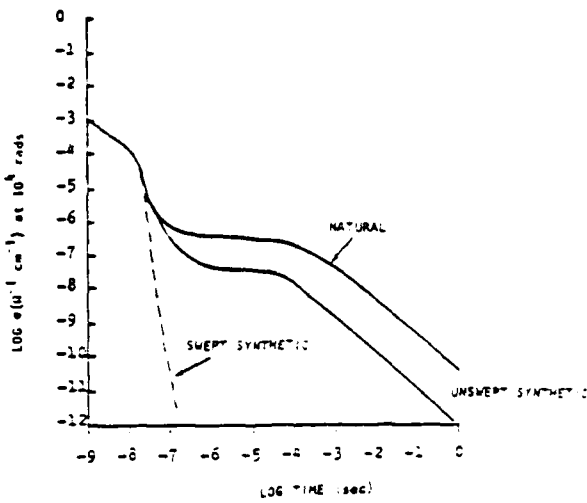


Figure 28. Radiation-Induced Prompt and Delayed Photoconductivity for Natural, Swept, and Unswept Synthetic Quartz

quartz there is a large and persistent increase in the conductivity. It is still measurable at times on the order of tens of seconds after the exposure. The magnitude of the conductivity of unswept synthetic quartz falls in between that of natural and swept synthetic material. It does have a measurable delayed component but is reduced by a factor of about two compared with natural quartz.

The equivalent series resonance resistance,  $R_s$ , (which is proportional to  $Q^{-10}$ ), also changes as a result of pulsed irradiation as indicated in Figure 29.<sup>35</sup> As was the case with the delayed conductivity the change in  $R_s$  depends on

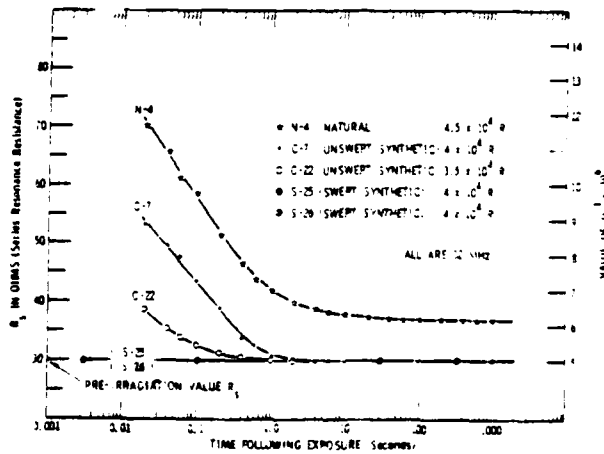


Figure 29. Radiation-Induced Change in the Series Resonance Resistance for 32 MHz Quartz Crystal Oscillators



the kind of quartz from which the oscillator was fabricated. The data in Figure 29 is for 32 MHz quartz resonators. The increase in  $R_s$  is greatest for natural quartz and it decays to a steady-state value that is somewhat larger than its pre-irradiation value. Unswept synthetic quartz also experiences an increase in  $R_s$  but it decays back to its original value. There is essentially no change in  $R_s$  for swept synthetic quartz.

The change in  $R_s$  for a 5 MHz natural quartz oscillator is shown in Figure 30.<sup>41</sup> The unit, after the first exposure of  $1 \times 10^4$  rad(Si) ceased

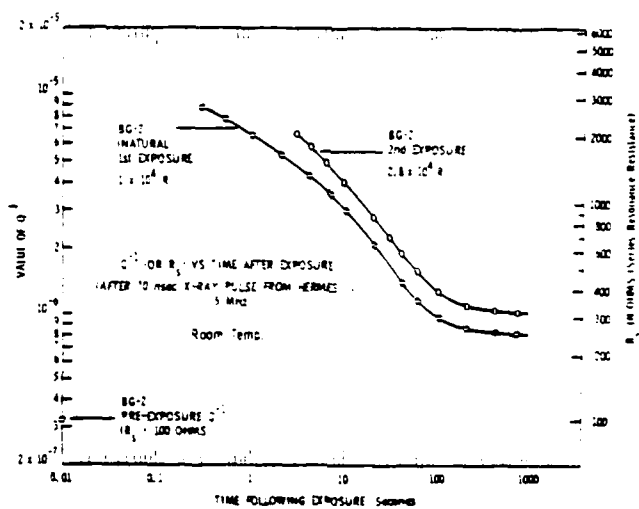


Figure 30. Radiation-Induced Change in the Series Resonance Resistance for a 5 MHz Natural Quartz Oscillator

oscillating for .05 sec. The unit ceased oscillating for 3 sec. after a second exposure of  $2.8 \times 10^4$  rad(Si). The extremely large increase in  $R_s$  in low frequency natural quartz crystals would seem to be the reason that oscillators employing such crystals fail for relatively long periods of time (several seconds).

Figure 29 indicates that .1 sec. after an exposure of  $4.5 \times 10^4$  rad(Si),  $R_s$  for the 32 MHz natural quartz crystal unit, N-4, has increased 100%. Figure 30 indicates that .1 sec. after an exposure of  $1 \times 10^4$  rad(Si)  $R_s$  for the unit BG-2 has increased 3000%. This comparison is made even clearer in Figure 31. This figure directly compares a 32 MHz unit with a 5 MHz unit



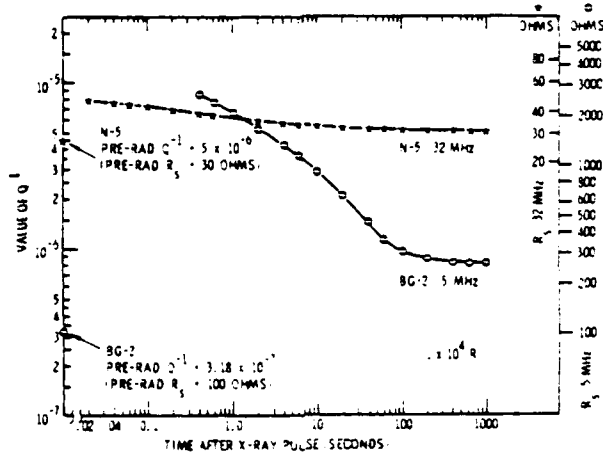


Figure 31. Comparison of the Changes in  $R_s$  in a 32 MHz Natural Quartz Oscillator with that of a 5 MHz Oscillator After an Exposure of  $1 \times 10^4$  rad(Si)

both of which were fabricated from natural quartz and exposed to  $1 \times 10^4$  rad(Si). This figure clearly indicates that the increase in  $R_s$  is inversely proportional to the frequency of the oscillator.

Data such as that in Figures 29, 30, and 31 constitutes another reason why natural quartz should be avoided. In addition to suffering a larger steady-state and permanent frequency offset natural quartz oscillators, also, are more likely to cease oscillating than are synthetic units.

Before leaving the subject of the transient response of quartz oscillators some comments should be made concerning the crystals and the tests themselves. The transient data listed previously was for very short radiation pulse widths ( $\approx 70$  nsec). In addition the data was obtained for resonators that were specially cut so as to have a flat frequency-versus-temperature characteristic.



Thus, temperature effects were unimportant in these tests and the changes do truly represent the response of the quartz crystals.

In order to understand the radiation response of quartz crystals the situation must be examined on a microscopic level. This was briefly discussed previously and that discussion will be summarized here and used as a basis for explaining the radiation response of quartz crystals. In unirradiated crystals, aluminum is located in the quartz lattice as a substitute for silicon. From an ionic viewpoint, aluminum is a +3 entity in a +4 silicon site and there is a general tendency to achieve charge compensation by the location of a +1 ion ( $H^+$ ,  $Li^+$ , and  $Na^+$ ) at a nearby interstitial site.

Irradiation of a quartz crystal generates approximately  $6 \times 10^{12}$  electron-hole pairs/cc per rad in quartz.<sup>51</sup> These electron-hole pairs, of course, undergo recombination processes. In general, holes are trapped at lattice imperfections more quickly than electrons.<sup>52</sup> The  $Al^{3+}$ - $Li^+$  or  $Na^+$  defect constitutes an ideal site for hole capture at one of the nonbonding oxygen orbital positions with a subsequent freeing of  $Li^+$  and  $Na^+$ . The remaining  $Al^{3+}$ -hole compensated center has an unpaired electron located in a nonbonding (unbonded to the aluminum) orbital of an oxygen atom adjacent to the aluminum ion. The hole is trapped on the nearest oxygen neighbor to the aluminum. The trapped hole is not stationary but rather jumbs back and forth between two of the four oxygen atoms. It must be mentioned that silicon in the quartz lattice is surrounded by four oxygens not quite tetrahedrally located, i.e., there are two equivalent pairs with  $SiO$  bonds of length 1.598 and 1.616 $\text{\AA}$  respectively.<sup>43</sup> Thus, there are two nearest oxygen neighbors to the aluminum. Electron spin resonance confirms the fact that the hole hops back and forth between the two nearest oxygen neighbors.<sup>53</sup>

There is agreement in the literature that the formation of the  $Al^{3+}$ -hole compensated centers are a major cause of the  $\Delta f/f$  offset. However, the exact reasons for this impact have not been completely formulated. A generalization is often used to explain the negative frequency offset which is based on the argument that ionization results in the removal of valence



electrons in the crystal. This weakens either the basic tetrahedral structure or the lattice structure in the vicinity of defect centers which reduces the elastic modulus of the crystal. However, it has also been proposed that the  $\Delta f/f$  is due to a change in the elastic modulus brought about by detrapping of positively charged compensating ions at the substitutional  $\text{Al}^{+3}$  sites. This is brought on by the formation of  $\text{Al}^{+3}$ - hole compensated centers. In any case, the formation of  $\text{Al}^{+3}$ - hole centers coupled with the radiation-induced mobility of interstitial ions are major factors in the radiation response of quartz.

A technique has been devised for determining the completeness of the sweeping process for quartz which was grown using  $\text{NaOH}$  or  $\text{Na}_2\text{CO}_3$  as a mineralizer and, hence, the concentration of the  $\text{Al}^{+3}$ - hole centers.<sup>42</sup> Essentially it consists of examining the  $\text{Al}^{+3}$ - hole center electron spin resonance (ESR) spectrum after each step of a sequence of three irradiations: an initial  $77^\circ\text{K}$  irradiation, a room temperature irradiation, and a re-irradiation at  $77^\circ\text{K}$ . The results of such measurements are shown in Figure 32<sup>42</sup> for an unswept Sawyer Premium Q quartz crystal used in a 5 MHz resonator. The intense set of closely-spaced lines centered at  $g_c = 2.0183$  has been determined to be caused by the  $\text{Al}^{+3}$ - hole center with the hole being trapped in a non-bonding orbital of an oxygen

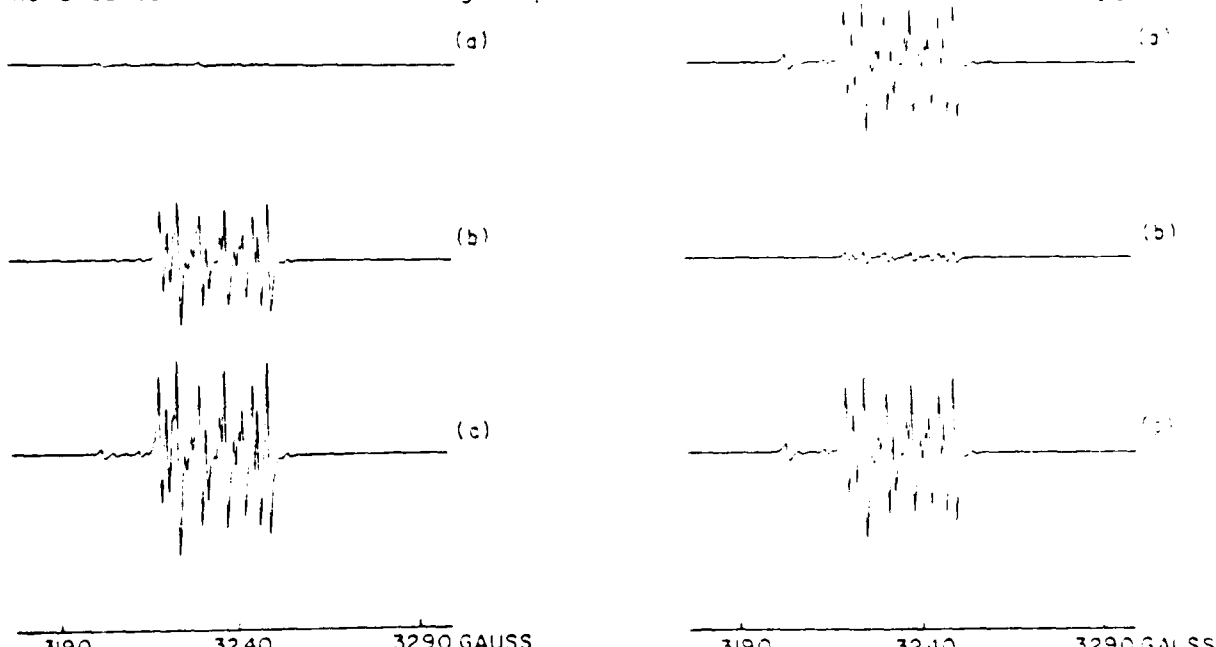


Figure 32.  $\text{Al}^{+3}$ - Hole Center ESR Spectra for Unswept Premium Q Quartz After Irradiation at a)  $77^\circ\text{K}$ , b) Room Temperature and Again at c)  $77^\circ\text{K}$

Figure 33.  $\text{Al}^{+3}$ - Hole Center ESR Spectra for Swept Premium Q Quartz After Irradiation at a)  $77^\circ\text{K}$ , b) Room Temperature, and Again at c)  $77^\circ\text{K}$



which is adjacent to a substitutional aluminum impurity.<sup>54,55</sup> By comparison, Figure 33 shows the results of ESR measurements taken after the same sequence of radiation exposures for a swept Sawyer Premium-Q crystal. It should be mentioned that the samples used for Figures 32 and 33 came from the same bar of quartz which was cut in half; one half was swept and the other half was unswept. The mineralizer was  $\text{Na}_2\text{CO}_3$ . Therefore, the differences in Figures 32 and 33 must be attributed to the sweeping process alone.

In unswept material the initial low temperature irradiation produced very few  $\text{Al}^{+3}$ - hole centers (Figure 32a). In swept material the same irradiation produced a significant number of such centers (Figure 33a). However, the room temperature irradiation of the unswept material created a large number of  $\text{Al}^{+3}$ - hole centers (Figure 32b) while for the swept samples this irradiation produced very few centers. The two samples exhibit essentially the same behavior for the second 77°K irradiation.

Additional samples were also subjected to this same three step irradiation process and the relative concentrations of  $\text{Al}^{+3}$ - hole centers based on the magnitude of their ESR spectrum are shown in Table 24.<sup>42</sup> The SQ samples are from Toyo while the PQ (Premium Quality) and EG (Electronic Grade) samples are

Table 24. Relative Concentration of  $\text{Al}^{+3}$ - Hole Centers As Determined by ESR. One Unit is Approximately  $8 \times 10^{13}$  Unpaired Spins

	PQ-E10 (Un- Swept)	PQ-F12 (Swept)	SQ-A1 (Un- Swept)	SQ-A2 (Swept)	PQ-A20 (Un- Swept)	PQ-D1 (Swept)	EG-C20 (Un- Swept)	EG-F20 (Swept)
Step 1 Initial Irradiation at 77°K	2	142	6	344	0	166	32	224
Step 2 Irradiation at Room Temperature	166	14	250	42	4	12	56	54
Step 3 Re-Irra- diation at 77°K	444	208	312	370	42	160	424	220



from Sawyer. One unit in the table corresponds to  $8 \times 10^{13}$  unpaired spins. The same pattern of behavior as that shown in Figure 32 and 33 is duplicated by all the samples. It is interesting to note that the number of  $\text{Al}^{+3}$ - hole centers generated by the second low temperature irradiation (step 3) indicates that the Sawyer sample PQ-A20 has a significantly lower aluminum content. However, as indicated by step 3, the other Premium-Q and the Supreme-Q samples contain approximately as many aluminum impurity ions as the Electronic-Grade samples.

The initial 77°K irradiation of unswept samples failed to produce many  $\text{Al}^{+3}$ - hole centers because of the presence of the interstitial alkali ion near the aluminum. Essentially, the  $\text{Na}^+$  ions are immobile at this temperature. They are frozen in place and no centers are formed. The onset of radiation-induced mobility of interstitial  $\text{Na}^+$  ions occurs at 200°K.<sup>42</sup> The second irradiation was performed at room temperature which, of course, allowed the  $\text{Na}^+$  ions to become mobile and move away from the aluminum ions. This allows the formation of  $\text{Al}^{+3}$ - hole centers and gives rise to the set of lines in Figure 32b. It should be mentioned that the ESR measurements were made at 77°K. The last irradiation of 77°K does not result in the liberation of any more  $\text{Na}^+$  ions but there is an increase in the intensity of the spectrum. This probably results from any uncompensated  $\text{Al}^{+3}$  ions which remain after the room temperature irradiation that trap the radiation-produced holes. However, it is not a temperature effect since the ESR measurements in step 2 and 3 were all made at 77°K.

The sweeping process for the samples in Figure 33 and Table 24 was done in a partial hydrogen atmosphere so that the interstitial ions were replaced from the aluminum sites by  $\text{H}^+$  ions. ESR results on hydrogen atoms<sup>53</sup> and IR results<sup>57</sup> on  $\text{OH}^-$  molecules both demonstrate that hydrogen is mobile in quartz under irradiation at temperatures below 77°K. Thus the initial 77°K irradiation of the swept sample (Figure 33a) essentially liberated the hydrogen ion from the aluminum site and produced large numbers of  $\text{Al}^{+3}$ - hole centers.

No explanation of the spectrum for swept samples irradiated at room temperature (Figure 33b) is given in the literature. Obviously, competing mechanisms are involved and, by comparison with Figure 33a, more  $\text{Al}^{+3}$ - hole centers are annihilated than are formed. There are several candidates for these competing mechanisms including the thermal release of trapped electrons which



were generated during the initial  $77^0\text{K}$  irradiation. The exact nature of the competing mechanism is not really pertinent to our discussion other than to note the temperature dependence of the mechanism indicated by Figures 33a.), b.), and c.).

The other important fact that is illustrated in Figure 33 is that for a completely swept sample the  $\text{Al}^{+3}$ - hole center ESR spectrum will have the same intensity after the first  $77^0\text{K}$  irradiation as after the second irradiation. For a partially swept sample, the ratio of the intensity of the ESR spectrum of the  $\text{Al}^{+3}$ - hole centers after the initial  $77^0\text{K}$  irradiation to that after the second  $77^0\text{K}$  irradiation is a sensitive indicator of what fraction of the interstitial alkali ions have been replaced by hydrogen ions. For a completely swept sample the ratio should be 1 as in Figure 33.

The basis for the technique, of course, resides with the fact that the alkali and hydrogen interstitial ions have substantially different temperatures for the onset of their radiation-induced mobility. This fact may, also, serve as a basis for developing a radiation tolerant quartz crystal. If as indicated in Figure 32a) at low temperatures essentially no  $\text{Al}^{+3}$ - hole centers are formed in unswept synthetic crystals then the radiation-induced frequency offset for these crystals should be minimal. Unfortunately, as mentioned previously, the Q of unswept quartz crystals is probably too low to allow for their application in precision oscillators. However, it should be noted that operation at low temperatures would, by itself, increase the Q of the crystal. Thus, it may be feasible to fabricate precision oscillators from partially swept synthetic crystals grown using  $\text{Na}_2\text{CO}_3$  as a mineralizer which are radiation resistant provided they are operated below  $200^0\text{K}$ . Obviously the minimal amount of sweeping would have to be determined along with the optimal operating temperature. In addition, the effect of different mineralizers should also be investigated. A larger ion should require a higher temperature for the onset of radiation-induced mobility. In any case, the use of partially swept crystals operated at less than  $200^0\text{K}$  is a possible solution to the radiation-induced frequency offset.

Although not as dramatic as the dose-induced transient response, frequency offsets can also be induced by neutron exposure. As discussed in section 2.0, this results from the displacement of atoms from their regular lattice



sites. There is not an abundance of data on this effect. Some of this data is summarized in Figure 34.<sup>45 57,58</sup> As indicated by this figure the slopes of

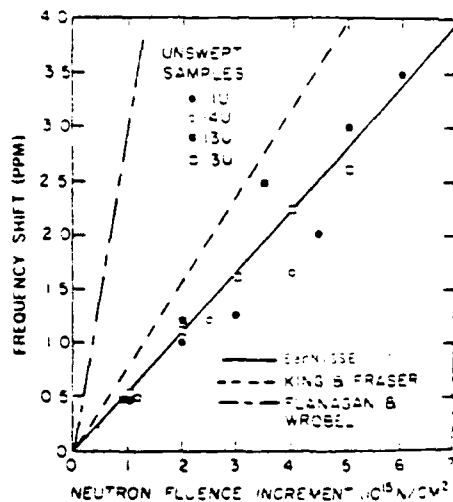


Figure 34. Frequency Shift as a Function of Neutron Fluence ( $>10$  KeV Fission Spectrum)

the curves do vary considerably but the figure does indicate that the frequency shift is a positive linear function of neutron fluence. Curve A was obtained from data on optical-grade unswept material and has a slope of  $0.5 \text{ ppm}/10^{15} \text{ n/cm}^2$  ( $>10$  KeV). Curve B was for data on natural and unswept synthetic quartz and has a slope of  $0.8 \text{ ppm}/10^{15} \text{ n/cm}^2$  ( $>10$  KeV). Curve C was for swept electronic-grade quartz<sup>58</sup> has a slope of  $3 \text{ ppm}/10^{15} \text{ n/cm}^2$ . Reference 58 also indicates that swept Premium-Q and swept electronic-grade quartz have a slope of  $6 \text{ ppm}/10^{15} \text{ n/cm}^2$ . This is disturbing since it gives some indication that better swept, higher quality quartz has a greater sensitivity to neutron exposure. However, it must be noted that the test fluences in Figure 34 are somewhat higher than the anticipated threat.

As alluded to in the preceding paragraph the differences between the curves in Figure 34 could have been caused by differences in the grade and type of

material. However, all neutron sources have gamma irradiation accompanying the neutron exposure and some method of accounting for the gamma-induced frequency shifts is required if the effects of neutrons alone are to be assessed. The difference between the curves may reside simply with the methods that were used to account for the gamma effects. In reference 45, these effects were treated by pre-exposing the crystals to 3 Mrad(Si) of radiation and relying on the saturation effect mentioned in the discussion on the effects of low dose region exposures. Reference 58 accounted for gamma effects by employing the gamma-induced frequency shift from a different resonator but cut from the same bar to correct the total shift resulting from a mixed gamma-neutron exposure. The results of this correction are depicted in Figure 35.<sup>58</sup> The two crystals

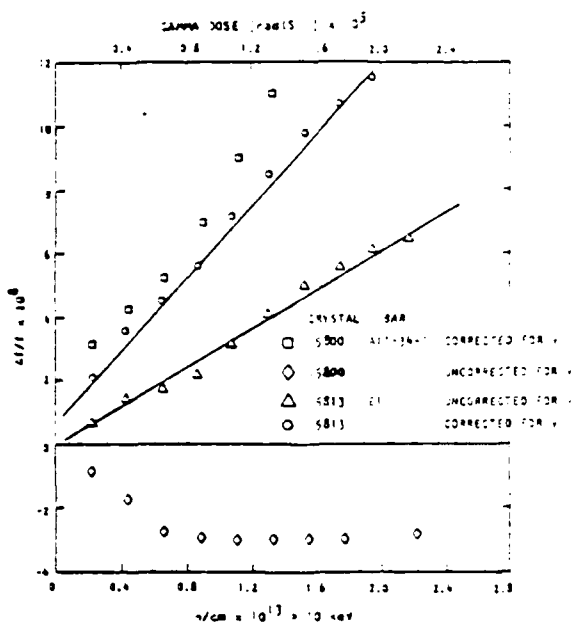


Figure 35. Frequency Offset Versus Neutron Fluence, Showing the Effect of the Correction for Gamma Radiation

depicted in the figure have quite different responses to a mixed gamma-neutron exposure yet after each was corrected for their respective gamma responses they are quite similar with a slope of roughly 7 ppm/ $10^{15} \text{ n}/\text{cm}^2$ . In any case, given the current scarcity of neutron effects data, it is recommended that the more



conservative data of curve C in Figure 34 be used as representative of the neutron response of quartz crystal oscillators. It is, also, recommended that the effects of neutrons and gammas be characterized separately and then be added.

This finishes the discussion of radiation effects on nonsemiconductor devices. As mentioned in the material section (section 3.0) the discussion in this section should be considered as guidelines and it is hoped that these guidelines will aid in the selection of resistors, capacitors, and quartz crystals which can survive the threat.



## 5.0 RADIO FREQUENCY SEMICONDUCTOR DEVICES

Any radar system whether radio frequency (RF), microwave, or millimeter wave will utilize RF devices in some form. They will appear in various applications including regulators and signal processors. In any case, any vulnerability study on state-of-the-art radar systems must include this type of device. In order to present the effort on these devices this section has been divided into two natural parts: 1.) discrete RF devices, and 2.) RF integrated circuits.

### 5.1 Discrete RF Semiconductor Devices

This section of the report will be confined to discrete devices. It is understood that these devices, although not state-of-the-art, will be incorporated in vital subsystems of every system (e.g., in voltage and current regulators associated with power supplies). This is the reason that a discussion of the vulnerability of radio frequency discrete devices will appear in any overview study of the vulnerability of an electronic system.

The two most popular technologies which are used to fabricate semiconductor devices (either discrete or integrated circuits) are bipolar and metal-oxide-semiconductor (MOS). Advanced radar systems will in all likelihood not incorporate to any great extent MOS devices because of its inherent speed and frequency constraints. Therefore, the study focussed almost solely on bipolar technology. The exception to this is gallium arsenide (GaAs). Gigahertz field effect transistors (FETs) are made from this technology and these are included in the section on microwave and millimeter wave devices (section 6.0).

#### 5.1.1 Diodes

The interaction of radiation with material is important only if it affects the performance of devices. In order to understand these effects it is best to start with a discussion of the operation of the simplest of semiconductor devices: namely, diodes. The next logical step is to indicate how radiation influences diode operation. Having this for a base the effort will then proceed to more complicated devices.

A diode, of course, is simply a p-n junction. In a crystal containing a p-n junction in thermal equilibrium the conduction electrons contributed

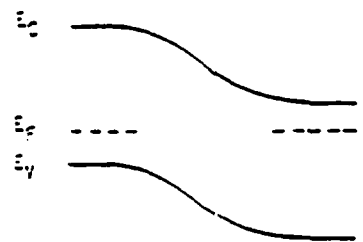


by the donors will be chiefly found in the n-region while, similarly, the holes contributed by the acceptor ions will be found chiefly in the p-region. It is not possible for the electrons and holes to remain entirely separated unless an electric field exists in the junction. Without an electric field the electrons and holes would intermix by diffusion. If it is assumed that, initially, there is no electric field across the junction, holes will diffuse out of the p-type material into the n-type leaving behind in the p-material negatively charged acceptor ions. Electrons will diffuse in the opposite direction leaving behind in the n-material positively charged donor ions. This initial diffusion will establish a dipole layer at the junction with an associated electric field which opposes any further diffusion across the junction. The region is called the space-charge region because the diffusion of carriers leaves behind charged donor and acceptor ions.

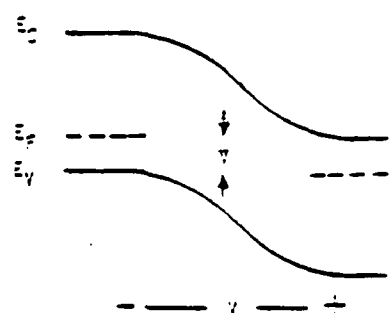
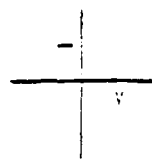
The holes which diffuse into the n-region recombine with free electrons in the space near the junction. Similarly, electrons which diffuse into the p-region recombine with holes near the junction. As a consequence of this action there are very few carriers in a small region on each side of the junction. This region which is the same as the space-charge region is called the carrier-depletion region or the transition region.

Figure 36a illustrates the electron potential energy in the neighborhood of a p-n junction.<sup>1</sup>  $E_c$  is the energy level corresponding to the bottom of the conduction band,  $E_v$  is the energy level corresponding to the top of the valence band, and  $E_f$  is the Fermi energy level. The current is carried by electrons in the conduction band and by holes in the valence band. The flow of current is controlled by the potential hill or barrier. The height of the hill is determined by an equilibrium between two factors: (1) The generation of electron-hole pairs on both sides of the junction by thermal ionization, and (2) the diffusion of carriers across the junction against the barrier by virtue of their thermally-generated kinetic energy.<sup>60</sup> At thermal equilibrium there is no net current flow and the two factors balance one another.

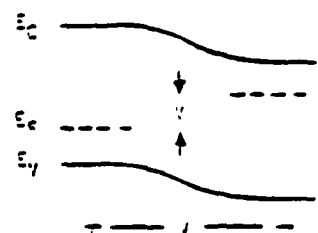
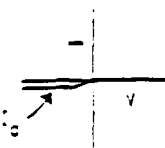
When the diode is reversed biased as in Figure 36b a negative potential is applied to the p-region and the height of the potential hill is increased.



a. No bias



b. Reverse bias



c. Forward bias

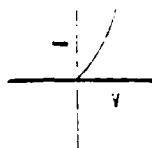


Figure 36. Potential Energy Diagrams and I-V Characteristics for a P-N Junction

51

For a reverse bias of a few tenths of volt or more, the hill is so high that a negligible number of holes have sufficient thermal energy to climb it and the hole current into the n-region essentially vanishes.<sup>61</sup> The hole current from the n-region (minority carriers) is practically the same as it was in the unbiased case. This current depends on the thermal generation of electron-hole pairs in the n-region and is almost unaffected by the applied potential. For this reason the reverse hole current saturates or reaches a limiting value as the reverse voltage increases. Similar comments apply to the electrons. That is, the potential hill which holds the holes in the p-region also holds electrons in the n-region.

When the diode is forward-biased the potential hill is lowered as in Figure 36c. More holes have sufficient energy to climb the barrier into the n-region and, similarly, more electrons will have sufficient energy to flow from the n- to the p-region. The flow of minority carriers (holes from the n-region and electrons from the p-region) is practically unaffected by the application of the forward bias.

Figure 37 is a typical V-I curve for a diode.  $V_B$  in this figure is the breakdown voltage. There are two types of physical phenomena which give rise to this breakdown, the avalanche effect and the Zener effect.<sup>62</sup> Thermally generated carriers from the p- and n-region will collide with atoms of the crystal lattice while crossing the transition region. When the junction voltage is high these carriers may gain enough energy between collisions to knock an

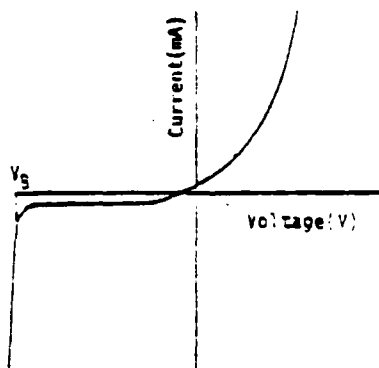


Figure 37. The Volt-Ampere Characteristic of P-N Diode

electron out of a covalent bond. This creates an electron-hole pair. The hole is swept into the p-region and the electron is swept into the n-region. These new carriers can also have ionization collisions creating new electron-hole pairs which in turn can have further ionizing collisions; thus, the process builds up in the manner of an avalanche. Breakdown occurs when the bias voltage is sufficient to maintain an ionization chain.

The breakdown potential is a function of the diode doping concentration. In a highly doped diode, breakdown occurs at a relatively low bias voltage through Zener breakdown. The Zener effect arises when the electric field in the transition region becomes so intense that the electric forces in this region are sufficient to tear electrons out of the covalent bonds, resulting in an electron-hole pair. The hole is swept by the field into the p-region and the electron is swept into the n-region. This movement of carriers, of course, constitutes a current across the junction. When the electric field in the transition region has become strong enough to break one covalent bond it is strong enough to break many. Thus, once the Zener effect has set in, large increases in reverse current through the diode can be accomplished with negligible increase in junction voltage, and, therefore, the voltage across the diode is nearly constant in the breakdown regions. The Zener effect is the breakdown mechanism when the diode is heavily doped and when the breakdown occurs at low voltages. The effect occurs in heavily doped diodes with a reverse bias of 10V or less.<sup>63</sup>

In order to understand the effects of neutrons on diodes it is necessary to express the forward current of a diode in the following form.<sup>2</sup>

$$I_f \approx \left(\frac{u}{\tau}\right)^{\frac{1}{2}} \left[ \exp\left(\frac{q(V_a - V_b)}{kT}\right) - 1 \right]$$

where  $u$  = minority-carrier mobility

$\tau$  = minority-carrier lifetime

$V_a$  = applied voltage

$V_b$  = potential drop across built-in region

Neutron-induced displacements actually produces three major effects in semiconductors: (1) minority-carrier lifetime degradation, (2) majority-



carrier removal, and (3) majority-carrier mobility decrease. The above equation indicates that, in order to maintain a constant current, the applied voltage must decrease if  $\tau$  decreases. To offset the decrease in carrier mobility,  $\mu$ , the applied voltage must increase. Majority carrier removal causes an increase in resistivity which results in an increase in  $V_0$ . Therefore, in order to maintain a constant  $I_F$  the applied voltage must be increased. The change due to minority-carrier lifetime degradation (for a constant forward current the applied voltage must be decreased) dominates at low fluence levels. The changes in mobility and resistivity dominates at high fluence levels. Thus, many diodes exhibit an initial decrease in  $V_F$  up to  $10^{12}$  to  $10^{13} \text{ n/cm}^2$ . At higher fluences,  $V_F$  increases to beyond its initial value. This behavior is depicted in Figure 38.<sup>34</sup>

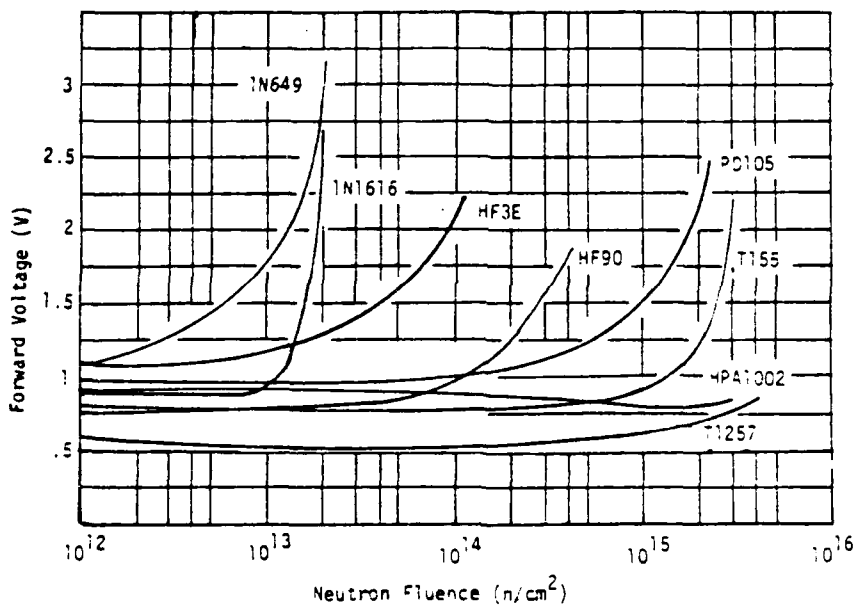


Figure 38. Forward Voltage at Constant Current Versus Neutron Fluence

Table 25 lists typical radiation responses of diodes. The table reflects that the leakage current does increase due to exposure to neutron fluence. This increase is produced by the generation-recombination centers in the junction depletion region. As the number of these centers increase, the leakage current will increase proportionally. In fact, the increase in leakage current along with the increase in forward voltage are the major neutron-induced effects on diodes. However, as indicated by the table the leakage current of modern diodes is extremely small and increases of several orders of magnitude can be tolerated without adversely impacting designs.<sup>65</sup>

Table 25. Neutron Response of Typical Diodes

Class: General Diodes		Leakage Current						Forward Voltage					
Type	Sample Size	Test Conditions VR(V)	Pre-test IR(mA)	IR at $10^{13} \text{ n/cm}^2$	$\frac{\text{Max } \Phi}{\text{Max }} \times 10^{13} \text{ (n/cm}^2)$	IR at $\frac{IR_{\text{max}}}{IR_0}$	IR at $\frac{IR_{\text{max}}}{IR_0}$	Test Conditions IR (mA)	Pre-test VR(V)	VR at $10^{13} \text{ (n/cm}^2)$	$\frac{\text{Max } \Phi}{\text{Max }} \times 10^{13} \text{ (n/cm}^2)$	VR at $\frac{IR_{\text{max}}}{IR_0}$	VR at $\frac{IR_{\text{max}}}{IR_0}$
IN2/0	10	50.0	3.60 ± 3	5.93 ± 3	4.10	13.35 ± 3	3.71	10.0	0.3962	0.3066	4.10	0.3894	1.01
IN4/9	10	100.0	1.97 ± 6	2.64 ± 6	4.40	8.99 ± 6	4.56	3.0	0.6910	0.6913	4.40	0.7410	1.00
Class: Rectifiers													
IN6/5	10	100.0	6.27 ± 7	6.52 ± 6	4.40	2.74 ± 5	4.7	30.0	0.7785	0.7643	4.40	0.9912	1.27
IN11/4A	10	100.0	1.01 ± 5	3.89 ± 5	4.3	1.43 ± 4	14.2	100.0	1.95	0.9638	4.10	6.96	
IN17/4	10	100.0	7.60 ± 3	7.56 ± 3	4.3	8.34 ± 3	1.10	100.0	0.7758	0.3658	4.30	1.52	1.96
IN45/25	8	30.0	3.43 ± 3	3.35 ± 4	4.7	1.17 ± 3	2.93*	200.0	0.8441	1.05	4.70	1.82	2.16
IN64/21*	20	50.0	6.61 ± 8	--	19.0	2.29 ± 7	2.66	10.0	0.5428	--	19.0	0.6280	1.16
IN110	10	75.0	6.03 ± 5	--	14.0	1.24 ± 4	2.06	50.0	0.7054	--	14.0	0.7054	1.11*
IN205	10	20.0	8.36 ± 6	--	13.0	3.01 ± 5	1.60	1.00	0.6110	--	13.0	0.5124	1.19**
Class: Switching Diodes													
IN6/3	10	30.0	6.76 ± 7	1.21 ± 6	4.5	2.43 ± 6	3.60	3.00	0.6743	0.6663	4.5	0.6591	1.02**
IN9/4B	10	20.0	8.90 ± 6	4.94 ± 6	69.0	1.23 ± 5	1.38	0.0100	0.169	--	69.0	0.3437	1.10**
IN30/2	10	20.0	4.94 ± 6	--	69.0	7.05 ± 6	1.43	0.0100	0.140	--	69.0	0.4222	1.02
IN16/3	3	600.0	0.170	--	0.2	0.2017	1.68	10.0	0.6743	--	0.2	0.6432	1.05**
IN18/4	10	10.0	8.67 ± 4	--	170.0	7.92 ± 3	9.14	180.0	0.6938	--	170.0	2.07	3.36
IN18/9	10	10.0	5.75 ± 5	--	160.0	2.05 ± 3	1.65	100.0	0.6713	--	160.0	2.16	3.74
IN19/1	4	10.0	1.68 ± 3	3.95 ± 3	4.5	1.54 ± 2	9.17	100.0	0.7097	0.7464	4.5	1.08	1.57
IN4/4H	10	75.0	1.05 ± 4	--	13.0	4.46 ± 4	2.41	400.0	1.22	--	13.0	1.23	1.01
IN4/4H	12	200.0	1.96 ± 8	5.68 ± 8	12.0	4.08 ± 7	20.37	22.00	1.72	0.9547	1.06	2.89	5.03
IN50/6/2*	20	50.0	1.48 ± 8	--	19.0	1.99 ± 8	1.35	200.0	0.9295	--	12.0	2.26	3.64
IN61/4	4	55.0	2.51 ± 8	--	21.0	3.30 ± 8	1.32	1.0	0.6617	--	19.0	0.9263	1.00**
UK25	5	500.0	2.11 ± 5	--	14.0	1.49 ± 4	7.06	50.0	4.09	--	21.0	0.5728	1.02
IN276/3	5	5.00	3.89 ± 5	4.52 ± 5	11.0	5.28 ± 5	1.36	0.500	0.5526	0.5535	11.0	0.449	1.01

\* These devices have been manufactured for particular defense systems and the identification of the nuclear vulnerability data with the system may by classified information. For these devices, the number of similar commercial device is given wherever possible. It must be remembered that defense system parts are manufactured under stringent quality assurance and control conditions, and commercial devices, listed as equivalent types, may not perform as the data indicates.

\*\* This value is measured value

† The following breakdown voltage data on these device types was also available:

		Reference Voltage*					
Type	Test Conditions IR(mA)	Pre-test BV <sub>0</sub> (V)	BV at $10^3 \text{ n/cm}^2$	Max $\Phi \times 10^3 \text{ n/cm}^2$	BV at $IR_{\text{max}}$	BV <sub>0</sub>	BV at $IR_{\text{max}}$
IN4/4B	.100	1.16	0	1.16	1.16	0	1.16
IN9/42	.001	6.74	0	6.74	7.3	0	6.74
IN4/4H	.005	106	0	106	19.0	0	106
IN6/3	.005	9.1	/	/	11.0	/	9.1

AD-A102 747

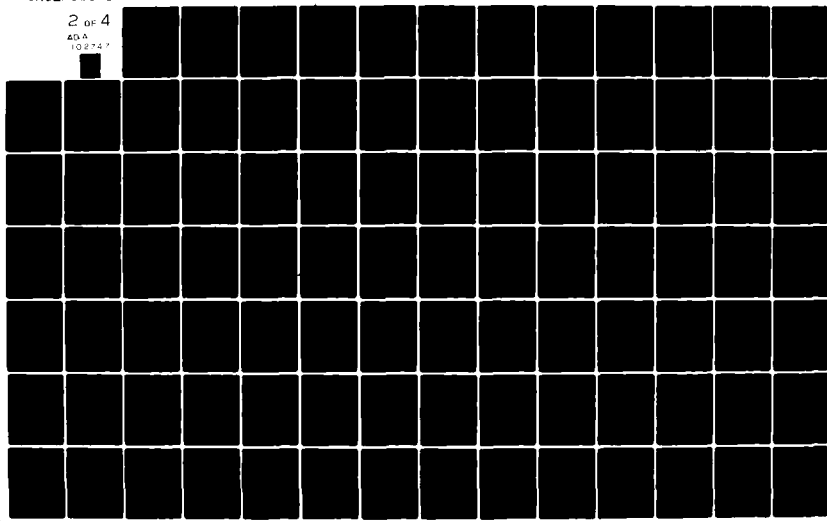
SCIENCE APPLICATIONS INC HUNTSVILLE AL  
NUCLEAR ANALYSIS AND TECHNOLOGY ASSESSMENT OF RADAR CONCEPTS. V--ETC(U)  
MAY 81 J P SWIRCZYNSKI, C S CHEEK  
DASG60-78-C-0029

NL

UNCLASSIFIED

SAI-82-604-HU

2 OF 4  
40A  
102747



The characteristics of reversed biased diodes are also impacted by neutron irradiation. Figure 39 is typical of the impact of neutron fluence on the V-I curve for diodes.<sup>2</sup> The magnitude of the breakdown voltage can show a small increase due to the increase in resistivity. However, it can also show a decrease as indicated in the supplement to Table 25.<sup>64</sup> For the diodes in both Figure 39 and the supplement to Table 25 avalanche is the breakdown mechanism. In general, the change in breakdown voltage is not large and can usually be tolerated. Although it is not clearly evident from Table 25 diodes which are used in rectifiers are expected to be less tolerant than those which are used as fast switching diodes. There are, obviously, many diode types on the market, and it is highly probable that diodes which have fast recovery times, low power, and small junction volume will survive  $10^{16} \text{n/cm}^2$ .

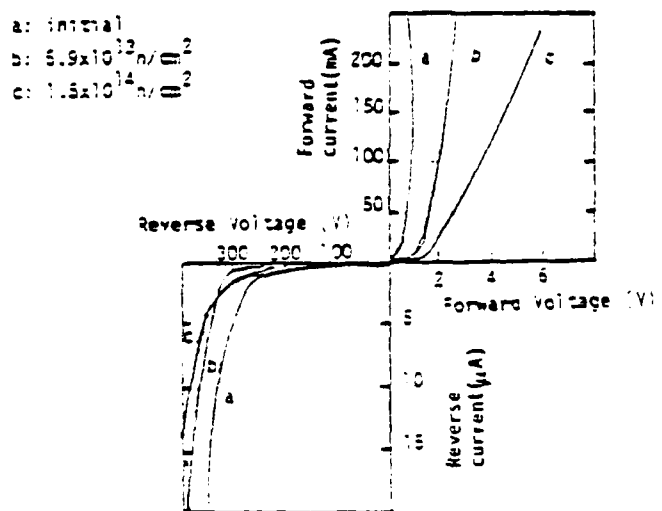


Figure 39. Effects of Neutron Fluence on Si Diodes

Precision Zener diodes, however, may exhibit a change of several millivolts in their reference voltage,  $V_z$ . The onset of the change occurs at  $10^{12} \text{n/cm}^2$  as indicated in Figure 40.<sup>1</sup>  $V_z$ , the breakdown voltage, usually decreases

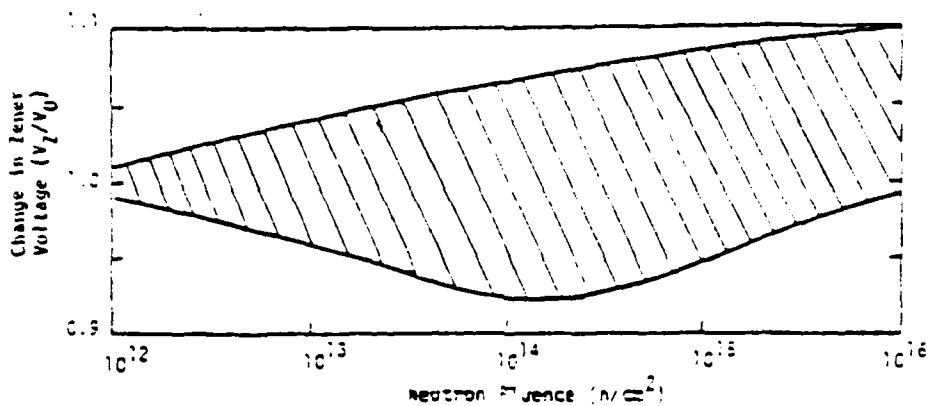


Figure 40. Change in Zener Voltage as a Function of Neutron Fluence

but occasionally can increase with neutron fluence. The Zener effect is the result of band-to-band tunneling. Exposure to neutron irradiation results in increased secondary tunneling due to neutron-induced defect states which cause a decrease in the breakdown voltage. However, as indicated in Figure 40 this is not always the case and, in fact usually, as indicated in Table 26, the breakdown voltage does not change.

Low-voltage, heavily doped Zener diodes are among the most radiation-resistant semiconductor devices. However, when they are used as voltage reference elements, they show an unusually large excursion due to temperature effects and temperature compensation must be employed. It must be mentioned that it has been reported that hardened types of temperature-compensated reference diodes exist which are unaffected by neutron fluences of  $10^{14}$  n/cm<sup>2</sup> or greater.<sup>65</sup> However, it has been reported that commercial devices of this type could be relatively soft and exhibit significant changes at fluences as low as  $5 \times 10^{10}$  n/cm<sup>2</sup> at 25°C.<sup>66</sup> Forward-biased reference diodes can be hardened by decreasing the lifetime by gold doping. Figure 41<sup>2</sup> indicates the effect of such a technique on the forward voltage. The reverse diodes may be hardened by increasing the initial dopant concentration.

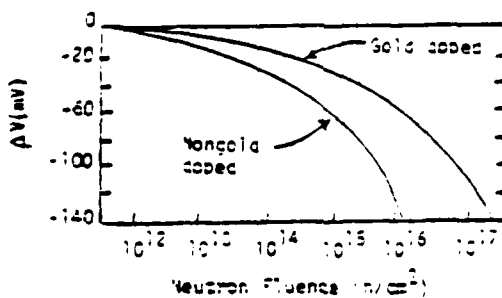


Figure 41. Change in Forward Voltage as a Function of Neutron Fluence for Reference Diodes

Table 26. Response of Reference Diodes to Neutron Irradiation

Type	Sample Size	Test Conditions		Reference Voltage				
		IR(mA)	Pre-Test BV(V)	BV at $10^{17} \text{n/cm}^2$	$\text{BV}_{\infty}/\text{BV}_0$	$\text{Max } \phi \times 10^{17} \text{n/cm}^2$	BV at $\phi_{\max}$	$\text{BV}_{\max}/\text{BV}_0$
IN758	8	3.0	9.96	9.96	1.00	4.6	9.96	1.00
IN9378	10	0.1	8.51	8.44	.992	5.5	8.38	.985
		10.0	9.10	9.27	1.02	5.5	9.94	1.09
IN963	8	10.0	11.5	11.5	1.00	4.1	11.5	1.00
IN2976	8	3.0	11.1	11.1	1.00	4.6	11.1	1.00
IN4461*	>20	100.0	7.07	7.07	1.00	6.5	7.08	1.00
IN4464	5	5.0	8.86	-	-	15.0	8.86	1.00
IN4467*	>20	1.0	11.7	11.7	1.00	8.7	11.7	1.00
IN4469	5	5.0	15.3	-	-	15.0	15.3	1.00
IN4470	5	5.00	15.9	-	-	15.0	15.9	1.00
IN4471	5	5.00	17.3	-	-	15.0	17.4	1.01
IN4474	5	5.00	23.2	-	-	15.0	23.2	1.00
IN4734	10	100.0	5.91	-	-	12.0	5.92	1.00
IN4748	10	10.0	22.6	-	-	12.0	22.7	1.00
IN4752	10	10.0	32.3	-	-	12.0	32.3	1.00
DZ2372*	>20	100.0	22.3	-	-	19.0	22.4	1.00
DZ3495*	>20	4.5	22.2	-	-	22.0	22.1	.996
DZ3554*	12	0.1	6.78	6.75	-	13.0	6.78	1.00
DZ4200*	>20	29	41.3	-	-	19.0	41.5	1.01
DZ4775*	>20	7.5	6.34	-	-	19.0	6.26	.987
DZ5409*	>20	650	8.73	-	-	20.0	8.75	1.00
DZ5690*	>20	20	3.33	-	-	19.0	3.32	.997
DZ5983*	>20	10	9.95	-	-	18.0	9.86	.991
DZ7425*	>20	10	4.70	-	-	21.0	4.68	.996
DZ9985*	>20	4.5	52.7	-	-	19.0	54.0	1.02
DZ9197*	>20	0.01	10.0	-	-	19.0	9.98	.998

\* These devices have been manufactured for particular defense systems and the identification of the nuclear vulnerability data with the system may be classified information. For these devices, the type number of a similar commercial device is given whenever possible. It must be remembered that defense system parts are manufactured under stringent quality assurance and control conditions, and commercial devices listed as equivalent types may not perform as the data indicates.

BV = Breakdown Voltage

$\text{BV}_{\infty}$  = Breakdown Voltage after exposure to  $10^{17} \text{n/cm}^2$

Max  $\phi$  = Maximum Fluence level used during the test

$\text{BV}_{\max}$  = Breakdown Voltage after an exposure to  $\phi_{\max}$



The levels of radiation tolerance exhibited by tunnel diodes generally exceed those for other semiconductor devices. The predominant effect of neutron damage to tunnel diodes is degradation of the negative resistance region of the current-voltage characteristics and the increase in the excess current over a range of forward-bias values. Both of these effects translate into a decrease in the ratio of the peak current to the valley current. Figure 42 illustrates the typical response of silicon tunnel diodes to neutron irradiation.<sup>68</sup> As indicated by this figure the peak current is relatively insensitive to neutron irradiation but the valley current steadily increases with fluence. Tunnel diodes which have higher peak-current values are more resistant to neutron irradiation. GaAs devices are harder than Si devices. GaAs diodes of 10 and 5mA do not degrade for exposures of  $1.5 \times 10^{15} n/cm^2$ . By comparison, the  $I_v$  at 0.45 V for Si tunnel diodes increased 75% at this fluence level.

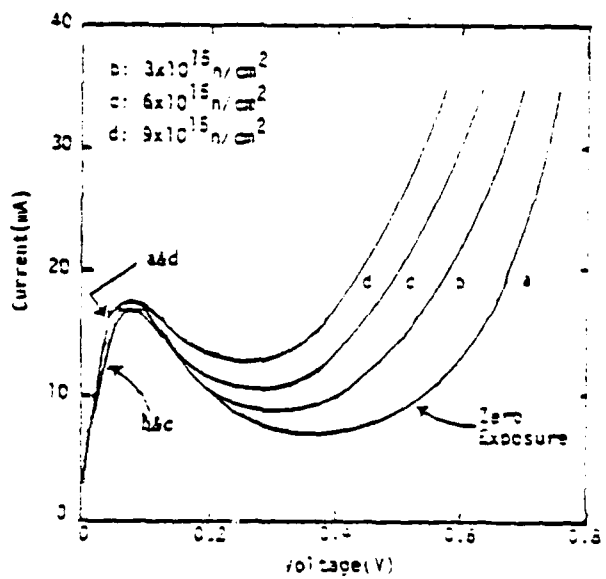


Figure 42. Effects of Neutron Fluence on Silicon Tunnel Diodes

In addition, GaAs diodes have certain advantages in a benign environment over Si or Ge diodes for switching-circuit design. Their peak-to-valley ratios for given peak currents and their switching voltages are higher than for Si or Ge diodes, which are generally desirable for high-speed low-power logic arrays. It is, therefore recommended that GaAs tunnel diodes be used instead of Si or Ge diodes and diode types be chosen which have the highest possible peak-current values. Radiation data on GaAs and Si tunnel diodes can be found in references 68 - 71.

This essentially ends the discussion of the effects of neutron irradiation on diodes. It is recommended that diodes be used which have fast recovery times, low power, and small junction volumes. Hardened versions of temperature-compensated reference diodes should be used. These will be gold-doped or use heavy doping. As indicated in the previous paragraphs, tunnel diodes usually present little problem with respect to neutron irradiation. However, it is recommended that GaAs tunnel diodes be used whenever possible and those types be chosen which have the highest possible peak-current values.

Ionization can also impact the performance of diodes. Radiation-induced ionization effects in semiconductor devices are produced by the generation of electron-hole pairs. In a silicon crystal the four valence electrons are shared in covalent bonds with four other silicon atoms. In a perfect crystal an electron cannot have an energy in the forbidden gap between the valence and conduction band. The magnitude of this gap in silicon is 1.11 eV. The majority of electrons forming the covalent bonds have energies in the valence band. However, it is possible for an electron to receive enough energy from thermal agitation or radiation to break the bond and become a free electron in the conduction band. This ejection of the electron creates a positive charge at the bond called a hole. The original ejection of an electron created two charge carriers: a hole and an electron. The process is called hole-electron pair generation. The opposite process consists of an electron returning from the conduction band to a covalent bond from which an electron is missing and is called recombination.

Typical crystals have imperfections which create energy states within the energy gap. These imperfections called defects can be crystal dislocations, vacancies (empty lattice sites), impurity atoms with available energy states in the energy gap, and displacement damage due to radiation. Figure 43 indicates the situation in which all the defects have an energy state,  $E_g$ , in the forbidden gap. An electron can make the transition from the conduction band

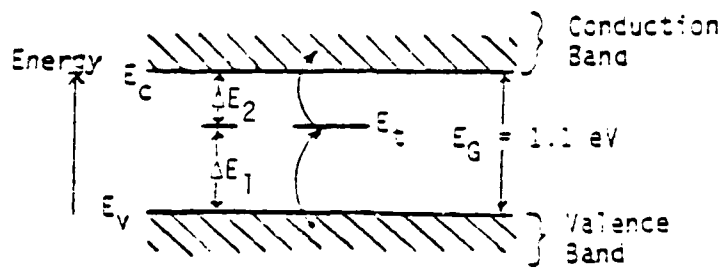


Figure 43. Carrier Generation through a Defect

to the valence band in two steps. The electron first receives energy,  $\Delta E_1$ , to carry it to the energy state,  $E_d$ , and later a second increment of energy,  $\Delta E_2$ , raises it to the valence band. The probability of the two step transition is much higher than for a one-step process. In fact, the rate of generation of electron-hole pairs is proportional to the number of defects in the crystal.

Similar to electron-hole pair generation the rate of recombination is determined by the number of defects that are available for the two step transition from the conduction band to the valence band. The situation is the same as that pictured in Figure 43 but with the arrowheads reversed on the transition changes since recombination involves an electron going from the conduction band back to the valence band. Since crystal defects determine the recombination characteristics of the crystal, they are called recombination centers. The mean time an electron spends in the conduction band or a hole spends in the valence band before recombination is called the minority carrier lifetime,  $\tau$ .

The generation rate of electron-hole pairs can be determined from:

$$g \approx \frac{\dot{y} s}{E} \frac{(100 \text{ ergs/gm-rad})}{(1.6 \times 10^{-12} \text{ ergs/eV})}$$

where  $\dot{y}$  = the absorbed dose rate in rads (material)/sec

$s$  = the mass density in gm/cm<sup>3</sup> of the material

$E$  = the average amount of energy required to form an electron-hole pair

For silicon with a bandgap of 1.1 eV, E must be approximately 3.6 eV. Using 2.33 gm/cm<sup>3</sup> for the density of silicon the above equation indicates that 1 rad/sec generates  $4 \times 10^{13}$  carriers/cm<sup>3</sup>-sec in Si.

The behavior of a semiconductor device, when exposed to ionizing radiation, depends on the number and rate of electron-hole pairs in the semiconductor and not on the type of radiation. When a p-n junction is exposed to a pulse of ionizing radiation a photocurrent will be produced due to the interaction between the junction and the electron-hole pairs produced by the radiation. This current is called the primary photocurrent. It is made up of a drift and a diffusion component.

The drift component results from carriers generated in the depletion volume or space-charge region of the junction. Carriers produced in this region are swept out by the field and cause a current in the external circuit. The diffusion component consists of minority carriers generated in the quasineutral region near the junction that can reach the depletion region before recombining. The average distance minority carriers travel before recombining is called the diffusion length. The diffusion component of the photocurrent consists of minority carriers produced within one diffusion length of the edge of the depletion region.<sup>72</sup> This component will be delayed when compared to the drift component due to the finite time required for the minority carriers to reach the depletion region.

The photocurrent is a function of the diode geometry and, in particular, the effective volume from which excess carriers can diffuse to the junction before recombining. There are several equations which attempt to describe the generation of photocurrents. For a rectangular radiation pulse the photocurrent can be expressed by:<sup>73</sup>

$$I_{pp}(t) = ? q g A \left\{ \left[ (W + L) \operatorname{erf} \left( \frac{t}{\tau} \right)^{\frac{1}{2}} \right] u(t) - \left[ (W+L) \operatorname{erf} \left( \frac{t-t_p}{\tau} \right)^{\frac{1}{2}} \right] u(t-t_p) \right\} \quad (1)$$

where

$I_{pp}$  = the diode photocurrent

W = effective width of the depletion region

L = diffusion length

A = junction area

q = charge of an electron

g = the generation rate of electron-hole pairs/cm<sup>3</sup>/sec in silicon

$\tau$  = minority carrier lifetime



$t_p$  = radiation pulse width  
 $\dot{\gamma}$  = dose rate in rads (Si)/sec  
 $t$  = time after the initiation of pulse  
 $u(t)$  = unit step function at  $t=0$   
 $u(t-t_p)$  = unit step function at  $t=t_p$   
 $\text{erf}$  = error function

The first group of terms in this equation expresses the buildup of  $I_{pp}$  when the pulse is applied and the second group described what occurs after the pulse ends. The typical waveform for  $I_{pp}$  resulting from such a square ionization pulse is shown in Figure 44. This figure indicated an exponential buildup in the current which peaks at the end of the pulse at time  $t_p$ . After the pulse ends the current decays exponentially.

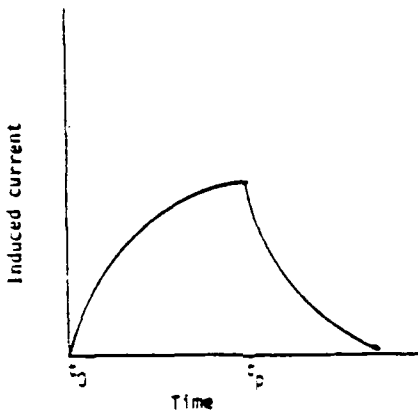


Figure 44. Typical Shape of Primary Photocurrent Induced by a Square Ionization Pulse of Width of  $t_p - t$

For nonrectangular radiation pulses, the photocurrent can be predicted more accurately if a convolution integral is used to relate the time dependent rate of radiation exposure to the photocurrent production as in the following:

$$I_{pp} = C \dot{\gamma}_p \left[ W \left( \frac{\dot{\gamma}(t)}{\dot{\gamma}_p} \right) + \left( \frac{1}{\dot{\gamma}_p \sqrt{\pi}} \right) \int_0^t \exp \left( \frac{-\lambda}{\tau} \right) \lambda^{-\frac{1}{2}} \dot{\gamma}(t-\lambda) d\lambda \right]$$

where  $C$  = an empirically determined scaling factor reflecting material and geometric constants

$\dot{\gamma}_p$  = peak value of the radiation pulse

$\lambda$  = dummy variable for integration

and all other variables have the same meaning as in equation 1.



A note of caution must be raised concerning the use of these equations. For dose rates greater than  $1 \times 10^9$  rad(Si)/sec, the amplitudes of the photocurrents do not necessarily scale linearly with increasing dose rates. Therefore, experimental data are usually necessary to accurately model photoresponse in this dose rate region. Also, the diffusion component of photocurrent is highly dependent on minority carrier lifetime. In addition, neither of the equations apply to a diode operating in avalanche breakdown since in this mode the diode has properties similar to a voltage source rather than a current source.<sup>74</sup>

Both of these equations indicate that the photocurrent of a heavily doped diode is less than that of a lightly doped diode since the depletion width ( $w$ ) decreases with an increase in doping density. This is true for forward biases and for reverse biases less than approximately one half of the breakdown voltage. Under bias conditions near but below breakdown, the transient response of the diode increases with bias voltage due to the avalanche multiplication of the photocurrent which has been created by ionizing radiation. Figure 45 shows the maximum transient photocurrent of a silicon diode with a 26 V breakdown plotted as function of reverse bias for various dose rates.<sup>75</sup>

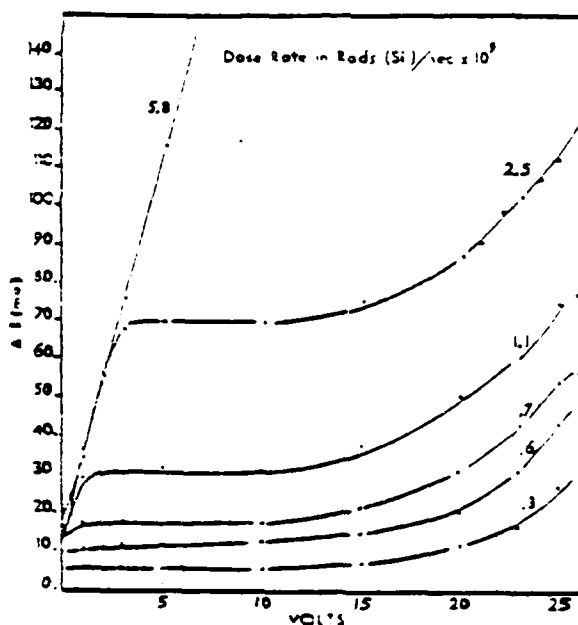


Figure 45. Diode Photocurrent versus Reverse Voltage for Various Radiation Dose Rates

The important feature of Figure 45 is the increase in photocurrent with bias voltage after the reverse bias has exceeded 13 V which is one half the avalanche breakdown voltage for this diode. The impact of this effect is, perhaps, better illustrated in Figure 46. This is a plot of the transient photocurrent as a function of

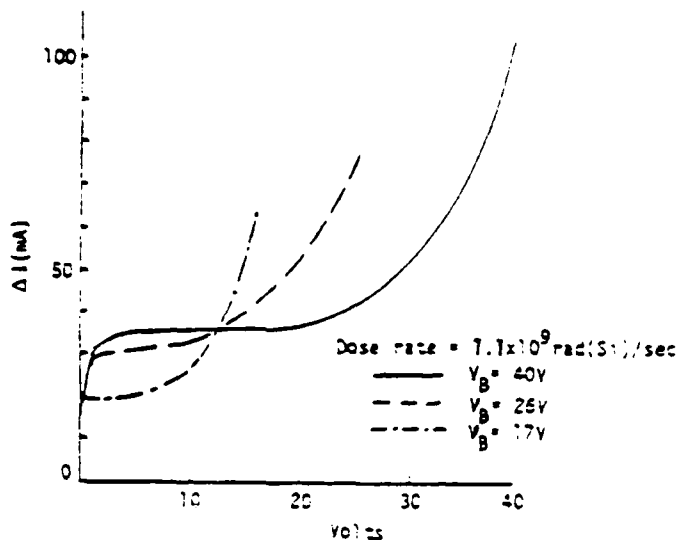


Figure 46 Diode Photocurrent versus Reverse Bias  
for Three Values of Breakdown Voltage

voltage for diodes with different breakdown voltages after being exposed to a dose rate of  $1.1 \times 10^9$  rads(Si)/sec. Theoretically, diodes with lower breakdown (corresponding to heavier doping) should exhibit smaller photocurrents due to both the smaller depletion width ( $W$ ) at any given voltage and the reduced minority carrier lifetime both of which result from the heavy doping. Figure 46 indicates that this, in fact, is true only for low bias voltages. However, it is not true for voltages near but still below breakdown. At a reverse bias of 20 V, the 26 V diode has a much larger photocurrent than a 40 V diode and, yet, for a reverse bias of 5 V just the opposite is true. For hardening purposes, this indicates that heavy doping, which is used for hardening against neutron-induced degradation, may not be advantageous for reducing photocurrents.

Table 27 is typical of the transient response of some common diodes.<sup>64</sup> In this table PW is the abbreviation for pulse width. The number of points is the number of measurement points that were taken on the waveform of the radiation pulse.  $V_R$  is, of course, the reverse bias. The relaxation time is the decay time of the photocurrent.

The multiple entries for the rectifiers and the general diodes correspond to diodes obtained from different manufacturers. The purpose of including these entries is to indicate the variations (factors of 2 to 4) in the transient response that can exist for diodes of the same type which come from different manufacturers.

As Table 27 indicates, the current can be quite large (e.g., 41 A for the IN1190 and a dose rate of approximately  $1.84 \times 10^{17}$  rads(Si)/sec) and obviously can cause havoc to any system. In order to minimize the photocurrent it is recommended that a low voltage (heavily doped) diode be used and be biased below one-half the breakdown voltage. This is compatible with the recommendations for neutron hardening.

The above remarks apply for a diode operating below its breakdown (i.e., the magnitude of the bias voltage is less than the breakdown voltage). There is some reported evidence that the same recommendation for a low voltage diode would apply when the diode is required to be biased into its breakdown. Figure 47 illustrates this.<sup>74</sup> This figure indicates that the photocurrent at any bias current is larger for higher voltage diodes. In addition, the magnitude of the transient response decreases as the bias current is increased. However, the explanation given in reference 74 for this figure made the assumption that the junction resistance is an increasing function of breakdown voltage.

Table 27. Dose Rate Response of Typical Diodes

Class: General Diodes

Type	Sample Size	Test Conditions VR(V)	Pulse Width (usec)	Number Points	Dose Rate Range (rads(Si)/sec)		I <sub>pp</sub> (mA)		Relax Time (usec)
					Min.	Max.	Avg.	Max.	
IN3595	4	75.0	.030	3	1.69E11	2.25E11	1.733	800	<PW
	5	75.0	.030	3	1.23E11	2.32E11	1.567	1,900	<PW

Class: Rectifiers

IN649	4	75.0	.030	3	6.60E10	8.80E10	3,367	4,000	.048
	3	75.0	.030	6	3.15E10	9.37E10	933	1,200	.10
IN1190	3	75.0	.030	2	1.38E11	2.39E11	35,000	36,000	-
	3	75.0	.030	2	1.55E11	2.08E11	41,000	42,000	-

Class: Switching Diodes

IN914	6	60.0	.030	2	2.50E11	2.53E11	100	100	<PW
IN3630	7	40.0	.030	5	1.48E11	1.57E11	158	200	<PW
IN3613	2	75.0	.030	2	2.88E11	3.10E11	10,000	11,000	.12
IN4148	3	60.0	.030	2	1.73E11	1.97E11	200	240	<PW
IN4942	5	75.0	.030	4	1.28E11	1.75E11	3,000	3,600	.0465
PS700	3	24.0	.030	2	2.05E11	2.48E11	120	120	<PW

Class: Reference Diodes

IN746A	2	18.0	.040	2	1.01E11	1.01E11	275	300	.25
IN750A	4	13.0	.040	8	3.76E10	1.06E11	302	350	.89
IN752A	2	36.0	.040	2	1.15E11	1.15E11	450	500	.89
IN753A	4	5.60	.030	2	2.80E11	3.30E11	260	300	.47
IN827	2	6.40	.030	2	1.51E11	1.71E11	770	900	.32
IN938B	2	12.0	.040	2	1.26E11	1.26E11	390	420	.14
IN3653	3	14.3	.030	3	1.82E11	2.03E11	967	1,000	.50
IN2993	3	46.0	.030	2	1.75E11	2.17E11	7,750	8,000	.69
IN4567A	3	6.40	.030	3	2.00E11	2.47E11	387	400	.50
IN4781A	5	9.40	.030	4	1.07E11	1.78E11	785	1,000	.26

Table 27. Dose Rate Response of Typical Diodes

Class: General Diodes

Type	Sample Size	Test Conditions VR(V)	Pulse Width (usec)	Number Points	Dose Rate Range (rad/sil/sec)		I <sub>pp</sub> (mA)		Relax Time (usec)
					Min.	Max.	Avg.	Max.	
IN3595	4	75.0	.030	3	1.69E11	2.25E11	733	800	<PW
	5	75.0	.030	3	1.23E11	2.32E11	1,567	1,900	<PW

Class: Rectifiers

IN649	4	75.0	.030	3	6.60E10	8.80E10	3,367	4,000	.048
	3	75.0	.030	6	3.15E10	9.07E10	933	1,200	.10
IN1190	3	75.0	.030	2	1.38E11	2.09E11	35,000	36,000	-
	3	75.0	.030	2	1.59E11	2.08E11	41,000	42,000	-

Class: Switching Diodes

IN914	5	60.0	.030	2	2.50E11	2.53E11	100	100	<PW
IN3600	7	40.0	.030	5	1.48E11	1.57E11	152	200	<PW
IN3613	2	75.0	.030	2	2.38E11	3.02E11	10,000	11,000	.12
IN4148	3	60.0	.030	2	1.73E11	1.97E11	220	240	<PW
IN4942	5	75.0	.030	4	1.28E11	1.75E11	3,000	3,500	.0465
FD700	3	24.0	.030	2	2.25E11	2.48E11	120	120	<PW

Class: Reference Diodes

IN746A	2	18.0	.040	2	1.01E11	1.01E11	275	300	.25
IN750A	4	13.0	.040	8	3.75E10	1.26E11	302	350	.89
IN752A	2	36.0	.040	2	1.15E11	1.15E11	450	500	.39
IN753A	4	6.50	.030	2	2.82E11	3.33E11	260	300	.47
IN827	2	6.40	.030	2	1.61E11	1.71E11	770	900	.32
IN9388	2	12.0	.040	2	1.25E11	1.26E11	390	420	.14
IN9658	3	14.3	.030	3	1.93E11	2.03E11	967	1,000	.50
IN2993	3	46.0	.030	2	1.75E11	2.17E11	7,760	8,000	.69
IN4567A	3	6.40	.030	3	2.00E11	2.47E11	387	400	.60
IN4781A	5	9.40	.030	4	1.37E11	1.73E11	785	1,000	.26

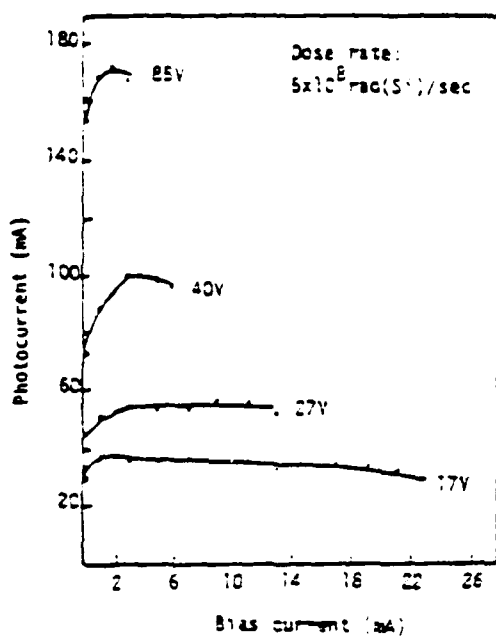


Figure 47. Peak Photocurrent versus Bias Current for Various Diode Breakdown Voltages

However, as indicated by Figure 48<sup>76</sup> this is not always true. In light of this, all that can be safely said is that to minimize photocurrents

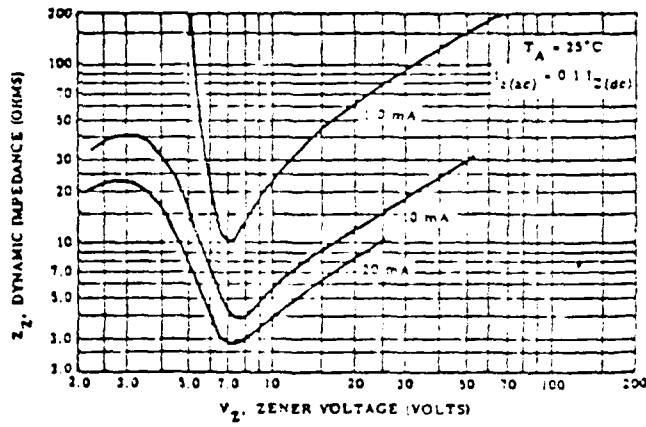


Figure 48. Zener Impedance versus Zener Voltage for Different Bias Currents

in applications such as a Zener reference element which is biased into breakdown, diodes with a breakdown voltage as near to 7 V as possible should be chosen and they should be operated at the highest practical bias current. It should also be noted that if temperature compensated units consist of more than one junction, a certain degree of photocurrent compensation is obtained by two opposing junctions in series.

Total dose effects on diodes result in changes in the leakage current, breakdown voltage, and forward voltage. Tables 28<sup>64</sup> and 29<sup>64</sup> list the response of some selected diodes to total dose. Figure 49<sup>1</sup> indicates the percentage change in diode characteristics as a function of total dose. In general, the leakage current increases and the forward voltage drops in all diodes with increasing dose. The breakdown voltage of switching and rectifying diodes usually decreases and that of reference diodes usually increases. The threshold for the onset of total dose effects appears at approximately  $10^4$  rad (Si) but the effects are usually tolerable (15 percent change or less) up to at least  $10^6$  rad (Si).

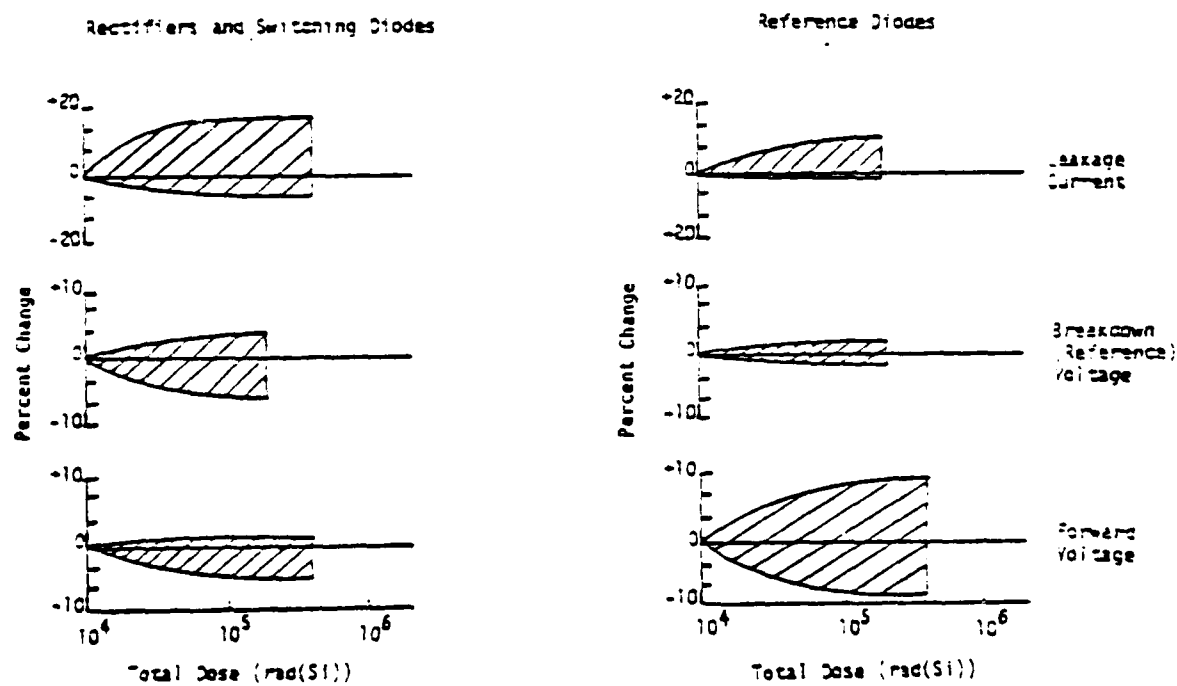


Figure 49. Composite Change in Diode Characteristics vs Total Dose

Table 28. Dose Response of Typical Diodes

**Class:** Rectifiers

Type	Sample Site	Leakage Current				Forward Voltage			
		Test Conditions V <sub>F</sub> (V)	Pre-test I <sub>L</sub> (mA)	I <sub>L</sub> at 10 <sup>5</sup> rad(SI)	I <sub>L</sub> at Max. Dose radi(SI)	Test Conditions I <sub>F</sub> (mA)	Pre-test V <sub>F</sub> (V)	V <sub>F</sub> at 10 <sup>5</sup> rad(SI)	Max. Dose radi(SI)
1N647	10	30	1.71E-9	-	5.01E-7	2.01E-9	1.17	1.00	.62
DN6102*	>20	600M	2.24E-7	-	6.08E-4	2.10E-7	0.97	.05	7.90
DN6108*	>20	60	1.72E-7	-	5.00E-4	1.20E-7	1.04	10.0	.56
DN6121*	>20	50	8.21E-9	9.35E-8	1.01E-5	9.35E-8	1.14	10.0	.63
DN6294*	>20	60	1.16E-6	1.20E-6	1.01E-5	1.20E-6	1.10	10.0	.49
<b>Class: Switching Diodes</b>									
1N9912	10	200	1.95E-8	-	5.04E-7	1.81E-8	.96	110.0	.96
034660*	>20	55	1.79E-8	1.95E-8	1.01E-5	1.95E-8	1.09	10.0	.68
053167*	>20	50	1.30E-8	1.40E-8	1.01E-5	1.40E-8	1.07	20.0	.72
053114*	>20	55	2.62E-8	-	5.01E-4	2.79E-8	1.06	10.0	.60
04164*	5	15	6.71E-9	-	2.51E-5	6.55E-9	.97	3.0	.73
<b>Class: Reference Diodes</b>									
04115*	>20	4.5	2.25E-6	2.49E-6	1.01E-5	2.49E-6	1.11	.001	22.1
015109*	>20	6.60	4.66E-5	4.65E-5	1.01E-5	4.65E-6	1.00	1000.0	.68
016201*	>20	0.001	3.22E-7	-	5.01E-4	3.30E-7	1.16	100.0	.81
017225*	>20	3.00	3.11W-5	-	5.01E-4	3.16E-5	1.05	20.0	.74
016149*	>20	3.00	4.96E-5	-	5.01E-4	6.16E-5	1.04	20.0	.69

\*These devices have been manufactured for particular defense systems and the identification of the nuclear vulnerability date with the system may be classified information. For these devices, the type number of a similar commercial device is given whenever possible. It must be considered that defense system parts are manufactured under stringent quality assurance and control conditions, and commercial devices listed as equivalent types may not perform as the data indicates.



Table 29. Effects of Total Dose Exposure on the Breakdown Voltage of Diodes

Class: Rectifiers

Type	Sample Size	Test Conditions IR(mA)	Reference Voltage			BV at Max. Dose	$\frac{BV_{max}}{BV_0}$
			Pre-test BV(v)	$10^5$ rads(ST)	Max. Dose rad(ST)		
DR2602*	>20	1.0E-4	8502.0	-	5.0E4	8530.0	1.00
DR3038*	>20	1.0E-2	98.3	-	5.0E4	90.5	.92
DR4921*	>20	0.1	134.0	135.0	1.0E5	135.0	1.01
DR9291*	>20	1.0E-2	87.9	84.3	1.0E5	84.3	.96

Class: Switching Diodes

Type	Sample Size	Test Conditions IR(mA)	Reference Voltage			BV at Max. Dose	$\frac{BV_{max}}{BV_0}$
			Pre-test BV(v)	$10^5$ rads(ST)	Max. Dose rad(ST)		
IN4947	10	1.0E-3	614	-	5.0E7	594.0	.97
DS4760*	>20	5.0E-3	96.0	97.3	1.0E5	97.3	1.01
DS5061*	>20	5.0E-3	100.0	106.0	1.0E5	106.0	.98
DS5814*	>20	5.0E-3	98.0	-	5.0E4	98.5	1.01

Class: Reference Diodes

Type	Sample Size	Test Conditions IR(mA)	Reference Voltage			BV at Max. Dose	$\frac{BV_{max}}{BV_0}$
			Pre-test BV(v)	$10^5$ rads(ST)	Max. Dose rad(ST)		
074775*	>20	7.50	6.33	6.34	1.0E5	6.34	1.00
075409*	>20	100.0	8.14	8.27	1.0E5	8.27	1.02
076903*	>20	0.30	9.73	0	5.0E4	9.79	1.01
077425*	>20	1.00	4.18	-	5.0E4	4.20	1.01
078149*	>20	20.0	4.67	-	5.0E4	4.70	1.01

\*Same comment applies here as in Table 12.

### 5.1.2 Silicon Controlled Rectifiers

The discussion on discrete semiconductor devices up to this point has focussed on the vulnerability of diodes. The discussion would be incomplete if it did not include silicon controlled rectifiers (SCRs). The device type finds wide application in voltage and current regulators where it often acts as a solid-state breaker switch. However, as will be seen, SCRs are among the most vulnerable semiconductor devices to radiation. In addition, SCR-like structures in integrated circuits (ICs) constitute one of the major problems for the survivability of ICs. For these reasons, it was decided to include a brief, separate section on SCRs.

A silicon controlled rectifier (SCR) is a semiconductor device which can be triggered to operate in one of two states, a high-resistance OFF state or a low-resistance ON state. The physical structure of a typical SCR is shown in Figure 50.

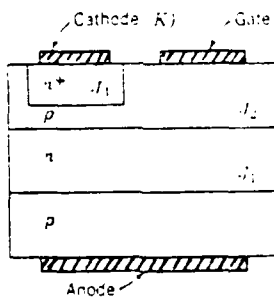


Figure 50. Physical Structure of a Silicon Controlled Rectifier

The SCR is fabricated by diffusing a p-layer into both sides of a lightly doped n-type silicon wafer and then diffusing an n+-type region (cathode) into one of the p-layers. This p-layer is termed the gate and the other p-layer is the anode. The three upper layers form an n-p-n transistor structure where the cathode is the emitter, the gate is the base, and the middle n-region is the collector. The lower three layers form a p-n-p transistor structure where



the anode is the emitter, the n-region is the base, and the gate is the collector.

This equivalence leads to the two transistor model commonly used to model the SCR, shown in Figure 51.<sup>81</sup> In normal operation the anode is positive and the cathode negative, so that both T1 and T2 have the emitter-base junction forward-biased and the collector-base junction reverse-biased.

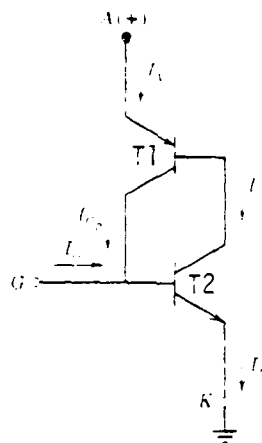


Figure 51. Schematic of the Two Transistor SCR Model

Note that  $I_{C1}$  is the pnp collector current crossing the high resistivity n-region.  $I_{C2}$  is the npn collector current crossing the base p-region. If  $\beta_1$  and  $\beta_2$  are used for the common emitter gains of T1 and T2 respectively, the current relations can be written as:

$$I_{C1} = (1 + \beta_1)I_{CBO} + \beta_1(I_{C2}) \quad (2)$$

$$I_{C2} = (1 + \beta_2)I_{CBO} + \beta_2(I_{C1} + I_G) \quad (3)$$

Where  $I_{CBO}$  is the leakage current, which is the same for both transistors since both have the same collector-base junction  $J_2$ ; and  $I_G$  is the gate current which is used to trigger the change in states. By noting that  $I_A = I_{C1} + I_{C2}$  and combining equation (2) and equation (3) the individual collector currents may



be eliminated, resulting in

$$I_A = \frac{2I_{CBO}(1 + \beta_1)(1 + \beta_2) + \beta_2 I_G}{1 - \beta_1 \beta_2} \quad (4)$$

At low currents the product of the gains is less than one and the anode current,  $I_A$ , is small. If the gains are increased by increasing the current level or by raising the voltage to increase the junction multiplication, the product of the gains will reach a value of  $\beta_1 \beta_2 = 1$ , making  $I_A$  indeterminate. When  $\beta_1 \beta_2 = 1$  the SCR will switch to the low resistance ON state. In an SCR this switching is accomplished by injecting a gate current,  $I_G$ , large enough to force  $\beta_1 \beta_2 > 1$ . Once the SCR has been switched to this ON state it cannot be switched OFF by reducing  $I_G$ . To switch to the OFF state  $I_A$  must be reduced to a point where  $\beta_1 \beta_2 < 1$ . This is usually done by reversing the anode voltage.

During turn-on, with a large voltage across the rectifier, burnout becomes a problem. The base current causes emitter crowding, which forces the initial current flow to the side of the anode nearest the gate contact. The buildup of current in this area can cause local thermal heating and burnout of the SCR at the edge of the anode. If the local heating is not excessive the region of high currents will propagate laterally until the entire anode area is turned on.<sup>81</sup>

The typical SCR is very sensitive to neutron irradiation because the gain and saturation voltage requirements demand a long minority carrier lifetime, and minority carrier lifetime degradation is a principal effect of neutron irradiation. This affects the SCR by taking it out of the ON state when the  $\beta$  degradation is sufficient to force  $\beta_1 \beta_2 < 1$ . Provided the SCR is not severely damaged it can be turned ON again by additional gate drive. Figure 52<sup>1</sup> shows the probability of this type of neutron-induced failure as a function of neutron fluence. No failures were observed at  $10^{12}$  n/cm<sup>2</sup> for the 55 SCR's tested; however, failures have been reported for fluences as low as  $5 \times 10^{11}$  n/cm<sup>2</sup>.

Total dose affects the SCR by increasing leakage currents. If this increase is sufficient the switching current gain will be boosted to a point where  $\beta_1 \beta_2 > 1$ , causing the SCR to switch from the OFF state to the ON state.



Total dose data on the 2N2323 SCR are presented in Table 30.<sup>1</sup>  $I_{R0}$ ,  $I_{F0}$ , and  $I_{RGO}$  are leakage currents.

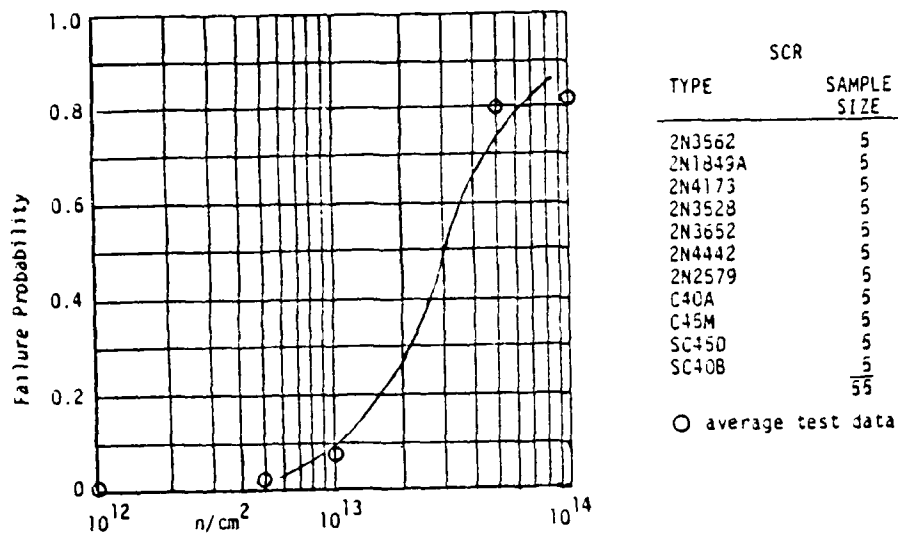


Figure 52. SCR Switching Failure Probability as a Function of Neutron Fluence

Unit No.	$V_{GT}$ (v)	Reverse Blocking I <sub>R0</sub> (amp)	Forward Blocking I <sub>F0</sub> (amp)	$I_{RGO}$ (amp)	Fused in Field
Pre-Irradiation					
1	0.5	$2.2 \times 10^{-9}$	$5.6 \times 10^{-9}$	$4.4 \times 10^{-6}$	-
2	0.6	$8.2 \times 10^{-9}$	$2.3 \times 10^{-8}$	$6.6 \times 10^{-10}$	-
3	0.545	$4.4 \times 10^{-9}$	$5.0 \times 10^{-9}$	$1.5 \times 10^{-9}$	-
4	0.55	$1.6 \times 10^{-9}$	$7.0 \times 10^{-9}$	$3.2 \times 10^{-10}$	-
5	0.6	$2.0 \times 10^{-9}$	$2.2 \times 10^{-9}$	$4.0 \times 10^{-10}$	-
After Exposure to $10^6$ rad					
1	0.5	$2.5 \times 10^{-9}$	$5.4 \times 10^{-9}$	$5.8 \times 10^{-9}$	Yes
2	0.55	$1.1 \times 10^{-8}$	$1.0 \times 10^{-8}$	$1.0 \times 10^{-9}$	No
3	0.55	$5.9 \times 10^{-9}$	$9.2 \times 10^{-9}$	$2.2 \times 10^{-9}$	Yes
4	0.55	$2.1 \times 10^{-9}$	$1.1 \times 10^{-8}$	$1.3 \times 10^{-9}$	Yes
5	0.56	$2.5 \times 10^{-9}$	$9.5 \times 10^{-9}$	$5.0 \times 10^{-10}$	No
After Exposure to $10^5$ rad					
1	0.5	$3.4 \times 10^{-9}$	$1.2 \times 10^{-7}$	$5.2 \times 10^{-6}$	No
2	0.56	$7.7 \times 10^{-9}$	$1.8 \times 10^{-7}$	$3.0 \times 10^{-9}$	No
3	0.55	$7.5 \times 10^{-9}$	$2.0 \times 10^{-7}$	$2.1 \times 10^{-9}$	Yes
4	0.58	$2.5 \times 10^{-9}$	$3.0 \times 10^{-7}$	$1.1 \times 10^{-9}$	Yes
5	0.56	$3.8 \times 10^{-9}$	$1.0 \times 10^{-5}$	$2.2 \times 10^{-9}$	Yes

Table 30. Total Dose Data for the 2N2323 SCR



Experimental studies have shown that SCR's can be triggered from the OFF state to the ON state by doses as small as 10 rads(Si).<sup>1</sup> The exact effect is dependent on the duration and shape of the ionizing pulse. A 1.5 ns pulse with peak dose rate of  $2.3 \times 10^{10}$  rad(Si)/sec can cause triggering in 15 ns. This extreme sensitivity to both total dose and dose rate leads to our recommendation of avoiding SCRs completely. In cases where the use of SCRs cannot be avoided, current limiting on the power supply buses can reduce the likelihood of latchup and device burnout.

It should be noted that p-n-p-n SCR structures occur frequently in integrated circuits. Dose rate induced photocurrents may be sufficient to cause these parasitic SCR paths to fire, leading to latch-up and burnout. This problem will be discussed in greater detail in the section on integrated circuits (5.2).



### 5.1.3 Transistors

A bipolar transistor in its simplest form is a three region device. This is illustrated in Figure 53. The three regions for the n-p-n transistor

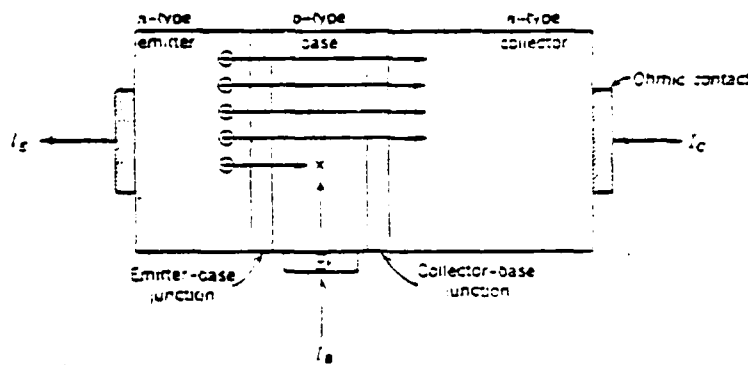


Figure 53. Simplified Picture of Transistor Operation.  
For the external circuit, arrows are in the direction of the flow of positive charge.

are, of course, an n-type emitter, a p-type base, and an n-type collector. The n-type emitter and the p-type base form a diode while the p-type base and the n-type collector form another diode. In simple terms, the operation of a transistor requires the electrons to migrate from the emitter to the collector without being captured or recombining in the base. The average time required for an electron to transverse the base region is known as the base transit time,  $t_b$ . For a uniform base transistor  $t_b$  is given by<sup>81</sup>

$$t_b = \frac{w_b^2}{2D} \quad (5)$$

where  $w_b$  is the base width and D is the diffusion constant.

For a graded base transistor, this equation is modified but the  $w_b^2$  dependence remains.

Letting  $R_n$  be the recombination rate per electron then the probability that an electron will recombine in the base region is approximately  $t_b R_n$ . According to the simplified picture in Figure 53  $I_E$  is essentially the number of electrons that leave the emitter and enter the base. The common emitter dc gain  $\beta$  is given by

$$\beta = \frac{I_C}{I_B} = \frac{I_E(1 - t_b R_n)}{I_E(t_b R_n)} = \frac{1}{t_b R_n} - 1 \quad (6)$$

As mentioned previously, neutron-induced displacements actually produces three major effects in semiconductors: (1) minority-carrier lifetime degradation, (2) majority-carrier removal, and (3) majority-carrier mobility decrease. The dominant mechanism is minority-carrier lifetime degradation in the base region and this degradation is principally determined by cluster defects in the base region. MOS devices are insensitive to variations in the minority carrier lifetimes and, for this reason, are reasonably invulnerable to neutron displacement effects. However, bipolar devices can be quite sensitive to degradation of the minority carrier lifetimes.

Carrier lifetime,  $\tau$ , is the most important semiconductor parameter to be affected by lattice defects. The reciprocal of the lifetime sometimes called the recombination rate per carrier is often used in analysis and prediction of displacement radiation damage effects. This is a very useful concept since all terms contributing to the recombination rate can be simply added together and because  $1/\tau$  is proportional to the number of defects and thus to the radiation exposure. This leads to the relationship between the neutron fluence and carrier lifetime given by<sup>77</sup>

$$\frac{1}{\tau_e} = \frac{1}{\tau_0} + \frac{\phi}{K_\tau} \quad (7)$$



where  $\tau_0$  is the pre-irradiation lifetime

$\tau_s$  is the post-irradiation lifetime

$\kappa$  is the lifetime damage constant in  $\text{cm}^2/\text{n-sec}$

$\phi$  is the 1 Mev equivalent neutron fluence in  $\text{n}/\text{cm}^2$

Messenger and Spratt<sup>78</sup> used the lifetime degradation equation (equation (7)) as the fluence-dependent volume recombination term together with an expression for a graded-base transistor similar to equation (7) by Wilson<sup>79</sup> to derive an equation relating the transistor current gain degradation with neutron fluence. In doing this they utilized Shockley-Read statistics<sup>59,61,80</sup> to describe the variation of lifetime with injection level and combined the effects of injection efficiency and surface recombination into a single, fluence-insensitive term.<sup>2</sup> A detailed derivation of this equation is quite involved and somewhat outside the scope of this study. For the purposes of this study the usual form of this somewhat famous equation will be used. This version is given by:

$$\frac{1}{\beta_s} - \frac{1}{\beta_0} = \frac{\kappa \phi}{2 \pi f_\alpha} \quad (8)$$

where

$\beta_s$  = post-irradiation common emitter dc forward current gain

$\beta_0$  = pre-irradiation common emitter dc forward current gain

$\phi$  = the neutron fluence

$K$  = lifetime damage constant

$f_\alpha$  = alpha-cutoff frequency or common-base cutoff frequency.

This expression is expressed in terms of  $f_\alpha$  where  $\alpha$  is the common-base dc forward current gain.  $f_\alpha$  is, of course, defined as the frequency at which the value of alpha drops to .707 times its 1 kHz value. Larin<sup>81</sup> expresses equation (7) in terms of the base transit time as

$$\frac{1}{\beta_s} - \frac{1}{\beta_0} = t_b K \phi$$

This form is perhaps less useful since values of  $t_b$  are not usually available. However, it does indicate the dependence of the gain degradation on the base transit time and, hence, on the base width of the transistor. Quite often  $f_2$  is not available and in those cases the gain bandwidth product,  $f_T$ , is used with the introduction of very small error. The gain bandwidth product is, of course, the frequency at which the common emitter dc forward current gain is unity. The relationship between  $f_T$  and  $t_b$  is, to the first approximation, given by

$$t_b = \frac{1}{2\pi f_T}$$

Another modification to equation (8) that is quite popular is the form

$$\frac{1}{\beta_0} - \frac{1}{\beta_0} = C \phi \quad (9)$$

where  $C$  is the neutron damage factor and, of course, is related to  $K$  by

$$C = \frac{K}{2\pi f_T}$$

The ease of this form is obvious since  $C$  is just the slope of the line which results from plotting  $\Delta(1/3)$  versus the neutron fluence.

The damage constant,  $K$ , takes into account the recombination in the emitter-base junction and the base region. It will also vary with the collector current,  $I_C$ , resulting in a variation in the neutron response of a transistor with  $I_C$ . Figure 54 indicates the effect of  $I_C$  on the neutron vulnerability of a 2N2708 transistor.<sup>1</sup> For a fluence of  $1.4 \times 10^{17}$  n/cm<sup>2</sup> the ratio of  $\beta_0/\beta_0$  is 0.22 for a collector current of 0.01 mA. For an  $I_C$  of 10 mA which corresponds to the maximum pre-irradiated current gain,  $\beta_0/\beta_0$  has a value of .4. This illustrates a general rule for designing survivable circuits. The biasing should be such that transistors are operated at or near the peak current gain.



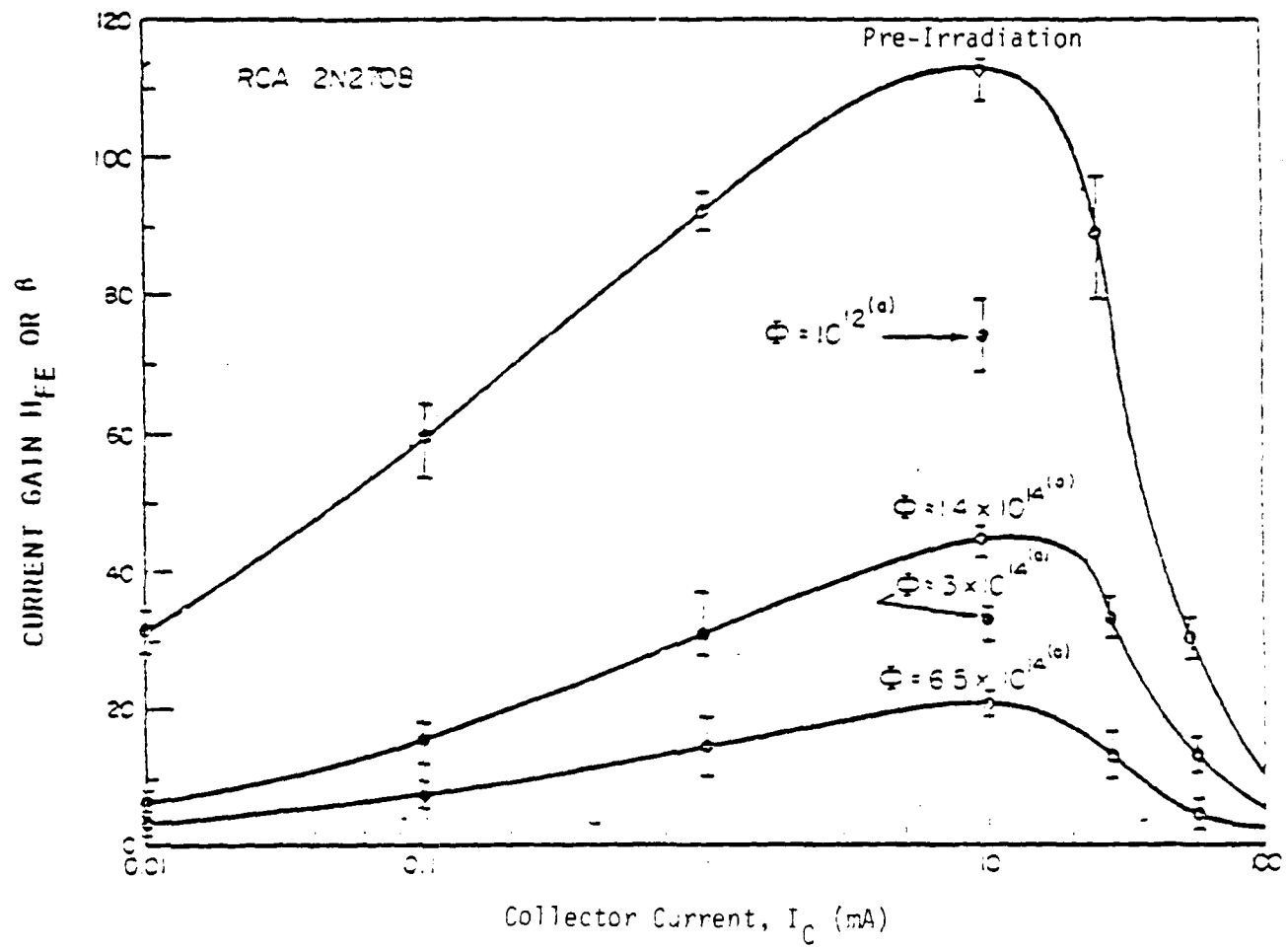


Figure 54. Current Gain versus  $I_C$  for a Family of Neutron Fluences

A vast amount of data has been taken on the neutron response of discrete bipolar transistors. The Component Response Information Center (CRIC) maintained by Harry Diamond Laboratories has data on over 450 transistor types.<sup>64</sup> This is only one of several data sources. It certainly is not possible or necessary for the purposes of this study-to assemble all of this data. Table 31 is representative of the data.<sup>64</sup> The data has been separated by frequency into roughly three groups corresponding to  $f_T$  less than or equal to 50 MHz,  $f_T$  less than or equal to 150 MHz but greater than 50 MHz, and  $f_T$  greater than 150 MHz. This, of course, assumes that  $f_{\alpha}$  has been replaced by  $f_T$  in equation 8 which is the usual form of the equation. Obviously, high  $f_T$  values indicate less change in  $S_e/S_0$  and, therefore, more radiation resistant devices. This constitutes the second design guideline. The devices with the highest possible  $f_T$  should be used to ensure a survivable design.

The dependence of vulnerability on  $f_T$  is borne out in Table 31. This is indicated by the  $S_e/S_0$  column for a fluence of  $10^{13} n/cm^2$ . The ratio of  $S_e/S_0$  varies from .06 for a 600 kHz device (the 2N1485) to over .9 for a 1000 MHz device (the 2N2857). The increase in hardness exhibited in the table is not a smooth monotonically increasing function of  $f_T$ . This is due to the fact that the ratio  $S_e/S_0$  also depends on  $S_0$ . This dependence of  $S_e/S_0$  can be illustrated by solving equation (8) for  $S_e/S_0$ . This yields

$$\frac{S_e}{S_0} = \frac{1}{1 + \frac{S_0 K_0}{2\pi f_T}} \quad (10)$$

This equation shows that the ratio,  $S_e/S_0$ , has a dependence on  $f_T/S_0$  so that the initial value of the gain should not be ignored. On the basis of  $f_T$  alone, the 60 MHz 2N3806 should be more radiation resistant than the 60 MHz 2N720A. However, radiation data indicates that the 2N3806 is more susceptible than the 2N720A since at  $10^{13} n/cm^2$  the 2N720A has a  $S_e/S_0$  value of .67 while the value of this ratio for the 2N3806 is .56. This anomaly occurred because the contribution of  $S_0$  was ignored. The parameter to minimize is really  $S_0/f_T$ . The value of  $S_0/f_T$  min for the 2N720A is 1.42 and for the 2N3806 the ratio has a value of 1.57. On this basis the lower frequency 2N720A is expected to be less vulnerable than the 2N3806.

Table 31. Effects of Neutron Irradiation on Transistor's Gain

Geometric Type	Transistor Type	$\theta_{\text{gain}}$ ( $^{\circ}\text{Rt}$ )	$\theta_0$	$\theta_{\text{dwell}}$	$\theta_0/\theta_{\text{dwell}}$	Avg. damage factor		$\theta_{\phi, \text{at}}$	$\theta_{\phi}/\theta_0 \times 10^{13} \text{ n/cm}^2$	$\theta_{\phi, \text{at}}$	$\theta_{\phi}/\theta_0 \times 10^{13} \text{ n/cm}^2$	$\theta_{\phi, \text{at}}$	$\theta_{\phi}/\theta_0 \times 10^{13} \text{ n/cm}^2$
						$\times 10^{-10}$	$\times 10^{-10}$						
2N1617	PNP	0.2	100	120	640.0	3.01	26.4*	21*	6.27	6.27	6.27	6.27	.04
2N1415	NPN	0.6	15	0.19	119.0	16.9	5.04*	0.06*	0.7	6.99	6.99	6.99	.06
2N116	NPN	2	75	69	45.5	2.50	27.0*	3*	0.92*	26.0	26.0	26.0	.32
2N1741		4	40	63.9	15.6	2.80	22.9*	.36*	0.95	23.7	23.7	23.7	.16
2N1740	NPN	10	150	270	9.0	0.565	106	.39	1.42	65	65	65	.32
2N1639	NPN	50	43	96	1.8	0.799	54.6	.61	3.00	24.6	24.6	24.6	.27
2N170A	NPN	50	40	71	1.42	0.683	47.8*	.67*	0.323	61.4	61.4	61.4	.06
2N1131	PNP	60	20	29.5	0.59	1.49	19.6	.66	5.51	6.00	6.00	6.00	.30
2N2104	NPN	60	100	311	6.6	0.612	174	.53	12.01	17.1	17.1	17.1	.05
2N2106	PNP	60	40	94.2	1.67	0.610	51.6	.56	6.46	17.4	17.4	17.4	.44
2N1613	NPN	60	40	60	1.33	0.542	55.8*	.70*	9.6	15.6	15.6	15.6	.20
2N1711	NPN	70	100	131	1.97	0.194	109.0	.79	3.70	70.0	70.0	70.0	.51
2N2270	NPN	100	50	121	1.21	0.645	74.1	.61	67.51	2.32	2.32	2.32	.07
2N1499	NPN	15.0	100	124	0.81	0.656	68.4*	.55*	1.05	60.1	60.1	60.1	.55
2N1501	NPN	45.0	100	101	1.22	0.284	123.0	.67	11.41	27.0	27.0	27.0	.27
2N2907	PNP	200	25	172	0.06	2.15	97.4	.57	12.34	1.3	1.3	1.3	.02
2N1502	PNP	200	140	211	1.06	0.470	105.9*	.50*	12.31	16.3	16.3	16.3	.06
2N2222	NPN	25.0	50	173	0.69	0.174	127	.73	12.31	37.0	37.0	37.0	.21
2N2119	NPN	25.0	100	116	0.54	0.291	96.0	.71	6.51	42.0	42.0	42.0	.32
2N1250	PNP	25.0	50	100	0.43	1.58	85.9	.80	12.31	4.61	4.61	4.61	.04
2N1906	PNP	25.0	100	169	0.66	0.340	101	.67	1.21	104	104	104	.67
2N110A	NPN	100	40	89	0.30	0.780	52.3*	.59*	2.09	16.1	16.1	16.1	.41
2N4124	NPN	100	120	171	0.41	0.134	81.1	.66	44.71	6.05	6.05	6.05	.06
2N1251	PNP	100	100	106	0.15	0.100	77.5	.71	9.6	26.5	26.5	26.5	.26
2N1175	PNP	15.0	10	50	0.14	0.161	45.9*	.92*	12.31	23.6	23.6	23.6	.47
2N1714	NPN	40.0	55	70.4	0.15	0.176	65.1*	.79*	0.19	67.3	67.3	67.3	.96
2N1727	NPN	50.0	100	100	0.20	0.108	81.9*	.05*	9.5	37.2	37.2	37.2	.37
2N1166	NPN	50.0	10	60.6	0.14	0.15	62.2*	.91*	14.21	16.9	16.9	16.9	.25
2N1110	NPN	60.0	20	119	0.20	0.17	99.0*	.03*	0.19	116	116	116	.96
2N1709	NPN	60.0	55.0	67	0.07	0.0005	52.5*	.95*	9.5	37.6	37.6	37.6	.66
2N2057	NPN	1000	30	99.4	0.10	0.015	91.0	.92	79.01	17.1	17.1	17.1	.17

\* Calculated

† Measured

‡fluence greater than  $10^{16} \text{ n/cm}^2$

This is not to say that one should use the transistor type with the lowest  $\beta_0$  value to minimize  $\beta_0/f_T$ . Instead this ratio should be minimized by using the highest  $f_T$  possible. There is some correlation between  $f_T$  and  $\beta_0$ , and in general, an increase in  $f_T$  means an increase in  $\beta_0$ . In addition, a higher value of  $\beta_0$  means a greater design margin and therefore the circuit can withstand more gain degradation. For a constant  $\beta_0/f_T$  ratio the combination with the highest value of  $f_T$  should be chosen since that choice will not only suffer less gain degradation but also has a greater design margin due to its higher gain. Thus, the third design guideline is to chose the device type with the highest  $\beta_0$  since this will increase the design margin.

Equation (10) has been used to generate two nomographs that can be used to estimate the value of  $\beta_e/\beta_0$ . These were first developed by J. R. Bilinski<sup>82</sup> but have since appeared in numerous places.<sup>83,84</sup> The nomographs are actually based on

$$\frac{\beta_e}{\beta_0} = \frac{1}{1 + 0.2 \frac{\beta_0 K e}{f_a}}$$

with  $K = 5.5 \times 10^{-7} \text{ cm}^2/\text{n-sec}$  for PNP silicon devices  
and  $K = 8.5 \times 10^{-7} \text{ cm}^2/\text{n-sec}$  for NPN silicon devices

The two nomographs have been combined into one in Figure 55. The procedure in using the nomograph is fairly obvious. The first step consists of connecting the value of  $f_a$  with the initial or unirradiated value of the current gain. The intersection of this line with the pivot line is then connected with the threat fluence. The value of  $\beta_e/\beta_0$  is then read off the  $\beta_e/\beta_0$  line. Usually  $f_T$  is used instead of  $f_a$  with the introduction of very little error.

Generally a designer will not know a priori the exact values of  $\beta_0$  and  $f_a$  or  $f_T$  for the devices in his circuit. To overcome this manufacturer's minimum specified values of  $\beta_0$  and  $f_T$  are frequently used. This, of course, yields a safe-sided estimate of  $\beta_e/\beta_0$ . However, this is balanced somewhat by the values of  $K$  which were used to create the nomographs. These are nominal or typical values. Within a generic type,  $K$  is essentially constant but it will vary by a factor of approximately 6 over all generic types.



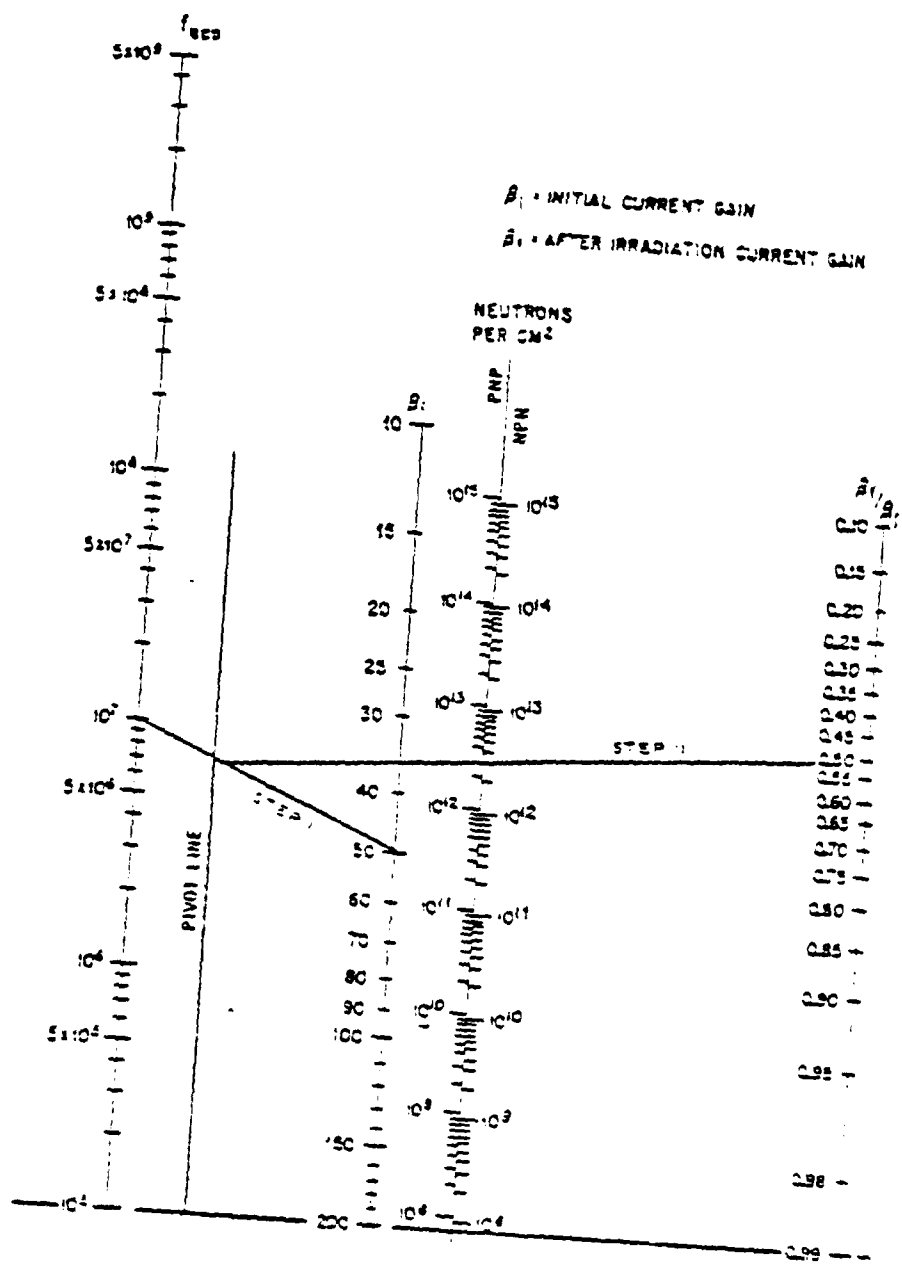


Figure 55. Silicon Transistor Nomograph for Determining Neutron-Induced Gain Degradation

Durgin, Alexander, and Randall<sup>65</sup> resolved this problem by realizing that the use of manufacturer's minimum specified values of  $\beta_0$  and  $f_T$  transformed equation (10) from a device equation to a generic type equation. For a particular device type,  $\beta_0 \text{ min}$  and  $f_T \text{ min}$  are known. The only uncertainty arises from K. They then treated K as a lognormally distributed random variable over all device types. This transforms equation (10) from an equation in four variables ( $\beta_0$ ,  $\beta_0$ , K, and  $f_T$ ) to an equation in two random variables ( $\beta_{\phi \text{ min}}$  and K). Basically, this changes equation (8) from an individual device equation to a device type equation since  $\beta_0 \text{ min}$  and  $f_T \text{ min}$  are characteristic of a generic device type (some particular 2NXXXX) rather than an individual device within a generic type. The resulting form of the equation is

$$\frac{1}{\beta_{\phi \text{ min}}} - \frac{1}{\beta_0 \text{ min}} = \frac{K\epsilon}{f_T \text{ min}} \quad (11)$$

Since K is now treated as a random variable, it is possible to derive an expression for the probability that  $\beta_{\phi \text{ min}}$  will degrade below some value  $\alpha$  after being exposed to a neutron fluence of  $\epsilon$ . This expression is given by:

$$P(\beta_{\phi \text{ min}} \leq \alpha) = F \left( \frac{-\ln(\frac{\beta_0 \text{ min}}{\alpha} - 1) - \ln(\frac{f_T \text{ min}}{\beta_0 \text{ min}}) + m}{\sigma} \right) \quad (12)$$

- where  $\beta_0 \text{ min}$  = manufacturer's minimum specified value of  $\beta$
- $f_T \text{ min}$  = manufacturer's minimum specified value of  $f_T$
- $\epsilon$  = neutron fluence
- m = mean value of  $\ln K$  and has a value of 16.36 at the lower 90% confidence bound for Si
- K = neutron damage constant
- $\sigma^2$  = the variance of the variable  $\ln K$  and has a value of 0.444 at the lower 90% confidence bound for Si
- F = the cumulative normal distribution function

A detailed derivation of this equation would be out of place. However, it can be furnished if required. It can also be found in reference 65 and summarized in reference 65. In any case the use of this equation yields a probabilistic answer and takes into account the variation or uncertainty in K. The equation is still safe-sided since it uses manufacturer's minimum specification values of  $\beta_0$  and  $f_T$ . These, of course, do not correspond to an actual device but are derated from the lowest value of  $\beta$  and  $f_T$  which have been measured by the manufacturer (typical derating factors are 10 to 20%).<sup>86</sup>

A useful concept for designers is the circuit tolerance factor (C.T.F.). This quantity is defined as

$$C.T.F. = \frac{\beta_0 \text{ min}}{\beta_T}$$

where  $\beta_T$  is the threshold or minimum value of gain that the circuit requires for proper operation. In other words,  $\beta_T$  defines circuit failure and the C.T.F. is a measure of the design margin or the allowable degradation of the gain. Using this concept equation (12) becomes

$$P_F(\beta_0 \text{ min} \leq \beta_T) = F\left(\frac{-\ln((C.T.F.)-1)-\ln\left(\frac{f_T \text{ min}/\beta_0 \text{ min}}{\phi}\right)+m}{\sigma}\right) \quad (13)$$

where, of course,  $P_F$  is the probability of failure. A nomograph was created and is shown in Figure 56.<sup>65</sup> It should be noted that no distinction is made between p-n-p and n-p-n devices since both the nomograph and its generating equation (equation 12) were based on the distribution of K over all devices types. The nomograph uses the probability of survival,  $P_S$ , which, of course, is simply  $1-P_F$ .

There are many ways this nomograph can be used. Essentially, two of the three quantities; C.T.F.,  $(f_T \text{ min}/\beta_0 \text{ min})/\phi$ , and  $P_S(c)$ ; are either known or assumed, are connected by a straight line, and the third is then determined by the intersection of the line with the remaining axis. Figure 56 is an example of its use. For this case a C.T.F. of 2 and a  $P_S$  of .99 was assumed. If the

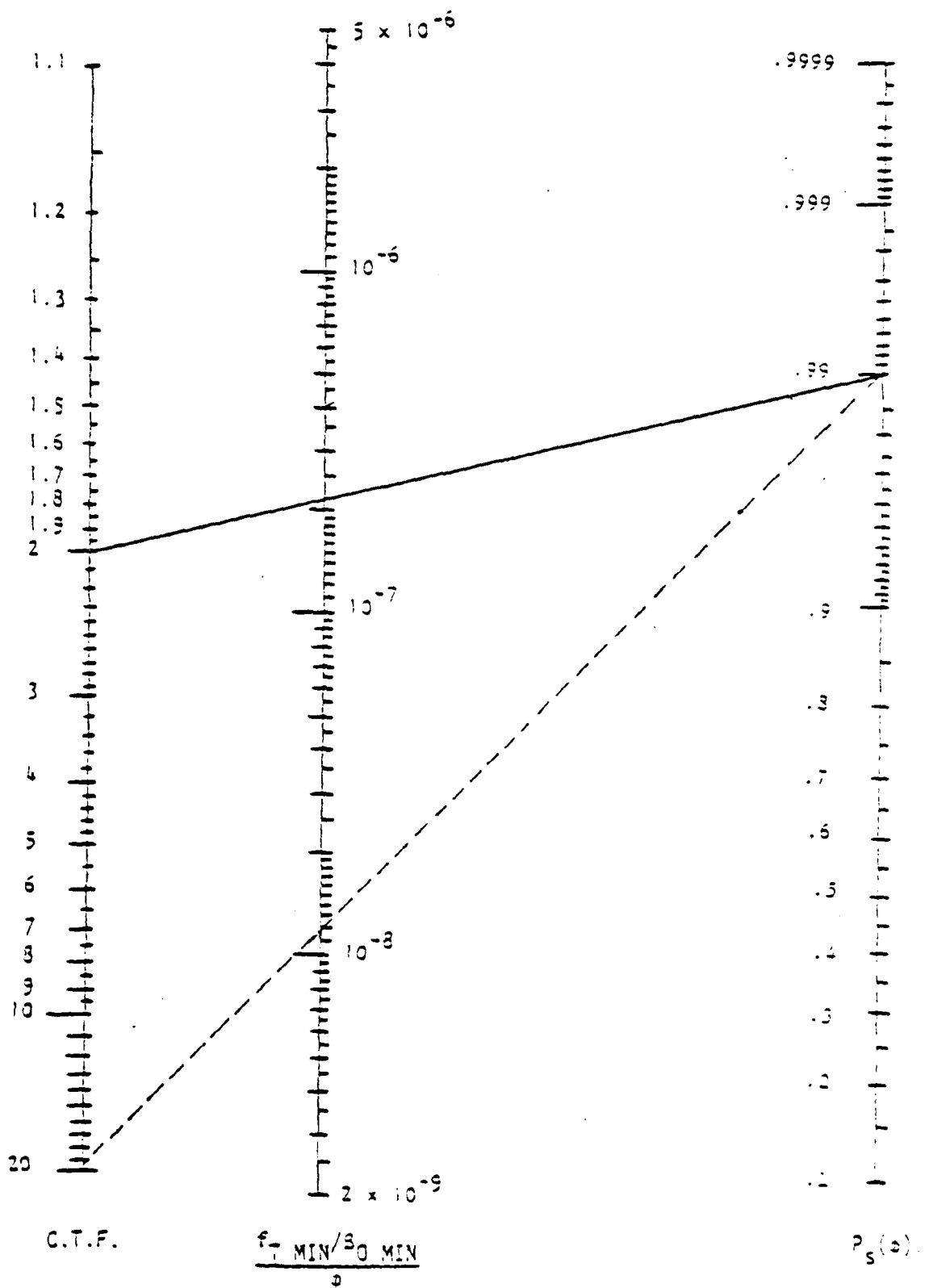


Figure 56. Silicon Transistor Nomogram Treating the Neutron Damage Constant as a Random Variable

circuit required a gain of 20 then, to achieve a C.T.F. of 2,  $S_0 \text{ min}$  would be required to be 4.0. According to the nomograph ( $f_T \text{ min}/S_0 \text{ min}$ )/c would be required to have a value of approximately  $2.2 \times 10^{-7}$  or  $f_T \text{ min}/c$  must have a value of  $8.8 \times 10^{-6}$ . At  $10^{14} \text{n/cm}^2$   $f_T \text{ min}$  must then be 880 MHz which is not an ordinary device. Of course it must be remembered that the use of manufacturer's minimum values yield a very conservative estimate of the maximum fluence that will still allow a given  $P_s$ . This fluence may be underestimated by a factor as great as 10 although factors of two to three are more common.<sup>86</sup>

It is very difficult to translate this underestimate into an impact on device parameter requirements used in the nomograph since this involves  $f_T \text{ min}/S_0 \text{ min}$ . However, the assumption that the failure fluence has been underestimated by a factor of 10 implies that the required value of  $f_T$  would be lower. This stems from the fact that  $f_T$  is proportional to the base width and the susceptibility of the device to neutron-induced degradation is dependent on the base width.

If the circuit is designed to be very tolerant of neutron-induced degradation then it obviously will have a much larger C.T.F.. For the same value of gain this translates into a lower required value of  $f_T \text{ min}$ . The situation is illustrated by the dashed line in Figure 56. For this case, with the same  $S_0 \text{ min}$  of 40 and a C.T.F. of 20 for an exposure to  $10^{14} \text{n/cm}^2$  the device would be required to have an  $f_T$  of 88 MHz in order to have a 99 percent probability of survival.

Of course this only applies to circuits containing one vulnerable transistor. In tactical scenarios where the threat levels are much lower this does not represent a serious constraint since many generic types can be considered invulnerable to these fluence levels. However, for strategic scenarios, this constraint assumes increasing importance. The solution to this problem rests upon the realization that the gains of any two transistors can be expressed in terms of the same random variable, K. For a circuit which contains two vulnerable transistors whose minimum output (M) can be expressed as the product of the gains of the devices within it this idea results in

$$M = S_{\phi_1} S_{\phi_2} = g(K) = \frac{f_{T_1} f_{T_2} S_{0_1} S_{0_2}}{(K S_{0_1} + f_{T_1})(K S_{0_2} + f_{T_2})} \quad (14)$$

where  $S_1$  is the gain of device 1 and  $S_2$  is the gain of device 2. This leads to an



expression for the probability that the circuit will survive a fluence  $\phi$  given by

$$P(B_1 B_2 \geq M) = F\left(\frac{-\ln u(M) + m}{\sigma}\right) \quad (15)$$

where  $B_{0i}$  = manufacturer's minimum specified gain for the  $i$ th generic device type

$B_{di}$  = gain of the  $i$ th device whose initial gain was  $B_{0i}$  after an exposure to a fluence  $\phi$

$$u(M) = -\frac{1}{2\phi} \left( \frac{f_{T_2}}{B_{02}} + \frac{f_{T_1}}{B_{01}} \right) + \frac{1}{2\phi} \sqrt{\left( \frac{f_{T_2}}{B_{02}} - \frac{f_{T_1}}{B_{01}} \right)^2 + \frac{4f_{T_1} f_{T_2}}{M}}$$

$m$  and  $\sigma$  are defined in equation (12)

$F$  = cumulative normal probability distribution.

The complete derivation of this equation is beyond the scope of this study. However, it can be found in reference 87. In addition, this reference also contains a more general form of this equation which utilizes a circuit output of the form

$$Z = AB_1 B_2 + B$$

where  $A$  and  $B$  are arbitrary constants. Both these forms are currently being used to assess the probability of survival of tactical systems.

Of course, since these equations are based on manufacturer's minimum specifications, they yield very conservative estimates of survival and, perhaps, are too conservative for BMDATC radar purposes. An expression that may be more suitable is based on radiation data. The form of the Messenger Spratt equation which is most suitable is given by equation 9 or

$$\frac{1}{B_d} - \frac{1}{B_0} = C \phi \quad (9)$$

Use of this equation leads to an expression for the probability of failure given by<sup>65</sup>

$$P(B_d \leq B_T) = F\left(\frac{\ln B_T + \pi_0 + \ln(A + b)}{\sigma_0}\right) \quad (16)$$

where

$\beta_T$  = minimum current gain which is required for proper circuit operation  
 $\beta_\phi$  = current gain after an exposure to a fluence of  $\phi$   
 $\phi$  = neutron fluence in 1 MeV equivalence

and  $\sigma_{\beta_0}$ ,  $m_0$ , and A are constants obtained from neutron effects data as shown below

$$\begin{aligned}\sigma_{\beta_0}^2 &= \ln\left(\frac{\sigma_{\beta_0}}{\mu_{\beta_0}}\right)^2 + 1 \\ m_0 &= \ln \mu_c - \frac{\sigma_{\beta_0}^2}{2} \\ A &= \frac{1}{\mu_c \mu_{\beta_0}} \left[ \frac{\sigma_{\beta_0}}{\left(\frac{\sigma_{\beta_0}}{\mu_{\beta_0}}\right)^2 + 1} \right]\end{aligned}$$

where

$\mu_{\beta_0}$  = estimated mean value of the current gain based on data  
 $\mu_c$  = estimated mean value of the neutron damage factor based on radiation data  
 $\sigma_{\beta_0}^2$  = estimated variance of the current gain based on data

Equation 16 can be readily modified to assess the survivability of a circuit containing two or more vulnerable transistors similar to the manner in which equation 13 was modified. This modification utilizes the fact that normal densities are closed under addition with the mean of the resulting density being the sum of the means of the individual densities and the variance being the sum of the variances.<sup>88</sup> Utilizing this idea, the probability of failure for a circuit whose output,  $y$ , can be expressed as the product of the gains of the devices within it is given by



$$P_F(y \leq M) = F\left(\frac{-\ln M + m_0}{\sigma_0}\right) \quad (17)$$

where

$$y = \prod_i^n b_i$$

$b_i$  = the gain of the  $i$  th device in the circuit after an exposure to a fluence  $\phi$

$$m_0 = \sum_i^n (m_{0i} + \ln(A_i + p))$$

$$\sigma_0^2 = \sum_i^n \sigma_{0i}^2$$

and  $m_{0i}$ ,  $A_i$ , and  $\sigma_{0i}^2$  are the parameters defined in equation 16 for the  $i$  th device.

This method, of course, is based on radiation test data and would tend to be less conservative than that based on manufacturer's minimum specifications. The predictions resulting from the two methods can vary widely. For the 2N2857 and a threshold gain of  $b_{0min}/2$  the ratio of the fluence associated with a probability of failure of 50 percent is 1.98 while for the 2N336 it is 32.1.<sup>89</sup>

It is difficult to say which model predicts failure more realistically. The model based on manufacturer's minimum specifications will, by definition, overestimate failure. However, the model based on radiation data has its faults also. The model predicts failure probabilities for a generic transistor type based on data which is usually taken on a small number of devices from that generic population. Unfortunately these devices usually come from the same manufacturer and the same diffusion lot. Consequently the data is not necessarily characteristic of either the total generic population or that portion of the population which would be used to build the system.

The problems arise from the attempt to apply subpopulation results to the total population. It is a consequence, primarily, of the nonrandom selection of the samples. Random selection means that all members of a population have an equal chance of selection. Since the selection is usually confined to one manufacturer and one diffusion lot, any prediction based on this data must be taken as being valid only for that particular subpopulation. Viewed in this light



the implication is that the prediction and confidence limits associated with the prediction have no absolute meaning when applied to the total population. Instead they must be used as indicators of possible problem areas.

Attempting to use data on one subpopulation to predict the response of the rest of the population can lead to over- or under-estimates of survival. The most serious of these is, of course, the overestimations. It has been found that survival can be overestimated by a factor as great as 17.4.<sup>90</sup>

The problem is further complicated by the fact that it is doubtful that the total population can ever be randomly sampled since this would entail sampling not only the present but also the past and future population. Messenger<sup>91</sup> has found that the neutron damage factors can vary by a factor of 8.1 for a captive line over a period of three years. Obviously it is not feasible to wait three years before being able to make a prediction of the radiation response of a generic type.

The question of the appropriate use of radiation data in generating a safe-sided estimate of the radiation response of the total population is still an active area for research. Various schemes have been proposed. One approach is to analyze the survivability of the circuit at  $\lambda$  times the threat fluence.<sup>92</sup> Acceptance decisions would then be based on the probability of survival at this higher fluence level. However, depending on the choice of  $\lambda$  this could lead to an overly safesided survival prediction at the actual threat level. Reference 90 indicated that the proper choice of  $\lambda$  will depend on the required survival probability and the threshold gain,  $\beta_T$ , of the circuit. The value of  $\lambda$  must be increased as  $\beta_T$  increases. However, a sensitivity analysis of the proper choice of  $\lambda$  versus  $\beta_T$  has not been performed so a general relationship between  $\lambda$  and  $\beta_T$  has not been established at this time.

Another approach to the problem of characterizing the total population's radiation response is to estimate and use parameters which pertain to the total population rather than the subpopulation. One approach of this nature developed in reference 89 consists of estimating the mean and variance of the gain and the damage factor based on manufacturer's specified maximum and minimum values of the device's parameters. In general, this method shows great promise but more studies must be performed before it can be safely applied.



The probability densities of the gain and the damage factor have been modified<sup>90,93</sup> in order to make these functions more realistic. Even with all of these modifications and approaches the problem of estimating the response of the total population to neutron irradiation is still unresolved. Perhaps this does not constitute a problem for SMDATC-radar. The number of systems that will be produced is very limited and they will be built from a very small portion of a device's total population. In addition it is true that the methods based on radiation data seem adequate in predicting the neutron response of the diffusion lot from which the samples were drawn. In addition, the method based on manufacturer's minimum specifications is always safe-sided. Thus, an approach based on a combination of the two methods can be developed to choose bipolar devices with the required probability of survival. The first step in such an approach would be to estimate the probability of survival based on manufacturer's minimum specifications. If this estimate is acceptable (e.g.  $P_s$  of .999 or greater) then there is no need to go further. If it is not acceptable then an attempt should be made to find a generic type which is. If this can not be done then several options are available. One consists of using manufacturer's minimum and maximum specifications to estimate the response of the total population. The other option is to radiate each diffusion lot in order to characterize not the total population but only that portion of the population from which systems will be built. If these less conservative estimates are still not acceptable then the circuit must be redesigned to incorporate a larger circuit tolerance factor. If this can not be done then shielding must be used to reduce the environment that the device will experience. It must be mentioned that because of the weight, volume, and cost penalties shielding against TRE and electromagnetic pulse (EMP) should be avoided whenever possible and can be justified only after all other approaches have been found to be unacceptable.

So much time and discussion has been devoted to neutron-induced gain degradation of bipolar transistors since this is the most mature assessment methodology. Basically the same approach has been used on other classes of devices and threat constituents. This consists of assuming a distribution for an operational parameter over the device's population. Experimental data is then used to establish a functional relationship between the radiation-in-



duced parameter degradation and the radiation level. The failure threshold value for the parameter is determined through detailed circuit analysis. These are combined in a probability equation that will allow the estimate of circuit failure as a function of threat level.

In addition the above discussion serves to illustrate some of the pitfalls associated with experimental data and testing. The variation in the radiation response within a piecepart population is amplified on the system and subsystem level. The more samples that are tested the better the estimate of the radiation response of the subpopulation from which they were drawn. However, the law of diminishing returns does apply here. Since the form of the distribution is known a sample size much greater than 10 will not provide much more additional information provided the samples were randomly drawn from the population that is being characterized. As with any statistical problem a great deal of care and caution must be devoted initially to defining the assumptions and definitions or the results may easily be misleading and misinterpreted. Random sampling is an absolute necessity. The degree of randomness must be maximized in order to insure the validity of the test results. Without random sampling it is better to have no data at all. Finally the above examples serve to illustrate the folly and danger in attempting to extend subpopulation test results to the whole population. References 90 and 92 demonstrated quite clearly that such attempts could lead a dangerous overestimate of survival. The total population from which a system is to be built must be randomly sampled in order for test results to have any applicability in a survivability assessment.

The above discussion focused on the gain degradation induced by exposure to neutrons. This should not be taken to mean that the gain is the only operational parameter which is affected. In fact, just the opposite is true. Many other transistor parameters which are of interest to a designer are also affected. However, these effects, in general, do not significantly change the operation of the device and are of secondary importance when compared to gain degradation. The exceptions to this statement include the collector resistance,  $r_{sc}$ ; the saturation voltage,  $V_{CEsat}$ ; the leakage currents,  $I_{EBO}$  and  $I_{CBO}$ ; and the collector emitter sustaining voltage,  $BV_{CEO}$ .



Saturation voltage changes resulting from neutron irradiation may be as important as gain changes especially in those applications requiring power transistors. A transistor is in saturation when both its emitter-base and collector-base junctions are forward-biased. For measurement of the saturation voltage, the collector current is constant and the saturation voltage is measured as a function of the base current or the forced beta,  $I_C/I_B$ . The voltage difference between the emitter and collector contacts is the saturation voltage designated as  $V_{CEsat}$ . This voltage has two components. The first one, called the junction saturation voltage,  $\Delta V_j$ , is the difference in the applied forward voltage at the two junctions or

$$\Delta V_j = V_{BE} - V_{BC}$$

The second component of the saturation voltage is the collector resistance component,  $V_R$ , due to the collector saturation current flowing through the collector bulk resistance,  $r_{sc}$ . The total saturation voltage is therefore

$$V_{CEsat} = \Delta V_j + V_R = (V_{BE} - V_{BC}) + I_C r_{sc}$$

The usual expression for the junction saturation derived by Ebers and Moll<sup>94</sup> in terms of the base and collector currents is given by:

$$V_{CEsat} = \pm \frac{kT}{q} \left[ \ln \left( \frac{\alpha_i (1 - \beta_F/\beta)}{(1 + \beta_F(1 - \alpha_i))} \right) \right] + I_C r_{sc}$$

where:  $\alpha_i$  = inverse common collector gain

$\beta$  = common emitter gain

$\beta_F$  = forced gain =  $\frac{I_C}{I_B}$

$I_C$  = terminal collector current

$I_B$  = terminal base current

$I_E$  = terminal emitter current

$k$  = Boltzmann's constant in eV/ $^0K$

$T$  = temperature in  $^0K$



The + sign is used for n-p-n transistors and the - sign for a p-n-p transistor. A different version of this equation is derived in reference 81 under slightly different assumptions but the two versions are in quantitative agreement. It should be noted that there is an error in the version of this equation in reference 85 in that the term  $(1 + \beta_F(1 - \alpha_I))$  is replaced by

$$\left( 1 + \frac{\beta_F}{(1 + \alpha_F)} \right)$$

The first term in the above equation is the junction saturation voltage and the second is, of course, the collector resistance component. As stated in the diode section, neutron damage causes a reduction in minority carrier lifetimes and carrier removal due to an increase in the density of recombination centers. This will occur in both the base and collector regions. In the base region the effect of displacement damage resulting from neutron irradiation is an increase in the base current required to drive the transistor into saturation. This is illustrated in Figure 57 for a 2N1613 transistor operating with an  $I_c$  of 100 mA after exposure.<sup>81</sup> After irradiation, about 24 mA of base current is required to drive the device into saturation.

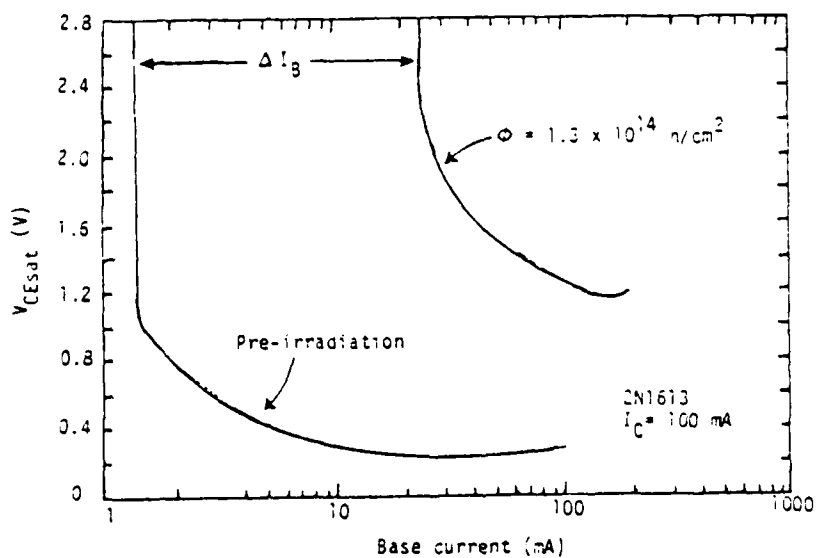


Figure 57. Change in Saturation Voltage with Neutron Irradiation

The most significant change in  $V_{CEsat}$  caused by neutron irradiation is that due to changes in the voltage drop across the collector bulk resistance,  $r_{sc}$ . The carrier removal effect results in effectively counterdoping all regions of the semiconductor.<sup>72</sup> One effect of this counterdoping is to increase the resistivity of the semiconductor. The increase in resistivity is especially pronounced in lightly doped regions simply because the carriers removed by neutron exposure is a greater percentage of the carrier concentrations in these regions than that which occurs in the more heavily doped regions. This is a serious problem for power transistors because the collector is lightly doped to obtain high breakdown voltage characteristics and the change in saturation voltage will be dominated by increases in the collector bulk resistance,  $r_{sc}$ .<sup>81</sup> The resulting increase in  $V_{CEsat}$  will require an increase in the power that needs to be dissipated or the transistor will suffer junction burnout.

Figure 58 is typical of the changes in  $V_{CEsat}$  as a function of neutron

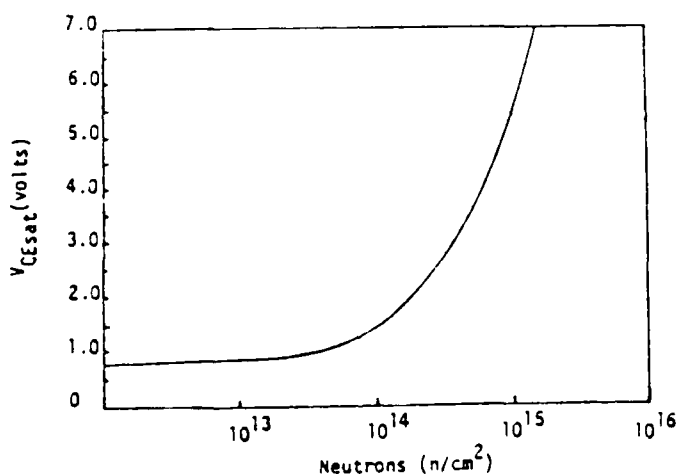


Figure 58. Saturation Voltage Versus Neutron Fluence for a 2N2907A Transistor and a Forced  $\beta$  of 10 with a  $I_c$  of 500 mA

fluence.<sup>1</sup> As is evident from this figure, the change is not linear with fluence. Table 32 lists the change in the saturation voltage due to exposure to neutron fluence for several common transistor types.<sup>64</sup> The large increase in the saturation voltage exhibited in Figures 57 and 58 and in the table is typical of nonepitaxial transistors with relatively low doping in the base region.



Table 32. Effects of Neutron Irradiation on Transistor's Saturation Voltage and Leakage Current

Class: Low Power

Type	Sample Size	Test Conditions			Saturation Voltage			Test Condition			Leakage Current			
		I <sub>B</sub> (mA)	I <sub>E</sub> (mA)	V <sub>Gsat</sub> (V)	V <sub>sat</sub> at 10 <sup>13</sup> n/cm <sup>2</sup>	V <sub>sat</sub> at p <sub>max</sub>	V <sub>GSat</sub> at V <sub>Coupe</sub>	V <sub>GSat</sub> at V <sub>GSat</sub>	I <sub>CE0</sub> (mA)	I <sub>CE0</sub> at t <sub>max</sub>	I <sub>CE0</sub> at t <sub>max</sub>	I <sub>CE0</sub> at t <sub>max</sub>		
2N335	10	0.20	1.20	.18	0.22	1.3	0.23	1.72	3.00	8.95E-7	1.3	1.15E-6	1.29	
2N397	10	20.0	120	.32	0.62	4.0	0.99	3.09	3.00	1.23E-7	4.00	3.39E-6	25.7	
2N3412*	>20	0.01	0.01	.095	-	2.18	0.94	9.98	0.70	3.64E-5	0.35	5.04E-5	1.39	
2N3834	20	0.33	1.33	0.20	0.073	3.7	0.032	1.6	3.00	7.93E-10	3.70	2.05E-10	0.27	
2N4126	10	0.33	1.33	.021	0.931	4.2	0.13	9.05	10.0	4.79E-7	42.0	6.43E-6	1.50	
Class: Switching		10	10.0	.260	.25	0.408	3.7	0.538	2.14	28.0	4.60E-7	3.7	1.99E-6	4.33
2N3222A	5	0.01	0.11	.70	0.21	11.0	1.43	7.16	10.0	9.70E-5	11.0	1.67E-4	1.87	
2N369A	5	3.33	13.3	.026	0.941	89.0	8.91	362.7	10.0	3.30E-7	89.0	7.63E-4	17.94	
2N3905	>20	6.00	36.0	.13	-	3.20	0.29	1.50	15.0	5.61E-9	32.0	5.18E-6	0.97	
2N3911	>20	9.00	36.0	.12	-	20.9	0.11	1.55	10.0	1.56E-6	20.0	1.62E-6	1.04	
2N4258	9	0.20	1.20	.071	-	-	-	-	-	-	-	-	-	
Class: High Power		10	100	400	.051	-	6.2	9.99	115.3	50.0	4.13E-7	6.2	1.16E-6	3.64
2N1495	10	333	1333	.20	0.23	1.0	3.77	18.9	5.0	8.04E-6	18.0	1.92E-4	24.6	
2N2860	10	10.0	40.0	.014	0.004	11.0	7.41	5.03	7.0	3.40E-9	12.0	5.81E-7	1.7	
2N3421	13	3.33	13.3	.011	-	15.0	7.03	194.6	19.0	1.33E-6	1.50	2.53E-4	17.9	
2N3553	5	3.33	13.3	.020	1.2	.015	.11	4.96	4.0	6.01E-7	10.0	9.70E-5	4.4	
2N3576	9	5.0	15.0	.042	21.6	1.1	6.3	111.4	-	-	-	-	-	
2N4011	10	5.0	15.0	.042	21.6	1.1	6.3	111.4	-	-	-	-	-	
2N3235	19	3.33	13.3	.688	0.11	0.10	1.13	3.43	6.0	6.01E-6	64.0	2.00E-4	41.1	
2N3160	5	0.50	5.5	.078	-	33.0	5.91	1.07	10.0	1.00E-7	13.0	2.44E-6	1.0	
1NPT4	10	34.3	53.3	.11	14.7	1.7	16.7	14.7	-	-	-	-	-	
1NPT6*	>20	100.0	1100	.38	-	1.6	9.14	12.1	10.0	4.00E-10	18.0	3.29E-8	59.4	
1N4749*	20	100.0	385.0	.081	-	21.0	6.03	1.03	1.0	1.00E-7	21.0	4.12E-7	2.0	

\*These devices have been saturated for particular drive conditions. Do not use saturation data with the system may be saturated. Information for these devices, the time of irradiation, or a detailed history of the device is not available. It must be considered that damage to these devices is guaranteed under standard operating conditions, and no guarantee is given that they may not perform as the data indicate.



The discussion serves as a basis for the formation of several design guidelines. For saturated operation, only epitaxial transistors should be used. Circuits should be designed to tolerate low breakdown voltage transistors which, of course, means using transistors with heavier doped collector regions.<sup>95,96,97</sup> This, however, cannot be done independent of reliability considerations. The maximum practical base current should be used for transistors required to operate in saturation. This will allow for the neutron-induced increase in the base current required to drive the transistor into saturation. Similarly, transistors with low  $V_{CEsat}$  and  $V_{BEsat}$  should be chosen to allow for neutron-induced increases. In addition, since  $V_{CEsat}$  increases as  $I_C$  increases, one hardening technique is to minimize  $I_C$ .

However, this is counter to the earlier recommendation of biasing the device so that it operates at or slightly below its maximum gain. Minimizing  $I_C$  will maximize the device's gain degradation. The recommended procedure will depend on the application and whether  $V_{CEsat}$  or the gain is more important for that application. In addition, power transistors are quite often used as series regulators of power supplies and, since power supplies have given current requirements, it may not be possible to lower  $I_C$ . In these cases it may be necessary to parallel two or more series regulator transistors.<sup>98</sup> Finally, it is important to minimize the requirements for ultrastable voltages, currents, and frequencies.<sup>83</sup> Since neutron degradation of device characteristics is primarily a gradual change, the larger the tolerance in parameters such as current, voltage, and frequency, the greater will be the neutron fluence required to cause circuit failure.

Table 32 also contains data on the effects of neutron irradiation on leakage current. Junction leakage is assumed to result from carrier generation-recombination centers in the depletion layer. As the number of these centers increases due to neutron displacement the leakage current will increase proportionately. Figure 59 depicts the variation of  $I_{CBO}$  as a function of neutron fluence.<sup>81</sup> This indicates that  $I_{CBO}$  varies linearly with fluence and displacement is the dominant damage mechanism.<sup>81</sup> However, as evident in this figure and in Table 32, the leakage current is typically in the microamp range and currents of this magnitude, even after neutron irradiation, generally will not pose a design problem.<sup>2</sup>



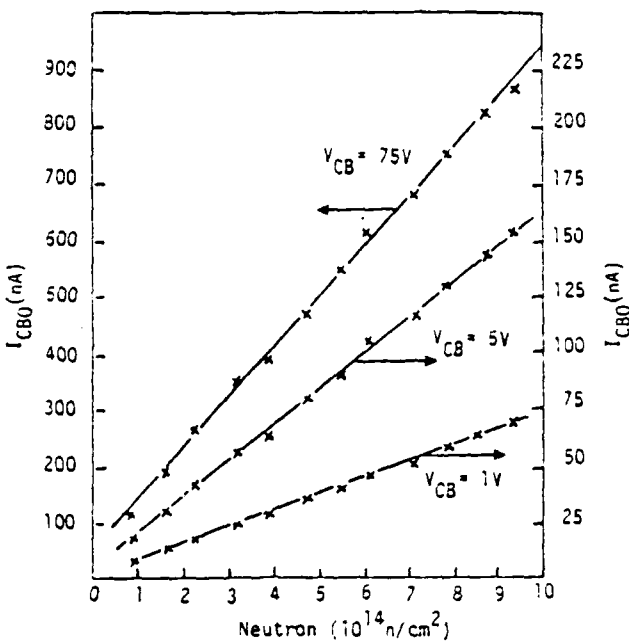


Figure 59. Leakage Current as a Function of Neutron Fluence for a 2N1613 Transistor

Changes in breakdown voltages are important design parameters for power transistors. The maximum reverse-biasing voltage which may be applied before breakdown between the collector and base terminals of the transistor, under the condition that the emitter lead be open-circuited, is represented by the symbol  $BV_{CBO}$ . Breakdown occurs because of avalanche multiplication of the current  $I_{CBO}$  that crosses the collector junction. At high enough voltages, namely  $BV_{CBO}$ , the multiplication factor becomes nominally infinite and the region of breakdown is then attained. The current rises abruptly and large changes in current accompany small changes in applied voltage.

$BV_{CBO}$  is determined in part by the doping or impurity concentration on the more lightly doped side of the junction. The dependence of the breakdown voltage on the doping levels for both a step and a graded junction is shown in Figure 60.<sup>81</sup> The linear grade constant,  $a$ , which appears in this figure is the proportionality constant in the approximation of the impurity concentration in a graded junction of the form

$$N(x) = a x$$

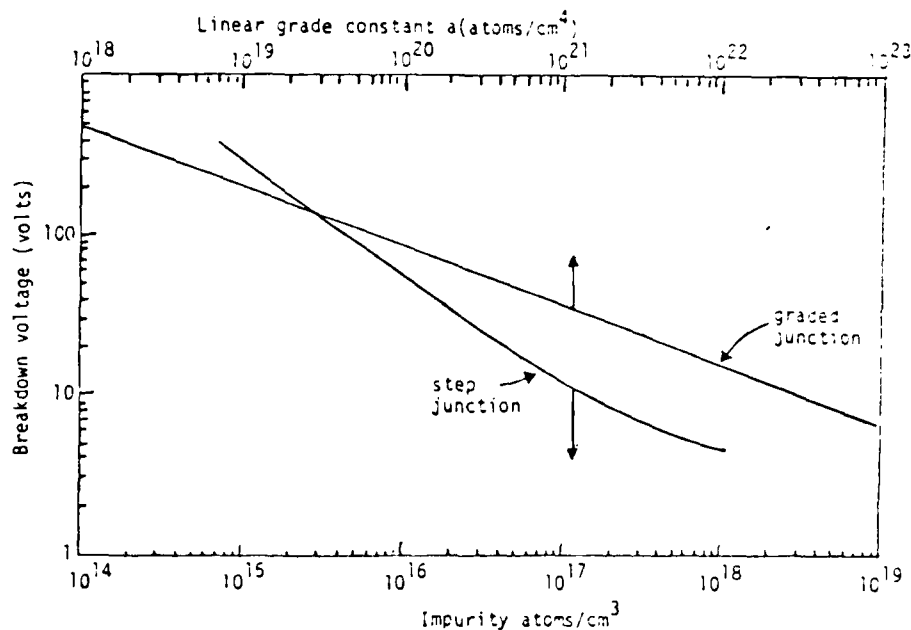


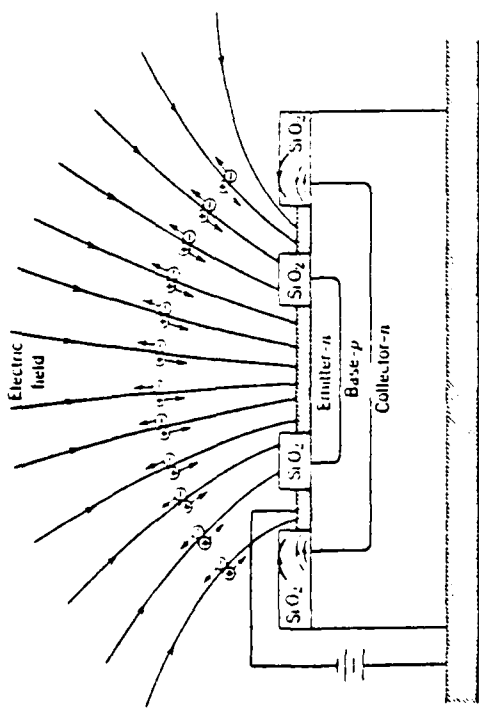
Figure 60. Avalanche Breakdown for pn Silicon Junction

where  $N$  is the impurity concentration at a particular distance,  $x$ , from the edge of the junction. As indicated in this figure the breakdown voltage increases with decreasing impurity concentration. Since one of the effects of neutron irradiation is carrier removal which lowers the effective doping level,<sup>72</sup> the breakdown voltage increases with neutron fluence.

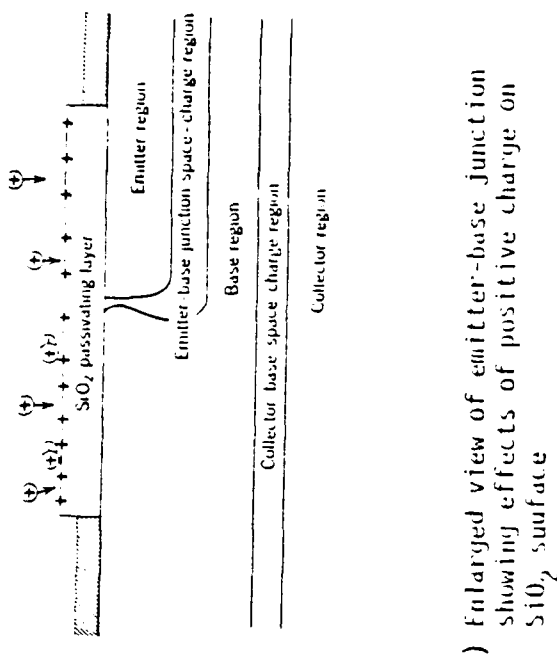
Usually, a more important breakdown voltage for transistors is the collector-emitter breakdown or sustaining voltage with the base open,  $BV_{CEO}$ . This voltage is related to the collector-base breakdown voltage by<sup>62</sup>

$$BV_{CEO} = \frac{BV_{CBO}}{(\beta)^{1/n}}$$

where  $\beta$  is the common base gain and  $n$  is an empirical fitting constant varying from 2 to 6.<sup>81</sup> As indicated by this equation, the increase in  $BV_{CEO}$  resulting from displacement damage is larger than that in  $BV_{CBO}$  due to the neutron-induced gain degradation. In any case, neutron irradiation causes all of the breakdown voltages to increase which is beneficial and will not result in device failure.



a) Electric fields for  $n-p-n$  transistor that cause deposition of charge on  $\text{SiO}_2$  surface



b) Enlarged view of emitter-base junction showing effects of positive charge on  $\text{SiO}_2$  surface

Figure 61. Dose Effects on  $n-p-n$  Transistor

Volume I covering the threat levels indicates that the nuclear environment that the radar will experience will be very stressing. These high radiation levels will impose a higher cost of radiation hardening if for no other reason than the effects of some of the threat constituents can no longer be ignored. The effects of total dose on bipolar transistors is a good example of this. In tactical scenarios bipolar devices are considered invulnerable to total dose exposure. However, this is not true for strategic scenarios. The damage threshold for bipolar devices is somewhere between  $10^4$  and  $10^5$  rad (Si).<sup>1,81,84,99,100</sup> In fact this range of thresholds is so well documented that the five cited references must be taken as a representative list rather than one that even approximates an exhaustive one.

For bipolar transistors total dose primarily causes an increase in the leakage currents and a degradation in the gain with the gain degradation being the most important. Several mechanisms are responsible for this degradation. One of these is the ionization of the gas in the transistor can. This results in the deposition of positive charge on the silicon dioxide when an electric field is applied between the transistor and the can.<sup>81</sup> Figure 61 illustrates this situation for an npn transistor.<sup>81</sup> In addition, the total dose irradiation produces ionization within the  $\text{SiO}_2$  layer itself. The electrons released during this ionization are more mobile than the ions or holes and some of them are swept out leaving behind the positive charged holes. All of these positive charges (those deposited on the surface of the  $\text{SiO}_2$  and those created by the ionization of the  $\text{SiO}_2$  itself) tend to migrate to the silicon-silicon dioxide interface and can significantly alter the potential at this interface.<sup>101,102</sup> Essentially a channel or an inversion layer is formed in the silicon as depicted in Figure 62.<sup>81</sup>

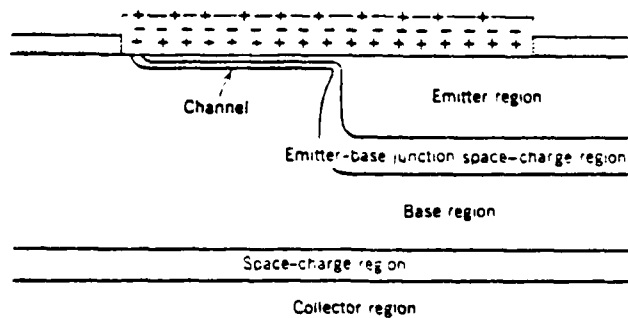


Figure 62. The Creation of a Channel in the Base Region Due to the Migration of Positive Charge to the Silicon-Silicon Dioxide Interface



As the ionization continues, electrons generated in the silicon by the radiation have enough energy to cross the interface and neutralize some of the positive charge that has migrated to the interface. This neutralization of the positive charge causes the channel to recede<sup>97</sup> as shown in Figure 63.<sup>81</sup>

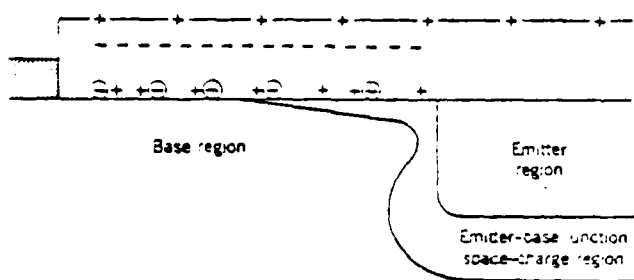


Figure 63. The Emitter-Base Junction After the Channel has Receded

Table 33 lists the total dose response of a number of transistor types.<sup>64</sup> This data should be used only as an indicator of the susceptibility of the devices. The dose response of a device is very sensitive to the oxide growth conditions and can vary widely even for devices produced by the same manufacturer. Table 33 also indicates the dependence of the gain degradation on collector current ( $I_C$ ). The degradation is greatest for transistors which are operated at low collector currents. At these low values of  $I_C$ , the gain is primarily due to surface currents which are sensitive to surface contaminants such as traps. Thus, low current, high gain transistors are particularly vulnerable to total dose effects.

The implication of the data in Table 33 is that bipolar devices cannot be considered invulnerable to total dose effects of  $10^5$  rad(Si) or greater. Degradation of 20% is not that uncommon even for normal  $I_C$  values. It must be also be remembered that the gain will also be degraded by neutrons. The total dose-induced degradation is due to surface damage and the neutron-induced degradation is due to bulk damage. The gain degradation due to total dose exposure can be considered independent of that due to neutron-induced damage.<sup>103</sup> The total damage is the sum of that caused by neutrons plus that caused by total dose with no synergistic effect. The neutron-induced degradation will, in most cases, be the greater component but the dose-induced degradation cannot be ignored.



Table 33. Total Dose Induced Gain Degradation (Average)  
in Irradiated Active Transistors with  
 $V_{CE} = 2$  v.; Sample Size = 10

Type	Measurement $I_c$ (mA)	Average Gain		
		0 rads(Si)	$10^5$ rads(Si)	$10^6$ rads(Si)
2N2222A	5	103	52.3	36.3
	50	109	36.5	56.4
2N2484	0.02	175	69.1	31.3
	1	348	221	148
2N2658	5	147	60	29
	500	225	181	138
2N2946A	1	188	145	42.8
	10	146	124	56.3
2N3019	10	116	39.9	59.9
	50	135	123	92.3
2N3553	10	20.2	15.3	9.22
	100	35	29.9	20.7
2N3752	100	117	87.4	78.5
	1000	97.4	89.5	76.9
2N5090	2	51.5	43.5	26.7
	10	62.5	54.3	36.6
2N5470	5	57.1	41	28.5
	50	63.1	45.5	35.9
2N6267	10	49.7	35.3	13.7
	100	53.3	41.5	20.9

Table 34. Effects of Total Dose Exposure on Transistor's Saturation Voltage and Leakage Current

Class: Lower Power

Type	Sample Size	Test Conditions		Saturation Voltage		Test Conditions	Leakage Current	
		I <sub>B</sub> (mA)	I <sub>C</sub> (mA)	V <sub>CBsat</sub> at 10 <sup>3</sup> rad(SI)	V <sub>CBsat</sub> at Max Dose rad(SI)		Pre-test V <sub>CE</sub> (V)	Max Dose rad(SI)
2N697	11	1.00	10.0	.13	.14	.14	1.00	-
2N1711	15	3.33	10.0	.0349	-	6.0E-4	1.34E-9	5.0E-4
2N2222	9	0.10	1.0	.0302	.042	8.6E-4	1.09	3.1E-10
2N2094	16	0.33	1.0	.0213	-	1.1E-3	.0225	1.06
2N2916A	10	2.0	20.0	.0212	.0408	1.5E-7	.0908	3.34

Class: Switch

Type	Sample Size	Test Conditions		Saturation Voltage		Test Conditions	Leakage Current	
		I <sub>B</sub> (mA)	I <sub>C</sub> (mA)	V <sub>CBsat</sub> at 10 <sup>3</sup> rad(SI)	V <sub>CBsat</sub> at Max Dose rad(SI)		Pre-test V <sub>CE</sub> (V)	Max Dose rad(SI)
2N2369	15	0.33	1.0	.12	-	1.3E-5	.12	1.00
2N2094	15	0.33	1.0	.0213	-	1.1E-5	.0225	1.06
2N3552	15	10.0	100.0	.0115	-	1.2E-5	.0366	1.16
1N2220*	10	1.0	10.0	.17	-	6.1E-4	.18	1.06
16730*	10	20.0	100.0	.15	.16	1.0E-5	.16	1.07

Class: High Power

Type	Sample Size	Test Conditions		Saturation Voltage		Test Conditions	Leakage Current	
		I <sub>B</sub> (mA)	I <sub>C</sub> (mA)	V <sub>CBsat</sub> at 10 <sup>3</sup> rad(SI)	V <sub>CBsat</sub> at Max Dose rad(SI)		Pre-test V <sub>CE</sub> (V)	Max Dose rad(SI)
2N1481	14	33.3	100.0	.04979	-	3.0E-4	.0401	1.00
2N2650	5	0.05	0.5	.25	.1E-7	.30	1.20	45.0
2N1421	10	10.0	30.0	.0104	-	6.1E-4	.0217	1.18
2N3501	4	3.33	10.0	.0403	-	1.0E-5	.0439	1.09
164749*	20	35.0	350.0	.0047	.0067	1.0E-6	.0949	1.12

\*These devices have been manufactured for particular defense systems and the identification of the nuclear vulnerability data with the system may be classified information. For these devices, the type number of a similar commercial device is given whenever possible. It must be remembered that defense system parts are manufactured under stringent quality assurance and control conditions, and commercial devices listed as equivalent types may not perform as the data indicates.

\*This rating is typical.

This device is also used for a low-powered switch.

Like the gain, total dose also impacts  $V_{CEsat}$  and the leakage current. The same mechanisms which cause the gain degradation also cause the impact on  $V_{CEsat}$  and the leakage current, i.e., formation of an inversion layer. Typical variations in  $V_{CEsat}$  due to total dose exposure are shown in Figure 64<sup>104</sup> and Table 34.<sup>64</sup> As

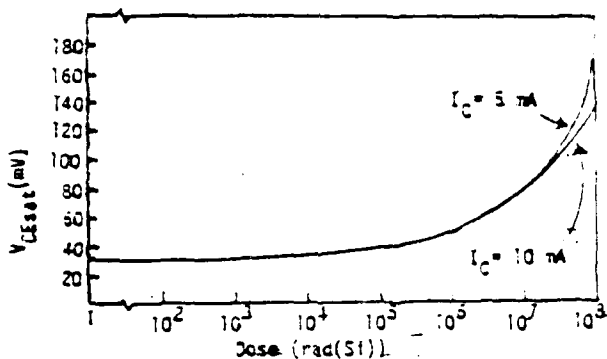


Figure 64.  $V_{CEsat}$  versus Dose for the 2N3752

indicated in this figure, the dose-induced change in  $V_{CEsat}$  is a function of  $I_C$ . However, as also indicated in the figure and in the table, these changes are usually minor compared to degradation in  $\beta$ .<sup>1</sup>

The leakage current,  $I_{CBO}$ , is also affected by exposure to total dose. The general tendency is for  $I_{CBO}$  to increase initially for low values of total dose and then decrease for higher values of the dose. This can probably be attributed to the formation of the channel or inversion layer depicted in Figure 62 and then, with increasing dose, the recession of the layer illustrated in Figure 63. However, there is considerable variation in the total dose response of transistors. This applies even to devices of the same type as shown in Figure 65.<sup>81</sup> The response of device 2 is more typical of most transistors of this type while device 1 has leakage of about two orders of magnitude greater at low exposures where channeling is a more significant damage mechanism. The very large difference in behavior is attributed to local defect sites contacted by the channel.



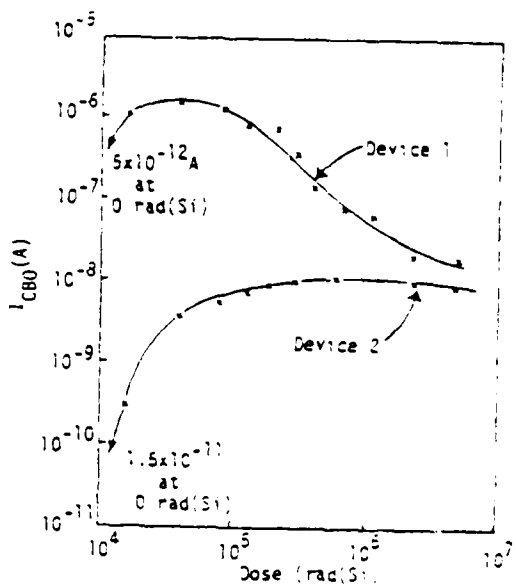


Figure 65. Variation in  $I_{CBO}$  for two 2N1613 Transistors as a Function of Total Dose Exposure

As evident from the figure and Table 34, the effects of total dose on the junction leakage of planar transistors is generally very large on a percentage basis. However, on an absolute current basis, the leakage current is still fairly small. As indicated by the table,  $I_{CBO}$  seldom exceeded a milliamp and this occurred only after an exposure to the very high level of  $1.5 \times 10^7$  rad(Si). Generally, the increase in leakage current is not significant in most circuit applications.

Up to this point, the impact of dose rate on the operations of a transistor has not been addressed. This is not to say that this threat constituent is not important. Quite the contrary is true for this constituent is one of the major sources of catastrophic failure. The problems arise from the dose rate induced photocurrents. As mentioned in the section on diodes, a dose rate of 1 rad(Si)/sec generates  $4 \times 10^{13}$  carriers/cm<sup>3</sup>-sec. In transistors these carriers are swept across the p-n junction in the same manner as within a diode. However, with transistors, the geometry and the interactions between the different regions (collector, emitter, and base) make the situation more complex.

Consider the schematic transistor depicted in Figure 66. Holes and electrons are produced uniformly throughout the silicon. Since the electric



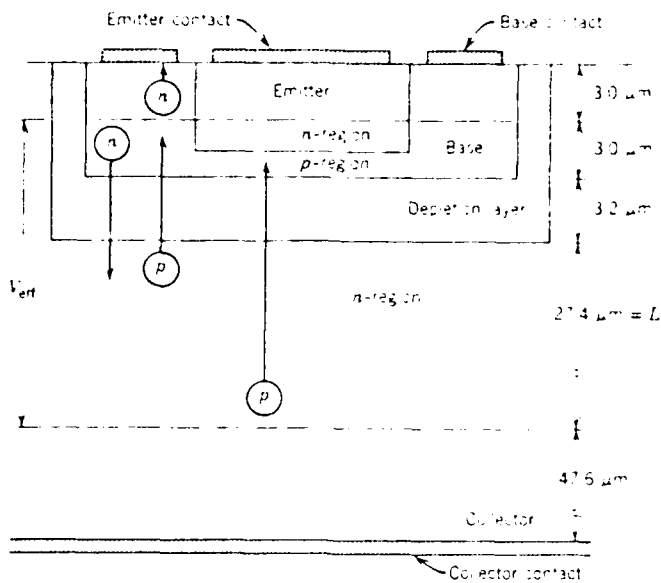


Figure 66. The Flow of Minority Carriers Producing Primary Photocurrents in an npn Transistor

fields at the junctions are in a direction to keep the majority carriers from flowing across the junction, these carriers remain in the region in which they were generated. However, the minority carriers in the vicinity of a junction will be swept across the junction which results in a current in the emitter-base or collector-base circuits. The term primary photocurrent ( $I_{pp}$ ) applies to the current flow across the junctions which is the result of actual carriers generated by the radiation.  $I_{pp}$ , of course, will be amplified by the inherent gain of the device. The term secondary photocurrent ( $I_{sp}$ ) applies to the current which flows out of a transistor as a result of dose rate exposure. There is some disagreement in the literature over the exact definition of  $I_{sp}$ . References 2 and 81 define  $I_{sp}$  as the primary photocurrent plus any additional current that flows due to carrier multiplication by transistor action. References 1 and 105 define  $I_{sp}$  simply as  $I_{pp}$  times the gain of the transistor. However, the two are essentially in agreement with one another since the approximation

$$I_{sp} = (1 + \beta) I_{pp} \approx \beta I_{pp}$$

is valid for any realistic value of  $\beta$ .

The effective volume for the collection of generated carriers is shown between the dashed lines in Figure 66.<sup>72</sup> Carriers generated above the upper line will diffuse to the surface where they will recombine and therefore will



not contribute to the photocurrent. Carriers generated below the lower dashed line are too far from the collector-base junction to diffuse to the junction before recombining since the mean distance for minority carrier diffusion is a diffusion length,  $L$ . When exposed to ionizing radiation, photocurrents are produced at both the base-collector junction and the base-emitter junction. The magnitude of each photocurrent component is directly proportional to the volume of the region contributing to the photocurrent. Since the base-emitter junction is geometrically smaller, the base-emitter photocurrent is usually much smaller than the base-collector photocurrent and is often ignored.<sup>85,106</sup> The photocurrent at the base-collector junction will consist of a prompt component that is made up of pairs generated within the depletion layer and a delayed component of minority electrons and holes generated one diffusion length away from the edge of the depletion region.

Table 35<sup>64</sup> lists the primary photocurrents induced in typical transistors as a result of various levels of dose rate. As indicated in this table  $I_{pp}$  can vary from millamps to tens of amps. Currents of this magnitude are of obvious concern and provide the incentive to examine their generation in more detail as well as methods for estimating their values. Utilizing the ideas of the previous paragraph leads to an expression for the steady-state primary photocurrent that flows across any p-n junction which is given by

$$I_{pp} = qg_0 V_{eff}\dot{\gamma}$$

where  $q$  = the electronic charge

$g_0$  = the carrier generation rate conversion factor  
 $= 4 \times 10^{13}$  carriers-sec/cm<sup>2</sup>-rad (Si)

$V_{eff}$  = effective volume from which all the generated carriers  
 can drift or diffuse to the junction before recombining

$\dot{\gamma}$  = dose rate in rad (Si)

The determination of  $V_{eff}$  is difficult and limits the usefulness of this equation. There are several methods which have been developed to predict  $V_{eff}$  by measuring certain electrical transistor parameters and relating them to physical and geometrical parameters. Generally this will allow the prediction of  $I_{pp}$  to within a factor of 2. These methods may include the determination of the collector-base junction area, the depletion layer width, diffusion length,



Table 35. Dose Rate Response of Typical Transistors

Class:	Low Power			Test Width ( $\mu$ sec)	Number of Points	Dose Rate Range		1 pp (mA) Avg	Relax Time ( $\mu$ sec)
	Type	Sample Size	Test Conditions $V_R$ (V)			Min	Max		
2N697	6	6.00	4.0	6	12	1.00E8	1.00E8	6.20	13.0
2N329A	12	6.00	4.0	6	12	1.00E8	1.00E8	22.1	53.0
2N1613	6	10.00	4.0	6	12	1.00E8	1.00E8	7.55	8.60
2N1132	6	6.00	4.0	6	12	1.00E8	1.00E8	2.97	4.00
2N285L	2	80.00	.03	4	4	3.55E10	5.97E10	2500	10000
2N2907A	3	48.00	.03	2	2	5.10E10	5.17E10	1025	1800
2N3019	3	75.00	.03	2	2	1.45E11	1.56E11	3300	3400

Class: Switching

2N404	6	6.00	4.0	6	1.00E8	1.00E8	18.8	22.0	
2N914	5	32.00	.03	5	4.57E10	7.27E10	202	340	.27
2N1132A	2	40.00	.2	2	1.5E9	1.5E9	43.0	46.0	
2N285I	2	80.00	.03	4	3.55E10	5.97E10	9500	10000	.41
2N3599	3	50.00	.03	5	7.97E9	2.50E10	16800	23000	.25
2N4002	5	50.00	.03	5	1.02E11	1.30E11	33600	38000	.34

Class: High Power

2N1490	3	6.00	4.0	3	1.00E8	1.00E8	2133	2800	
2N1016B	2	80.00	.2	2	1.00E8	1.00E8	2000	2000	
2N2907A	3	48.00	.03	2	9.20E9	1.33E10	230	240	<PW
2N3467	2	32.00	.03	1	2.30E11	2.30E11	1100	1100	<PW
2N3499	2	80.00	.20	2	1.00E8	1.00E8	6.50	6.50	
2N3599	6	50.00	.03	1	5.83E10	5.83E10	32000	32000	
2N4002	5	20.00	.03	5	1.02E11	1.30E11	33600	38000	.46



and minority carrier lifetimes in the collector.<sup>83,107,108,109</sup> These are very costly and time consuming experiments and calculations. In addition, these methods require a number of sample devices which, for BMDATC radar systems, may not be available. However, a set of equations based on manufacturers' data sheets has been developed.<sup>110</sup> The equations differ slightly for switching and amplifier transistors, for npn and pnp transistors, and for different power ratings. The full set of these equations is listed in Table 36. In this table  $C_{CB}$  is the base-collector capacitance,  $V_{CB1}$  is the reverse bias voltage at which  $C_{CB}$  in the data sheet has been measured,  $C_{CB}$  is the measured capacitance,  $V_{CB2}$  is the reverse bias voltage during the irradiation, and  $V_{CBC}$  is the maximum allowable collector-base voltage (i.e. the collector-base breakdown voltage).

A comparison between the results of these equations and empirical data is shown in Figure 67.<sup>110</sup> These equations appear to give reasonable agreement with experimental results. However, the data in Figure 67 may be misleading. Some of the  $I_{pp}$  data was taken at lower dose rates and simply extrapolated to  $10^{10}$  rad (Si)/sec<sup>110</sup>, under the assumption that  $I_{pp}$  varies linearly with dose rates above  $10^8$  or  $10^9$  rad (Si)/sec. In fact, the primary photocurrent exhibits four basic regions with respect to dose rate: 1) linear with dose rate, 2) transition region between  $10^8$  and  $10^9$  rad (Si)/sec, 3) sublinear with dose rate, and 4) saturation. In some transistors the transition region is superlinear while in others it is sublinear.<sup>1,110</sup> Both types of reactions are shown in Figure 68.<sup>1</sup>

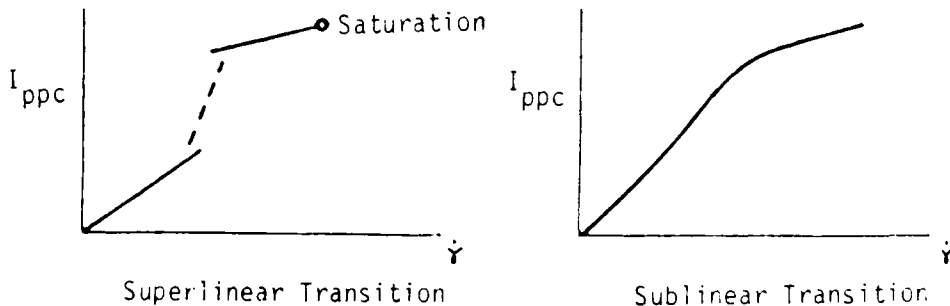


Figure 68. Characteristics of Primary Photocurrent Versus  $\gamma$

This behavior may be due in part to changes in the effective volume. For a transistor operating in the active region the effective volume  $V_{eff}$  for the collection of minority carriers is a function of the collector current since

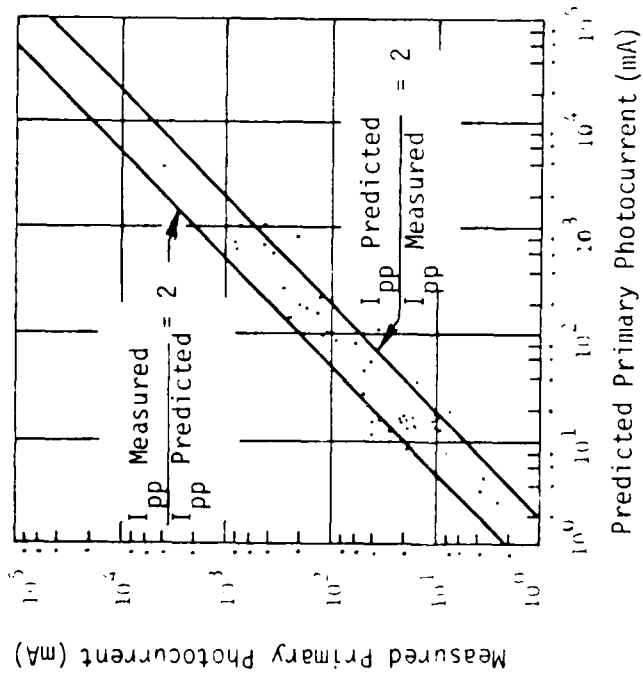
Table 36. Defining Equations

			Prediction Equation
Polarity	P <sub>D</sub> (Watts) (Note 1)	Type (Note 2)	I <sub>pp</sub> =
NPN	to 0.6	SW	$\dot{v}C_{CB1} V_{CB1} t_s^{1/3} \left( 6.47 + V_{CB2}^{1/3} \right)$
PNP	to 0.6	SW	Same as Above
NPN	0.8 to 1.0	SW	Same as Above
PNP	0.8 to 1.0	SW	Same as Above
NPN	2.0 and over	SW	Same as Above
PNP	2.0 and over	SW	Same as Above
NPN	A11	Amp	$\dot{v}f_T^{-2/5} V_{CBO} \left( C_{CB1} V_{CB1}^{1/3} + 1.08 \right) \left( 21.6 + V_{CB2}^{1/3} \right)$
PNP	A11	Amp	Same as Above

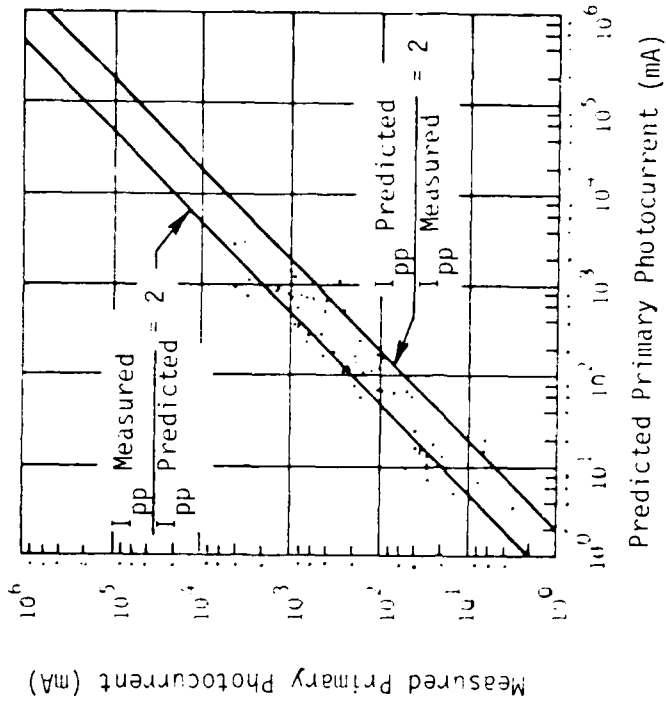
## NOTES:

1. Power Dissipation at T<sub>A</sub> = 25°C.
2. SW = Switching; Amp = Amplifier.
3. Units are mA, rad (Si)/s, pf, Volts, GHz, ns.
4. V<sub>CB1</sub> is voltage at which C<sub>CB1</sub> is specified.
5. V<sub>CB2</sub> is voltage at which device is to be operated.





(a) Predicted vs Measured Primary Photocurrents in  
Silicon Switching Transistors at  $10^{10}$   $\text{rad}(\text{Si})/\text{sec}$



(b) Predicted vs Measured Primary Photocurrents in  
Silicon Amplifier Transistors at  $10^{10}$   $\text{rad}(\text{Si})/\text{sec}$

Figure 67. Predicted Versus Measured Primary Photocurrents in Silicon  
Switching and Amplifier Transistors (After Notthoff,  
Reference III-2)



the collector current creates an electric field in the collector by flowing through the collector body resistance,  $r_{sc}$ .<sup>73</sup> However, the increase in the effective volume by the electric field in the collector is relatively unimportant for thin epitaxial transistors. This results from the fact that it is difficult for the added volume to penetrate the substrate because for epitaxial devices, the substrate has a short lifetime and diffusion lifetime. However, the effect should be taken into account for thick nonepitaxial collectors.<sup>81</sup>

The effective volume will also be influenced by the injection level. The injection level simply is the ratio of the minority carrier concentration to the impurity concentration. Low injection means the minority carrier concentration approaches that of the impurities. High injection will cause an electric field in the collector region that is in the direction to increase the effective area. The reasons for this are beyond the scope of and, perhaps, not pertinent to this study. It is sufficient to be aware that a transition from low injection to a high injection level will result in an increase in the effective volume and an increase in the photocurrent. Low levels of dose rate will cause a transition from a low injection to high injection level for devices that have low-doped collections.<sup>81</sup> Consequently devices with such collectors are more sensitive to dose rate.

It has been reported in reference 107 that the primary photocurrent variation as a function of junction voltage is in excess of that caused by variations in the effective volume. This voltage effect is not linear with radiation rates between  $1 \times 10^9$  rad (Si)/sec and  $5 \times 10^9$  rad (Si)/sec,<sup>81,111</sup> - essentially the transition region. No explanation for this nonlinear behavior has been formulated.

The primary photocurrent can, also, undergo a step increase as a function of dose rate. This is illustrated for a 2N915 transistor in Figure 69.<sup>81</sup> Similar behavior has been reported in reference 2, 113, and 114. In order to understand this behavior it must be kept in mind that what is of concern here is the primary not the secondary photocurrent. This simply means that the transistor must be "turned off". The desired situation is for the observed collector photocurrent to be equal to the primary photocurrent generated in the collector-base junction. This will be true only if the transient emitter voltage is zero. The best approximation to this results from shorting the external emitter and base terminals. For a shorted emitter, the transistor will turn on when the voltage drop across the internal base resistance is large enough to forward bias the emitter-base

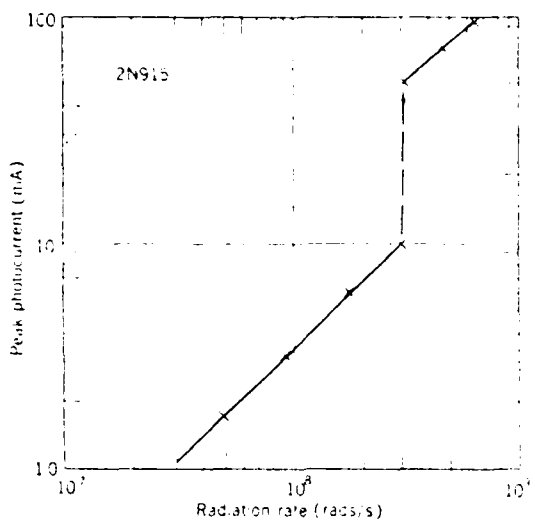


Figure 69. The Response of a 2N915 Transistor With an Open Emitter

junction to approximately 0.7V. Even with no external base resistance, that portion of the primary photocurrent flowing across the collector-base junction opposite the emitter can generate a substantial transverse voltage from the center of the emitter to the periphery due to the relatively high intrinsic base resistance. The explanation in reference 113 for the turn-on phenomenon for the case of the open emitter is that the voltages that build up across the emitter-base junction due to the flow of the primary photocurrent are large enough to exceed the breakdown voltage of the emitter-base junction. This junction breakdown essentially shorts the base and emitter and permits a large secondary photocurrent to flow due to the inherent gain of the transistor. The abrupt discontinuity is typical of high-resistivity collectors. The transition is more gradual in lower resistivity collectors which implies that devices with heavier doped collectors will be less sensitive to dose rate.

The secondary photocurrent in transistors is affected by internal base bulk resistance as well as the external circuit resistance connected to the base. In the simple transistor circuit of Figure 70, secondary photocurrents will not appear until turn-on or until the forward bias across the base-emitter junction reaches the cut-in voltage (.7V). This level for the circuit in Figure 70 is given by

$$i_{pp} \left( r_B + \frac{R_1 R_2}{R_1 + R_2} \right) = 0.7V$$

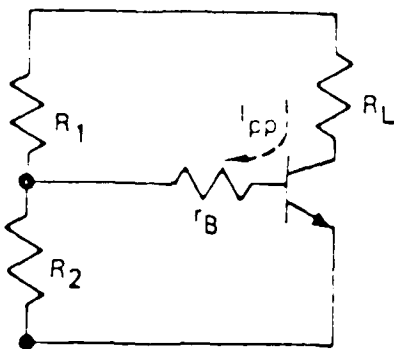


Figure 70. Photocurrent Compensation

This indicates that the base bulk resistance,  $r_B$ , can have a large impact on the turn-on threshold and also that because of  $r_B$  secondary photocurrents can occur even when the base is externally shorted to ground. For small area transistors,  $r_B$  is typically between 200-1000 ohms and for power transistors it is between 1-100 ohms.<sup>105</sup>

A common technique for mitigating the effects of the external resistor consists of connecting a compensation diode to the base of the transistor across the load resistor. This essentially removes the same amount of charge from the base region as flows into the base region as primary photocurrent. This is illustrated with two transistors in Figure 71.<sup>81</sup> The effectiveness of compensation is limited by photocurrent mismatch and by the base bulk resistance, which may cause turn-on of the internal junctions even with exact primary photocurrent matching. The photocurrent matching is dependant on the differences in the effective volumes of the transistors. If the effective volume of the compensating transistor is much larger than the original transistor, the net effect will be to turn a transistor off which should be on. Compensation works well for integrated circuits (ICs) since the collector-base diode of an adjacent transistor has essentially the same primary photocurrent and base bulk resistance. It is for this reason that the topic of compensation will also be discussed in Section 5.2 on ICs. It should be mentioned that compensation can help prevent secondary photocurrents by preventing the transistor from turning on but it will not reduce the primary photocurrents.

There is a second type of abrupt discontinuity in the collection current at high radiation rates which is due to second breakdown. This is a



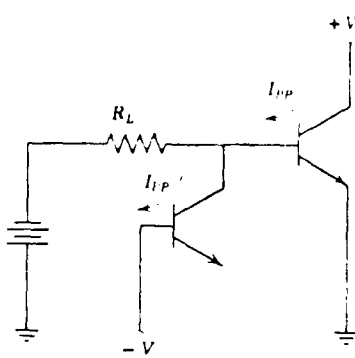


Figure 71. Photocurrent Compensation

very serious problem for power transistors. Second breakdown is a local thermal runaway effect at the junction which is induced by severe current concentration within the device.<sup>81</sup> A review of second breakdown in reference 115 distinguishes between two primary types of initiation of second breakdown: (1) thermally-induced second breakdown, and (2) current mode second breakdown. The damage mechanism appears to be localized heating<sup>116</sup> within the junction which results in the formation of hot spots and finally junction failure due to excessive current conduction over a portion of the junction area.<sup>117, 118</sup> Essentially, the problem results from power being dissipated within the junction. As a consequence of this dissipation, the junction temperature rises, and this, as a result of thermal generation, increases the current which results in a subsequent increase in power dissipation. If allowed to continue this self-heating phenomena will locally melt the silicon. The resolidified region at the junction results in decreased gain, decreased breakdown voltages, and a significant increase in junction leakage current.<sup>119</sup>

The effect was first reported in 1958.<sup>120</sup> A transistor was swept through its  $V_{CE}$  versus  $I_C$  characteristics as shown in Figure 72.<sup>81</sup> When the collector was allowed to increase to  $I_M$  the voltage suddenly dropped and the transistor was found either to be shorted between the emitter and the collector or to have reduced  $BV_{CEO}$ . The sudden decrease in voltage has been ascribed to a sudden drop in the effective resistance.<sup>121</sup> The decrease in voltage has been termed second breakdown. It should be noted that the V-I curve in Figure 72 is doubled valued - at relative low voltage either a very low or a very high current can be present. Under normal operating conditions the low-current state is maintained. The application of a relatively large voltage is required to initiate a breakdown before the low-voltage

*SA*

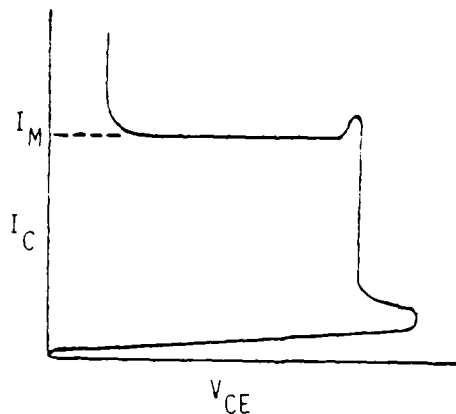


Figure 72. Second Breakdown for Typical Forward-Biased Transistor

high-current state is attained.<sup>122</sup>

It must be pointed out that second breakdown does not in itself cause failure. Devices have been placed in this second-breakdown state with sufficient current limiting to allow recovery without electrically measurable degradation. However, very little additional energy is required to cause the component to fail when in the second-breakdown state.<sup>123</sup> In many references second breakdown and failure are considered synonymous.

It has been noted that a transistor operating at a current and voltage large enough to cause second breakdown required a delay time before the transistor failed by second breakdown.<sup>124</sup> Since the phenomenon in most cases is thermal in origin, there is a finite amount of time required to raise the temperature of the small region of the transistor where breakdown takes place. The self-heating process proceeds until breakdown and has a typical time lag associated with it<sup>125</sup> indicating that energy dissipation is a factor.<sup>81</sup>

In any case, the possibility of second breakdown is enhanced by the choice of high frequency, narrow base width transistors, and represents an example where nuclear survivability must be traded against reliability. In addition to tradeoff problems, second breakdown itself constitutes a serious problem for applications in a nuclear radiation environment. Displacement damage resulting from exposure to a neutron fluence increases emitter crowding, decreases storage time, and increases the transistor fall time all of which favor the conditions for second breakdown. Furthermore, photocurrents resulting from dose rate can drive a transistor into regions where second breakdown can occur which, of course, can lead to burnout. Although it is not a subject for this project, it should be

mentioned that second breakdown constitutes one of the major EMP damage mechanisms for devices.

The previous discussion on dose rate effects has concentrated on the generation of steady-state photocurrents for exposure times that are long compared to the minority carrier lifetimes. There are two other situations which must be considered: 1) saturating photocurrent pulses due to a short, intense, radiation exposure and 2) nonsaturating photocurrent pulses resulting from a prompt gamma pulse. The saturating photocurrent, as was the case with steady-state photocurrents, can be determined from fairly simple hand calculations. However, a computer solution is usually required to determine the nonsaturating photocurrents as a function of time. The discussion will focus first on the saturating photocurrents.

A small prompt gamma pulse can drive a transistor into saturation because the number of carriers generated per rad is large and the pulse can be delivered in a time that is short compared to the minority carrier lifetime in the collector. A transistor driven into saturation will remain in saturation even after the radiation pulse has disappeared. The prolonged saturation time is called the radiation storage time,  $t_{sr}$ . This is the time required to reduce the excess carrier concentration after the gamma pulse to the concentration required to give the saturation current,  $I_{cs}$ . The radiation storage can be express as

$$t_{sr} = \tau \ln \frac{\Delta p(0)}{\Delta p(sat)}$$

where  $\Delta p(0)$  = excess carrier concentration after a pulse of  $\gamma$  rads.

$\Delta p(sat)$  = excess carrier concentration required to maintain saturation.

$\tau$  = minority carrier concentration in the collector.

The radiation storage time is a function of dose rate since  $\Delta p(0)$  is a function of dose rate. For a square radiation pulse  $\Delta p(0)$  is given by

$$\Delta p(0) = g_0 \gamma t (1 - \exp(-t_p/\tau))$$

where  $t_p$  is the radiation pulse width. For this case, the relationship between  $t_p$  and  $t_{sr}$  is depicted in Figure 73.<sup>126</sup> For dose rates greater than  $10^8$  rad (Si)/sec, reference 2 lists the following simplified expression for  $t_{sr}$

$$t_{sr} = .138 t_s \log_{10} \dot{\gamma}$$

where  $t_s$  is the transistor storage time. However, the note was also made that



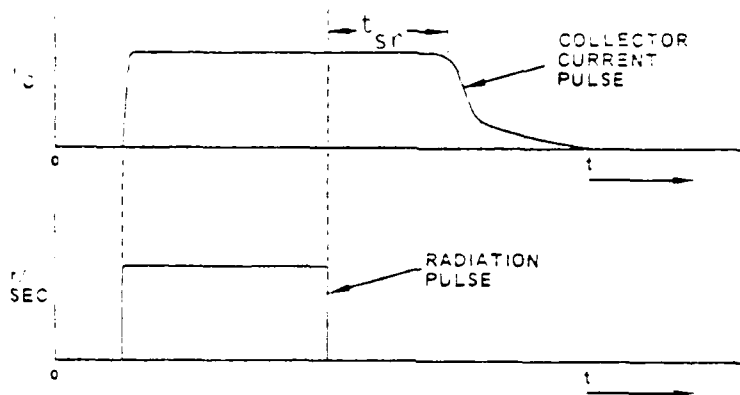


Figure 73. Relationship between  $t_p$  and  $t_{sr}$

this expression would yield values that may be high. In any case,  $t_{sr}$  will generally vary from  $10^{-5}$  to  $10^{-8}$  sec.

An expression for the primary photocurrent is given by<sup>1,81</sup>

$$I_{pp} = \frac{I_{CS} - I_B^3}{1 + 3}$$

where  $I_{CS}$  is the saturation collector current and  $I_B$  is the corresponding base current. The upper limit on  $I_{pp}$  is, of course,  $I_{CS}$  and this can be obtained from manufacturer's data sheets.

The last situation that must be discussed is the generation of nonsaturating photocurrents due to an exposure to a prompt gamma pulse. Essentially this situation corresponds to the transistor being in the active region. Besides defining the effective volume, the solution of the current as a function of time in this situation must account for the buildup of the primary photocurrent as a function of time and the charging of the emitter and collector capacitances and the base region by the primary photocurrents. Computer solutions are generally required to evaluate circuit operation in a transient radiation environment.<sup>73,83</sup>

For a step radiation pulse of magnitude  $\gamma$  and width  $t_p$ , the time response of the primary photocurrent is the sum of a prompt component coming from the volume of the base and the collector-base junction and a delayed component from the collector. As was the case with diodes, the delay in the current from the collector is the time required for carriers to diffuse to the collector-base junction. The expression for the primary photocurrent as a function of time for a square radiation pulse width,  $t_p$ , is<sup>81</sup>

$$I_{pp} = GA_c \left[ \left( x_c + \frac{r_j}{2} \right) + L_c \operatorname{erf} \left( \frac{t}{\tau} \right)^{\frac{1}{2}} \right] \quad \text{for } t < t_p \quad 18a.$$

$$I_{pp} = GA_c L_c \left[ \operatorname{erf} \left( \frac{t}{\tau} \right)^{\frac{1}{2}} - \operatorname{erf} \left( t - \frac{t_p}{\tau} \right)^{\frac{1}{2}} \right] \quad \text{for } t > t_p \quad 18b.$$

where  $G$  = bulk current generation rate =  $6.4 \mu\text{A}/\text{cm}^3\text{-rad(Si)}/\text{sec}$

$A_c$  = area of the collector

$L_c$  = minority carrier diffusion length in the collector

$x_c$  = width of the collector-base depletion layer

$r_j$  = base width

$\operatorname{erf}$  = error function

A typical transistor primary photocurrent for a radiation pulse width of approximately  $0.8\tau$  is depicted in Figure 74.<sup>81</sup>

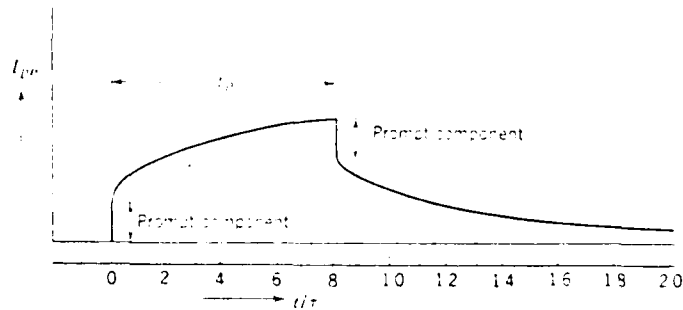


Figure 74. Typical Transistor Primary Photocurrent response to a Step Radiation Pulse with a Pulse Width of  $t_p$ .

The secondary photocurrent can be estimated by approximating the primary photocurrent with a step rise in photocurrent, equation 18, and

$$I_C = I_{CS} = \beta I_{pp} (1 - \exp(-t/\beta(t_b + 1.7R_L C_{TC}))$$

where  $R_L$  = load resistance

$C_{TC}$  = collector junction capacitance

$t_b$  = base transit time

In order to use this equation, the value of  $I_{pp}$  and the time,  $t$ , must be determined. The maximum possible secondary photocurrent will be for a square  $I_{pp}$  pulse with amplitude equal to the primary photocurrent at  $t_p$  calculated by equation 18a. The time of the square wave pulse can be determined by making the total charge collected



equal to the steady state  $I_{pp}$  (i.e.,  $I_{pp}(t)$  evaluated in equation 13a at an infinite time) times the radiation pulse width. This can be expressed as:

$$\int_0^t I_{pp}(t_p) dt = I_{pp}(\infty)t_p$$

or

$$t = \frac{I_{pp}(\infty)t_p}{I_{pp}(t_p)}$$

Equation 18 can be used to determine the appropriate values of  $I_{pp}$  using the fact that  $\text{erf}(\infty)$  has a value of 1.

It must be remembered that above procedure yields only a rough estimate of the peak secondary photocurrent. The problem in calculating the unsaturated secondary photocurrent is the lack of a detailed description of the currents as a function of time when many quantities such as the radiation, primary photocurrents, voltages and capacitances are all varying during the pulse. This is important when a circuit is being evaluated for transients generated by a radiation pulse. A number of computer codes have been developed which address this problem and are summarized in reference 83. Both Ebers Moll,<sup>81</sup> charge control,<sup>127</sup> and Linville models<sup>128</sup> have been applied to this problem. This is a very complex problem which requires a computer for its solution. It is certainly beyond the scope of this study. All that can be said is that the time varying unsaturated secondary photocurrent,  $I_{sp}$ , can be determined and its peak value will be less than the steady-state value of  $I_{sp}$ .

Several guidelines for device selection and circuit design which mitigates the vulnerability of transistors have been presented. It has been briefly mentioned that some of these guidelines will have an adverse effect on reliability. One instance of this was the recommendation to use devices that employ high doping levels. This will limit the affect of neutron radiation on bulk resistivity which in turn will result in less change in  $V_{CDsat}$ . However, high doping levels are related to low junction breakdown voltages, both  $BV_{CBO}$  and  $BV_{EBO}$ . Obviously this will have an impact on reliability. A somewhat similar situation exists with the recommendation to decrease neutron vulnerability by using devices with the highest practical  $f_T$ . This, of course, implies a very thin base width. As has been mentioned previously, unfortunately this means that these devices will be more susceptible to second breakdown.

These represent examples where nuclear survivability must be traded against reliability and is indicative of the fact that the commitment to harden a system



is a significant decision from a technical point of view. It establishes a definitive engineering task which must be fully integrated into the system management since the hardening procedure impacts device selection, circuit design, testing, reliability, qualification, logistics, and documentation. Aside from the technical and management aspects, hardening will incur both nonrecurring and recurring cost increases during system acquisition. The reason for this is that the primary cost drivers in a hardening program are the analysis and testing. In addition, nuclear survivability will require an increase in documentation associated with the system. The costs of the hardware modifications (e.g., redesign for greater base drive to a transistor, insertion of current-limiting resistors, or substitution of a hardened transistor) are negligible by comparison with the analysis and testing costs.

Same comments on testing must be made. Radiation facilities cost roughly \$2000 per day to use.<sup>129</sup> This is only a small part of the total cost of a test because this is dominated by pre-test and post-test analysis. The pre-test analysis must include benign environment characterization of the material, piece-part, circuit, subsystem, or system to be tested. Obviously, it must include the design of the test. In addition, it should include a careful evaluation of the expected radiation response of the sample. This is especially true for tests on higher levels of samples (such as systems, sub-systems, or modules). The evaluation should lead to an identification of the weak links in the system and to a prediction of the transient voltages and currents and degradations of part parameters. The evaluation then serves as a basis for system level tests in that particular attention can then be paid to monitoring the identified weak links and the test points to measure the predicted transients and degradations. Thus, the test serves as a verification of not only the system's survivability but also of the analytical techniques used to predict the radiation response of the system.

The post-test analysis must include a determination of the level of confidence associated with the test. This is necessary because of the variation in the radiation response of piece-parts and becomes an extremely important consideration. Since no simulator will exactly duplicate the threat environments, the post-test analysis must extrapolate the test results to the threat. The analytical tools which were used in the pre-test predictions and then verified by the test, itself, should be used to do this extrapolation. In addition, consideration should be given to synergistic effects (such as the combined effects of

thermal and blast or EMP and gamma.)

In any case, the cost of irradiating the equipment is a very small portion of the total cost of a radiation test. The analysis dominates both a test and a hardening program. In general the cost is a function of the threat levels. References 130 through 134 do provide some data on the incremental RDT&E (research, development, testing, and evaluation) costs of hardening a tactical system to a balance threat associated with  $5 \times 10^{11} \text{ n/cm}^2$ . A three percent increment was associated with hardening to the complete spectrum of blast, thermal, TREE, and EMP. For hardening against neutrons only, RDT&E cost deltas for hardening a system in development and in production have been reported<sup>65</sup> for a range of neutron fluences and are shown in Table 37. It should be noted that these last deltas are based on strategic systems while the delta associated with the  $5 \times 10^{11} \text{ n/cm}^2$  fluence is based on tactical systems.

Table 37. RDT&E Costs for Hardening Against Neutrons

NEUTRON FLUENCE ( $\text{n/cm}^2$ )	DEVELOPMENT COST DELTA (%)	PRODUCTION COST DELTA (%)
$1 \times 10^{10}$	0	0
$1 \times 10^{12}$	3-5	5
$5 \times 10^{12}$	25	17
$1 \times 10^{13}$	60	25

The costs associated with obtaining nuclear survivability vary widely due to several reasons. Besides technology and risk factors, the methods of measuring or determining the survivability costs are not uniform. Moreover, increasing the survivability of a system quite often helps in meeting other performance specifications such as conventional survivability, and electromagnetic compatibility (EMC) requirements. In fact, in spite of the above discussion on the tradeoff between nuclear survivability and reliability, nuclear survivability can also aid in meeting reliability requirements since survivability requires a more careful screening of piece-parts, increased design margins, and may introduce a certain amount of redundancy into the system - all of which will increase the reliability of the system. Thus, the true cost of survivability can be masked or appear misleadingly high compared with the cost of meeting other performance specifications, depending

on how the costs are tallied. Nuclear survivability costs can be estimated realistically only when the other performance parameters have been assessed their fair share.

The magnitude of the costs associated with developing a survivable system depends to great extent on the knowledge and expertise residing in the Program Manager's Office, their nuclear vulnerability advisors, the contractor, and the entire chain of participants or their nuclear advisors in the life-cycle management of developing nuclear survivable equipment. This really means participants are required who understand how the nuclear environments affect the performance of materials, piece-parts, circuits, subsystems, and systems. The phenomenology which created the environment is of lesser importance when it comes to hardening a system to a defined threat. Like any requirement, the less the expertise and knowledge applied, the greater the risk in not meeting the requirement and the greater the cost incurred in actually meeting the requirement.

## 5.2 INTEGRATED CIRCUITS

### 5.2.1 Introduction

The previous section discussed semiconductor devices (diodes, SCR's, and transistors) when implemented as discrete devices. This section will extend that work on discretes into semiconductor devices when fabricated into integrated circuits (IC's). Obviously, it would be naive to think that this report could completely cover this area. For this reason it was necessary to focus this report on a more specific family of IC's. The fact that most of the work on semiconductor discretes concentrated on bipolar discretes made it natural to concentrate on bipolar IC's. The decision to study Transistor-Transistor Logic (TTL) and Emitter-Coupled Logic (ECL), both bipolar technologies, was motivated by several factors. TTL is by far the most popular technology and has a vast amount of radiation hardening research behind it. TTL is currently used in the MX system, and both TTL and ECL are candidates for LOADS. ECL is the fastest commercial technology available today and in addition has been proposed for use in the BMDATC-radar preprototype endo NNK homing and fusing sensor.

Before one can understand the operation of and the radiation effects on integrated circuits it is necessary to understand some fundamentals of semiconductor logic. This introduction may be unnecessary for the reader who is familiar with electronics; however, many have not been exposed to these areas before. This introduction will be followed by 5.2.3, TTL operation and radiation effects on TTL integrated circuits, 5.2.4, ECL operation and radiation effects on ECL, 5.2.5, a discussion of technologies which didn't merit an entire section - Gallium Arsenide (GaAs) and n-channel-metal-oxide-semiconductor (NMOS).

### 5.2.2 Fundamentals of Electronic Logic

A logic gate is a circuit which is capable of implementing a Boolean algebraic operation by taking one or more inputs and generating the proper output. This circuit can be electrical, mechanical, hydraulic, pneumatic, etc., but in this case will be electronic. Although Boolean algebra may be trivial to many, it is likely that many others have only heard of it. As in any algebra



it deals with variables. The difference is that a Boolean variable may take on only two values, 0 and 1. It is immediately obvious that Boolean algebra is ideally suited to the binary operations of digital computers.

The three most fundamental operations are NOT, AND, and OR. These are represented by the operators " $\neg$ ", " $\cdot$ ", and " $+$ ". These operations are easily seen in the truth table of Figure 75 where  $x_1, x_2, \dots, x_N$  are the input variables, and  $x_0$  is the output variable or answer. The truth table, which is a table of all possible combinations of inputs and their corresponding outputs is a common and useful tool in Boolean algebra and logic circuit design.

Input		Output	Input		Output	Input		Output
$x_1$	$x_2$	$x_0$	$x_1$	$x_2$	$x_0$	$x_1$	$x_2$	$x_0$
0		1	0	0	0	0	0	0
1		0	0	1	0	0	1	1
			1	0	0	1	0	1
			1	1	1	1	1	1

$$\bar{x}_1 = x_0 \quad x_1 \cdot x_2 = x_0 \quad x_1 + x_2 = x_0$$

NOT                    AND                    OR

Figure 75. Fundamental Boolean Operations

A number of other operations exist, but two of these are the most important operations in digital logic. They are NAND ( $\uparrow$ ) and NOR ( $\downarrow$ ) from the contractions of NOT AND and NOT OR. Their truth tables are given in Figure 76.

Input		Output	Input		Output
$x_1$	$x_2$	$x_0$	$x_1$	$x_2$	$x_0$
0	0	1	0	1	1
0	1	1	0	1	0
1	0	1	1	0	0
1	1	0	1	1	0

$$x_1 \uparrow x_2 = x_0 \quad x_1 \downarrow x_2 = x_0$$

NAND                    NOR

Figure 76. NAND and NOR Operations



In logic circuit design the gates which implement these operations are given the symbols shown in Figure 77.

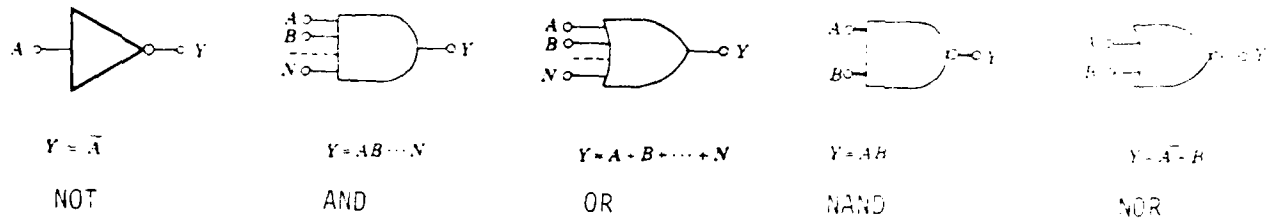


Figure 77. Logic Gate Symbols

The application of Boolean algebra to logic gates can easily be seen in one of the earliest electronic logic families, Resistor-Transistor Logic (RTL). An N input RTL gate is shown in Figure 78.<sup>134</sup>

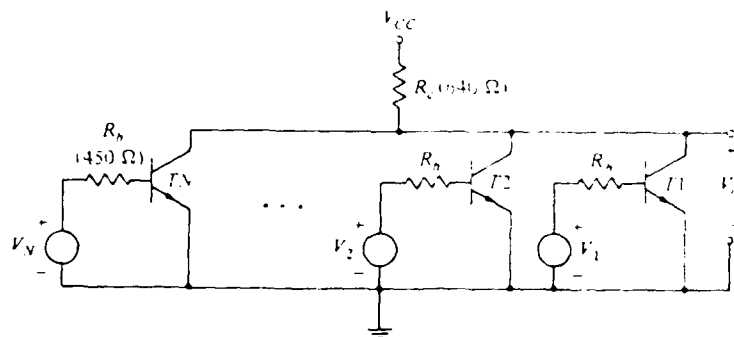


Figure 78. RTL Gate

The input voltages  $V_1, V_2, \dots, V_N$ , representing input variables, are applied to the bases of the transistors through  $R_b$ . The logic levels,  $V_i$ , are not fixed values but are such that  $V_i$  is at logic level zero if it is below the cut-in voltage,  $V_Y$ , of the transistor and is at logic level 1 if  $V_i$  is sufficient to drive the transistor into saturation. For an RTL gate typical values for "0" and "1" are < 0.2 V and > 0.3 V respectively.



It can be seen that if any of the transistors are in saturation ( $V_i = "1"$ ) the output of the gate,  $v_o$ , will be "0". The output will be "1" only when all inputs are "0". From the truth table of Figure 76 it can be seen that the RTL gate performs the NOR operation and is thus a NOR gate. Using this NOR gate, we can build a logic circuit that can implement any Boolean algebraic expression. This is the reason NAND and NOR gates are so important to logic design. One may design a logic circuit solely of NOR or NAND gates to realize any algebraic expression. This connecting of logic gates is the essence of combinational logic. A flip-flop, the basic memory element of a digital computer, is built by wiring a set of gates together such that they, the gates, are forced to respond to a clock. These flip-flops are also used to construct logic circuits. Sequential logic involves the combining of flip-flops and other logic gates.

### 5.2.3 Transistor-Transistor Logic (TTL)

#### 5.2.3.1 TTL Operation

The foreunner of TTL was Diode-Transistor Logic (DTL). Figure 79 shows a three input DTL gate as realized with discrete components. It can be seen that when all the inputs are logic level zero then the output,  $V_o$ , is 5V which is a logic level one. If any input is 5V = "1" then the output is "0" since  $T_1$  saturates. The DTL gate performs the NOR operation making it a NOR gate.

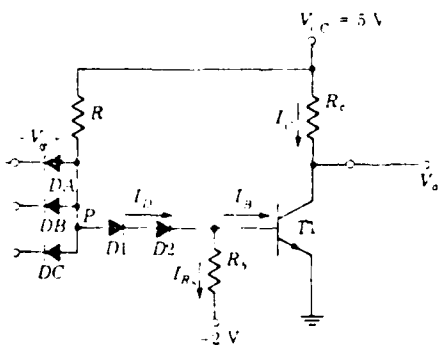


Figure 79. DTL NOR Gate



By examining the change of states the motivation behind TTL becomes apparent. Consider one of the inputs to the DTL gate to be at logic level one (5V). The current flows through D1 and D2 and into the base of T1, eventually driving T1 into saturation. But what happens when the input changes to logic level zero? The output of the gate will go to "1", but not instantaneously. T1 must come out of saturation, pass through the active region, and go into cutoff. During this transition D2 is cutoff, requiring the base charge of T1 to be removed through recombination and as a current flowing through  $R_b$ . This is a slow mechanism and the fundamental speed limitation of DTL.

The speed problem associated with the removal of base charge was solved with TTL. The simplest TTL gate is shown in Figure 80.

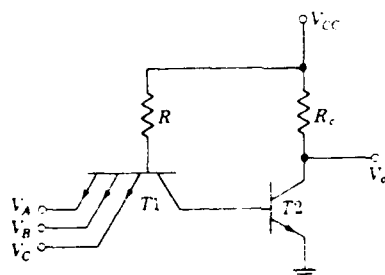


Figure 80. Simple TTL Gate

When the input is at logic level one the emitter-base junction of T1 will be reverse biased and current will flow through R, through the collector-base junction of T1 and into the base of T2, saturating T2 and taking the output to logic level 0.

What happens when the input drops to "0"? The emitter-base junction of T1 becomes forward biased and allows the stored base charge of T2 to flow through the collector of T1. To illustrate the difference in switching times assume  $V_{BE(sat)} = 0.75V$ ,  $R_C = 2K\Omega$ ,  $R = 4K\Omega$ , and  $h_{FE} = 20$ . It can easily be shown that the initial currents carrying the base charge are 0.38 mA for DTL and 22 mA for TTL. This leads to propagation delays for TTL which are 1/10 those of DTL.<sup>135</sup>



The propagation delay ( $t_{PD}$ ) of a gate is one of several parameters used to characterize a logic gate. Two others, rise time ( $t_R$ ) and fall time ( $t_F$ ), can be seen in Figure 81.

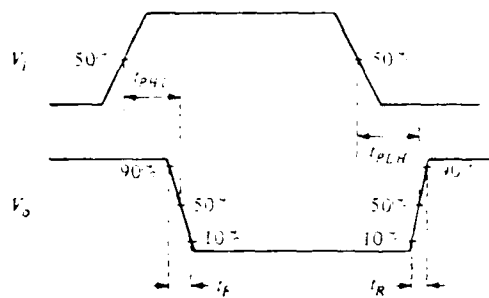


Figure 81. Measurement of Propagation Delay and Rise and Fall Times

The propagation delay is the time it takes for the output wave form to respond to the input.  $t_{PD}$  is measured between the 50% voltage levels of the respective waves. The time required for the output to respond to a rising pulse will usually differ from the time required to respond to a falling pulse, justifying the need for two propagation delays,  $t_{PHL}$  (input going High and output going Low) and  $t_{PLH}$  (input going Low and output going High).  $t_{PD}$  is simply the average of the two delays. The rise time and fall time are measured between the 10% and 90% voltage levels.

After decreasing the time necessary to remove the base charge of the output transistor there is only one principal limitation on gate speed left to overcome. This is the time required to charge the output capacitance. The output capacitance,  $C_0$ , comes from the capacitance of the output transistor and the input capacitance of the gates being driven. In Figure 80 it can be seen that when the output transistor T2 is driven to cutoff the output capacitance measured from the collector of T2 to ground must charge through  $R_C$  with a time constant  $R_C C_0$ . A reduction in  $R_C$  would lower this time but presents an unwanted increase of power dissipation in  $R_C$  ( $i = v/R$ ,  $P = i^2 R$ ). Thus, active



elements (semiconductor devices) are used in place of  $R_C$ . This is shown in Figure 82<sup>135</sup> without detailing its operation. For those interested, an excellent description can be found in Reference 135.

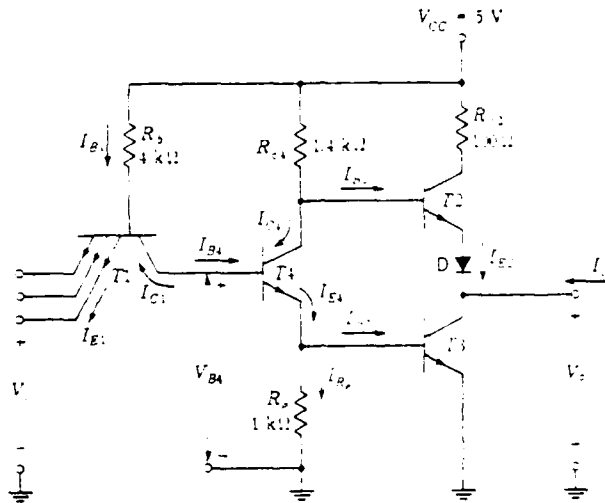


Figure 82. TTL NAND Gate with Active Pull-Up

This is the TTL gate as implemented in most TTL IC's and is the gate referred to in all further discussions of TTL. Additional modifications can be made for applications requiring low power or high speed.

Before discussing radiation effects it is necessary to have been exposed to some peripheral information on TTL logic circuit operation.

#### Fan-Out

In logic circuit applications a TTL gate is supplied current by the driving TTL gate which is in saturation. Often, this driven gate is supplying current to other gates as well. This ability of the gate to supply driving current to additional gates is termed fan-out. Thus, the fan-out of the gate is limited by the amount of current that the output transistor, T3, can sink while in saturation and the amount of current required to drive the driven gates, T1 - T1N (Figure 83).



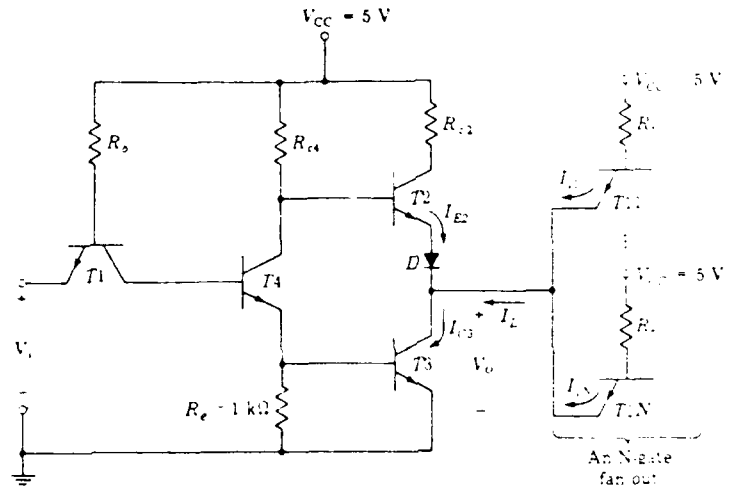


Figure 83. TTL Gate With N-Gate Fan-Out

The current that T3 can sink while in saturation is determined by the gain of T3 and by the input current  $I_{B3}$ . The current required to drive the second stage of gates is determined by  $R_b$  and  $h_{FC}$  of the driven transistors. In a typical gate we find that when the driving-gate output is logic zero it must supply about 1 mA to each driven gate.

Fan-out also affects propagation delay time and saturation time. The dependence of  $t_{PD}$  on fan-out is due to the capacitive loading added by each driven gate. For example, with a capacitive load of 15 pF and a fan-out of 10,  $t_{PD}$  is typically 10 ns.

The fan-out of a gate may be calculated from the required input current to the driven gates and from the output current of the output transistor of the driving gate. Data on the minimum current necessary to drive the next stage of gates is usually given in the manufacturer's specs. The output current can be found from the equation describing dose-induced gain degradation. This is important because it enables the fan-out to be accurately modeled.



### Input-Output Characteristics

In order to quantitatively discuss the performance of a TTL gate some relation between the input and output voltage levels needs to be examined. The most common is the curve relating  $V_{\text{OUT}}$  to  $V_{\text{IN}}$ . This is known as the voltage transfer characteristic and is usually given as one of the manufacturer's specifications. The voltage transfer characteristic for an SN54/74 TTL NAND gate is given in Figure 84.<sup>134</sup>

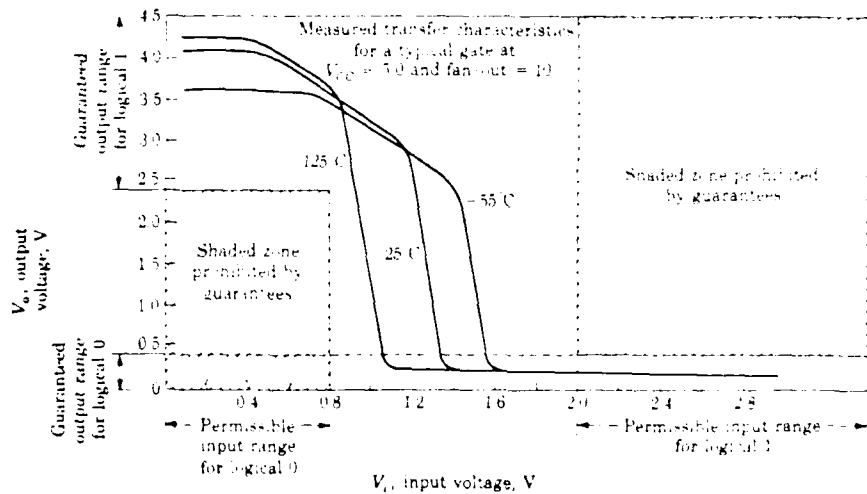


Figure 84. Voltage Transfer Characteristics for Typical SN54/74 NAND Gate

### Speed-Power Product

What the voltage transfer characteristic does not show is the speed or the power characteristic of the gate. These two parameters are often used to characterize the performance of a logic gate. It is obvious a tradeoff is involved between maximum speed and minimum power. This inverse relationship between speed and power leads to another parameter which is often used to characterize performance: the speed-power product, in which the speed and power are combined.

The importance of high speed is obvious. What might not be so clear is the importance of low power. The power a gate dissipates in an IC is going

to directly affect the level of integration attainable. The packing density of gates on an IC is limited by the amount of heat (power) that the IC can dissipate.

### Schottky TTL

It has been seen that a change of states in TTL involves coming out of cutoff, passing through the active region, entering saturation, and going deep into saturation. To obtain the fastest circuit operation, a transistor must be prevented from entering saturation. This can be achieved by using a Schottky diode as a clamp between the collector and base. This can be implemented in an IC as shown in Figure 85(a).

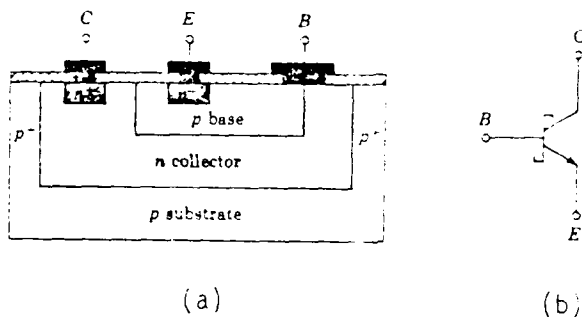


Figure 85. (a) Schottky TTL IC Structure  
(b) Schottky Transistor Symbol

An aluminum metallization is used for the base lead and is allowed to make contact with the n-type collector region, but without the intervening n+ section. This procedure forms a metal-semiconductor diode between the base and collector. This is referred to as a Schottky transistor and is represented by the symbol in Figure 85(b). When TTL is implemented with Schottky transistors it is referred to as Schottky TTL.

The latest advancement in Schottky TTL is Advanced Schottky TTL, introduced by Fairchild in 1979. This version of Schottky TTL employs smaller geometries, higher frequency transistors, and oxide separation to attain speed and power characteristics which are superior to Schottky TTL. Aside from Fairchild's FAST (Fairchild Advanced Schottky TTL), Motorola has introduced



SS (Super Schottky) and TI/National has introduced ALS (Advanced Low Power Schottky) and AS (Advanced Schottky). It should be noted that military specifications have been generated for FAST, the military has a captive line for SS, and is considering ALS.

A comparison of the speed and power characteristics for Standard TTL, Schottky TTL, and Advanced Schottky TTL is shown in Table 38.<sup>134,135,136</sup>

Table 38. Speed/Power Characteristics of Standard TTL,  
Schottky TTL, Advanced Schottky TTL

		<u>Propagation Delay</u>	<u>Power</u>
54	Standard TTL	10 ns	10 mW
54L	Low Power	33 ns	1 mW
54H	High Speed	6 ns	22 mW
54S	Schottky	3 ns	20 mW
54LS	Low Power Schottky	10 ns	2 mW
	FAST	2.5 ns	4 mW
	SS	1.5 ns	20 mW
	ALS	3.8 ns	1 mW
	AS	1.8 ns	20 mW

#### 5.2.3.2 Radiation Effects and Radiation Hardening of TTL Integrated Circuits

Radiation hardening of TTL will be discussed on the gate level, assuming the gate is to be incorporated in an IC. From there the report will proceed to flip-flops and then to shift registers, the building blocks of the CPU.

The radiation threshold of a TTL gate is defined as the level of radiation (neutron fluence, total dose, or dose rate) for which the output response exceeds the noise margin, i.e., the radiation level necessary to cause a change of state of the output logic level. This threshold is dependent on noise immunity, element construction, and packing arrangement.



5.2.3.2.1 Neutrons. Irradiation of TTL IC's with neutrons causes bulk damage in the form of lattice dislocations. These dislocations cause changes in the electrical characteristics of silicon, namely reductions in mobility, effective free carrier concentration, and minority carrier lifetime.

The reduction in minority carrier lifetime causes a proportional decrease in the forward gain ( $\epsilon_f$ ) of the transistor as shown in the Messenger-Spratt equation.<sup>1</sup>

$$\epsilon_f = \frac{2D}{W^2} \left( \frac{\tau_0}{1 + \frac{\tau_0}{\tau_0 K \phi}} \right)$$

where      D    = diffusion constant  
              W    = effective base width  
               $\tau_0$  = pre-irradiation minority carrier lifetime  
              K    = damage coefficient (material dependent)  
               $\phi$    = neutron fluence

This reduction in gain causes the obvious reduction of the output current of the output transistor of the gate. Recalling the previous discussion of fan-out, it can be observed that a reduction of the output current will cause a corresponding reduction of the fan-out capability of the gate. Simply stated, if the gain degradation is sufficient the gate will be unable to deliver enough current to drive the next stage of gates. This effect is shown in Figure 86<sup>2</sup> for a Motorola MC201 DTL gate. The curve is characteristic of a TTL gate, too. Another problem associated with gain degradation is that of maintaining saturation. Recall that a minimum base current,  $I_B = I_C/h_{FE}$ , is necessary to drive and keep the transistor in saturation. Thus, if the gain degradation is sufficient the minimum value of base current required to drive the transistor into saturation will increase past the value of base drive designed into the circuit. This will cause the transistor to come out of saturation and will result in a change of states of the gate output.

There are several approaches to fighting this degradation. The first of these, and perhaps the most important, is the designing of a large



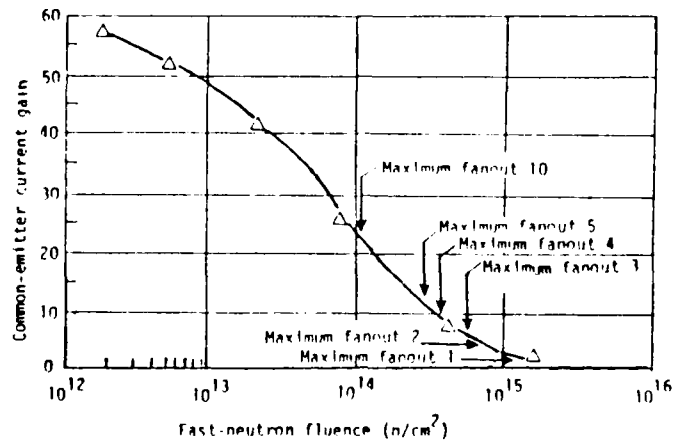


Figure 86. Neutron-Induced Gain Degradation and Decreased Fan-Out Capability

gain margin into the circuitry. This is done by overdesigning the circuit so that a decrease in gain will not affect the operation of the gate. For example, if a gate required a transistor with a gain of 20, a similar transistor with a gain of 100 could be substituted. Obviously, this would allow an 80% degradation of gain without affecting gate operation. The design margin alone can allow for a 10%-90% reduction of gain.

Another effective method is to reduce the fan-out requirements of the gates in the design of the circuit. By reducing the number of gates to which the output transistor must supply current, the effect of any reduction in output current can be negated.

By increasing the reverse bias and increasing the collector current the transistor can be driven harder into saturation. This will aid in keeping the transistor in saturation when it is supposed to be there. The above methods are used to harden against all types of radiation-induced gain degradation.



Permanent gain degradation can be lessened by using as large an emitter current as practical and as high an ambient temperature as possible. Both of these increase the annealing of displacement damage and thus reduce permanent gain degradation.

The reduction of carrier mobility and carrier concentration causes a reduction in the resistivity of the silicon. The decrease changes the quiescent operating point of the transistor. This effect can be negated by using a small resistor in the emitter or by using low resistance bias circuitry.

Neutron irradiation also affects the static parameters of the IC gate. The input threshold voltage will increase moderately and the output low-level voltage will increase significantly. The latter of these is by far the most common mode of neutron induced failure.<sup>2</sup> This increase in the output low-level voltage is caused by a combination of gain degradation and increased resistivity. If the increase in the output low-level voltage is sufficient a logic level zero will be read as a logic level one. To illustrate this effect a voltage transfer characteristic for a Motorola MC201 DTL gate is shown in Figure 87<sup>2</sup>.

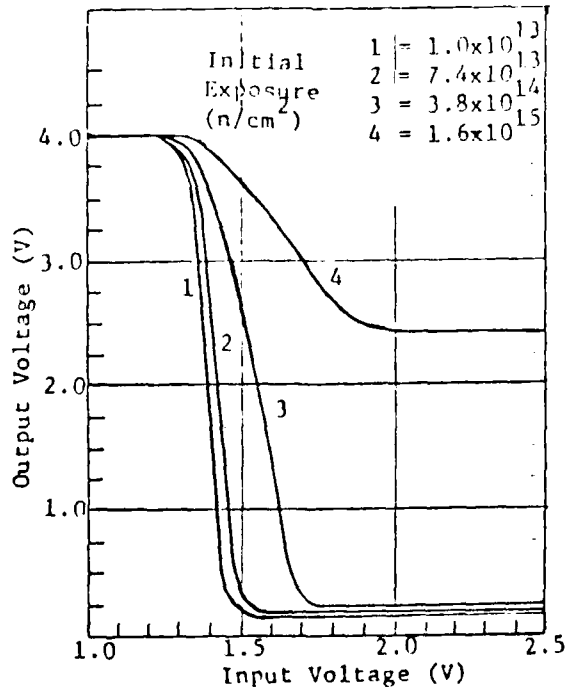


Figure 87. Neutron Induced Increase of Output Low-Level Voltage

SRI

This curve is representative of TTL behavior as well, as shown in Table 37.<sup>137</sup> Measurements were made on a total of 80 radiation-hardened, low power, TTL quad 2-input NAND gates, namely the RSN54L00, after exposure to neutron fluences ranging from  $4.6 \times 10^{13}$  n/cm<sup>2</sup>. Only the values of those devices which remained within the manufacturer's specifications were used in the average of the output low-level voltage. The figure in parentheses gives the number of devices included in this average. These gates employed dielectric isolation, thin-film resistors, quartz-surface passivation, and photocurrent compensation for radiation-hardening. It should be noted that pre-irradiation testing revealed two electrical problems. Two gates had an apparent electrical short between the two output emitters. Thus, when an unused input was connected to the power supply through a 1KΩ resistor and the other input held low excessive supply current was drawn. During testing at the White Sands Missile Range LINAC, one gate began to draw excessive current after exposure to a dose of only  $10^4$  rads(Si). Examination with a Scanning Electron Mirror Microscope revealed a possible pinhole short in the device die through the oxide from the emitter metalization to the base region. This may have been caused by electrical overstress rather than radiation.

TABLE 39

Average Low State Output Voltage ( $V_{O0}$  in units of volts) of Surviving Devices after Neutron Irradiation to Specified Fluences. Numbers in parentheses indicate the number of devices in each sample.

FANOUT (Fluence (n/cm <sup>2</sup> ) (1 MeV equiv))	10	9	8	7	6	5
0	0.168(80)	--	--	--	--	--
$4.6 \times 10^{13}$	0.200(80)	--	--	--	--	--
$9.6 \times 10^{13}$	0.208(80)	--	--	--	--	--
$2.2 \times 10^{14}$	0.247(4)	0.240(8)	0.223(8)	0.208(10)	0.189(10)	0.172(10)
$2.5 \times 10^{14}$	0.247(2)	0.236(4)	0.226(4)	0.213(5)	0.209(9)	0.189(10)
$7.2 \times 10^{14}$	--	--	--	--	0.255(1)	0.256(3)
$1.2 \times 10^{15}$	--	--	--	--	--	--



Since this increase of low-level output voltage varies among devices it is important to test candidate gates at the anticipated threat levels to insure that this problem will not interfere with the circuit operation.

Dynamic characteristics of the gate are also affected. The propagation delay will increase slightly, the rise time will decrease initially and then increase rapidly as the gain degrades. The fall time may either increase or decrease depending on the loading and other circuit characteristics.

The vulnerability of TTL devices to neutron irradiation has been summarized in Figure 88.<sup>64,136,138,139,140</sup> The point where the bar starts indicates the radiation level at which the first device of that type has been observed to fail. The last point on the bar represents the radiation level above which no devices have been observed to survive.

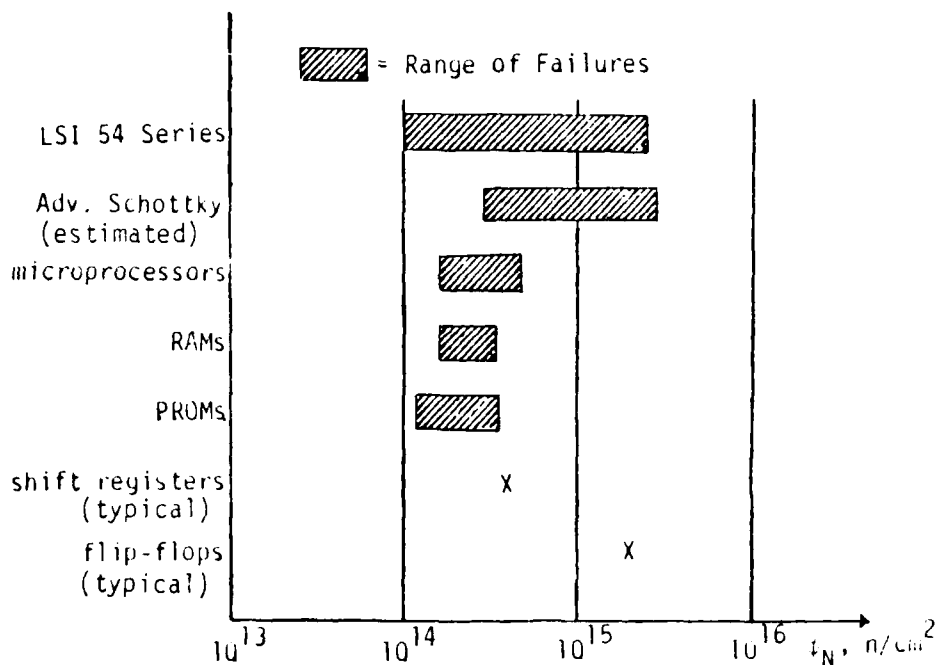


Figure 88. TTL Neutron Failure Levels



A set of design guidelines for neutron hardening are summarized below.

- Design a large gain margin into circuitry
- Reduce fan-out requirements in design
- Large emitter current
- Large collector current
- High ambient temperature
- Increased reverse bias
- Emitter resistor
- Low impedance bias circuitry

5.2.3.2.2 Total Dose. Total dose exhibits itself as a degradation of gain and an increase in leakage currents. Although the leakage currents may increase by an order of magnitude they are generally insignificant when compared to the operating currents of the transistor. The level of gain degradation necessary to cause circuit failure is dependent on a number of factors. As with neutron induced gain degradation the design margin and fan-out requirements are the most critical of these. All comments regarding the effects of gain degradation from neutrons also apply to total dose induced gain degradation.

The mechanism behind the gain degradation is ionization of the atmosphere, the  $\text{SiO}_2$  insulation layer, and the bulk silicon. In the atmosphere positive ions and electrons are produced. Electric fields produced during transistor operation are in a direction to drive the positive ions toward the base region (for an n-p-n transistor), hence a deposition of positive charge on the  $\text{SiO}_2$  insulation layer. This charge then migrates to the Si- $\text{SiO}_2$  interface. Ionization in the  $\text{SiO}_2$  layer leads to the production of electrons and holes. The holes migrate to the Si- $\text{SiO}_2$  interface, causing a charge inversion at the interface; p becomes n and n becomes p. This effect is illustrated in Figures 89(a) and 89(b).<sup>81</sup> The charge inversion causes the emitter-base junction space-charge region to be extended by the formation of a space-charge channel.



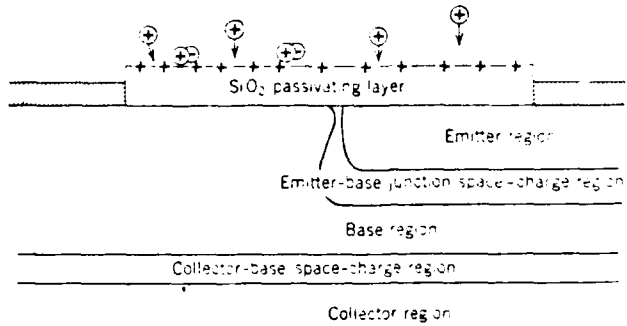


Figure 89(a). The Emitter-Base Junction With Positive Charge Collected on the  $\text{SiO}_2$  Surface

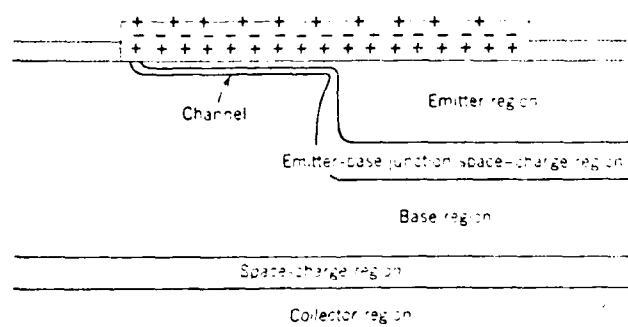


Figure 89(b). The Creation of a Channel in the Base Region

**SAI**

Ionization of the bulk silicon also occurs as the formation of electrons and holes. As the positive charge layer forms at the interface the electrons are attracted to the interface and absorb enough energy to allow them to cross the interface and neutralize the positive charge. This causes the channel to recede to a point between the original state and the maximum channel length. The gain degradation is a direct result of the forementioned charge inversion.

The level of dose-induced gain degradation experienced by a TTL IC is dependent on a number of factors. At low current densities the percentage gain degradation will be much greater, and depends on the bias conditions both during and after irradiation.<sup>105</sup> For npn transistors,  $\beta$  degradation is greatest when irradiated under an active bias condition; the magnitude of the degradation being controlled primarily by  $V_{CB}$  during irradiation. pnp transistors show the greatest degradation when irradiated under a passive bias condition with the degradation being controlled primarily by  $I_C$  during irradiation.<sup>2</sup>

TTL IC's can be hardened using some of the same techniques discussed under neutrons. In the design of the circuit a large gain margin and reduced fan-out requirements are very effective.

In the fabrication stage gold doping is very effective in hardening against total dose. This hardening is due to the gain degradation of the output transistor at low injection levels caused by the introduction of traps and recombination centers. Gold doping simply degrades the gain before the dose has a chance to do so. The net result is the use of transistors with a degraded gain of 30, for example, which show little or no gain degradation upon total dose exposure, rather than the use of transistors with a gain of 100 which degrade to a gain of 30 upon irradiation. Gold doping is not the luxury it sounds since it is also used to increase switching speeds and harden against dose rate. Pre-irradiation with neutrons affects the transistor in the same way as gold doping and is often used as an alternative to gold doping.

All things considered, hardened TTL is hard to total dose at the threat being considered, and should not be a primary problem. The vulnerability of TTL to total dose has been summarized in Figure 90.<sup>64,136,138,139,140</sup> As before, the beginning of the bar corresponds to the first observed failure and the end of the bar indicates that all devices have been observed to fail by this point.



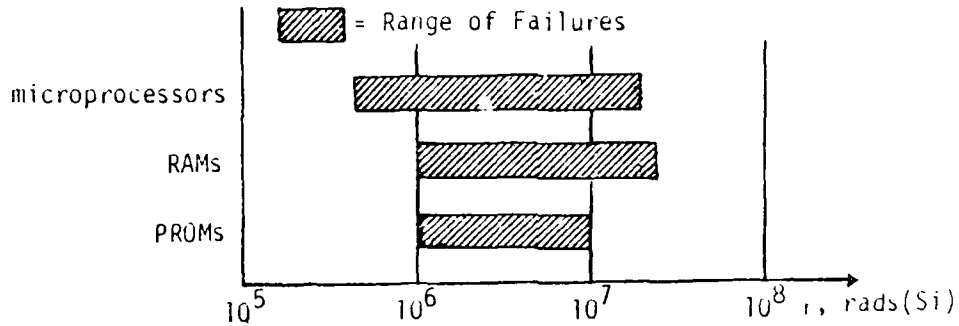


Figure 90. TTL Total Dose Failure Levels

A summary of design guidelines for hardening against total dose is given below.

- Large gain margin in design
- Reduced fan-out requirements
- High current levels
- Increased reverse bias
- Gold doping of collector region
- Pre-irradiation with neutrons

### 3.3.2.3 Dose Rate

Dose rate induced effects in IC's are caused by the generation of electron-hole pairs. The behavior of the IC depends on the number and rate of generation of these electron-hole pairs. The generation rate,  $g$ , can be determined from



$$g = \frac{\dot{Y}\rho}{E} \left( \frac{100 \text{ ergs/gm-rad}}{1.6 \times 10^{-12} \text{ ergs/eV}} \right)$$

where  $\dot{Y}$  = absorbed dose rate in rads (material)/sec.

$\rho$  = mass density in gm/cm<sup>3</sup> of material

E = average energy required to produce an electron-hole pair.

The number of electron-hole pairs produced is directly proportional to the generation rate, g, and the volume of semiconductor exposed to the threatening radiation. These electron-hole pairs move under the influence of the applied electric fields to form a photocurrent. This photocurrent is called the primary photocurrent,  $I_{pp}$ . Typically, a dose rate of 1 Mrad(Si)/sec. generates a primary photocurrent of 10mA.<sup>1</sup> This primary photocurrent is indistinguishable from the normal operating current of the transistor and thus will be amplified just as the operating currents. The amplified primary photocurrent is called the secondary photocurrent and is the principal dose rate damage mechanism. These photocurrents can cause permanent damage in the form of device latchup and component burnout.

Latchup occurs when internal p-n-p-n paths have sufficient gain to create an SCR within the circuit and the current flow after irradiation exceeds the holding current of the SCR. This holding current may be less than the normal operating current.<sup>141</sup> Recall that when the SCR fires, a low-impedance, high-current path is formed. The device will remain latched in the high state until primary power is removed. This means the output will not respond to any input signal. If primary power is not removed the high current levels will cause device burnout, possibly within microseconds. Radiation hardening often consists of trying to control these photocurrents rather than hardening the device against them. This approach is called photocurrent compensation.

Two of the many circuits used in photocurrent compensation are shown in Figure 91<sup>2</sup>. Base-emitter compensation (Figure 91(a)) uses the forward biased collector-base junction of a neighboring transistor to shunt the primary photocurrent to ground, thus preventing it from being amplified.



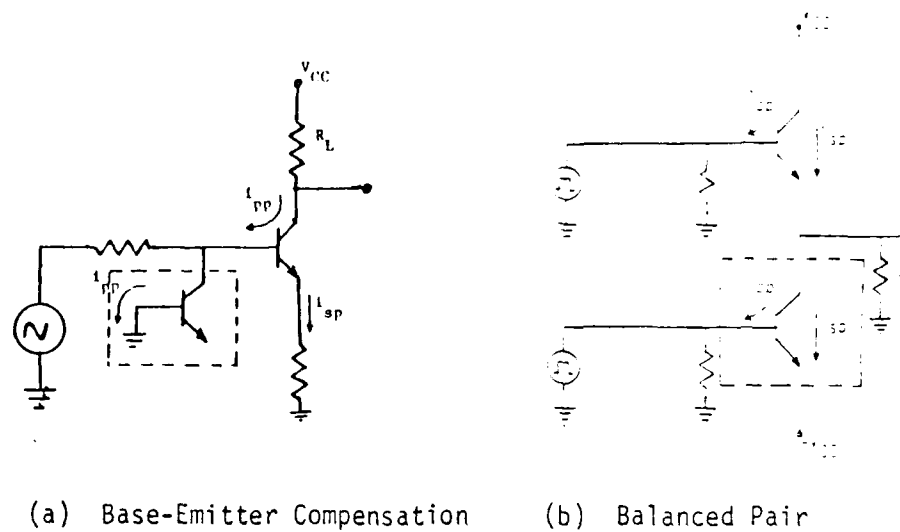


Figure 91. Photocurrent Compensation

Transistors connected in pairs are very effective in reducing the transients caused by photocurrents. The balanced pair (Figure 91(b)) also provides a low source and sink impedance for the following stages. For good rejection the transistors should have the same photocurrents and base input resistances. This is a minor problem in IC's since neighboring transistor structures have nearly identical characteristics. The designer should, however, exercise caution when designing a photocurrent compensation circuit into a system as these circuits may have increased susceptibility to total dose, variations in power supply voltages, and transient voltage and current spikes caused by EMP.<sup>2</sup> Many other circuit tricks have been found which are useful in controlling primary and secondary photocurrents and can be found in reference 2.

Photocurrent generation can be minimized in the fabrication process by using shallow diffusion depths and small p-n junction widths, allowing less area in which photocurrents can be produced. Heavy gold doping of the collector to minimize carrier lifetime is also effective. Gold doping, however, is seeing less use as a method to increase speed as Schottky TTL becomes more



popular for high speed applications. Schottky TTL has never been observed to be susceptible to photocurrent-induced latchup but may be susceptible to high temperature Schottky latchup. This is due to a difference in the temperature dependance of Schottky current,  $2\%/\text{ }^{\circ}\text{C}$ , and collector p-n junction current,  $8\%/\text{ }^{\circ}\text{C}$ . If the dose rate-induced photocurrents are large enough to heat the IC to the upper end of the military spec. range the p-n junction current may be sufficient to cause high temperature latchup. This leads to a condition similar to that of non-gold doped transistors discussed previously. In newer Schottky versions the Schottky barrier diode is replaced by Darlington transistors, eliminating all latchup possibilities.

Even if the photocurrents are not of sufficient magnitude to cause latchup they can still cause transient upset. Transient upset is a term which is used to collectively describe a variety of noncatastrophic logic errors. A photocurrent flowing in the junction which isolates the collector of the output transistor can cause the gate output (which is a bit in a computer) to change states. Another common logic error is the production of a photocurrent-induced extraneous command signal or clock signal which will trigger a change of state. It is also possible for photocurrents to cause the computer to mis-read a bit of data.

Larger photocurrents are capable of causing permanent damage even if latchup does not occur. Metalization patterns are very susceptible to electrical overstress brought about by excessive photocurrents. For example, the current density in aluminum metalization is limited to  $5 \times 10^5 \text{ A/cm}^2$  due to reliability considerations. If a typical value of  $25 \text{ nA}/(\text{cm}^2\text{-rads-sec})$  is used for the photocurrent produced in an IC p-n junction aluminum electrical overstress can be calculated to occur at  $\dot{y} = 2 \times 10^{11} \text{ rad(Si)}/\text{sec.}^2$ . The possibility of dose rate-induced overstress can be reduced by using metalization patterns with small cross sections and by using current limiting resistors.

It should be noted that metalization burnout is not the only dose rate-induced electrical overstressing failure mode associated with IC's. Two others, junction breakdown and interface breakdown,<sup>264</sup> are both more common than metalization burnout and, in fact, are the most common dose rate-induced permanent damage mechanisms. Although junction breakdown and interface break-



AD-A102 747

SCIENCE APPLICATIONS INC HUNTSVILLE AL  
NUCLEAR ANALYSIS AND TECHNOLOGY ASSESSMENT OF RADAR CONCEPTS. V--ETC(U)  
MAY 81 J P SWIRCZYNSKI, C S CHEEK  
DASG60-78-C-0029

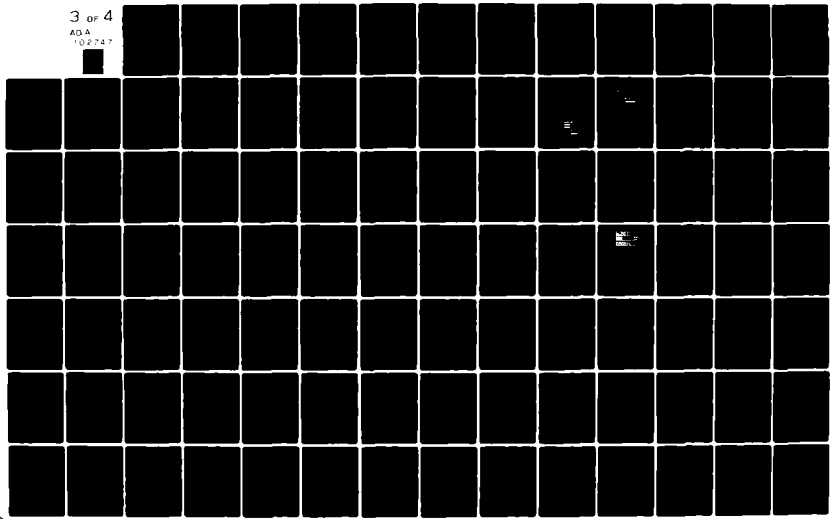
F/G 17/9

NL

UNCLASSIFIED

SAI-82-604-HU

3 of 4  
ADA  
102 747



down are not photocurrent-induced it is felt their importance merits a discussion at this point.

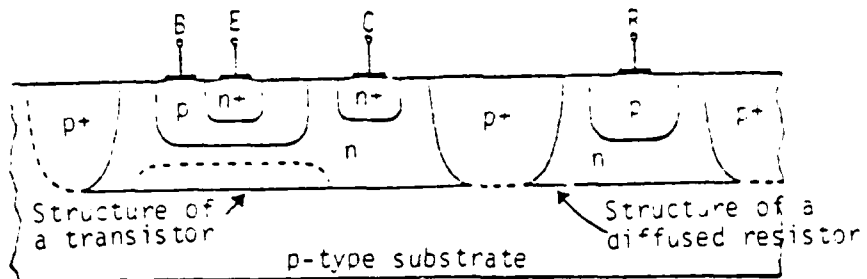
Junction breakdown is caused by second breakdown, a phenomenon previously discussed in section 5.1 under dose rate-induced damage to discrete bipolar transistors. Recall, second breakdown is caused by a sudden decrease in the effective resistance of a reverse-biased avalanching transistor (thermal runaway). In a submicrosecond time frame this resistance decrease is seen as a simultaneous increase in junction current and a decrease in voltage across the junction. On the transistor level this causes localized heating within the junction which eventually melts the silicon and results in a melt channel which extends across the junction. This channel acts as a resistive short circuit between the collector and emitter and is referred to as junction breakdown.

Interface breakdown, commonly called a flash-across short, is the result of a breakdown path which usually appears across the emitter-base junction that is caused by a voltage transient. The models that have been proposed to explain the process do not agree on the initiation mechanism but it appears that a melting of the aluminum metalization is involved. This effect is one of the principal EMP-induced damage mechanisms<sup>264</sup> and, as such, merits further study.

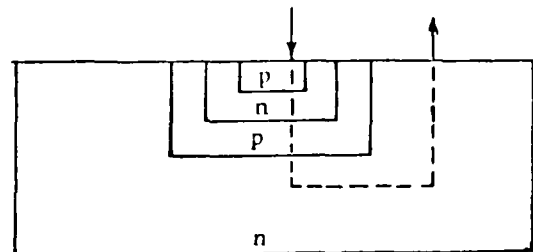
Junction breakdown can be hardened against by using current limiting resistors, an approach which can be used to harden against all types of photocurrent-induced damage mechanisms; using wider base widths, a hardening approach that involves a tradeoff with neutron hardness, reliability, and switching speed; and using transistors with higher power ratings, an option which is prohibitive in regard to level of gain attainable.

The most effective way to prevent damage from latchup is to prevent latchup. This can be done by eliminating the parasitic SCR paths associated with latchup. Figure 92(a) shows the cross section of an IC fabricated using dielectric isolation in which p-n junctions are used to separate different transistor regions. This leads to the formation of many possible p-n-p-n paths as shown in Figure 92(b). Dielectric isolation, shown in Figure 92(c), uses an isolating  $\text{SiO}_2$  layer between regions to prevent the formation of parasitic p-n-p-n SCR paths and parasitic capacitances.

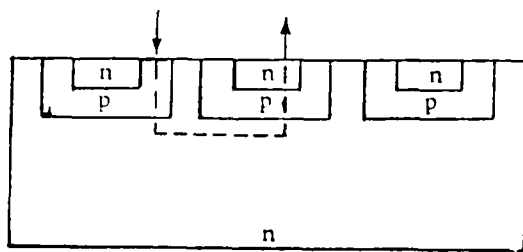




(a) Junction Isolation

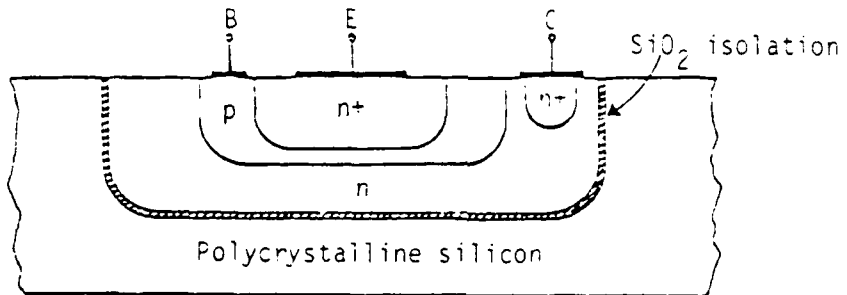


Vertical PNP Transistor



Multiple Diodes or Transistors

(b) IC p-n-p-n Latchup Paths



(c) Dielectric Isolation

Figure 92.

The most common method used to fabricate an IC with dielectric isolation is the lapback technique, outlined in Figure 93<sup>2</sup>. A buried n+ region below the collector is used to lower collector resistance. A simple way to include this region is to begin step 1 with a substrate having either a diffused or epitaxially grown n+ skin. After step 6 the cross section resembles the sketch of Figure 94<sup>2</sup>.



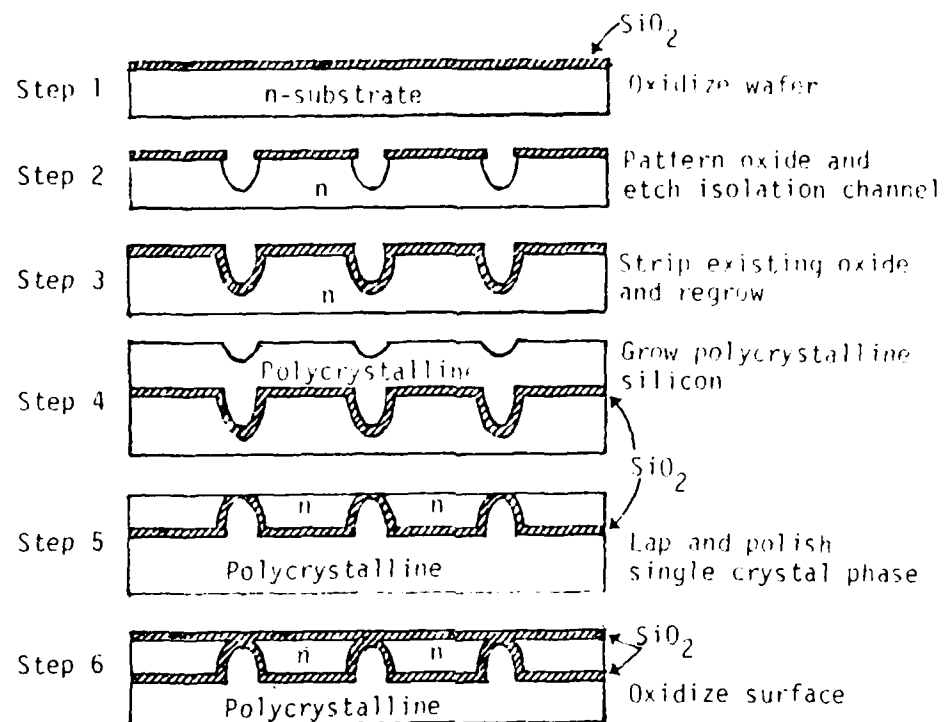


Figure 93. Lapback Technique of Dielectric Isolation

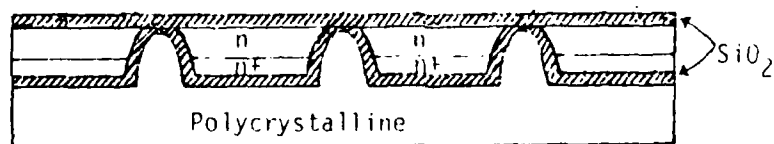


Figure 94. Cross Section After Lapping When Using an Epitaxial n+ Layer on an n Substrate

A modified lapback technique diffuses the n+ skin after the moat etching of step 2 and before the oxidation of step 3. The lapback process demands skillful lapping and polishing techniques during the lapback, step 5, since the circuits must be diffused through this surface.

Other oxide insulation techniques replace the lapback step with an extra deposition step and thin the crystal from the bottom to reduce the importance of the quality of the finish. These are known as double handled processes.<sup>2</sup>

The mesa isolation technique of dielectric isolation uses a wafer into which the circuits have already been diffused.<sup>2</sup> After the top plate has been reinforced with a rigid material such as silicon or glass, moats are etched completely through the underlying oxide in the appropriate regions. The area between these exposed silicon areas is either left empty (air isolation) or filled with a ceramic (ceramic isolation) and leads are attached. Dielectric isolation has been proven effective in raising interdevice breakdown voltages, lowering parasitic capacitances and increasing resistance to radiation damage.

The problems present at the transistor and gate level lead to new problems at the flip-flop level. The flip-flop is the basic memory element of the computer and is simply a group of gates wired together and made to respond to a clock pulse. A sufficient dose rate will cause a change in logic states, either from an extraneous clock signal or from a photocurrent induced signal.

Table 40 summarizes the sensitivity of flip-flops to dose rate induced upset.<sup>141</sup> The SN54L72 uses unhardened gates while the RSN54L71 and RSN54L74 use hardened gates. The flip-flops were loaded at a fan-out of 10 and toggled at 1 MHz. A logic or phase error was said to have occurred if a device incorrectly changed states or failed to respond to a command immediately after irradiation. The apparent increased hardness of the flip-flops over the gates used to build the flip-flops is largely a matter of failure definition. The table also shows the peak supply current drawn by the flip-flop.



TABLE 40. FLIP-FLOP TRANSIENT RADIATION FAILURE LEVELS

SN54L72

## J-K Master-Slave Flip-Flop

<u>Dose Rate</u>	<u>Logic Failure</u>	<u>Peak I<sub>cc</sub>(mA)</u>
$3 \times 10^9$	No	23
$5 \times 10^9$	Yes	40
$1.5 \times 10^9$	Yes	85
$1 \times 10^{10}$	Yes	135

RSN54L71

## R-S Master-Slave Flip-Flop

<u>Dose Rate</u>	<u>Logic Failure</u>	<u>Peak I<sub>cc</sub>(mA)</u>
$9 \times 10^9$	No	12
$2 \times 10^{10}$	Yes	18

RSN54L74

## Dual-D Flip-Flop

<u>Dose Rate</u>	<u>Logic Failure</u>	<u>Peak I<sub>cc</sub>(mA)</u>
$1.6 \times 10^9$	No	3
$3.0 \times 10^9$	No	3
$9 \times 10^9$	Possible	5
$2 \times 10^{10}$	Yes	15

Transient upset of flip-flops may be mitigated by using circumvention, an alternative which requires a large amount of redundancy. Circumvention requires the contents of a shift register (string of connected flip-flops) to be stored in a hardened memory during the period that a threatening dose rate exists. This is also an expensive alternative as a plated wire memory, the most commonly used hardened memory, costs \$15 per bit.<sup>143</sup> It should be noted that dollar values as low as \$1.80 per bit for plated wire memories can be found in the literature<sup>144</sup>, but it has been impossible to verify these values. This technique is necessary only for volatile memories, memories whose contents will be destroyed if power is removed. A nonvolatile memory on the other hand can have power removed and retain its contents. This would allow the memory to be turned off for the duration of a threatening dose rate with no effect on the memory. Metal-nitride-oxide-semiconductor (MNOS), magnetic bubbles, and amorphous semiconductors are the only nonvolatile memories available. These technologies



are also the least mature and therefore have the poorest performance of memory technologies; but the nonvolatility advantages insure low module power dissipation, high module reliability, and intrinsic radiation hardness in a pulsed nuclear environment. These facts make these three technologies prime contenders for nuclear radiation tolerant systems.

TTL's susceptibility to dose rate induced transient upset has been summarized in Figure 95<sup>64,136,138,139,140</sup>. Transient upset is defined as a change of states, a failure to read properly, or an extraneous command signal.

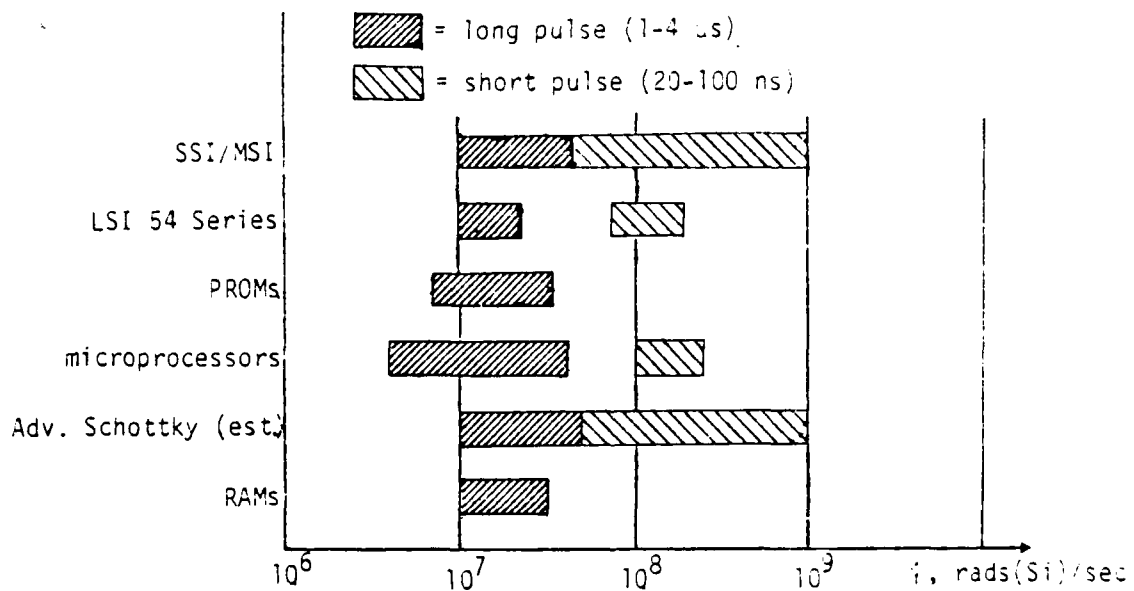


Figure 95. TTL Dose Rate-Induced Transient Upset Failure Levels



It can be seen from Figure 95 that the dose rate failure levels are dependent on the pulse width, similar to total dose failure levels. This dependence can be seen in Figure 96 for a 64-bit Schottky TTL RAM.<sup>139</sup> As the pulse width varies from .01  $\mu$ s to 1.0  $\mu$ s the dose rate failure level decreases by an order of magnitude from  $3 \times 10^8$  rads (Si)/sec to  $3 \times 10^7$  rads (Si)/sec. Similar pulse-width vs. failure level data for the AM2901A, AM2910, and 74S481 TTL microprocessors presented in reference 145 shows a factor of two more upset sensitivity than the forementioned Schottky RAM. This makes it important that a dose rate time history, showing pulse width, is known when designing a radiation hardened system.

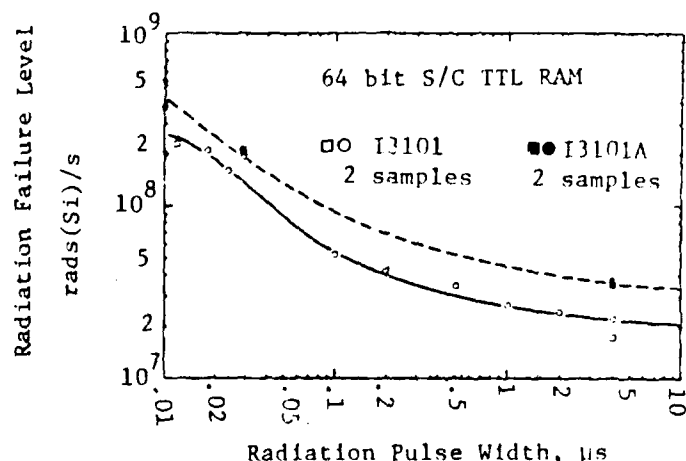


Figure 96. TTL Pulse-Width Dependence of Transient Vulnerability

A summary of dose rate hardening design guidelines is given below.

- Minimum transistor geometries
- Gold doping
- Dielectric isolation
- Current limiting resistors
- Photocurrent compensation
- Circumvention
- Nonvolatile memories
- Wide base widths



propagation delay time caused by the transistor going into saturation. To counter this problem it was necessary to find a way to operate a gate with one logic level in the active region and the other in cutoff. It must also be possible to achieve switching between the active region and cutoff with a small input voltage swing. ECL accomplishes this by using a difference amplifier (Figure 97).

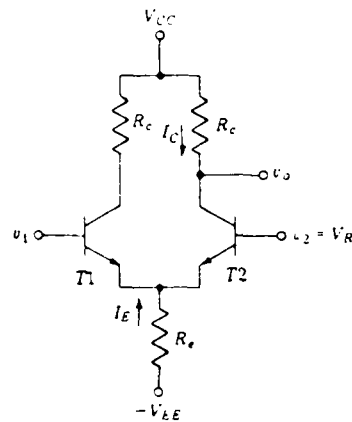


Figure 97. The Difference Amplifier

When used as a logic gate, the base of T2 is held at a fixed reference voltage,  $V_R$ , and an input,  $V_1$ , is applied at the base of T1. When  $V_1$  is sufficiently larger than  $V_R$ , T2 will be cut off and the current will flow through T1.

As  $V_1$  drops to equal  $V_R$ , the currents in the two transistors will be equal. When  $V_1$  is sufficiently lower than  $V_R$ , T1 will be cut off and current will flow through T2. From this it can be seen that ECL accomplishes switching by switching current from one transistor to the other rather than by turning a transistor ON and OFF. This switched current is, in fact, a nominal emitter current which varies by less than 2% as it is switched.

This leads to an ECL gate as shown in Figure 98. The component values given correspond to the Motorola MECL III, a medium speed, medium power gate.<sup>135</sup>



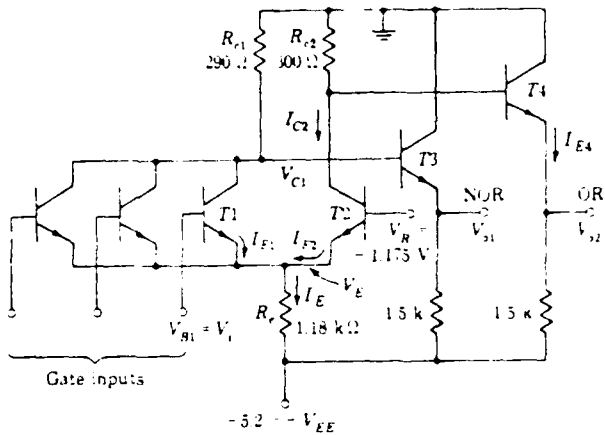


Figure 98. Motorola MECL III Gate

The gate has several important features which should be given special attention. First, the gate is equipped with OR and NOR outputs which, of course, are complements of each other. Since one or both of the outputs can be used, the gate provides the designer with flexibility that is not available with other gates.

The reference voltage,  $V_R$ , is also worth examining. The gate is designed such that the  $\Delta 0$  and  $\Delta 1$  noise margins are approximately equal ( $\Delta 1 = \Delta 0 = 0.175$  V). But since there is a temperature dependence of  $2 \text{ mV}/^{\circ}\text{C}$  the noise margins will be equal at only one temperature if the reference voltage remains fixed. This problem is countered by using a temperature compensated reference voltage. The circuit used in the MECL II gate is given in Figure 99.

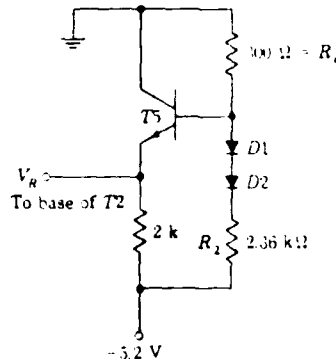


Figure 99. Reference Supply Circuit for ECL Gates



Using this compensated reference voltage, as the temperature changes, the midpoint of the range from logic 1 to logic 0 changes by the same amount at the reference voltage  $V_R$ . This setup maximizes noise immunity over a large range of temperatures and also provides a significant amount of compensation for variations in the supply voltage,  $-V_{EE}$ .

The relationship of the noise margins, reference voltage, and the input and output voltages is easily seen by examining the voltage transfer characteristics (Figure 100).<sup>135</sup>

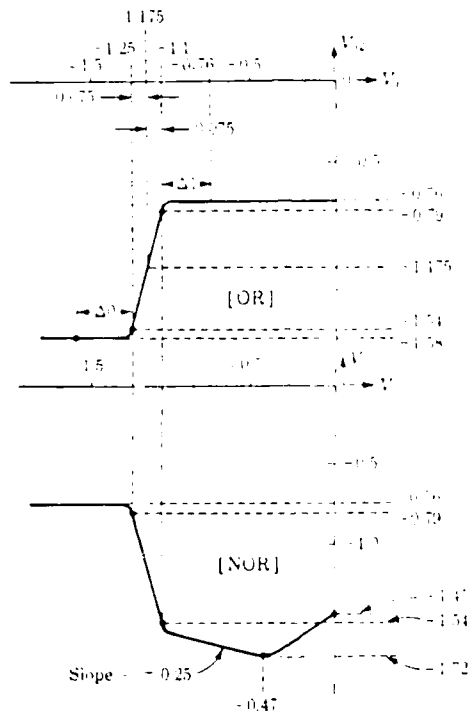


Figure 100. ECL Transfer Characteristic

The transfer characteristic of a particular type of gate is included in the manufacturer's specifications and will show good agreement with the derived transfer characteristic.

The noise margin also directly affects the fan-out. In DTL (Diode-Transistor Logic) and TTL (Transistor-Transistor Logic), where the outputs are taken across a saturated transistor, as long as the allowable fan-out is not exceeded the output voltage and noise margin remain essentially constant. This is not the case with ECL, a non-saturating logic. In fact fan-out is strictly a function of what the designer considers an acceptable noise margin. In a typical case if the allowed noise margin is 0.3V the fanout will be approximately 25, while if the noise margin is 0.1V the fan-out will increase to 250. This makes it apparent that fan-out is no problem if the only worry is availability of driving current. However, fan-out does affect gate speed, the main attraction of ECL. To keep propagation delay times below the specified limits it is only necessary to conform to the manufacturers specified ac fan-out and dc fan-out, typically 15 and 25 respectively.

In any case, as with TTL, a good design incorporates a minimum fan-out. This maximizes the speed in a benign environment and minimizes the effects of gain degradation in a nuclear environment. The effects of fan-out on the propagation delay of a MECL II gate are presented in Table 41. The table gives fan-out values for only 0 and 20 because the effect of dose rate on  $t_{pd}$ ,  $t_r$ , and  $t_f$  is linear between 0 and 20.<sup>135</sup>

TABLE 41. EFFECTS OF FAN-OUT ON MECL II

Fan-Out	$t_{pd(HL)}$	$t_{pd(LH)}$	$t_r$	$t_f$
0	3.5 ns	3.5 ns	6 ns	4 ns
20	18 ns	5 ns	8 ns	30 ns

One last note on the use of ECL is of importance. Whenever the propagation delay time approaches the line delay time (the time necessary for the signal to go from the output of one gate to the input of the next) the output signal will begin to oscillate. To explain this effect requires the use of transmission line theory that is not appropriate here. It is sufficient to know that the oscillations can be minimized by using short connections between gates and by properly terminating these gates. For this reason the manufacturers



generally provide information concerning maximum unterminated line lengths and the most effective termination of longer lines.

The latest development in ECL technology was the introduction of Fairchild's 100K series in 1978. This series offers propagation delays of 0.5 - 1 ns and an operating frequency of 5 GHz. These speeds make ECL by far the fastest logic family on the market. With these outstanding speed and frequency characteristics one might ask why ECL is used only sparingly. Not surprisingly, the reason is power. A gate from the 100K series dissipates from 10-40 mW depending on the switching speed.

For applications where there is no alternative but to use ECL the dissipation of this power becomes the prime consideration. The Cray II, the world's fastest computer, circulates liquid nitrogen to act as a heat sink for its ECL gates. Schemes such as this will likely be necessary if LSI levels of ECL are to be used.

This power problem is also the reason ECL hasn't achieved the levels of integration of other technologies. An ECL gate would literally melt during operation if fabricated using VLSI. Fairchild has introduced a low power version for RAM applications but the authors have been unable to find any useful data on this series.

The State-of-the-Art in ECL is an ECL/TTL 4K RAM (93471) which utilizes the high speed characteristics of ECL and the low power characteristics of TTL. Although the latest advances in ECL have been introduced by Fairchild, Motorola is still the authority on ECL. They introduced their first ECL gate in 1962 and have continued developing this technology ever since. Motorola possesses the most mature ECL production line available today.

#### 5.2.4.2 Radiation Vulnerability of ECL

High switching speed is not the only attraction of ECL. ECL is harder to radiation than any commercial logic family. Combined, these two factors make ECL the most desirable bipolar logic to use in a radiation environment where high speeds are necessary. Although very little work has been done on ECL vulnerability, the problem is beginning to receive the attention it merits.



There are several factors contributing to the radiation tolerance of ECL. First, the higher the operating frequency of ECL, the higher the radiation tolerance. This is true of ECL in particular but not of logic families in general. This is because higher operating currents are required for high speed operation, lessening the effects of gain degradation. Also, the construction of high speed ECL requires a very narrow base region. This contributes to neutron hardness. As a rule failure levels of ECL are on order of magnitude higher than those of TTL as by comparing Table 42<sup>146</sup> with the data presented in the discussion on TTL.

TABLE 42. ECL RADIATION VULNERABILITY

<u>THREAT</u>	<u>FAILURE LEVEL</u>
$\dot{N}$ ( $n/cm^2$ )	$>10^{15}$
$\gamma_T$ (rad(Si))	$10^7$
$\dot{\gamma}_{UPSET}$ (rad(Si)/sec)	$>10^8$
$\dot{\gamma}_{PERMANENT}$ (rad(Si)/sec)	$10^{11}$

These levels of hardness do not apply to the 93471 ECL/TTL 4K RAM mentioned earlier. In dose rate testing performed by Boeing, 50 ns and 1  $\mu$ s pulses were applied while the device was in the active low output state.<sup>147</sup> For the 50 ns pulses, transient responses exceeding 0.8V were observed at  $7 \times 10^7$  rads(Si)/sec. Data upset was observed at  $10^9$  rads(Si)/sec. For the 1  $\mu$ s pulses, voltage transients exceeding 0.8V were observed at  $7 \times 10^6$  rads(Si)/sec and data upset at  $1.5 \times 10^7$  rads(Si)/sec. These values of transient upset are well below those of RAMS which are only TTL or ECL.

Just as TTL total dose and dose rate failure levels are dependent on pulse width, so are ECL failure levels. This means it is important to consider the nature of the pulse when evaluating gate hardness. For an MC1678L, a typical ECL NOR gate, the radiation tolerance is as shown in Table 43.<sup>138</sup>



TABLE 43. ECL IC PULSE-WIDTH FAILURE LEVEL DEPENDENCE

ECL Transient Susceptibility ( $\gamma$ ,  $\frac{\text{rad(Si)}}{\text{sec}}$ )

Narrow Pulse

( $t_p = 10 \text{ ns}$ )

$3-5 \times 10^8$

Wide Pulse

( $t_p = 4 \text{ us}$ )

$1-1.5 \times 10^8$

This concludes the work on ECL. As mentioned previously the scarcity of ECL radiation data prohibited an in-depth study. Points to remember are that ECL is both faster and harder than any commercial bipolar technology. These advantages are offset by the very high power consumption which is the one factor that has restricted the use of ECL.

#### 5.2.4.3 Radar System Parts List

Table 44 represents a list of semiconductor discretes and integrated circuits which might be found in a typical radar system. Also included are selected manufacturer's specifications and an estimate of neutron irradiation damage for fluences of  $10^{12}$ ,  $10^{13}$ , and  $10^{14} \text{ n/cm}^2$  as predicted by the Messenger-Spratt equation. The Messenger-Spratt equation is presented in the section on discrete semiconductor devices but may be approximated at high frequencies as

$$\frac{1}{\beta_\phi} = \frac{1}{\beta_0} + \frac{K_f}{2\pi f_T}$$

where  $\beta_\phi$  = post-irradiation common emitter dc forward current gain.

$\beta_0$  = pre-irradiation common emitter dc forward current gain.

$\phi$  = neutron fluence

K = material dependent neutron damage factor,  $5.5 \times 10^7 \text{ cm}^2/\text{n-sec}$  for PNP silicon devices,  $8.5 \times 10^7 \text{ cm}^2/\text{n-sec}$  for NPN silicon devices<sup>82</sup>

$f_T$  = gain-bandwidth product



Table 44. The CAT Radar System. Parts 1-15.

Part No.	Vendor	Device Type	Electrical Characteristics & Operating Conditions				
			Min. Output Current (A)	Max. Output Current (A)	Min. Transfer Function	Max. Transfer Function	
MC14441-2 LM123J	Harris Motorola	Quad D-Amp Quad Op. Amp	25 26	100 200	2.5M	3.5M	25
					Type Max. Open Freq. (Hz)	Tech	Type Max. Freq. Open (Hz)
SN64973	TI	Binary Rate Multi.		3.0M		170	4.0M
			Min. Output Voltage (V)	Max. Input Voltage (V)	Max. Logic Current (A)	Max. Fanout =	
MC14454M MC14455M MC14456M MC14457M MC14458M	Fairchild Fairchild Motorola Motorola	Voltage Regulator Voltage Regulator Voltage Regulator Voltage Regulator	15 5 15 5	35 35 35 35	1.0mA 1.0mA 1.0mA 1.0mA	Internally ESD Protected Internally ESD Protected Internally ESD Protected	
					Max. Pwr. Diss. (W)	V <sub>DD</sub> (V)	Current Consumption
MC14564	Motorola	Balanced Modulator- Demodulator	20	330	8	100 mA	100 mA
					Type Max. Open Freq. (Hz)	Tech	Type Max. Freq. Open (Hz)
SE665F	Sigmetics	Phase-Locked Loop		500 Hz		300	100
				Type Logic Level (V)			Type Logic Level (V)
MC4344L	Motorola	Phase-Freq. Detector		2.4	4		800
				Min. Forward Current $I_F = 3 \times I_{F(1)}$	Max. Reverse Current $I_R = 3 \times I_{R(1)}$		
1N4143 1N4858	Fairchild	Switching Diode Diode	100 100	1.0 1.0	200 200	100 100	100 100
				Power Dissipation $\theta_{COP} = 2000 \text{ m}^2$	Min. F <sub>DD</sub> (Hz)	Min. F <sub>DE</sub>	Max. Power Diss. (W)
2N4357 2N4360 2N4359	-	PNP Low Power Transistor PNP Low Power Transistor NPN Low Power Transistor	200 200 400	1.50 1.50 1.50	20 20 100	20 20 100	10 10 50
				Type Max. Open Freq. (Hz)	Tech	Type Max. Open Power Diss. (W)	Type Max. Power Diss. (W)
MC10175L MC10641L	Motorola Motorola	Quad Latch Shift Register	15M 15M	ECL ECL	400n 400n	4.5n 3.8n	
				Min. Output Sink Current (A) / 3 V <sub>DD</sub>	Tech	Type Max. Open Pwr. Diss. (W)	Max. Power Delay (s)
MC10153L MC10164L	Motorola Motorola	Quad Line Receiver 1 of 8 Selector	12m 20m	+.78 +.96	300 300	100 300	2.3n 6.0n
				Max. SW P-P Current (A) / Volt. (V)	Tech	Type Max. Open Pwr. Diss. (W)	Type Max. Power Time (ns)
MC14066BAL MC14066BAL	Motorola Motorola	Quad Analog Switch Quad Analog Switch	10m 10m	16 16	CMOS CMOS	16u 16u	10n 10n
				Type Max. Open Freq. (Hz)	Tech	Type Max. Open Pwr. Diss. (W)	Max. Power Delay (s)
MC10153IL	Motorola	Dual D-Flip-Flop		150M	ECL	200n	4.3n
					Tech	Max. Prop. Delay (s)	Type Max. Total Pkg. Diss. (W)
MC10502L	Motorola	Quad OR NOR		ECL	2.9n		100M
				Tech	Min. Delay (s)	Max. Int. Delay (ns)	Max. Int. Delay (ns)
MC10198L	Motorola	One Shot Time Delay		ECL	10n		50n



It should be noted that since the values used for  $f_0$  and  $f_T$  are manufacturer's minimums, the resulting estimate of post-irradiation gain is a conservative one. From the Messenger-Spratt equation it can be seen that the most vulnerable devices are those with high gain and low injection levels. The effects of radiation on most of the devices was unavailable. Since the Messenger-Spratt equation is only applicable to transistors the effects of neutron irradiation on the gain degradation of transistors is the only radiation damage prediction presented. More extensive predictions of the effects of neutron irradiation on bipolar IC's could be formulated if the constituent transistors were known.

### 5.2.5 Other Technologies

During our study of the radiation vulnerability of integrated circuits it was felt necessary to study some technologies which are currently very popular or are just emerging. These technologies are Gallium Arsenide (GaAs) and N-Channel Metal-Oxide-Semiconductor (NMOS).

#### 5.2.5.1 Gallium Arsenide

Gallium Arsenide (GaAs) has been the subject of intensive R&D programs over the past few years in several companies including Rockwell, McDonnell Douglas, The Aerospace Corp., Lockheed, and IBM. This work has concentrated on the fabrication of GaAs IC's. Much of this activity is aimed at developing a VHSIC (Very High Speed Integrated Circuits) capability. The remarkable speed and power characteristics of GaAs ( $t_{PD} = 100\text{ps}$ ,  $P = 5 \text{ nW}$ ) make it the natural choice for future high speed IC's. What has gone unnoticed is the outstanding radiation resistance of GaAs. In Reference 148 McDonnell Douglas performed a set of theoretical calculations to determine GaAs vulnerability to neutrons, dose, and dose rate.

By predicting the magnitudes of the photocurrents generated, one can predict the vulnerability to dose rate. Dose rate, as has been discussed, presents a severe, yet unsolved hardening problem for IC's. Of all the technologies studied, only GaAs offers any hope of providing an inherently dose rate hardened IC at the anticipated threat.

As was discussed in the section on semiconductor discretes (5.1), photocurrents are caused by electron-hole pairs moving under the influence of electric fields. The rate of formation of these electron-hole pairs can be used as a base for predicting the photocurrents. If all the electron-hole



pairs generated were collected by the electrodes, the primary photocurrent is given by

$$I_{pp} = qg_0 \dot{\gamma} A_j L_c \quad (19)$$

where  $A_j$  = the junction area  
 $q$  = the electron charge  
 $g_0$  = the carrier generation constant of ionizing radiation  
 $L_c$  = effective collection length  
 $\dot{\gamma}$  =  $d\gamma/dt$  = radiation energy deposition rate density

The conversion factor  $g_0 = g(t)/\dot{\gamma}$ , where  $g(t)$  is the carrier generation rate density, is

$$g_0 = 6.25 \times 10^{13} \frac{d}{E_{E-H}} \text{ carriers/cm}^3\text{-rad}$$

where  $d$  = specific density of the irradiated material in  $\text{g/cm}^3$   
 $E_{E-H}$  = the energy required to produce one electron-hole pair in eV

For silicon,  $g_0(\text{Si}) = 4.33 \times 10^{13}$  carriers/ $\text{cm}^3\text{-rad}$ . The value for GaAs is  $g_0(\text{GaAs}) = 6.63 \times 10^{13}$  carriers/ $\text{cm}^3\text{-rad}$ , 50% larger than silicon.<sup>148</sup>

The transient primary photocurrent produced in a pn junction is given by<sup>266</sup>

$$I_{pp}(t) = qA_j \left\{ Wg(t) + \int_0^t g(t-\lambda) \left[ \frac{D_n \exp(-\frac{\lambda}{t_n}) + D_p \exp(-\frac{\lambda}{t_p})}{\sqrt{\pi\lambda}} \right] d\lambda \right\} \quad (20)$$

where  $W$  = depletion width

$Wg(t)$  = the instantaneous photocurrent due to carriers generated in the depletion region

$D_p$  = diffusion constant of holes

$D_n$  = diffusion constant of electrons

$t_p$  = characteristic recombination or trapping time of holes

$t_n$  = characteristic recombination or trapping time of electrons

In tests on GaAs JFET structures the response to pulsed, ionizing radiation was studied.<sup>267</sup> The photocurrents were seen to increase linearly with dose rate at low dose rates but sublinearly at high dose rates. This characteristic is either caused by the onset of band-to-band recombination or recombination through energy states in the bandgap. If the excess carrier concentration is much greater than the initial majority carrier concentration, direct recombination becomes proportional to the square of the excess carrier concentration.<sup>267</sup> The



generation rate at which the transition between linear and square dependence occurs is<sup>267</sup>

$$g_{tr} = 2\delta \left( n_0 + \frac{1}{\delta\tau} \right)^2 \quad (21)$$

where  $\delta$  = direct recombination coefficient

$n_0$  = equilibrium electron concentration

$\tau$  = hole lifetime

By comparing equation (21) to experimentally obtained values the best fit was found at  $\delta = 3.3 \times 10^{-11} \text{ cm}^3/\text{s}$  and  $\tau = 8 \times 10^{-7} \text{ s}$ .

The transient peak photocurrent of a GaAs FET with pn junction gate from equation (20) can be approximated by<sup>267</sup>

$$I_{pp} = qg_0 \dot{\gamma} LW(a + L_D) \quad (22)$$

where  $g_0 = 6.63 \times 10^{13} \text{ electron-hole pairs/cm}^3$

$\dot{\gamma}$  = dose rate in rad(GaAs)/s

$(a + L_D)$  = collection length of about  $5\mu\text{m}$  for typical GaAs FET structures

$L$  = channel length

$W$  = channel width

To see when this photocurrent will cause logic upset it is necessary to find the logic upset current,  $I_{DS}(\text{UPSET})$ . Without irradiation<sup>265</sup>

$$I_{DS} = K(V_G - V_T)^2 \quad (23)$$

where  $I_{DS}$  = drain-to-source current

$K$  = constant

$V_G$  = gate voltage

$V_T$  = threshold voltage

Where near the threshold voltage,  $V_T$ , a relation analogous to MOSFETs is obtained<sup>134</sup>

$$K = \frac{\mu C_0 W}{2aL} = K' (W/L) \quad (24)$$

where  $C_0$  = gate capacitance per unit area

$\mu$  = majority carrier mobility



When the logic upset current for a gate is defined as<sup>268</sup>

$$I_{DS}(\text{UPSET}) = K' \frac{W}{L} (V_{NM} - V_T)^2 \quad (25)$$

where  $K' = \mu C_0 / 2 = 1 \times 10^{-4} \text{ A/V}^2$   
 $V_{NM} = 0.5\text{V}$  is the noise margin  
 $V_T = 0.25\text{V}$  = threshold voltage  
 $L$  = channel length

the logic upset dose rate,  $\dot{\gamma}_{\text{UPSET}}$ , can be evaluated.

Equating equations (22) and (25) yields an upset dose rate of

$$\dot{\gamma}_{\text{UPSET}} = \frac{K' (V_{NM} - V_T)^2}{q g_0 L^2 (a + L_D)} \quad (26)$$

Using numerical values for a gate with a channel length of 2.5 $\mu\text{m}$ ,  
namely

$$\begin{aligned} K' &= 1 \times 10^{-4} \text{ A/V}^2 \\ V_{NM} &= 0.5\text{V} \\ V_T &= 0.25\text{V} \\ a + L_D &= 5\mu\text{m} \\ L &= 2.5\mu\text{m} \\ g_0 &= 6.63 \times 10^{13} \text{ e-h pairs/cm}^3 \end{aligned}$$

gives a value for  $\dot{\gamma}_{\text{UPSET}}$  of

$$\dot{\gamma}_{\text{UPSET}} = 1.175 \times 10^{11} \text{ rad(GaAs)}/\text{s.}$$

It should be mentioned that the levels measured in rad(GaAs) may be compared to rad(Si) since the conversion factor is 1.06 rad(Si) = 1 rad(GaAs).

These theoretical predictions were compared to experimentally obtained values for three integrated circuits.<sup>148</sup>

A. Nine-stage ring oscillator

B. Buffer stages

C. Memory cell circuits with ion implanted resistors and external resistors



For the oscillator, oscillations were suppressed at  $i = 1.14 \times 10^{10}$  rad(GaAs)/sec. For the buffer circuit, logic upset had occurred in a majority of the devices by about  $1 \times 10^{10}$  rad(GaAs)/s. Memory cells, consisting of a flip flop with read and write circuitry, had upset levels in excess of  $1.2 \times 10^{10}$  rad(GaAs)/s. The first failure mode regarding circuit survivability occurred at  $1 \times 10^{11}$  rad(GaAs)/s with the occurrence of gold metalization burnout. By using thicker and wider metalization a survival dose rate of greater than  $10^{11}$  rad(GaAs)/s can be achieved with present technology.<sup>148</sup>

The correlation of the theoretical and experimental failure levels gives credence to the validity of the theoretical calculations. The above devices were SSI planar circuits, but are capable of being expanded into MSI and eventually into LSI. The state-of-the-art technology is able to offer radiation tolerance of GaAs IC's with negligible degradation of electrical performance for<sup>148</sup>

Fast Neutrons	$1 \times 10^{15}$ n/cm <sup>2</sup> ( $E > 10\text{KeV}$ )
Total dose of ionizing radiation	$1 \times 10^7$ rad (GaAs)
Dose rate for logic upset	$8 \times 10^9 - 2 \times 10^{10}$ rad(GaAs)/s.
Survival dose rate	$1 \times 10^{11}$ rad(GaAs)/s

These levels are expected to increase due to advances in fabrication and material technology and device and IC design and should result in the following levels.<sup>148</sup>

Fast Neutrons	$\sim 5 \times 10^{15}$ n/cm <sup>2</sup> ( $E > 10\text{KeV}$ )
Total dose of ionizing radiation	$\sim 1 \times 10^8$ rad(GaAs)
Dose rate for logic upset	$\sim 5 \times 10^{10}$ rad(GaAs)/s
Survival dose rate	$\sim 5 \times 10^{11}$ rad(GaAs)/s

While GaAs has outstanding radiation resistance to total dose and neutron fluence, so do other commercially available technologies. However, only GaAs appears to have the ability to withstand the dose rate threat that has been imposed on the system. The combination makes GaAs devices and IC's the logical candidates for use in hardened system electronics required to operate in severe nuclear radiation environments.



Additional data on GaAs tunnel diodes and GaAs FET's can be found in the sections on discrete semiconductors (5.1) and microwave devices (6) respectively.



### 5.2.5.2 N-Channel Metal-Oxide-Semiconductor (NMOS)

This section has been included to warn of the problems posed by a radiation environment for NMOS devices, in particular microprocessors ( $\mu$ P's). NMOS offers high densities along with moderate speed and power. These attributes together with the fact that NMOS is a fairly mature technology (pre-1970) has allowed NMOS to become the dominant semiconductor technology, particularly at the LSI level. But these advantages lose their importance in a radiation environment since is among the softest technologies to total dose. Fortunately the wide use of NMOS has prompted considerable work on NMOS radiation testing and hardening.

Among the state-of-the-art devices are a number of  $\mu$ P's, including the Intel 8086, Motorola 68000, Zilog Z8000, and the Texas Instruments TMS9985. National recently introduced a 32K Static Random Access Memory (RAM), the 6132, and a 65K Dynamic RAM, as have TI and Motorola. 64K Read Only Memories (ROM's) and 65K Programmable ROM's (PROM's) have also been recently announced. Japanese manufacturers have announced the introduction of a 256K RAM.

As is true with all MOS technologies, NMOS is inherently hard to neutron irradiation and does not have problems below fluences of  $10^{15}$  n/cm<sup>2</sup>.

Failure from total dose has been reported as low as 500 rad(Si) for the Intel 8080  $\mu$ P.<sup>149</sup> The vulnerability to total dose has been summarized in Figure 101<sup>64,136,138,139</sup> where the bar represents the range of observed failures. Note that no devices have been observed to survive a total dose of greater than  $2 \times 10^4$  rads(Si) and that all device types have been observed to fail by  $7 \times 10^2$  rads(Si). R&D efforts, begun by EMM-SEMI and NRL in 1979, have produced hardened NMOS devices which may be able to survive a total dose of  $10^5$  rads(Si)<sup>136</sup> at low dose rates.

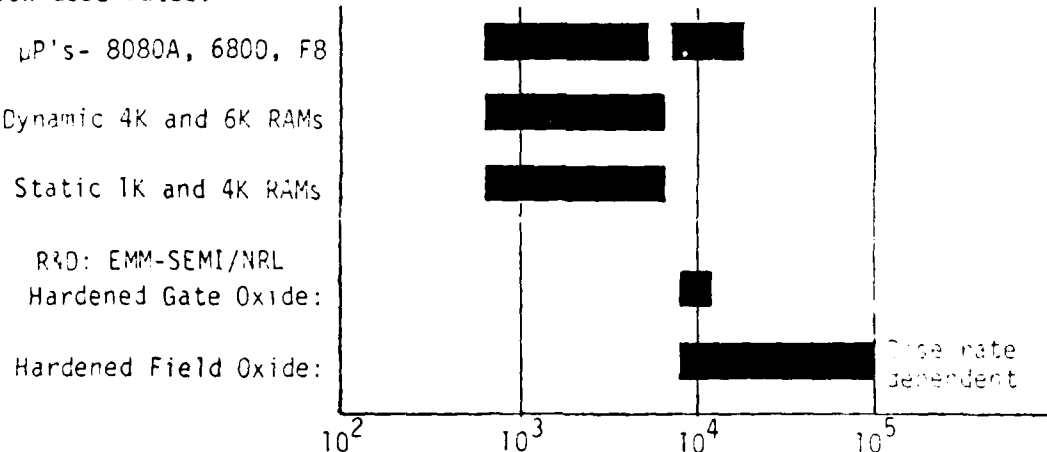


Figure 101. NMOS Total Dose Failure Levels



NMOS is also among the most vulnerable to dose rate, the Intel 8080 EP having been observed to fail at dose rate less than  $10^5$  rads(Si)/sec.<sup>149</sup> Dose rate vulnerability has been summarized in Figure 102,<sup>64,136,138,139</sup> for two pulse widths.

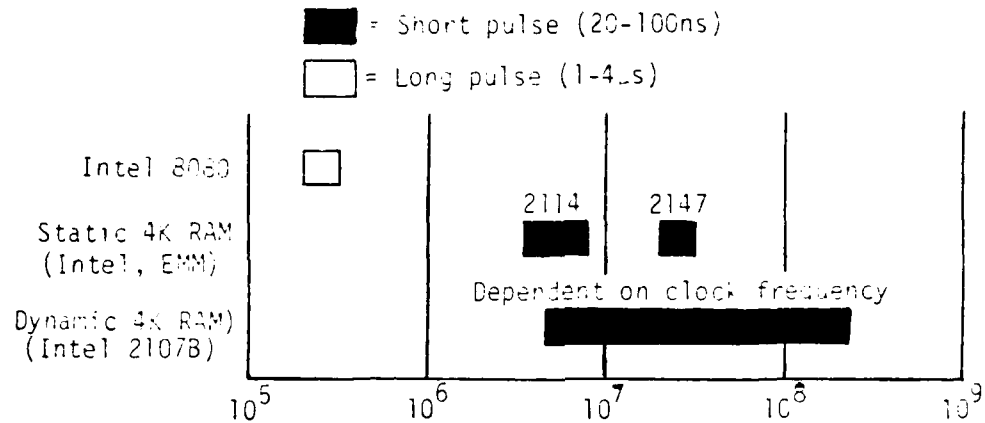


Figure 102. NMOS Dose Rate-Induced Transient Upset Failure Levels

At the anticipated threat levels for both total dose and dose rate, Figure 101 and Figure 102 show that no NMOS devices will survive. This leads us to make the following total dose and dose rate hardening recommendation.  
DO NOT USE NMOS!



## 6.0 MICROWAVE AND MILLIMETER WAVE DEVICES

BMDATC-radar is exploring systems concepts in the high frequency region. Therefore, it was appropriate to include some typical classes and types of devices that operate in the microwave region and above in this study. Specifically, the classes that were included were: 1.) Impatt-like devices, Gunn diodes; 3.) PIN diodes; 4.) Ferrite phase shifters; and 5.) Gigahertz GaAs field effect transistors (FETs). Compared to device classes discussed previously in section 6.0 these are rather specialized classes and, as such, there is less radiation data on these classes than on RF devices. However, the data that does exist has been compiled, summarized, and is included in the report.

### 6.1 Impatt-like devices

As the title of this subsection implies this portion of the report will not be confined to just Impatts but will also include Trapatts and Baritt diodes. In order to understand the impact of transient radiation on these type of devices a brief discussion of the operation of Impatts in elementary terms would be appropriate. It was felt that this discussion should concentrate primarily on Impatts since the operation of Trapatts and Baritts are very similar.

The term Impatt is an acronym that stands for " impact ionization avalanche with transit time ". Conventional semiconductor devices operate by controlling the flow of charge carriers at a p-n junction and, therefore, are subjected to the fundamental transit time limitation. From the early 1950s, the possibility was considered of using the effects of the finite carrier transit time rather than allowing it to remain as a limiting factor. Starting in the early 1950s, various schemes were proposed to achieve this. One such scheme was the avalanche transit time diode structure first proposed by Read<sup>150</sup> in 1958.

Before examining the internal mechanism of Impatt diodes used as oscillators, it must first be realized that there are two basic requirements for a feedback oscillator. First the feedback from the oscillator must be of sufficient magnitude to drive the input and, second, the frequency of the oscillation is determined by the phase condition of the output with the phase difference between the

input and output differing by a multiple of  $2\pi$ . A two terminal diode device can act as a delay by storing the information within itself for a finite time. This is the "transit time" referred to by the last two letters in Impatt. In the forward biased case, there is certainly a transit time involved in getting the charge carriers across the junction. However, there is no gain so the diode cannot sustain oscillation.

A junction biased in the reverse direction would seem just as useless because very little current flows in this condition by definition. However, as discussed in the section on diodes, the application of a large enough reverse potential results in a breakdown of the blocking condition, i.e., the impedance is reduced and the current is multiplied. As was discussed previously, there are really two mechanisms whereby breakdown can occur: the Zener effect and avalanche breakdown. Avalanche breakdown is the mechanism of concern for Impatts. This mechanism results from the acceleration of carriers by the applied reverse electric field to the pn junction such that they are capable of and, in fact, do collide with and ionize lattice atoms in the junction. The resulting carriers are further accelerated which results in more ionization causing more free carriers to be formed. This is the "impact ionization avalanche" that is referred to by the first four letters in Impatt.

The width of a junction in the reversed biased condition depends, among other things, on the doping densities. One model that illustrates this is the abrupt junction pictured in Figure 103. The total width of such a

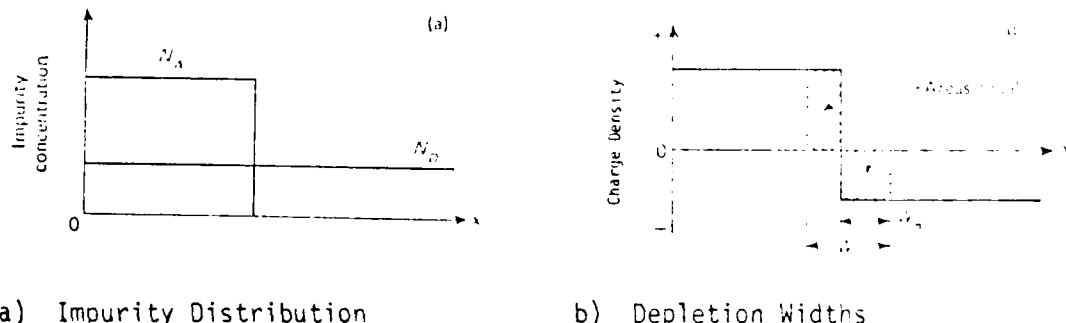
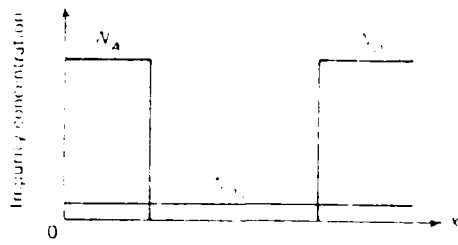


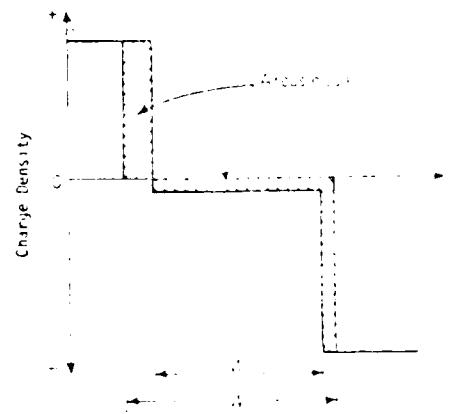
Figure 103. Idealized Abrupt pn Junction

junction is dominated by the density of impurities in the portion of the material with the lowest doping density. This results simply from the fact that charge neutrality must be maintained and, therefore, the number of uncovered charges (i.e., donors that have given up an electron or acceptors which have accepted an electron) on each side of the junction must be equal. This implies that the penetration of the depletion region is the greatest on the lower doped side of the junction. One method of forming an abrupt junction is depicted in Figure 103a. It consists of introducing a high density of acceptors ( $N_A$ ) into a region that was uniformly more lightly doped. Figure 103b compares the total depletion layer width,  $W$ , with that of the lightly doped side,  $W_1$ .

A modification of this method which produces a PIN diode structure that is related to that proposed by Read is illustrated in Figure 104. In this method, a high density of acceptors is introduced into one end of homogeneous material which has been lightly doped and a high density of donors is introduced into the other end (Figure 104a). For an Impatt-type device, it is immaterial whether the lightly doped region contains donors, acceptors, or any impurities at all. The original structure proposed by Read was  $n^+ipi^+$  where + denotes high doping and i means intrinsic<sup>150</sup>. A variety of similar structures have been proposed, analyzed, and fabricated including  $n^+pp^+$ <sup>151</sup>,  $p^{++}nn^{++}$ <sup>152</sup>, and  $p^{++}n^+nn^{++}$ <sup>152</sup>. The only thing concerning the doping densities that is critical to the operation of an Impatt is that the total number of uncovered charges in the entire lightly doped region should be less than the



a) Impurity Distribution



b) Depletion Widths

Figure 104. Ideal Abrupt PIN Junction

number in either of the heavily doped regions when the diode is reversed biased.<sup>153</sup> This ensures that, for a reversed bias, a punch-through condition extends throughout the lightly doped region, i.e., the space-charge region extends from the p<sup>+</sup>i junction to the n<sup>+</sup> junction. Rather than totally relying on doping profiles to ensure conditions for punch-through, the reverse bias may simply be increased until it exceeds the punch-through voltage of the device.<sup>150</sup>

The region between the heavily doped areas is sometimes referred to as the intrinsic region even though it is one in which a space charge and an electric field do exist. A better descriptor would be "depletion region" since the charge in this region consists of uncovered impurity ions which are stationary and the region is depleted of mobile charges. The field across this depletion region is not necessarily constant. Essentially the depletion region between the heavily doped P and N regions constitutes a relatively long path in which mobile charge carriers will be subjected to an electric field. They will drift along the path under the influence of the field provided the field is in the correct direction. This path is called the "drift space". In this space, free electrons will drift towards the n<sup>+</sup> region and holes toward the p<sup>+</sup> region. Essentially the Impatt diode can be regarded as an accelerator. Minority carriers (holes from the n region and electrons from the p region) as well as electrons and holes generated thermally in the region will be swept through the drift space.

In the drift space, the carriers will not be accelerated to higher and higher velocities. Electrical potential energy is being converted to kinetic energy of the carriers and their velocity increases. However, the carriers interact with and transfer energy to the atoms which make up the crystal. Essentially the lost carrier energy results in increasing the thermal vibration of the lattice atoms and the temperature of the crystal rises. In crossing the drift space, the carriers attain a stable velocity which for silicon is approximately  $10^7$  cm/sec or about 2 million miles per hour.<sup>153</sup> Although this velocity is high, it is still not in the relativistic region since the speed of light in free space is still a factor of 300 greater.

The above discussion should not be taken to imply that the carriers will attain a saturating value of velocity for all values of fields. The

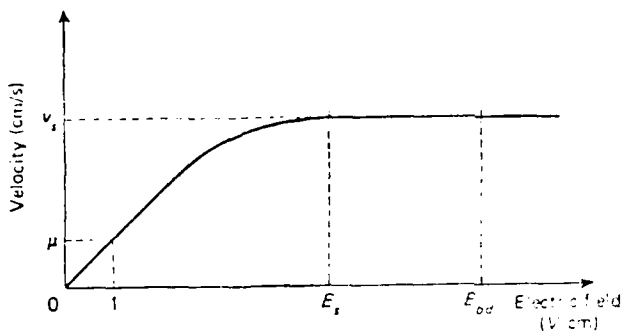


Figure 105. Idealized Plot of the Velocity of Free Electrons in Semiconductors Versus Electric Field

actual situation is depicted in Figure 105.<sup>153</sup> As indicated in this figure, the curve is linear at low fields and velocities. The linear region is the area where RF devices are operated. In this area a concept known as mobility is valid. The electron mobility,  $\mu$ , is simply the velocity of a free electron in that material at a condition in which the value of the electric field is unity. Utilizing this concept, the velocity can be expressed simply as

$$v = \mu E$$

Mobility is an important concern to the operation of Gunn diodes and will be discussed more fully in the portion of the report on these devices.

In any case, there exists a saturation field,  $E_s$ , such that further increases in the field will not result in a substantial increase in the electron velocity. The field throughout the drift space does not have to be constant but simply above  $E_s$  in order to ensure that the carriers all have attained the saturated value of velocity,  $v_s$ . The constant velocity, of course, implies that the transit time is determined by the length,  $W$ , of the depletion region and, hence, the time delay between the output and input to an Impatt is controlled by  $W$ .

The discussion up to this point has viewed the PIN structure primarily as a delay line. However, the feedback signal must be of sufficient magnitude to sustain oscillation. As mentioned previously, the mechanism that is used to attain sufficient gain is the avalanche effect of impact ionization. The reader should not be misled by the discussion on the saturation velocity. The concept of a constant value of a saturated velocity is a convenient approximation which allows the easy determination of transit times with a very

small error. In addition, the curve in Figure 105 approaches  $v_s$  asymptotically. The fact that increasing the field to  $E_{bd}$  (the value of the field in Figure 105 necessary for avalanche breakdown) does not substantially increase the free electron velocity above  $v_s$  does not mean that the kinetic energy of the electron and, hence, the energy that is available to be transferred to lattice atoms has not been increased. It must be remembered that the energy varies as the square of the velocity and, therefore, small increases in velocity are reflected in larger increases in kinetic energy.

The field has a large peak at the junction of the  $p^+$  and n regions (the n region has been referred to as the intrinsic region in the foregoing discussion). This is a result of the potential gradient,  $dV/dx$ , in going from the  $p^+$  to the n region. The rate of pair production is a sensitive nonlinear function of the field which has been found to be<sup>154</sup> given by

$$\alpha = E^m$$

A value of 6 for  $m$  has been found to yield a good fit to the data below about 500 kilovolts/cm. By proper doping the field can be given a relatively sharp peak so that multiplication is confined to a very narrow region at the  $p^+$ -n junction.<sup>150</sup> In addition, if the doping profile over the n region varies logarithmically the field will be constant over the rest of the n region.<sup>153</sup> A typical field distribution for a Read diode is shown in Figure 106.<sup>153</sup>

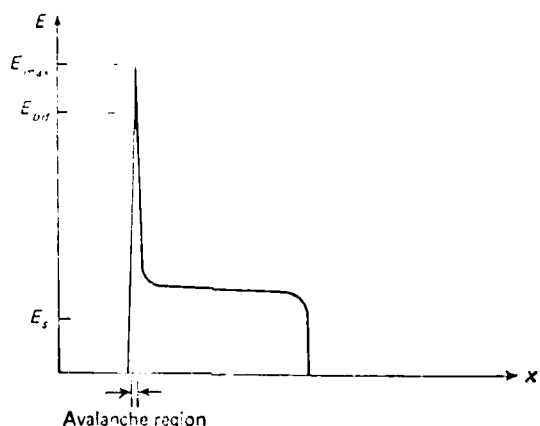


Figure 106. Electric Field Distribution Through a Read Diode.

In order to maintain a constant velocity, the field must exceed  $E_s$  at all points in the diode and, for avalanche ionization to occur, the peak field must exceed the breakdown field,  $E_{bd}$ . For this situation electrons will be generated in the avalanche region and swept into and across the drift space. After a delay of one transit time, they will appear at the  $n^+$  region.

There is one unusual phenomenon in an Impatt which deserves mention. Consider the effect of a single square pulse superimposed on a d.c. bias potential which momentarily causes the peak value of the field to exceed  $E_{bd}$ . Free electrons will be formed and swept into the drift space for a time  $\Delta t$  as indicated in Figure 107. Assume that  $\Delta t$  is less than the transit time,  $t_t$ . Under these conditions the voltage pulse is translated into a current pulse which is swept through the drift space. Because velocity saturation is occurring the amount of diffusion that occurs is minimal.<sup>153</sup> Diffusion will only occur when there is an assembly of mobile particles which are free to move in any direction. However, in this case, the mobile particles are constrained by the field to move in one direction so the conditions for diffusion are not present. Therefore, the current pulse will be just as abrupt in passing out of the drift space as it was when it was formed and the

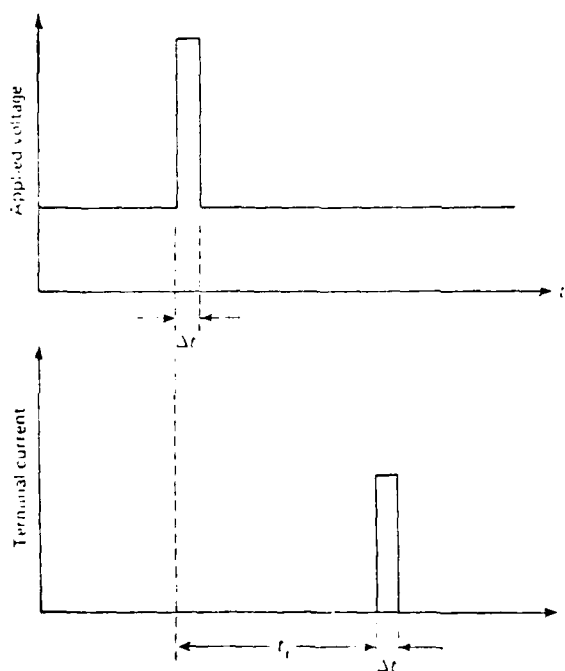


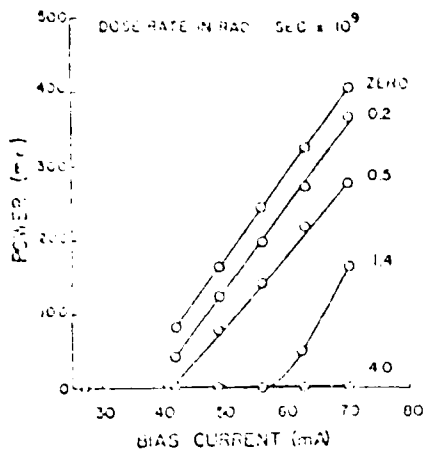
Figure 107. Time Displacement of a Square Voltage Pulse Applied to an Impatt Diode and Its Resultant Square Current Pulse

situation exists in which a signal will not be degraded as it moves through a piece of semiconductor material.

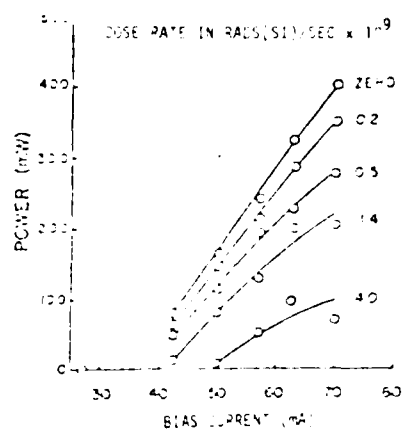
Returning to the main topic, i.e., the operation of an Impatt oscillator, the above discussion indicates that the Impatt diode does satisfy the two requirements for oscillation: gain and a controllable phase relationship between the input and output. In order to form an oscillator the current pulse from an Impatt is used to form a potential which is fed back to the diode terminals. This is achieved by mounting the diode in a tuned microwave cavity in which the transit time of the diode is consistent with the frequency to which the cavity is tuned and thus oscillation is attained and maintained. This ends the discussion on the operation of Impatts. For a more complete discussion on the generalized Impatt theory, the reader is referred to references 151 and 155.

An Impatt oscillator is composed, of course, of two parts: the diode itself and the microwave cavity. Transient radiation affects both parts. The impact of radiation on the cavity is to ionize the air or gas which fills the cavity. The fact that ionizing radiation does impact a gas-filled microwave cavity is well known.<sup>156</sup> In fact, this effect has been used to monitor power levels inside reactor cores.<sup>157,158,159</sup> It has been shown that the ionization of the air causes a shift in the resonant frequency and a change in the cavity Q.<sup>156,157</sup> The change in the resonant frequency is very small but the change in Q can be as large as 30% for a dose rate of  $3 \times 10^9$  rads(Si)/sec.<sup>160</sup> This loss in Q results in a reduction in the RF power from the oscillator. In addition, the air ionization provides a shunt path for the diode bias current which further reduces the power. It has also been observed that there is a delay in the build up of RF power after the radiation pulse (on the order of 50 nanoseconds) which has been attributed to air ionization - recombination effects.<sup>160</sup>

However, the reduction in RF power due to the ionization of air in the cavity does not occur at all levels of dose rate. The threshold appears to be between 1.4 and  $4.0 \times 10^9$  rads (Si)/sec as can be seen by a comparison of the two parts of Figure 108<sup>160</sup>. It should be noted that this effect is not unique to Impatts but occurs for all microwave devices requiring a cavity including traveling wave tubes (TWTs). Even though the ionized air-induced



a) Evacuated Microwave Cavity



b) Air-filled Microwave Cavity

Figure 108. RF Power From an Impatt

reduction in  $Q$  will be present at the threat levels, it is easily mitigated by simply evacuating the cavity.

The other part of an Impatt oscillator is, of course, the diode itself. The oscillator characteristics of Impatt diodes are virtually unchanged after exposures to neutron fluences of  $10^{15} \text{ n/cm}^2$ .<sup>161,162</sup> This threshold is based on empirical data but it is in agreement with theoretical calculations.<sup>163</sup> Typical data for Impatts is depicted in Figure 109<sup>161</sup> for the output power and

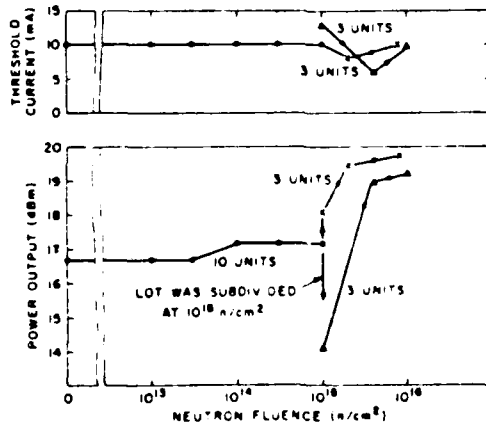


Figure 109. Threshold Current and Output Power for X-Band, Silicon Impatt Oscillators as a Function of Neutron Fluence

the threshold current for oscillation. In this figure, the original lot of 10 was divided into two sublots at  $10^{15}$  n/cm<sup>2</sup>, one with a high-average output power and one with a low-average power. As indicated by the figure, these type devices should essentially suffer little or no degradation at the threat level of neutron fluence.

Although neutrons present no problem, the same cannot be said of ionizing transient radiation. The primary effect of this radiation is the same as for any other semiconductor, namely, the generation of electron-hole pairs throughout the Impatt. This additional generation of electron-hole pairs manifests itself as an increase in the leakage current of the diode. This current is proportional to the dose rate and the sum of the volume of the depletion region and the volume bounded by one diffusion length from the depletion region (i.e., the effective volume). The effect of this additional leakage current is a premature build up of the avalanche current which results in reduced RF power and an increase in the frequency of oscillation.<sup>164,165</sup> In addition, reference 166 concludes that the affect of leakage current on the operation of Impatt oscillators is to damp the oscillations and, thereby, reduce the power output and the oscillator's efficiency. Computer calculations indicate that a bias current to leakage current ratio of 100 to 1 reduces the RF power output to one-half that which would have been obtained without any leakage current.<sup>164</sup>

This predicted quenching effect has been well substantiated by empirical data.<sup>167-173</sup> Reference 167 indicates that a ceasing of RF power (5 mW or less) in silicon oscillators occurs during and for 15 minutes after a 15 millisecond pulse of a combined neutron and gamma flux of  $3 \times 10^{15}$  n/cm<sup>2</sup> and  $5 \times 10^6$  rads(Si)/sec, respectively. Full recovery of RF power occurred only after the bias was reduced to zero and then increased back to preirradiation levels. At approximately twice these radiation levels, irreversible diode failure occurred.<sup>119</sup> Reference 170 indicates that 100 mW silicon Impatt oscillators ceased oscillation after an exposure to  $7 \times 10^7$  rads(Si)/sec. However, in this case, the oscillation resumed immediately after the exposure with no change in operating conditions. Reference 171 indicates that 200 mW GaAs Schottky barrier Impatt oscillator only experienced a small fractional change in RF power after an exposure to  $7 \times 10^9$  rads(GaAs)/sec. In this case, full power was obtained



immediately after the pulse with no change in operating conditions. The reduction in RF power has also been observed in injection locked Impatt oscillators following an exposure to rates of  $1 \times 10^8$  and  $3 \times 10^9$  rads(Si)/sec.<sup>173</sup> Figure 110

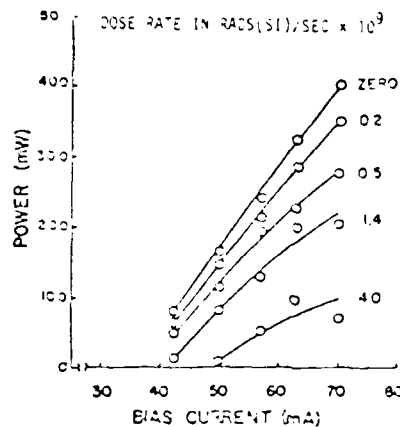


Figure 110. RF Power From a 10 GHz Impatt Oscillator For Various Dose Rates

is indicative of the data.<sup>160</sup> This data was for a X-band silicon double epi Impatt diode. However, it should be noted that oscillation did cease when the dose rate was increased beyond  $5 \times 10^9$  rads(Si)/sec.

As mentioned previously, the effect of the additional leakage current generated by the ionizing radiation pulse is the premature buildup of the avalanche current. This means that the  $90^\circ$  phase lag between the voltage and current is reduced, i.e., the leakage current leads to a premature buildup of the avalanche current which, in turn, deteriorates the optimum phase relationship between the current and voltage. The smaller the transit time through the avalanche region, the greater will be the reduction in the  $90^\circ$  phase lag between the current and voltage.<sup>160</sup> Therefore, Impatt diodes with thin avalanche regions are predicted to be more susceptible to leakage current effects.

Oscillators will also experience a temporary dose rate-induced frequency shift. Typical shifts are shown in Figure 111.<sup>160</sup> As can be seen, these are in the MHz range. However, it must be noted that these changes during the pulse are critically dependent upon the RF circuit as well as the

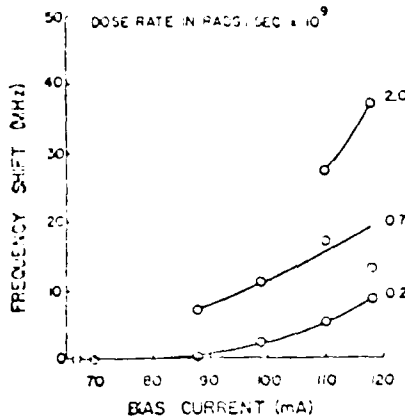


Figure 111. Dose Rate Induced Frequency Shifts in a 10 GHz Impatt Oscillator

Impatt diode itself. This data was for a X-band silicon diffused Impatt diode.

The effects discussed above are temporary in the sense that the diode and oscillator do return to preirradiation values. However, it has been briefly mentioned previously that permanent effects have also been reported.<sup>167,169,172,174</sup> In some cases catastrophic failure occurred<sup>169,172</sup> and in others a lower power but a stable oscillating condition was obtained even though the device does not necessarily undergo irreversible change.<sup>172,174</sup> Reference 174 indicates that the permanent effects reported in references 167,169 and 172 could have been caused by the long cable length that is often used between the diode and the bias network to allow for the incorporation of the proper radiation shielding. It has been shown that bias circuit instabilities are possible for cable lengths greater than 4 feet.<sup>175</sup> Based upon the reported descriptions of the radiation facilities, reference 174 concludes that the failures reported in references 169 and 172 were due to improper bias circuit impedance and that reference 175 should be used as a guide in this area.

Three major conclusions were reached in reference 174, which is the latest published report on radiation-induced permanent effects on Impatts the authors have been able to uncover. These are:

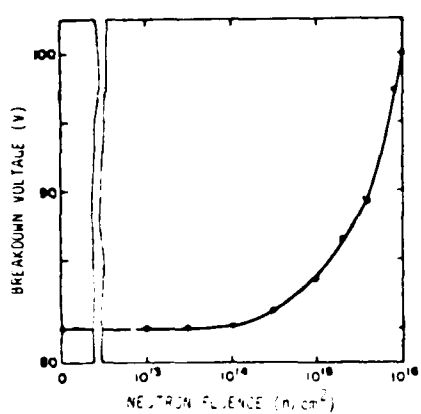
1. The permanent effects are related to a diode-circuit interaction.
2. The principal cause of the permanent effects is not improper

bias circuit impedance that results in bias circuit oscillations. However, it is believed that bias circuit oscillations, combined with the permanent effects, have caused diode failures reported in references 169 and 172.

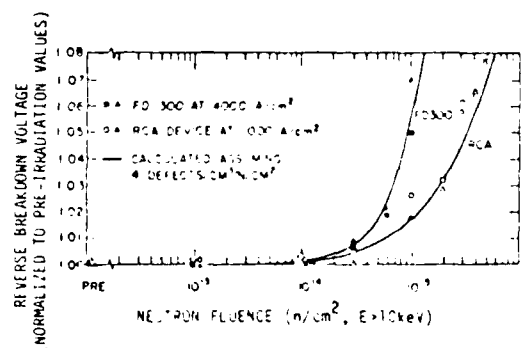
3. The GaAs Schottky diode is more prone to permanent effects. They occur at power levels above 200mW and dose rates above  $2 \times 10^9$  rads(GaAs)/sec. The permanent effects in Si and GaAs diffused diodes only occur with the diode operating slightly below power saturation and/or spectrum deterioration and at dose rates of approximately  $8 \times 10^9$  rads (Si)/sec. The GaAs diffused diode was more prone to these permanent effects than the Si diffused diodes.

This finishes the discussion on Impatts. However, as indicated at the beginning of this section, there are a number of variants of the basic Impatt structure. One of these is the Trapatt diode. Trapatt is an acronym that stands for trapped plasma avalanche triggered. Like Impatts, these devices are punch-through  $p^+nn^+$  devices. Also like Impatts, neutron exposure does not affect the breakdown voltage until the fluences are large enough to cause carrier removal at the edges of the space-charge region in the  $p^+$  and  $n^+$  region.<sup>176</sup> Devices with heavy doping in the  $p^+$  and  $n^+$  regions and an abrupt doping profile will be more resistant to carrier removal at the edges of the space-charge region than a diffused junction device.

Figure 112 indicates the affect of neutron irradiation on the



a) IMPATT



b) TRAPATT

Figure 112. Effects of Neutron Fluence on the Breakdown Voltage of Impatts and Trapatts

breakdown voltage for both Trapatt<sup>176,177</sup> and Impatt<sup>161</sup> diodes. In Figure 112b, there is data on two Trapatts as well as a theoretical calculation.<sup>163</sup> The two device types were operated at the current densities at which the devices worked the best as Trapatt oscillators: the FD300 at 4000 amps/cm<sup>2</sup> and the RCA device type at 1000 amps/cm<sup>2</sup>. The RCA device has a more abrupt doping profile and is indeed more resistant to breakdown voltage increases with neutron fluence. In fact, if the RCA device were operated at the same current density as the FD300 then the difference between the curves would even be more pronounced since increasing the current density decreases the breakdown voltage due to charge trapping.

The vertical scale to the right of Figure 112a has been normalized to a pre-irradiation value of 82 volts. As indicated in this figure, the response of the Impatt is close to that of the RCA device. This is to be expected since this Impatt device that generated this data is a "nearly abrupt" diode and, essentially, the same comments apply for the Impatt that applied for the RCA device. Essentially the guideline for both Impatts and Trapatts is to use heavily doped devices with abrupt doping profiles.

It must be remembered that the increase in breakdown voltage is really advantageous. Unfortunately there are other effects associated with neutron irradiation which are not desirable. One of these is associated with the device's temperature coefficient. For avalanche devices this coefficient is normally defined as  $V^{-1} dV/dT$  for a given bias current and units of  $^{\circ}\text{K}^{-1}$ .<sup>176</sup> As mentioned in the previous paragraphs, the increase in breakdown voltage is due to carrier removal at the edges of the space-charge region. This removal effect is reduced with an increase in temperature because of increased thermal release of trapped charge. The result is a negative contribution to the device's temperature coefficient.<sup>178</sup>

For an unirradiated device, the temperature coefficient is positive because of the positive temperature coefficient of avalanche breakdown. The negative contribution from carrier trapping and the positive contribution from avalanche generation compete with each other to determine the device's overall temperature coefficient. A more abrupt doping profile will reduce the negative contribution from carrier trapping at the edges of the space-charge region.

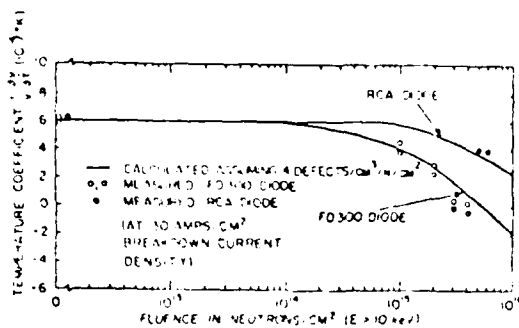


Figure 113. Calculated and Measured Temperature Coefficient at 30 A/cm<sup>2</sup> Versus Neutron Fluence.

Figure 113 is a plot of the measured and calculated temperature coefficient versus neutron fluence at a current density of 30 A/cm<sup>2</sup>. The device with the more abrupt junction (the RCA diode) is more radiation resistant than the FD300. It should be noted that the coefficient for the FD300 becomes negative at the higher fluence. This is important since a negative temperature coefficient implies thermal instabilities (i.e., thermal runaway) and the possibility of current filament formation.<sup>176</sup> The net result, of course, is an increase in the probability of burnout with increasing neutron fluence. This, in fact, has been observed in irradiated Impatt diodes<sup>161</sup> which are very similar to Trapatt in terms of this effect. Fortunately, this effect does not appear to be evident below  $10^{14}$  n/cm<sup>2</sup> and should not be a serious problem in the scenarios proposed for BMDATC-radars. However, it is still recommended to use heavily doped devices with abrupt doping profiles.

As the neutron fluence increases there is a slight increase in frequency for both Impatts and Trapatts.<sup>161-163</sup> Since the frequency is primarily determined by the cavity, the frequency shift is typically one percent or less.<sup>176</sup> In addition, no appreciable degradation of Trapatt mode instantaneous RF output power has been observed below  $6 \times 10^{15}$  n/cm<sup>2</sup>. This is attributed to the alternating "off-on" nature of the Trapatt which switches between a high voltage, low current state and a low voltage, high current state. Neither state is appreciably sensitive to neutron damage. Neutron damage should affect the device's operation only during the transition period by increasing the rate of trapped plasma extraction through added recombination. Since the transition period is only a small portion of an RF cycle, the overall effect on the RF power output should be small.<sup>176</sup>

The degradation of RF output power of a Trapatt oscillator after neutron irradiation is actually due to failure of the ordinary Impatt mode whose presence is necessary to initiate the Trapatt phenomenon.<sup>176</sup> Since Trapatt devices require the presence of a number of harmonically related signals, devices quite often require the existence of an Impatt mode to initially build up RF energy in the microwave cavity to a level sufficient to initiate the first Trapatt oscillation. The time delay between the application of a bias pulse and the actual initiation of the Trapatt phenomenon (i.e., the buildup time) is inversely related to the small-signal growth rate of the ordinary Impatt mode.<sup>176</sup> Neutron exposure degrades the small-signal growth rate of Impatts because some of the carriers injected by the avalanche mechanism recombine as they transit the space-charge region.<sup>163</sup> The buildup time decreases the amount of time during the application of the bias pulse when RF power is being generated and thus reduces the average output power. This effect is depicted in Figure 114 where the average output power for a 500 nsec bias pulse length is plotted versus neutron fluence.<sup>176</sup> As indicated by this figure, the RCA device is essentially unaffected by fluences of  $10^{15} \text{ n/cm}^2$  or lower. The RCA diode is a 1 GHz device with a depletion width of 6 microns and the FD300 is a 600 MHz device with a depletion width of 10 microns. A narrower depletion width, of course, means a shorter transit time which also means less chance of avalanche injected carriers recombining as they cross the space-charge region. Basically, this means that higher frequency devices have a shorter buildup time and, hence, are more resistant to neutron-induced degradation.

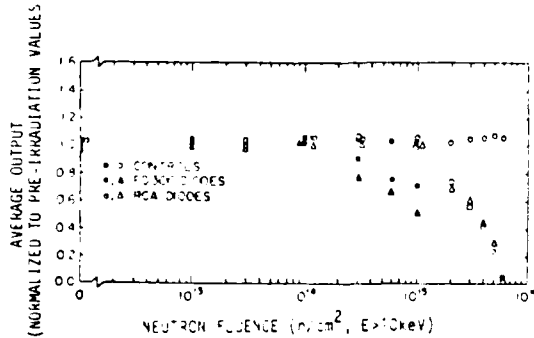


Figure 114. Average RF Output Power Normalized to Pre-irradiation Values Versus Neutron Fluence for 500 nsec. Bias Pulses.

By defining RF failure to mean an increase in the buildup time on the order of 250 nsec, using the equations in reference 173 which define the optimum space-width for a given frequency (optimum width is proportioned to  $f^{-1}$ ), and using the results in reference 161 on carrier lifetime as a function of neutron fluence (lifetime inversely proportional to the fluence at high fluence levels), the frequency of operation has been found to be linear with the level of neutron fluence required to produce RF failure. Such a qualitative result is depicted in Figure 115<sup>176</sup> with the unity slope line representing expected behavior for RF failure as a function of neutron fluence. This line has been matched to the 1 GHz RCA device. The area above  $10^{16} \text{ n/cm}^2$  results from an increase in the probability of DC burnout due to the negative temperature coefficient effect. It should also be noted that the threshold is very high and probably poses no problem for Ghertz devices at the threat level.

The discussion up to this point has focused on the affects of neutron irradiation on the performance of Trapatts. However, these devices can also be affected by dose rate. It has been shown that various Trapatt parameters are strongly dependant on the reverse saturation current of the device.<sup>180</sup> Specifically, an increase in the reverse saturation current results in a decrease in the peak electric field and the width of the avalanche region which, in turn, reduces the mobile charge generated by the avalanche shock front. Moreover, these effects occur at unexpectedly low values of the reverse saturation current.<sup>181</sup> As with any semiconductor device, the primary effect of a radiation pulse is the generation of electron-hole pairs throughout the Trapatt diode. This results in an increase in the leakage current which, in

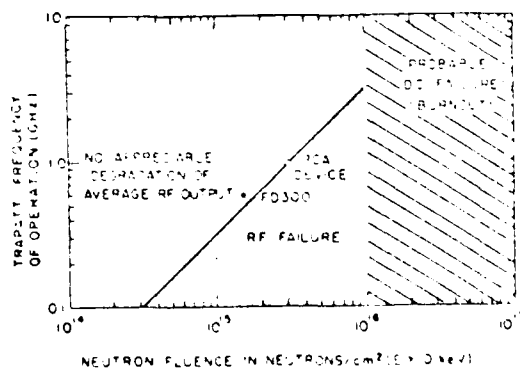


Figure 115. Plot of Trapatt Frequency of Operation Versus Neutron Fluence. RF Failure is Defined as the Buildup Time Exceeding 250 nsec.

turn, serves to increase the reverse saturation current. Thus, Trapatts are expected to be susceptible to dose rate induced effects.

The RF output power from a Trapatt oscillator as a function of dose rate is shown in Figure 116.<sup>181</sup> As this figure indicates, the oscillators exhibited the same behavior in either an air-filled or an evacuated cavity. This is to be expected at these dose rates and for these 1cw Q cavities. Cavity effects are not expected to be significant below approximately  $5.0 \times 10^8$  rads (Si)/sec. The RF power does show a gradual decrease with dose rate up to  $1.8 \times 10^8$  rads (Si)/sec. At this point the power drops to almost zero within a factor of 2 increase in dose rate. Beyond  $3.6 \times 10^8$  rads (Si)/sec, the RF output power is virtually zero. This same behavior has been found in other diodes from the same manufacturer with the critical dose rate ranging from  $8 \times 10^7$  to  $2 \times 10^8$  rads (Si)/sec.<sup>181</sup> However, it must be mentioned that only limited data is available and no attempt has been made to characterize variations between manufacturers.

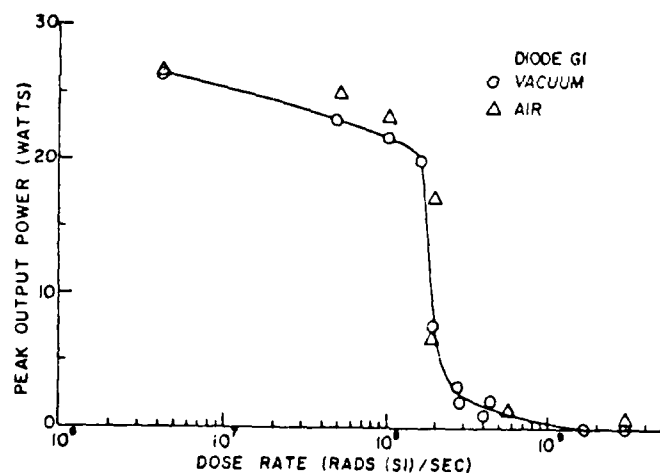


Figure 116. RF Output Power From a 2.5 GHz Trapatt Oscillator as a Function of Dose Rate

The RF power does recover to its original value within 50 nsec after the radiation pulse has ended. It has been found that the behavior of the RF power during the radiation pulse was independent of the position of the radiation pulse with respect to the bias pulse so long as they overlapped.

With nonoverlapping radiation and bias pulses, the radiation had no affect on the RF behavior of the diode. However, it has been observed that if the oscillator has not been carefully tuned, a radiation pulse at the beginning of the bias pulse would turn the oscillator off through the whole bias pulse. Even in these cases, the pre-irradiation characteristic will be restored on further bias pulsing.<sup>181</sup> Thus, it would appear that the RF output power from Trapatt oscillators will drop to zero at threat levels of dose rate but it will return to its original value after 50 nsec.

A first order model of Trapatt operation has been developed to calculate the RF power during the radiation pulse. This model combines the circuit model described in reference 182 and the device equations found in reference 180 to determine the total charge generated during the charging period.<sup>181</sup> A detailed description of this model is beyond the scope of this study. However, a comparison of its results with empirical data is shown in Figure 117.<sup>181</sup> Although the curves do not match exactly, at least the theory does predict a decrease in output power. This simply means that the model is only a rough approximation of the true behavior of a Trapatt diode.

Baritt diodes are another device type that is related to Impatts which deserves some mention. Baritt is an acronym that stands for "barrier injection transit time." They are low-power, low-noise microwave oscillators

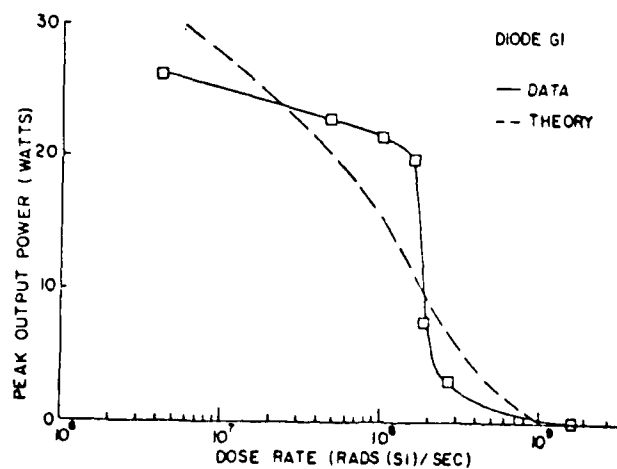


Figure 117. A Comparison of the Theoretical and Experimental Performance of Trapatt Oscillators as a Function of Dose Rate.

which operate on thermionic injection of minority carriers and the transit time delay of these charge carriers.<sup>183</sup> These devices utilize punch-through injection (PTI) rather than avalanche injection used in Impatts and Trapatts.<sup>184</sup> Baritts also differ from Impatts and Trapatts in that their structure is  $n^+pn^+$ , or MSM (metal-semiconductor-metal) with contacts made only to the end regions. This configuration is illustrated in Figure 118<sup>184</sup> and as can be seen closely resembles an open base transistor.

Because of their different structure it will be helpful to briefly discuss the operating principles of Baritts. The application of a small bias voltage ( $V_1$ ) across the diode causes one of the p-n junctions to be forward biased and the other to be reverse biased as shown in Figure 118. The current will be very small since there is a very small probability that charge injected at the forward biased junction (left-hand junction in Figure 118) will be able to diffuse through to the reverse saturation current of the reverse biased junction. As the bias voltage is increased, the depletion region of the reverse biased junction widens while the depletion region of the forward biased junction narrows. Eventually the bias voltage reaches a value ( $V_2$  in Figure 118) where the depletion region reaches the forward biased junction and PTI occurs. Under these conditions, carriers injected at the forward biased junction are swept across the depletion region by the large electric field and the current

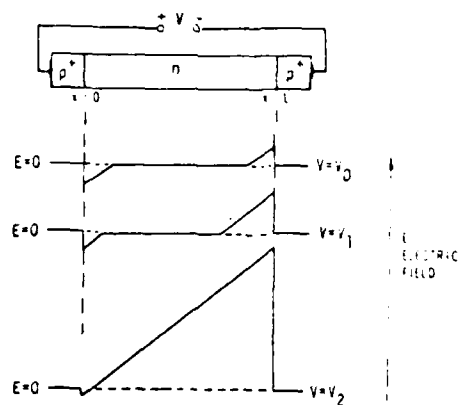


Figure 118. Typical Structure of Baritt Diode and the Electric Field Profile.

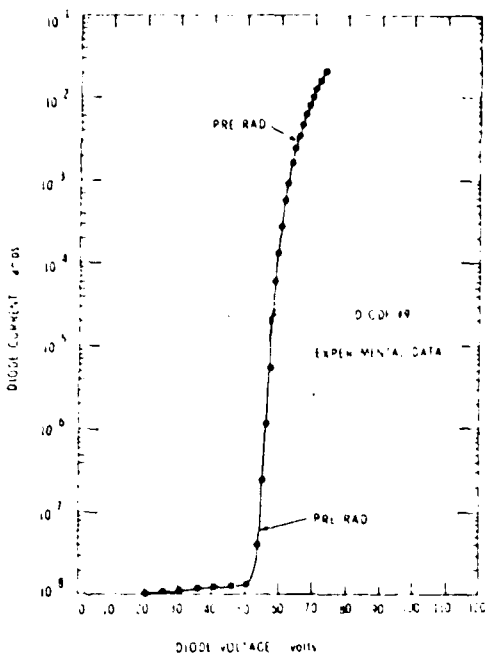


Figure 119. V-I Characteristic of a Baritt Diode

increases quite rapidly as indicated in Figure 119.<sup>184</sup> The voltage at which PTI occurs is given by<sup>185</sup>

$$V \approx eN_D L^2 / 2\epsilon$$

where

$e$  = charge on an electron

$N_D$  = N region uncovered donor density

$L$  = N region width

$\epsilon$  = Dielectric constant

The maximum value of the electric field has been shown<sup>185</sup> to be

$$E_m = eN_D L / \epsilon$$

The only drifting carriers of importance are the holes injected at the forward biased junction.<sup>185</sup> If the field is large enough so that the carriers attain the saturated drift velocity,  $v_s$ , then a transit angle,  $\theta$ , can be defined as  $\omega L/v_s$  where  $\omega$  is the operating frequency.<sup>184</sup> It has been shown<sup>185</sup> that if  $\theta$  has a value of  $3\pi/2$ , then the combination of PTI and carrier drift will cause

the terminal voltage and current waveforms to be such that a negative resistance occurs at a frequency of  $1.5\pi v_s/L$  at a bias of approximately  $V_2$ . The design values of  $N_D$ ,  $L$ , and the optimum operating current density,  $J_{op}$ , vary with frequency.<sup>184-186</sup> Their values are given by<sup>184</sup>

$$N_D = 4 \times 10^5 \omega_0 \varepsilon / (3\pi v_s e)$$

$$L = 3\pi v_s / (2\omega_0)$$

$$J = 10^{-9} \omega_0$$

A comparison of typical V-I characteristics on platinum silicide Schottky diodes before and after neutron exposure is depicted in Figure 120.<sup>184</sup> This figure indicates that at low currents the voltage required to produce a given current decreases with neutron fluence. At high currents the situation is reversed in that the voltage increases with fluence. The reason is that neutron irradiation introduces traps which trap the predominant carrier (electrons) and compensation occurs, i.e., the positively charged uncovered donors are neutralized by the trapped electrons. (For a more complete description of compensation the reader is referred to Section 4.2 on quartz crystals.) This electron trapping lowers the punch-through voltage and causes the current to increase at lower voltages. At higher current levels, the N

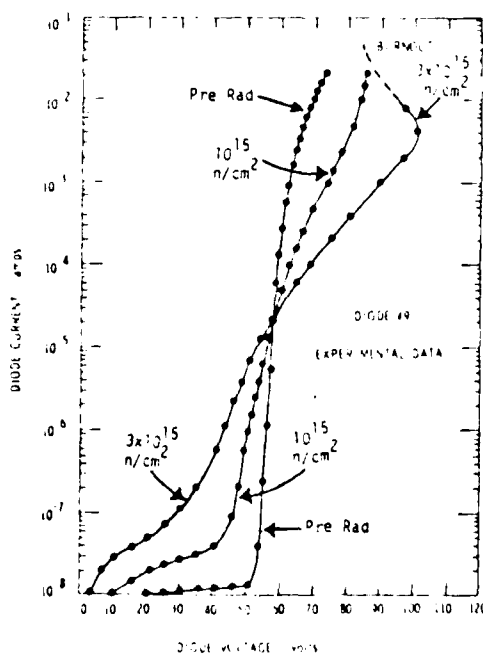


Figure 120. V-I Characteristics of MSM Baritt Diodes Before and After Neutron Exposure.

region is depleted of electrons (by definition of punch-through) and the only carriers available to be trapped are the drifting holes and, therefore, the traps become occupied in the positive state. In effect, this increases the uncovered donor density. Remembering that the definition of  $V_2$  is  $eN_D L^2/2\epsilon$ , the net effect is to increase the punch-through voltage.

Figure 121<sup>184</sup> indicates the affect of neutron irradiation on the microwave output power of a Baritt oscillator operated at a constant input current of 15mA. The increase in power is due mainly to the increase in operating voltage required to maintain a constant current. With further increases in neutron fluence, the output falls off rapidly due to avalanche multiplication of the hole current.<sup>184</sup> This phenomenon occurs when the maximum electric field approaches the avalanche breakdown value of  $2.8 \times 10^5$  V/cm.<sup>187</sup> A prediction of the fluence at which the falloff in power occurs is given by<sup>184</sup>

$$\phi_f = 4.8 \times 10^4 \omega_0 \text{ (n/cm}^2)$$

where  $\omega_0$  is the design frequency. Reference 184 indicates that use of this equation for the device used to generate Figure 121 yields a prediction of  $1.4 \times 10^{15}$  n/cm<sup>2</sup>. However, when the quoted nominal value of frequency of 4.5 GHz for the design frequency was used a value of  $2.16 \times 10^{14}$  n/cm<sup>2</sup> was obtained. It should be noted that the 4.5 GHz value was for nominal operating values of 60V for the voltage and 15 mA for the current. The nominal output power

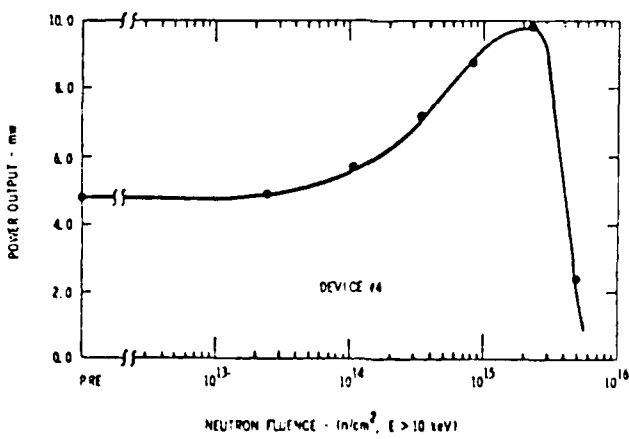


Figure 121. Output Power From a 4.5 GHz Metal-Semiconductor-Metal Baritt Oscillator as a Function of Neutron Fluence.

was 5mW. If the quoted value of  $1.4 \times 10^{15} \text{ n/cm}^2$  is used in the above equation, the required design frequency is 29 GHz - roughly a factor of 6 above the nominal value. Either the design frequency of the device in Figure 121 was considerably higher than the nominal value, the operating conditions in the test caused an increased in frequency, or the multiplier in the equation is wrong and should be replaced by  $3.11 \times 10^5$ . The situation is further complicated by the fact that the derivation of the equation is not given in reference 184 and, as such, the authors view this equation with a great deal of caution and misgivings.

In any case, Figure 121 does indicate that Baritt MSM diodes should be unaffected by neutron fluences levels below  $10^{15} \text{ n/cm}^2$ . Thus, it would appear that they can be used in neutron tolerant microwave oscillators.<sup>184,188</sup> In addition to being neutron tolerant, Baritts are also low noise devices. The same cannot be said for Impatts. Impact ionization is a noisy mechanism. The discontinuous creation of mobile charges results in the discontinuous rise and fall of the space charge in the base region. When Impatt oscillators are working at their optimum condition as feedback devices (i.e., at their resonant frequency) the noise is very great because of the violent fluctuations of current in the ionization region. For silicon Impatt diodes, the noise can be as large as 40 dB.<sup>153</sup> By comparison Baritt diodes are neutron tolerant as are Impatts but have the advantage of being low noise devices.

However, the effects of dose rate on the performance of Baritt oscillators cannot be ignored. Table 45 shows the results of transient ionizing radiation exposure on a variety of Baritt diodes.<sup>189</sup> The characteristics of these devices in a benign environment are listed in Table 4b. The diode labeled Ch was that used to generate the neutron data.<sup>184</sup> The junction of importance is, of course, the injecting contact (i.e., the forward biased junction). Thus, the diodes, S1 and C4, are similar to the Ch diode in that they are flat-profile Schottky diodes with characteristics that bound those of the Ch diode. They are dissimilar in that they have chrome-gold junctions while the Ch diode has a platinum Schottky junction. The diode A4 has a different device design which was proposed in Reference 190 but it still has a chrome-gold Schottky contact. The notation,  $\text{MNV}^+$ , used to designate this device has not been explained in the literature. However, it should be

Table 45. Effects of Dose Rate on Baritt Diodes

Characteristic	Ch(2)	S1 MNP <sup>+</sup>	C4 MNP <sup>+</sup>	A4 MCP <sup>+</sup>	D1 P <sup>+</sup> NP <sup>+</sup>
Type	MNM				
Bias Circuit Impedance (ohms)	500	500(5000)	500(10,000)	330	330(300)
Air-filled or Vacuum Cavity	air	air*	vacuum	vacuum	vacuum
Dose rate for 3dB drop in power (rads/sec)(normalization dose rate)	$2 \times 10^8$	$1.3 \times 10^8$	$\sim 10^9$	$\sim 10^9$	$2 \times 10^7$
Measureable charge storage	Yes	Yes	No	No	Yes
Storage time at $10^9$ rads/sec (nsec)	125	200(300)	-	-	500(25)
Measured photocurrent at $10^9$ rads/sec (mA)	16	15	0.7	2	30
Voltage drop at $10^9$ rads/sec (V)	20	4(14)	0.3 (2)	< 2	17(32)
Measured Secondary Photocurrent $I_s$ at $10^9$ rads/sec (mA)	16.	15.	0.7	2.	30.
Calculated Primary photocurrent $I_p$ at $10^9$ rads/sec (mA)	3.1	9.5	0.75	2.4	0.59
Extrapolated $I_s$ at dose rate for 3dB drop in RF power (mA)	3.2	2.1	0.7	2.	0.6
$I_s$ at dose rate for 3dB drop in RF power divided by nominal operating bias current (later given in Table 46)	0.21	0.12	0.04	0.07	0.04

\* Some vacuum tests were taken with no appreciable change in characteristics under radiation.

Table 46. Baritt Diode Characteristics in a Benign Environment

Characteristic	Ch(2)	S1	C4	A4	D1
Type	MNM	MNP <sup>+</sup>	MNP <sup>+</sup>	MCP <sup>+</sup>	P <sup>+</sup> NP <sup>+</sup>
Area ( $\text{cm}^2$ )	$4.0 \times 10^{-4}$	$9.0 \times 10^{-4}$	$1.8 \times 10^{-4}$	$3.5 \times 10^{-4}$	$1.4 \times 10^{-4}$
Doping Conc. ( $\text{cm}^{-3}$ )	$5.6 \times 10^{14}$	$5 \times 10^{14}$	$1 \times 10^5$	$10^{15}/10^{14}$ *	$2 \times 10^{15}$
Thickness ( $\mu\text{m}$ )	12	16	6.2	1/3.2*	.3
Nominal Operating Voltage (V)	60	80	33	70	55
Nominal Operating Current (mA)	15	18	19	30	14
Nominal Power (mW)	5	7	2	3	1
Nominal Frequency (GHz)	4.5	2.5	6.5	6.5	8.9

\* First number refers to N layer and second refers to P layer.

\*\* cw power, although some diodes tested with pulse bias in irradiation testing under vacuum at identical pulse power levels.



noted that doping concentrations fall from a value of  $10^{16} \text{ cm}^{-3}$  in the N layer to  $10^{14} \text{ cm}^{-3}$  in the v layer. In addition, the thickness of the v layer is  $9.2\mu\text{m}$  while the thickness of the N layer is  $1\mu\text{m}$ . The four diode types; S1, C4, A4 and D1; had various chrome thicknesses on the Schottky contacts<sup>189</sup> which resulted in slightly different barrier heights.<sup>191</sup> All the devices were operated in the continuous wave (CW) mode at room temperature in evacuated cavities.<sup>189</sup>

As indicated in Table 45, the RF output power of all the diode types is reduced by dose rate. The reduction increased with increasing dose rate with the dose rate required to reduce the RF power by one-half (i.e., 3dB) being listed in Table 45. The RF power is quenched entirely at a dose rate which is dependent upon the junction characteristics. Figure 122 indicates the normalized RF output power during a radiation pulse (power during the pulse divided by the pre-irradiation power) versus the normalized dose rate (dose rate during the pulse divided by the dose rate required to reduce the

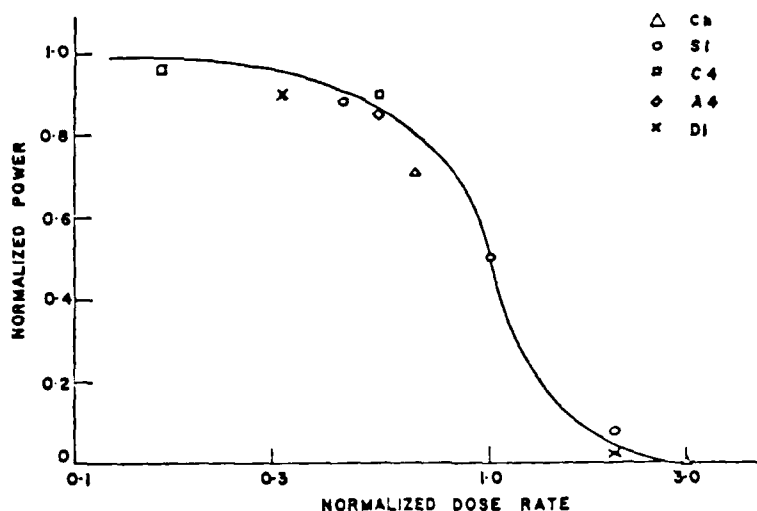


Figure 122. Normalized RF Output Power as Function of Normalized Dose Rate for Five Types of Baritt Diodes.

RF power by one-half). It should be noted that all the diodes have similar drops of the normalized power with normalized dose rates, even though the dose rate required to produce a 50% drop in the RF power varied by a factor

of 50 ( $2 \times 10^7$  rads (Si)/sec to  $10^9$  rads (Si)/sec as in Table 45).

It must be mentioned that the RF power remains reduced after the radiation pulse (pulse width of 100 msec) for approximately 500 nsec in some diodes. Other than this temporary reduction of RF power immediately after the pulse there are no permanent effects which have been observed in Baritt diodes (as have been observed with Impatts<sup>172, 174</sup>). All the oscillators returned to their pre-irradiation characteristics within 1 micro-second after the end of the pulse. The amount of time that power remained reduced is independent of the relative positions of the bias and radiation pulses but does depend on charge storage.<sup>189</sup> The charge storage is related to the injection efficiency of the injecting contact. The time the reduction persists increases as the injection efficiency increases. The time the characteristics of a Baritt diode are perturbed by the radiation pulse will be reduced for Schottky injecting contacts with low injection efficiency.<sup>189</sup>

This ends the discussion on Impatt-like devices. In conclusion it can be said that these devices will be affected by threat levels of radiation. Impatts seem to be the only device types that will suffer permanent effects. The next class of microwave semiconductor devices to be discussed is Gunn diodes.

## 6.2 Gunn Diodes

The semiconductor devices which have been discussed up to this point have been junction devices, i.e., the properties of the devices depend on the properties of the p-n junctions within the device. Gunn diodes do not depend upon junction properties but rather upon the properties of the semiconductor material itself. The microwave oscillations occur in the bulk of the semiconductor rather than in the junction. This effect was first discovered by J. B. Gunn in 1963 while investigating n-type GaAs.<sup>192</sup> It was found that, upon reaching a threshold field value in the neighborhood of 2 to 4 kV/cm, random noise-like oscillations appeared in the sample current with amplitudes on the order of an ampere.<sup>193</sup> For shorter samples (below .2 mm) the oscillations of some of the samples became coherent with frequencies of several gigahertz. The frequency was determined mainly by the sample and not by the external circuitry. The period of oscillation was approximately inversely proportional to the sample length which indicates

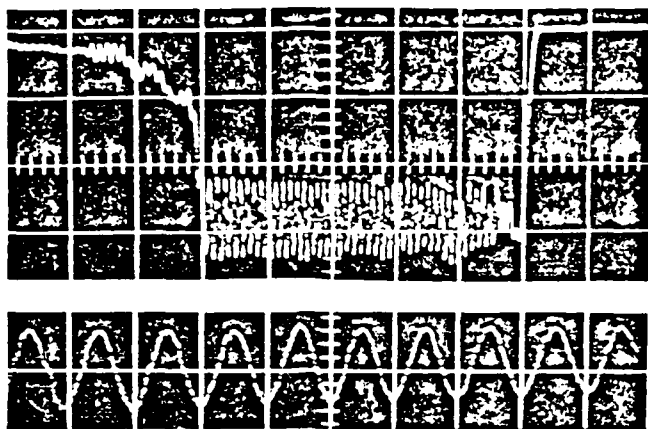


Figure 123. Current Versus Time of n-type GaAs. Lower Trace: 2nsec/cm, horizontally; .23 amp/cm vertically. Upper Trace: expanded view of lower trace.

a transit-time effect.<sup>192</sup> This behavior is depicted in Figure 123.<sup>192</sup> By measuring the potential distribution along a GaAs sample, it has been established that a marked electric-field inhomogeneity was moving from the cathode to the anode in a cyclic manner.<sup>194</sup>

The bulk effect that lies at the root of the Gunn effect can be explained by the so-called transferred-electron effect.<sup>195,196</sup> This effect was proposed one to two years prior to Gunn's observation and contained all the essential details for an explanation of the effect.<sup>193,197</sup> Transferred-electron devices utilize a relationship between the electron-drift velocity and the electric field of the form depicted in Figure 124.<sup>198</sup> This effect is well documented in the literature and verified many times from both a theoretical and experimental standpoint.<sup>199-204</sup> As indicated in this figure, the drift velocity increases linearly (ohmically) with the electric field starting from the origin. However, it passes through a maximum at a threshold field  $E_T$ . There is a region of negative - differential mobility beyond  $E_T$  where the drift velocity falls asymptotically towards a valley velocity,  $v_v$ .

This phenomenon is very complex and a detailed description is well beyond the scope of this study. Suffice it to say that the effect is a consequence of the many valley conduction band structure in GaAs and

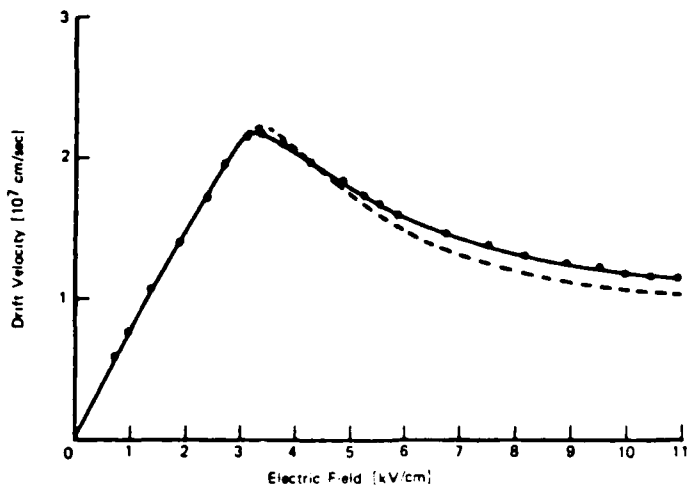


Figure 124. Electric Field-Dependent Average Drift Velocity of Electrons in n-type GaAs. Experimental Values (●) From Reference 199 and Theoretical Values (—) From Reference 200.

other similar materials. An idealized illustration of two possibilities for the band structure is depicted in Figure 125.<sup>153</sup> In this figure,  $k$  is the wavevector and  $E$  is energy. The lower band is the valence energy band, the top band is the conduction band, and the two are separated, of course, by the energy gap. In silicon the center energy valley is flanked by side valleys that are somewhat deeper than the center one. On the other hand,

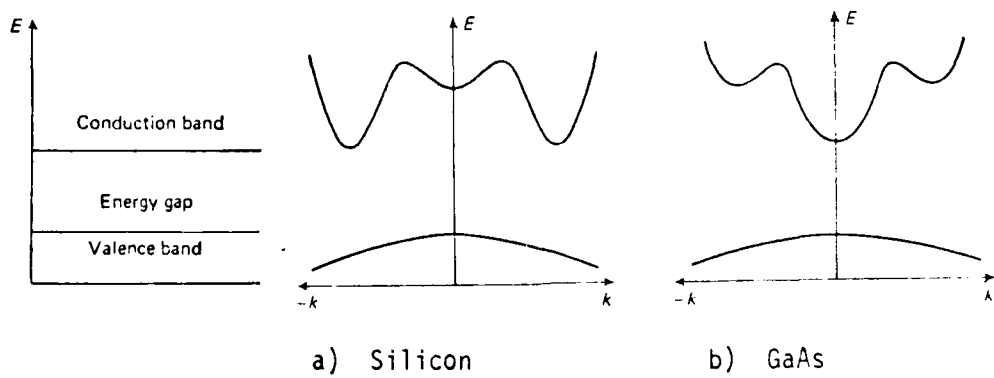


Figure 125. Idealized Energy Band Structure for Semiconductors.

GaAs has side valleys that are shallower than the center valley. In the conduction band, free electrons will collect in the lowest available level or

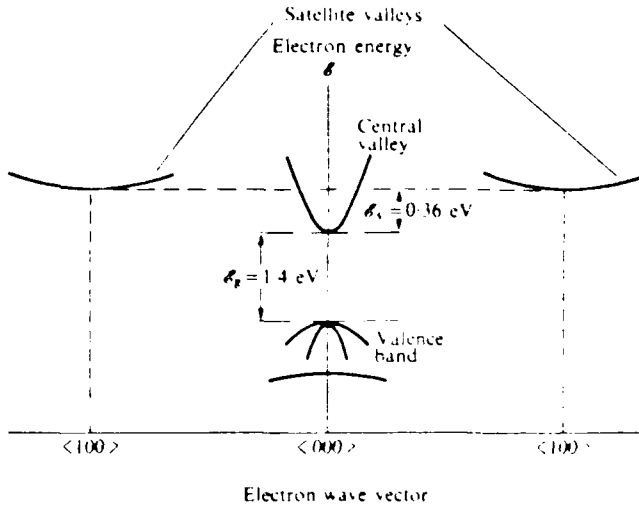


Figure 126. Band Structure of GaAs.

energy state which in GaAs is the central valley.

The band structure for GaAs is depicted in more detail in Figure 126.<sup>197</sup> As the electric field increases, the kinetic energy of the electrons in the central valley increases. When the kinetic energy of the electrons exceeds 0.36 eV, they have the additional choice of occupying energy states in the satellite valleys.

In semiconductor physics it is customary to assign to the mobile charge carriers an effective mass,  $m$ , which differs from the gravitational mass,  $m_0$ , which for electrons is  $9.108 \times 10^{-28}$  gm. This effective mass is introduced to allow for the influence of the lattice forces on the carriers. For mobile electrons in GaAs, the effective mass,  $m_1$ , in the central valley has been found to be approximately  $.066 m_0$ .<sup>205,206</sup> For reasons that are not pertinent to this discussion, the effective mass of electrons in the satellite valleys is a tensor. However, generally a mean value called the combined-density-of-states mass,  $m_2$ , is used and has a value of  $.85 m_0$ .<sup>207,208</sup> The density of states,  $N$ , of a valley denotes the number of allowable energy states per unit volume and energy intervals which are available to conduction electrons, and is proportional to the effective mass raised to the three halves power. The density of states ratio between the satellite and central valleys is approximately 46.<sup>193</sup> Those electrons which have sufficient energy will exist predominantly in the satellite valleys. As the electric field is

increased further more electrons have sufficient energy for the intervalley transition so more of them will occupy the satellite valleys.

As was mentioned in Section 6.1 on Impatts the electron mobility is essentially a proportionality factor relating the average electron drift velocity,  $v$ , and the applied electric field,  $E$ . The electron mobility in the satellite valleys,  $\mu_2$ , is smaller than that in the central valley,  $\mu_1$ , by a factor of approximately 70 because of the higher effective mass and the stronger scattering processes present in the satellites.<sup>209</sup> If the electron density in the central valley is  $n_1$  and in the satellite valleys is  $n_2$  then the mean drift velocity is given by

$$v = \mu E = \left( \frac{n_1}{n} \mu_1 + \frac{n_2}{n} \mu_2 \right) E$$

where  $n$  is the total electron density. The rapid growth of  $n_2$ , in conjunction with the fact that  $\mu_1$  is much less than  $\mu_2$ , leads to the crucial result that beyond a certain field value, the average drift velocity falls with increasing field, i.e., negative differential conductivity is obtained. A popular name for the decrease in free electron velocity with increasing field is negative differential mobility which would account for the decrease in velocity.

The material requirements, not all of which have been covered in the discussion, for a significant transferred-electron negative differential mobility are as follows:<sup>197</sup>

- 1) The conduction band must have a many valley structure with  $E_s$ , the satellite to central valley energy gap in Figure 126, being several times larger than the thermal energy (approximately .025 eV at room temperature) in order to avoid populating the satellite valleys at low values of the electric field.
- 2)  $E_g$ , the energy gap in Figure 126, must be greater than  $E_s$  in order to prevent impact ionization of electrons across  $E_g$  occurring before intervalley transfer.
- 3) The effective mass in the satellite valleys must be appreciably larger than that in the lower valley. Electrons with sufficient energy to have the choice of occupying either valley will then have a much greater probability of occupying the satellite valleys



owing to their relatively high density of states.

- 4) The electron mobility in the satellite valleys must be much smaller than that in the lower valley.
- 5) Transfer of electrons between the valleys must occur over a small range of electric fields.

If an attempt is made to apply a d.c. potential to the terminals of a piece of n-type GaAs so as to produce an electric field in the negative differential conductivity region there is a tendency for the material to form high and low field domains within itself. Essentially a sample with velocity-field characteristic shown in Figure 124 is thermodynamically unstable when biased in the negatively sloped portion of the curve. The most favorable state energetically is reached if, instead of having a homogenous field distribution over the sample length, the field splits into a high-field region and a low-field region.<sup>197</sup> In the high-field region or domain the field tends to a value which, in general, is in excess of the peak field,  $E_p$ , of the E-V characteristic curve and the velocity declines. However, the field outside this high field region declines.<sup>197</sup>

Poisson's equation demands that at the interface of the regions with differing field strengths, there must exist space-charge layers (i.e. space-charge dipole domains). The dipole domain is composed of an accumulation

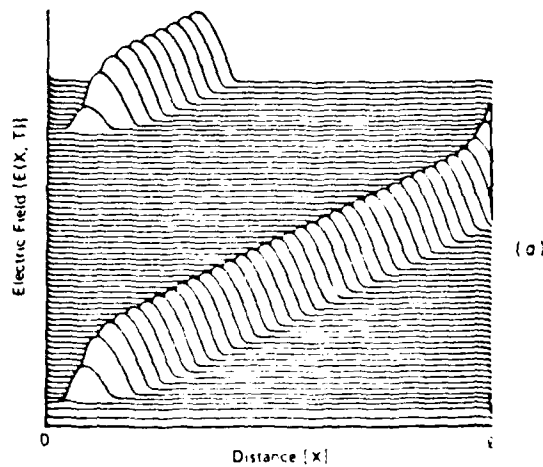


Figure 127. Numerical Simulation of the Generation and Propagation of a Dipole Domain Through n-Type GaAs. Time Between Successive Vertical Displays is  $16t$  sec Where  $t$  is the Dielectric Relaxation Time.

layer which consists of mobile electrons and a depletion layer which has a deficiency of electrons. Since the domain consists of mobile electrons, it will separate from the source and drift toward the drain. As the depletion layer reaches the drain, the dipole will collapse and the system will recycle as indicated in Figure 127.<sup>210</sup> This figure is for the formation of single dipoles near the cathode. The sudden collapse of the domain gives rise to a current pulse at the anode.

When a transferred-electron device is placed in a microwave cavity several modes of operation are possible. Three of the more common modes will be discussed: the transit-time mode, the delayed-domain mode, and the quenched-domain mode. In the transit-time mode of operation, the frequency is determined only by the space-charge transit time across the device. Typical waveforms are illustrated in Figure 128.<sup>197</sup> In this figure,  $T_D$  is the space-charge or domain transit-time,  $V_B$  is the bias voltage,  $V_T$  is the voltage associated with the threshold field for the Gunn effect,  $I_p$  is the current corresponding to the peak of the v-E curve, and  $I_v$  is the current corresponding to the valley.

As indicated in Figure 128, the current spike occurs when a domain enters the anode and the growth of the next domain is initiated at the cathode. This is the form of the effect originally observed by Gunn.<sup>192,194</sup> The phase of the voltage with respect to the current depends on the impedance in the resonant circuit, the load impedance, and the transit-time of the device. The efficiency of this mode is low and the frequency is limited to the natural domain

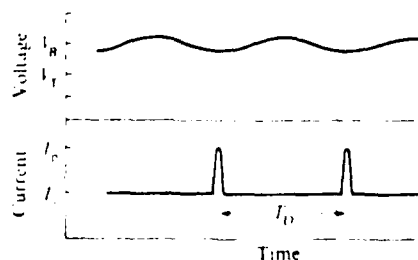


Figure 128. Typical Waveforms for Transit-Time Mode Operation of a Gunn Oscillator.

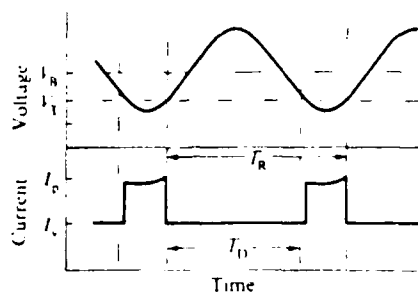


Figure 129. Typical Waveforms for Delayed-Domain Mode Operation of a Gunn Oscillator

transit-frequency. Usually this lies between 7 and 25 GHz.<sup>211</sup>

The transit-time mode of operation is one in which the voltage is always above the threshold. Because of jitter in the formation, drift, and extinction of domains, this mode is the most noisy of all the operating modes. Better oscillator performance is obtain by controlling the formation and/or the extinction of the domains with the external circuitry. In the delayed-domain mode only the domain formation is controlled. Typical waveforms are illustrated in Figure 129.<sup>197</sup> The notation in this figure has the same meaning as in Figure 129. For this mode, the circuit Q must be large enough and the load impedance small enough to allow a sinusoidal voltage waveform with a large enough amplitude at the device's terminals so that voltage falls below the threshold for a portion of each cycle. The domain transit-time must be less than the resonant period,  $T_R$ , of the tank circuit so that the domain may be extinguished at the anode while the voltage is below threshold. The formation of the next domain is not initiated until the voltage rises above the threshold. During this delay period, the diode behaves as a resistor. The efficiency is higher than for the transit-time mode since the current is above  $I_v$  longer than for the transit-time mode (compare Figures 128 and 129). If the ratio of  $I_p$  to  $I_v$  is two, the efficiency can be as great as 7.2%.<sup>212</sup> A further advantage is the controllability by the circuit subject to the restriction that<sup>197</sup>

$$2T_D > T_R > T_D$$

The quench-domain mode operation relies on the fact that the traveling dipole domain is annihilated if the voltage across the sample drops below the



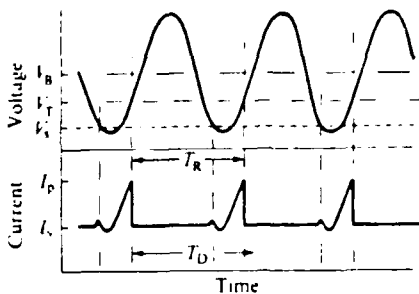


Figure 130. Typical Waveforms for Quench-Domain Mode Operation of a Gunn Oscillator.

domain sustaining value  $V_s$ .<sup>213</sup> The domain is essentially quenched in flight but the next one is not formed until the terminal voltage of the device has risen to the threshold. Figure 130<sup>197</sup> depicts typical waveforms for this mode of operation. Frequencies higher than the transit-time frequency can be generated. However, the high-frequency limit for this mode is not infinity, but is limited by the time,  $\tau_s$ , required for domain formation and extinction. The frequency constraint is approximately<sup>197</sup>

$$2T_D > T_R > \tau_s$$

Thus the frequency can be controlled over a wider range of frequencies in this mode than in the delayed-domain mode. The circuit requirement is that the load impedance be reduced so that the terminal voltage falls below  $V_s$  during a portion of each cycle. This mode is not as efficient as the delayed-domain mode with a maximum predicted efficiency of approximately 5%.<sup>197</sup>

Another mode of operation is the limited space-charge accumulation (LSA) mode. This technique avoids the domain-formation and transit-time effects. It results in a substantially homogeneous electric field over the sample.<sup>214</sup> In this mode the conversion of the d.c. power conveyed to the device into a.c. power is achieved by the negative differential mobility of the individual electrons rather than by the movement across the sample of space-charge bunches as in the case of the dipole-domain mode.<sup>193</sup> Efficiencies as high as 18% are predicted.<sup>215</sup> This mode of operation differs significantly from the Gunn effect in that a dipole domain is never formed and the accumulation layer is quenched after it has been initiated, grown, and moved toward the cathode. A detailed discussion of this mode is even more complex than the Gunn effect because it involves

accumulation-layer dynamics since, in contrast to dipole domains, the accumulation layer is never in a steady state. Suffice it to say that devices are operated in the LSA mode because of their high frequency and efficiency.

As a brief digression, the discussion on the operation of Gunn diodes would be incomplete without mentioning the work contained in reference 216. This was the first explanation of the mechanism which causes the Gunn-effect. Essentially, this reference couples the prediction in reference 196 of the existence of field-induced "transferred electrons" effects which could lead to negative differential mobility (NDM) together with the conclusion found in reference 194 that the presence of NDM could cause homogeneous material to become heterogeneous. The explanation of the Gunn effect was formed by the joining of these two separate pieces of information. The theory was later verified by an examination of the threshold voltage as a function of hydrostatic pressure<sup>217</sup> (the intervalley separation energy varies with pressure). The threshold voltage decreased with increasing pressure and vanished completely at 26 kbar. In another experiment, the intervalley separation was varied by varying  $x$  in  $\text{GaAs}_x \text{P}_{1-x}$ .<sup>218</sup> As  $x$  decreases from 1.0 to .5 the intervalley separation decreases from 0.36 eV to zero. The threshold voltage disappears at a value for  $x$  of 0.52. These two experiments left little doubt that intervalley transfer was the mechanism responsible for the Gunn effect.

Gunn and Gunn-like devices (i.e., transferred-electron (TE) devices) are appearing in a number of electronic systems. However, in many applications they have to compete with other microwave devices such as Impatt, Trapatt, and Baritt diodes; bipolar or field-effect transistors; or electron tubes. Table 47<sup>219</sup> compares TE devices with each of these device classes. As is indicated in this table the strengths of TE devices are their low noise properties and low bias-voltage requirements in moderate power continuous wave applications and their high peak power available in pulsed operation. However, this is in a benign environment and their performance is degraded in a radiation environment.

Similar to other bipolar devices, these devices experience two types of radiation-induced effects: displacement effects caused by neutrons and ionization effects which are related to either total dose or dose rate. Neutron irradiation results in three main effects on the Gunn diode efficiency:



Table 47. Comparison of TE Oscillators (TEO) and Reflection-Type Amplifiers (TEA) with Other Microwave Devices

(a) State of the Art of TEOs		Strengths	Weaknesses
vs	IMPATT diodes	Lower noise Higher pulsed power Higher pulsed efficiency Lower bias voltage	Lower C.W. efficiency and power
vs	TRAPATT diodes	Lower noise Higher duty-cycle operation Higher frequency operation Lower bias voltage	Lower pulsed power and efficiency Less temperature stable GaAs vs Si
vs	Transistors	Higher frequency operation Higher pulsed power Less complicated structure	No C.W. L & S band devices GaAs vs Si
vs	Tubes	Longer life, more reliable Equivalent noise performance Lower bias voltage Simpler power supplies	Lower power and efficiency Less temperature stable
vs	BARRIT diodes	Higher power and efficiency	GaAs vs Si

(b) State of the Art of TEAs (reflection-type)		Strengths	Weaknesses
vs	IMPATT amplifiers	Greater bandwidth (Higher gain-bandwidth product) More linear Lower noise Wider dynamic range	Lower C.W. efficiency and power
vs	TRAPATT amplifiers	Much greater bandwidth (Much higher gain-bandwidth product) Much more linear Much lower noise Much wider dynamic range Higher frequency operation	Much lower pulsed power and efficiency No UHF or L-band operation GaAs vs Si
vs	Transistor amplifiers	Greater bandwidth (Higher gain-bandwidth product) Higher power in C, X, and Ku bands	Two-terminal device GaAs vs Si
vs	Tubes	Longer life, More reliable Low bias voltages Simpler power supplies	Less power and efficiency Less temperature stable
vs	BARRIT-diode amplifiers	Greater bandwidth (Higher gain-bandwidth product) Higher power and efficiency	GaAs vs Si

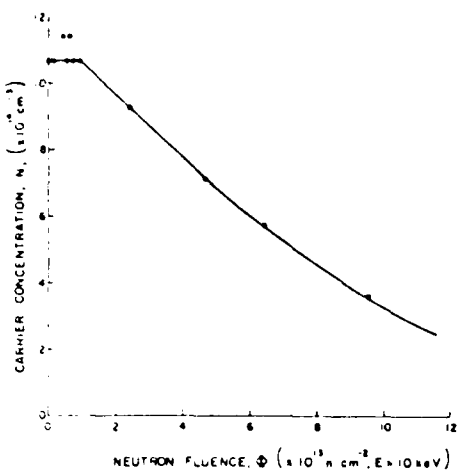


Figure 131. Carrier Concentration Versus Fluence  
For a Typical Gunn Device

- 1) carrier removal, 2) reduction of the peak to valley current ratio ( $\alpha$ ), and
- 3) slow trapping of high-field conduction electrons.<sup>220</sup>

A typical curve of the carrier concentration versus neutron fluence is shown in Figure 131.<sup>221</sup> This curve has some interesting features. The carrier concentration maintains its initial value until the fluence reaches a damage threshold value which in this case is approximately  $.9 \times 10^{13} \text{ n/cm}^2$ . The carrier concentration then falls off at a constant rate until roughly  $5 \times 10^{13} \text{ n/cm}^2$ . At this fluence point, although it isn't clearly evident from the figure, the rate of decrease in the carrier concentration begins to slow due to a decrease in the carrier removal rate.<sup>221</sup>

If a degradation parameter is defined as<sup>222</sup>

$$a = -\frac{1}{n_0} \left( \frac{dn}{d\phi} \right)_{\phi \rightarrow 0}$$

where  $n_0$  = initial carrier concentration  
 $\phi$  = neutron fluence

The carrier concentration can then be expressed as

$$n = n_0 (1 - a\phi) \quad (27)$$

Another parameter called the mobility damage constant which is used to relate the effects of neutron irradiation on mobility is defined as<sup>222</sup>

$$b = \mu_0 \left( \frac{d}{d\phi} \frac{1}{\mu} \right)_{\phi \rightarrow 0} \quad (28)$$

where  $\mu_0$  is the initial carrier mobility. Using this parameter the mobility can be expressed as a function of neutron fluence by

$$\frac{1}{\mu} = \frac{1}{\mu_0} (1 + b\phi) \quad (29)$$

where  $\mu_0$  is the initial or unirradiated carrier mobility and  $\mu$  is the mobility after irradiation. Equations 27 and 28 are reasonably accurate for changes in  $n$  and  $\mu$  of less than 25% but loses accuracy for large fluences.<sup>222</sup>

The parameters,  $a$  and  $b$ , can be determined from conductivity and Hall measurements. Data from references 222-225 was used in reference 222 to generate the plot of  $a$  and  $b$  versus initial carrier concentration shown in Figure 132.

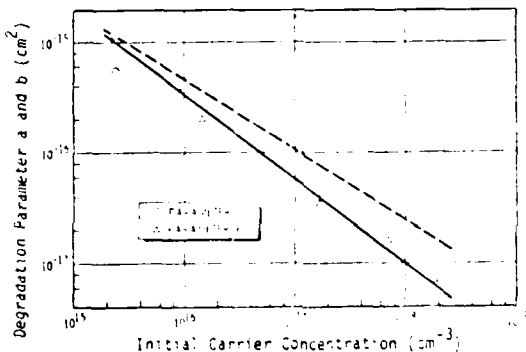


Figure 132. Degradation Parameters  $a$  and  $b$  for Bulk GaAs Versus Initial Carrier Concentration.

The equations for these lines are

$$a = 7.2 \times 10^{-4} n_0^{-0.77}$$

$$\text{and} \quad b = 7.8 \times 10^{-6} n_0^{-0.64}$$

The data for parameter  $a$  in Figure 132 lie closely along the curve but the data for  $b$  shows considerably greater deviation. In fact, there is some disagreement in the literature over the exact expression for  $b$ . References 222 and 226 agree with the above expression but reference 220 used Figure 133 to obtain the equation.

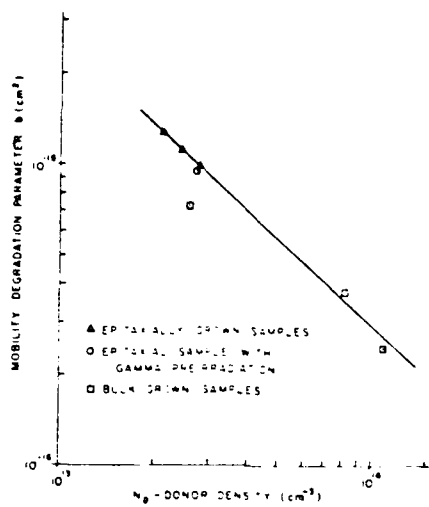


Figure 133. Mobility Degradation Parameter Versus Donor Density

$$b \approx 2.7(n_0)^{-1} \quad (30)$$

The carrier removal rate can be determined by differentiating equation 27 or

$$\frac{dn}{d\phi} = -n_0 a = -7.2 \times 10^{-4} (n_0)^{.23} \quad (31)$$

However, empirical data from references 221, 227 and 228 yields a plot of removal rate versus the initial carrier concentration depicted in Figure 134. There is some disagreement since the equation for this curve is

$$\frac{dn}{d\phi} = -9.08 \times 10^{-6} n_0^{0.4} \quad (32)$$

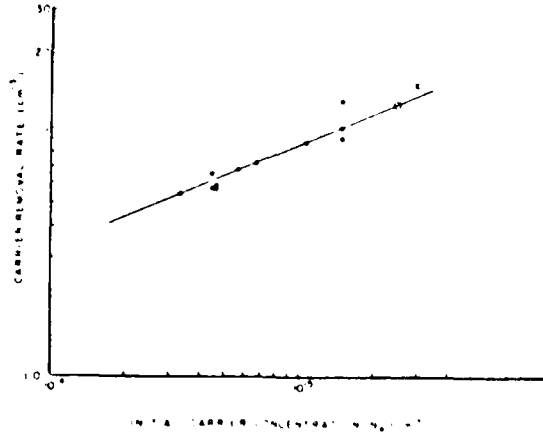


Figure 134. Carrier Removal Rate Versus Initial Carrier Concentration

This equation yields higher values of  $\frac{dn}{d\phi}$  than equation 31. For example at  $10^{15}$ , equation 31 yields a value for  $\frac{dn}{d\phi}$  of approximately  $2.0 \text{ cm}^{-1}$  while equation 32 yields a value of approximately  $9.0 \text{ cm}^{-1}$ . At higher fluences, the disagreement is even greater. The bulk of the literature uses equation 31.

In any case, both equations do indicate that the carrier removal rate depends on a fractional power of the initial carrier concentration. One consequence of this dependence is that devices with higher initial carrier concentration should withstand the effects of neutron irradiation better than devices with lower concentrations. The carrier removal rate will be somewhat higher but the fractional change,  $\frac{dn}{n_0}$  is proportional to  $n_0$  raised to a negative fractional power. Thus,  $\frac{dn}{n_0}$  will decrease as  $n_0$  increases.

The same argument also applies to the neutron-induced mobility degradation. This becomes apparent when equations 29 and 30 are converted to a common form such as

$$b = An_0^{-B}$$

where A and B are positive constants. Rearranging equation 28 for the change in reciprocal mobility yields

$$\Delta \left( \frac{1}{\mu} \right) = \left( \frac{1}{\mu} - \frac{1}{\mu_0} \right) = \frac{A\phi}{n_0 B}$$

This indicates that the change in mobility will be less for devices with higher carrier concentrations.

Some results for typical devices are shown in Table 48.<sup>220</sup> This data includes one sample of a wafer that was preirradiated with gamma rays and then neutron irradiated. The dose level for this exposure was  $8 \times 10^7$  rads (GaAs). In this table  $N_D$  refers to the donor impurity density rather than the actual carrier density, n, which is also listed.

The carrier removal rate for all the samples in Table 48 varies between 4 and  $5 \text{ cm}^{-1}$ .<sup>220</sup> This is consistent with results reported in other work<sup>221,227-229</sup> for this initial carrier concentration. As indicated in this table, the carrier concentration does decrease with neutron fluence. Unfortunately, the neutron fluences in this table are above  $10^{13}$  to  $10^{14} \text{ n/cm}^2$  so the data does not demonstrate the threshold effect. However, even though the



Table 48  
Transport Properties of Epitaxially Grown GaAs versus Fluence  
(T = 300°K)

Sample No.	Accumulated v Fluence	Accumulated Neutron Fluence	Carrier Density	Mobility	Resistivity
	$\phi_v (10^{16} \text{eV/cm}^2)$	$\phi_n (\times 10^{13} \text{n/cm}^2)$	$n (\times 10^{15} \text{cm}^{-3})$ (E > 10 keV)	$\mu \text{ cm}^2/\text{V-sec}$	$\Omega \cdot \text{cm}$
950-1 $N_D = 2.1 \times 10^{15} \text{cm}^{-3}$	---	0	1.67	7137	1.51
	---	5.1	1.41	7137	1.51
	---	10.3	1.36	7132	1.51
	---	16.8	1.21	7134	1.51
1-3 $N_D = 2.8 \times 10^{15} \text{cm}^{-3}$	---	0	2.13	7386	1.34
	---	5.3	1.91	7115	1.41
	---	11.7	1.63	6713	1.46
	---	16.6	1.42	6710	1.46
	---	21.8	1.24	6681	1.51
1-32 $N_D = 2.76 \times 10^{15} \text{cm}^{-3}$	0	---	1.93	7948	1.43
	9.4	---	1.81	7420	1.43
	19.0	---	1.19	7663	1.12
	---	11.4	1.71	6844	1.17
	---	16.3	1.56	6713	1.33
	---	21.5	1.47	6382	2.01
124 $N_D = 2.47 \times 10^{15} \text{cm}^{-3}$	---	0	1.82	7932	1.43
	---	5.3	1.72	7735	1.47
	---	10.4	1.47	7211	1.51
	---	15.7	1.26	6449	1.71
	---	20.5	1.07	6613	1.87

spread in initial carrier concentrations between devices is not great, the data in the table does indicate that devices with higher initial carrier concentrations,  $n_0$ , experience less fractional losses in carrier concentration than those with lower values of  $n_0$ . Device 95C-1, with an initial value of  $1.69 \times 10^{15} \text{ cm}^{-3}$  for  $n_0$ , experiences a loss of .51 after being exposed to a fluence of  $1.68 \times 10^{14} \text{ n/cm}^2$ .<sup>220</sup> Device 143, with an initial value of  $2.13 \times 10^{15} \text{ cm}^{-3}$  for  $n_0$ , only experiences a loss of .33 after an exposure of  $1.66 \times 10^{14} \text{ n/cm}^2$ . Hence it would appear that the percentage change in the carrier concentration due to neutron exposure is very sensitive to the initial concentration.

As expected the data also indicates a decrease in mobility with an increase in neutron fluence. In addition, the data also indicates that the loss in mobility is less for devices with high initial carrier concentrations. For the same two fluence levels as in the previous paragraph, device 95C-1 experiences a loss of  $1261 \text{ cm}^2/\text{V-sec}$  which is 18 percent of the unirradiated value while device 143 has a loss of  $876 \text{ cm}^2/\text{V-sec}$  which is 12 percent of the initial value. Thus, devices with higher carrier concentrations experience less mobility degradation due to neutron exposure from both an absolute and a percentage standpoint.

The impact of neutron fluence on the doping profile has been studied by measuring the carrier concentration versus depth profile. The results of this work are portrayed in Figure 135.<sup>220</sup> This data indicates that the doping

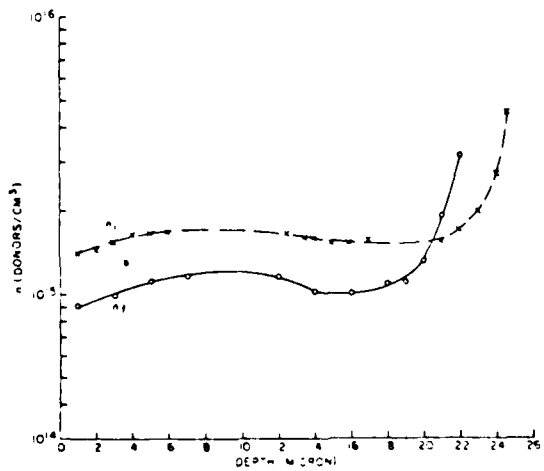


Figure 135. Donor Impurity Concentration Versus Depth Before and After Exposure to a Fluence of  $1.5 \times 10^{14} \text{ n/cm}^2$ .

profile is essentially unchanged while the carrier concentration decreases due to neutron irradiation.

References 230 and 231 indicate that a Gunn oscillator should cease oscillating when the doping-length product,  $n \times l$  (where  $n$  is the doping density and  $l$  is the specimen length), is less than roughly  $5 \times 10^{11} \text{ cm}^{-2}$ . This would imply that neutron-induced decreases in carrier concentration would lower the  $n \times l$  product until failure occurred. Output power does decrease with increasing fluence with device failure eventually occurring between approximately  $10^{13} \text{ n/cm}^2$  to  $10^{14} \text{ n/cm}^2$ . In addition, data indicates a much higher  $n \times l$  product at device failure<sup>221,227,228</sup> than was predicted in references 230 and 231. This data is depicted in Figure 136 in the form of the neutron fluence required to produce a failure in the output power (i.e., oscillation ceased) versus initial carrier concentration. This data indicates that carrier concentration depends linearly on the initial concentration.

Device efficiency is also related to device failure and is influenced by neutron irradiation. There are a number of factors which control the efficiency of a Gunn diode. The carrier-concentration and length product ( $n \times l$ ),<sup>231</sup> and the ratio of the peak current to valley current,  $\alpha$ ,<sup>232</sup> are generally

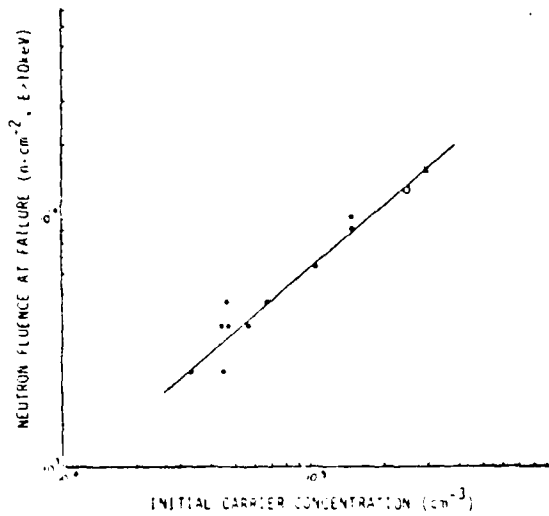


Figure 136. Neutron Fluence at Device Power Failure Versus Initial Carrier Concentration

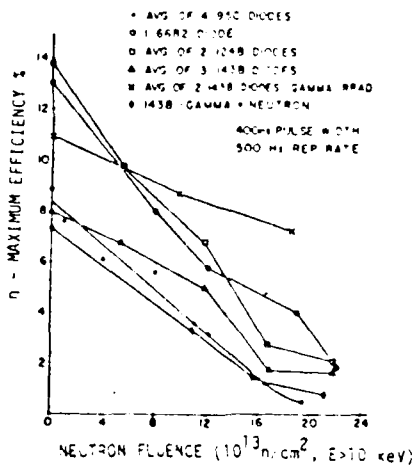


Figure 137. Maximum Efficiency of Gunn Diodes Versus Neutron Fluence

considered to be important factors in determining the efficiency.<sup>220</sup> For a specific device, there is a value of the  $n \times l$  product where efficiency is a maximum. As the carrier concentration is decreased due to neutron irradiation, the efficiency falls and finally oscillation ceases. Figure 137 is a plot of the efficiency versus fluence.<sup>220</sup> The data that was used for this figure is listed in Table 43.<sup>220</sup> The efficiency was reduced approximately 50% by an exposure to roughly  $10^{14} \text{ n/cm}^2$ .

As was the case with Table 48, this table also contains data on a diode (143B-14) that was irradiated first with gamma rays and then neutrons. The efficiency data of the two gamma irradiated diodes is also shown in Figure 137 where they have been plotted versus equivalent neutron fluence. Equivalence in this case is determined by carrier removal alone. This essentially means that all the gamma ray induced degradation is assumed to be due to carrier removal. This assumption is justified by the work in reference 233. As indicated in Figure 137 the efficiency decreases linearly with carrier removal. The rate for this decrease is consistent with failure resulting from too small an  $n \times l$  product. Thus, this curve gives an indication of the behavior of a device whose only failure mechanism is carrier removal.

A comparison of the curves for the gamma-irradiated diodes with those for the neutron-irradiated diodes in Figure 137 indicates that there are other neutron-induced degradation mechanisms present in addition to carrier removal.

**SJ**

Table 49  
I-V Gunn Diode Characteristics versus Neutron Fluence

Diode No.	Accumulated Fluence ( $\times 10^{17}$ n/cm <sup>2</sup> )	Low Field Resistance (M)	Breakdown Voltage (V)	Peak Current I <sub>P</sub> (A)	Recovery Current I <sub>R</sub> (A)	I <sub>P</sub> × 10 <sup>3</sup>	$\alpha = \frac{I_P}{I_R}$	$\beta = \frac{I_P}{I_V}$	$\gamma = \frac{I_P}{I_{P0}}$
12-B2-18	0	1.37	7.1	3.71	.11	3.71	1.1	1.1	1.1
	11.7	1.47	7.2	2.47	.17	2.47	1.4	1.4	1.4
	16.6	2.17	7.2	1.74	1.01	1.74	1.71	1.71	1.71
	21.4	3.21	7.2	1.3	*1.1*	1.3	1.1	1.1	1.1
12-B2-27	0	1.37	7.1	3.75	2.01	3.75	1.1	1.1	1.1
	11.7	2.15	7.1	2.2	1.11	2.2	1.91	1.91	1.91
	16.6	2.6	7.2	1.75	1.21	1.75	1.41	1.41	1.41
	21.3	3.04	7.2	1.21	*1.07*	1.21	1.11	1.11	1.11
143B-6	0	1.37	7.55	3.72	3.72	3.72	1.01	1.01	1.01
	11.7	2.04	7.5	2.71	1.71	2.71	1.11	1.11	1.11
	16.6	2.34	7.3	1.95	*1.14*	1.95	1.71	1.71	1.71
	21.3	2.75	7.2	1.75	1.75	1.75	1.01	1.01	1.01
143B-10	0	1.37	7.25	4.42	3.71	4.42	1.11	1.11	1.11
	11.7	1.75	7.2	2.75	1.51	2.75	1.81	1.81	1.81
	16.6	2.13	7.2	2.07	1.41	2.07	1.48	1.48	1.48
	21.3	2.55	7.2	1.73	*1.27*	1.73	1.31	1.31	1.31
143B-19	0	1.37	7.2	4.92	3.71	4.92	1.11	1.11	1.11
	11.7	1.39	7.2	3.85	2.92	3.85	1.01	1.01	1.01
	16.6	1.72	7.2	2.8	2.15	2.8	1.3	1.3	1.3
	21.3	2.04	7.2	2.05	*1.73	2.05	1.11	1.11	1.11
143B-14	0	1.07	7.4	5.0	3.2	5.0	1.51	1.51	1.51
	$\sim 1.3 \times 10^{17} \text{ } \gamma/\text{cm}^2$	2.20	7.1	2.4	1.7	2.4	1.31	1.31	1.31
	11.1	3.88	7.3	1.3	.96	1.3	1.31	1.31	1.31
	16.0	5.9	7.2	.81	.64	.81	1.11	1.11	1.11
	21.2	9.62	7.2	.43	.41	.43	1.01	1.01	1.01

These values were corrected for trapping effects.

\*\* Diode was first irradiated with gamma rays to this fluence and then irradiated with neutrons.



The efficiency,  $\eta$ , is related to the peak-to-valley-current ratio,  $\alpha$ , by the expression<sup>233</sup>

$$\eta = \frac{(\alpha - 1)}{(\alpha + 1)}$$

Data for  $I_p$ , the peak current;  $I_v$ , the valley current; and  $\alpha$ , their ratio are listed in Table 49. It is evident in every case that  $\alpha$  decreases with neutron fluence.  $I_p$  is given by<sup>220</sup>

$$I_p = \frac{V_T n q A}{L}$$

where  $V_T$  = Gunn threshold voltage

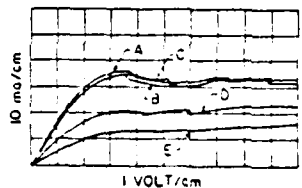
$q$  = electronic charge

$A$  = device area

$L$  = active electrical length of the device

Table 49 indicates that  $V_T$  is relatively unchanged over a fairly wide range of fluences. Figure 138<sup>234</sup> also indicates this. The break point in the curves which represents the onset of negative resistance that marks the onset of the Gunn effect occurs essentially at the same voltage point. In addition, this figure indicates  $I_p$  steadily decreases with fluence until the Gunn effect has virtually disappeared in curve D.

In any case, for a specific device  $I_p$  is a function of only  $n$ , the concentration, and  $\mu$ , the mobility, since all other quantities are constants.



CURVE A • BEFORE EXPOSURE  
 CURVE B • AFTER NEUTRON FLUENCE OF  
 $2.89 \times 10^2 \text{ N/cm}^2$   
 CURVE C • AFTER  $1.26 \times 10^3 \text{ N/cm}^2$   
 CURVE D • AFTER  $1.25 \times 10^4 \text{ N/cm}^2$   
 CURVE E • AFTER  $1.88 \times 10^4 \text{ N/cm}^2$

Figure 138. V-I Characteristics of a Gunn Diode After Various Levels of Neutron Irradiation

The valley current,  $I_v$ , is given by

$$I_v = nqv_s A$$

where  $v_s$  is the saturation velocity. It seems highly unlikely that neutron-induced displacement damage would have any effect on the high-field phonon scattering upon which  $v_s$  depends.<sup>220</sup> Therefore

$$\frac{I_p}{I_v} = \alpha = \frac{V_T n q \mu^4}{n q v_s L} = \text{constant} \times \mu$$

Therefore,  $\alpha/\mu$  should be a constant with neutron fluence. This is borne out reasonably well in Table 49 in the last column. Thus, the reduction in  $\alpha$  is related to degradation in the mobility.

In addition to the degradation in efficiency resulting from carrier removal and changes in  $\alpha$ , there is evidence in the literature that slow traps are introduced by irradiation which also degrade the efficiency.<sup>220</sup> Unfortunately, the data in the literature<sup>220</sup> which demonstrates this effect is in the form of oscilloscope traces which are completely obliterated in the available reproduction processes. Therefore, a descriptive account of the experiment and the effect will be used instead.

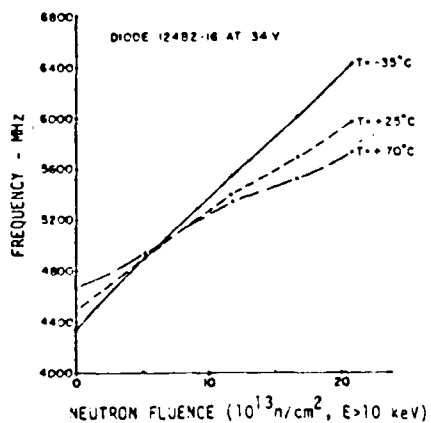
A bias voltage in the form of a double trapezoidal pulse with an amplitude of approximately 50 V was applied to diodes that had been exposed to  $2 \times 10^{14}$  n/cm<sup>2</sup>. The width was .3  $\mu$ sec at the base and .2  $\mu$ sec at the top. The time between the initiation of the separate pulses was approximately .5  $\mu$ sec. The resultant power output of the devices was detected. The output power from the first voltage pulse was initially high. Unfortunately, the value was not given in the literature. After approximately 75 nsec, this initial value drops to a value that was roughly 50 percent of the initial value. The output from the second pulse degrades even more (roughly 65 percent) with the initial output being reduced 50 percent when compared to the initial output resulting from the first voltage pulse. Before the diodes were irradiated the power output was constant during the voltage pulse and identical from one pulse to another.

The behavior after irradiation is due to trapping of electrons in the high field portion of the domain by radiation created field-dependent

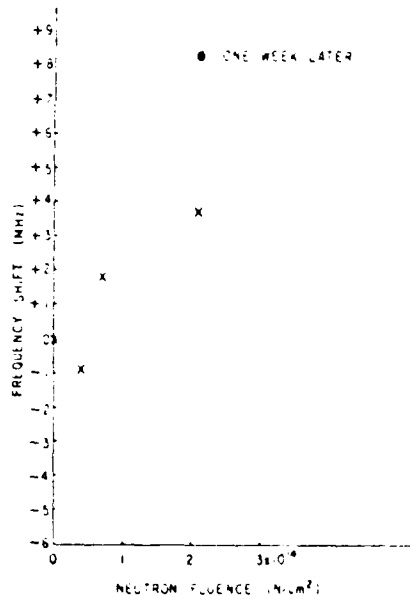


traps.<sup>220</sup> The traps are filled during the initial part of the pulse by the high fields associated with the moving dipole domains. As the electrons become trapped, the RF current and output power drop.<sup>235</sup> The diodes were also subjected to multiple exposures of many double pulses with various time delays between the individual pulses of each double pulse. A 3 usec lifetime was measured.<sup>220</sup> Similar experiments were performed on the gamma-ray irradiated diodes. There was no indication of gamma-induced formation of slow traps.

Besides degrading the efficiency and, thus, the output power neutron irradiation also affects the frequency of Gunn diodes. There is very little data on this effect but what does exist indicates that frequency will be increased by neutron exposure. The data that does exist is shown in Figure 139.<sup>220, 226</sup> The data for the diode 124B2-16 in Figure 139a is listed in Table 49. The diode for Figure 139b had an operating frequency of 9 GHz and a bias voltage of 9 volts. The device temperature was not given. The frequency



a) Reference 220

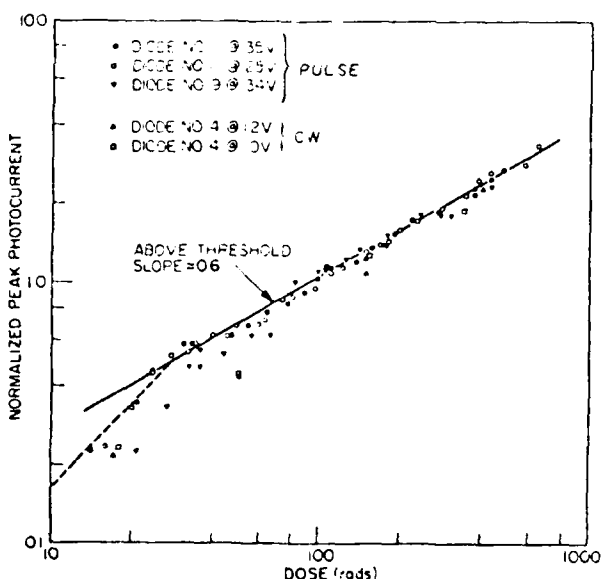


b) Reference 226

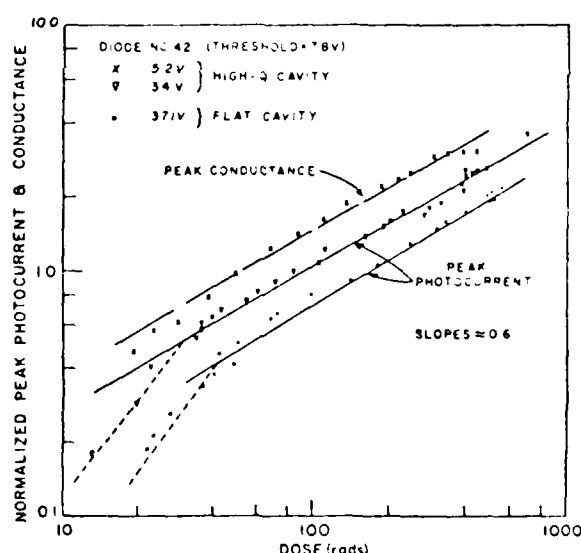
Figure 139. Effect of Neutron Irradiation on the Frequency of Gunn Diodes

behavior is not understood beyond noting that the temperature coefficient is radically altered.<sup>220</sup> Apparently studies involving the sensitivity of the change in frequency to the initial frequency or the mode of operation have never been performed. The diode in Figure 139a was operated in the hybrid mode. No mention was made of the mode of operation for the diode in Figure 139b but it was probably transit-time. In any case, it would appear that at threat levels of fluence the frequency of Gunn oscillators will experience a significant increase ranging from a few MHz to roughly 1 GHz.

Besides neutron irradiation, Gunn diodes are also susceptible to transient ionizing radiation. As with any semiconductor, exposure to ionizing radiation results in the generation of electron-hole pairs. Dose rate exposure results in the production of photocurrents. Figure 140<sup>236</sup> is a plot of the peak photocurrent that was generated in response to a 25 nsec radiation pulse as a function of dose. The photocurrents are normalized to the Gunn threshold current for each diode. The data in Figure 140a is for a number of diodes operating in



a) Different Diodes in a High-Q Cavity.



b) One Diode in a High-Q and Flat Cavity.

Figure 140. Peak Photocurrent of Gunn Diodes Versus Dose (Pulse Width of 25 nsec).

a high-Q cavity at different voltages. All of these voltages were above the threshold voltage. The data in Figure 140b is for one diode operated in both a high-Q and a flat cavity.<sup>236</sup> The conductance data was taken below threshold and normalized to the conductance at threshold.

Figure 140a indicates that the peak photocurrent above the threshold is independent of the voltage.<sup>236</sup> This implies that the current-voltage characteristic above threshold is saturated, even during irradiation. It must be realized that since the pulse width was constant Figures 140a and b are plots of photocurrent versus not only dose but also dose rate. Thus, the excess carrier-concentration produced by radiation is directly proportional to the photocurrent and must also exhibit a power law to the 0.6 power of dose rate as is the case with the photocurrent. The value of  $\alpha$  (i.e.,  $I_T/I_V$ , the ratio of the Gunn threshold current to the valley current) for diodes in the flat cavity in Figure 140b is 1.6. In a pure Gunn mode  $\alpha$  can approach two. Negative resistance will be present only if  $I_T$  is greater than  $I_V$  and  $\alpha$  is greater than unity. It can be shown that<sup>236</sup>

$$\frac{G_{pp}/G_T}{I_{pp}/I_T} = \frac{\alpha}{a} \quad (33)$$

where  $G_{pp}$  = peak conductance  
 $G_T$  = conductance at threshold  
 $I_{pp}$  = peak photocurrent  
 $I_T$  = Gunn threshold current  
 $a$  = numerical factor  $\approx .8$

The factor "a" accounts for the slight departure of the velocity-field curve from linearity at threshold.

For the data in Figure 140b, the ratio in equation 33 has a value of approximately 2.0 which means that  $\alpha$  is 1.6. Since  $\alpha$  is greater than unity, this means that even during the radiation pulse, the negative resistance and the Gunn effect are not quenched. For the high-Q cavity, the value of  $\alpha$  was found to be roughly 1.1. Thus, the Gunn effect is still present during radiation and the number of carriers generated by the radiation pulse is given by<sup>236</sup>

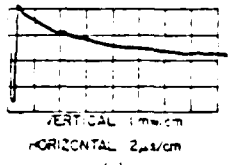
$$n_{pp} = k (\dot{\gamma})^b \text{ cm}^{-3}$$

where  $b \approx .6$   
 $k \approx 3 \times 10^9$

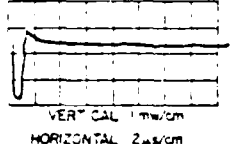
$\dot{\gamma}$  = dose rate

Two modes of failure are associated with dose or dose rate exposure:

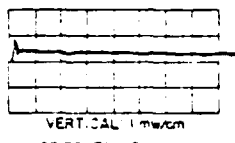
1) temporary cessation of output power and 2) avalanche breakdown when large currents surge through the diodes. The first mode of failure is nondestructive with a recovery time of 300 ns<sup>234,236</sup> for Gunn oscillators. Figure 141<sup>234</sup> indicates the output power during and after a radiation pulse of  $3 \times 10^8$  rads(Si)/sec



(a)

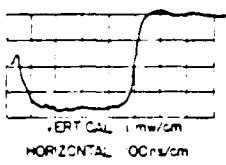


(b)

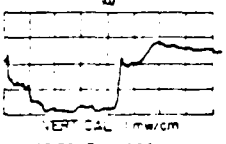


(c)

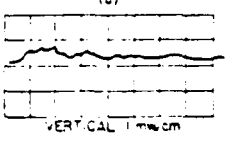
a) Overall



(d)



(e)



(f)

b) Expanded View of a)

Figure 141. Radiation-Induced Transients in Three Gunn Diodes' Output Power for a Dose Rate of  $3 \times 10^8$  rads (Si)/sec

The recovery time,  $\tau_0$ , associated with this mode of failure is plotted in Figure 142<sup>236</sup> for a number of operating voltages. The data in this figure was taken from pulse-diode test results. The onset of this failure mode is  $10^9$  rads(Si)/sec. CW diodes exhibit similar behavior except that the effect first appears at approximately  $10^8$  rads(Si)/sec.

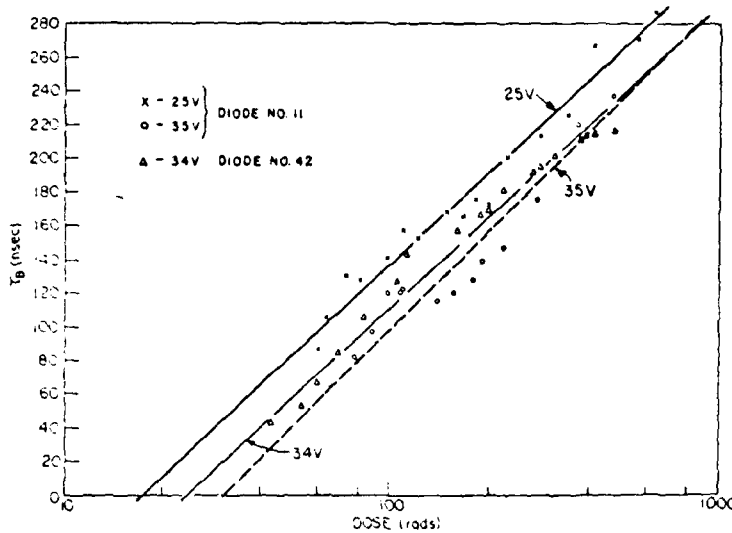


Figure 142. Recovery Time Versus Dose (Pulse Width of 25 nsec) for Pulsed Gunn Diodes.

From Figure 142, the recovery time,  $\tau_0$ , can be expressed as

$$\tau_0 = c \ln(\gamma-d)$$

The values of "c" and "d" vary with the operating voltage and operational mode (CW or pulse). Table 50<sup>236</sup> lists values of "a" and "d" for different voltages and modes of operation.

Table 50. Factors For Determining the Recovery Time

<u>Operating Voltage (Volts)</u>	<u>Diode Mode</u>	<u>a (nsec)</u>	<u>d (nsec)</u>
10	CW	137	2673
12	CW	139	2777
25	Pulse	73.6	1.71
34	Pulse	77.7	1.72
35	Pulse	36	1789

The behavior is also influenced by the types of cavity. This can be summarized as follows:<sup>236</sup>

- 1) There is an abrupt termination and recovery, after  $\tau_0$ , of the output power in a high-Q cavity. This is illustrated in Figure 141. For a flat cavity, the output power degrades during the

SAC

radiation pulse and then gradually recovers.

- 2) In a high-Q cavity the photocurrent seems to decay in steps and after  $\tau_D$  there is an abrupt drop. With a flat cavity, however, there is a more gradual exponential decay.

In the high-Q cavity, the mode in which the diode oscillates is critically dependent on the RF impedance matching between the device and the cavity. During ionizing radiation, the carrier concentration is increased, the RF current waveform changes, the diode suddenly becomes detuned and output power ceases. The diode is still oscillating but the power is not coupled to the output circuit. As the carrier concentration decays back to equilibrium the device will return to the original operating mode and the output power will resume.<sup>236</sup>

With a flat cavity, there is almost no RF tuning and the output power and device current are determined mainly by the diode itself. Therefore, as long as the device is oscillating, some output will be observed and the diode current will smoothly follow the changes of the decreasing carrier concentration.

The second failure mode is associated with avalanche breakdown. It is typified by the diode current gradually increasing to a large value and then decaying. The threshold for avalanche breakdown varies from manufacturer to manufacturer and with the mode of operation. The threshold for Monsanto diodes is approximately  $1 - 2 \times 10^{10}$  rad (Si)/sec whereas other manufacturer's diodes had an order of magnitude lower threshold. This applies to pulse operated diodes. Breakdown was not observed for diodes operated in the CW mode up to  $5 \times 10^{10}$  rad (Si)/sec.<sup>236</sup>

It has been observed that breakdown occurs in some instances long after the radiation pulse has ended. This suggests a thermal effect. Photocurrents generated by the ionizing radiation increase the operating temperature of the diode. This increased temperature can quench the negative resistance phenomenon<sup>237</sup> and stop the formation of the domains. The large electric field associated with the domain could then be trapped at the electrode and results in the injection of large currents into the diode and hence, breakdown. The increased temperature could also cause "hot spots" at localized imperfections. The radiation-induced hot spots would explain the delayed breakdown since this



is a heating effect which depends on the total integrated current through the device. In addition, it has been observed that diodes which exhibit poor thermal characteristics experience avalanche at lower dose rates.<sup>236</sup> The hardness of CW diodes can be accounted for by noting that these devices are operated at a much lower voltage than pulsed diodes. Therefore, the incremental heating due to radiation-induced photocurrents is less.

The above discussion applied to Gunn oscillators. Gunn amplifiers are, also, susceptible to the effects of ionization radiation. Similar to oscillators, two failure modes have been observed: 1) transient cessation of amplification and 2) destructive permanent failure. The threshold for transient failure occurs at  $2 \times 10^8$  rads (Si)/sec.<sup>238</sup> When the radiation pulse occurs, the power drops - not to zero but rather to a value that corresponds to zero dB gain (i.e., to the input power level). The output level remains at this low level for a period of time called the recovery time and then returns to the pre-irradiated value. The operating voltage, current, and gain also regain their preirradiation values. Figure 143<sup>238</sup> depicts the normalized output power ( $P/P_0$ , where  $P_0$  is the preirradiated output power and  $P$  is the output power after irradiation) and the recovery time versus dose rate. It should be noted that at the highest dose rate depicted,  $4 \times 10^{10}$  rads (Si)/sec, the off time was less than 400 nsec.

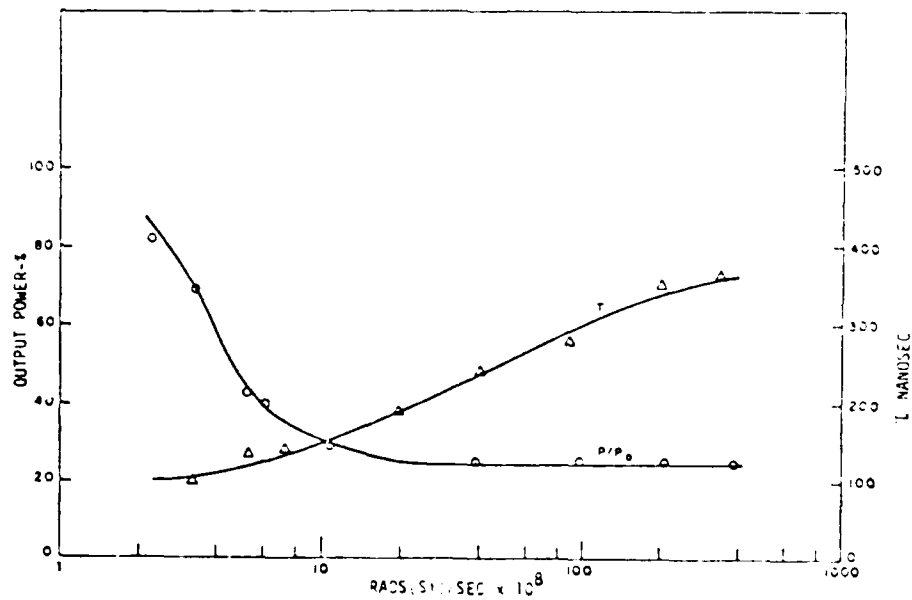


Figure 143. Recovery Time and Normalized Output Power Versus Dose Rate



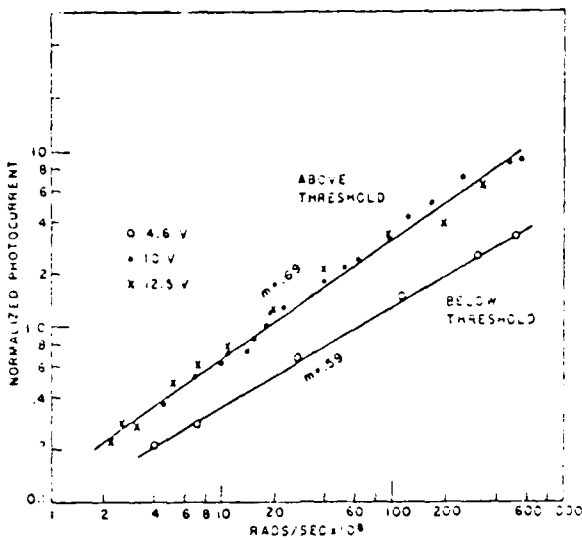


Figure 144. Peak Photocurrents in Gunn Amplifiers Versus Dose Rate

The peak photocurrents induced in Gunn amplifiers by transient ionizing radiation are plotted versus dose rate in Figure 144.<sup>238</sup> This was done for diodes biased above and below threshold. In this figure, the photocurrents are normalized to their preirradiated operating values. Similar to oscillators, the photocurrent and, hence, the radiation-induced excess carrier concentration, is proportional to  $\dot{\gamma}^{.65}$  (.65 is the average of the two slopes in Figure 144). The reader is reminded that for oscillators, the photocurrent varied as  $\dot{\gamma}^{.6}$ . This behavior is believed to be due to a trap distribution in the forbidden gap.<sup>239</sup> The photocurrent for the diode biased above threshold is independent of voltage which indicates, as was the case with oscillators, that the Gunn effect was not quenched by the radiation pulse.

The transient mode can be explained in terms of radiation-induced excess carrier concentration. This essentially changes the electric field distribution across the diode, reducing the negative conductance to zero. This is depicted in Figure 145 for two different carrier concentrations. For the diode that was irradiated (curve b) the region of the diode where negative differential mobility exists (region of the curve between  $E_1$  and  $E_2$ ) has been greatly reduced by radiation. The figure gives some indication that heavier doped diodes will be more radiation resistant. Computer analysis for the field distribution of curve b indicates that the negative conductance has decreased



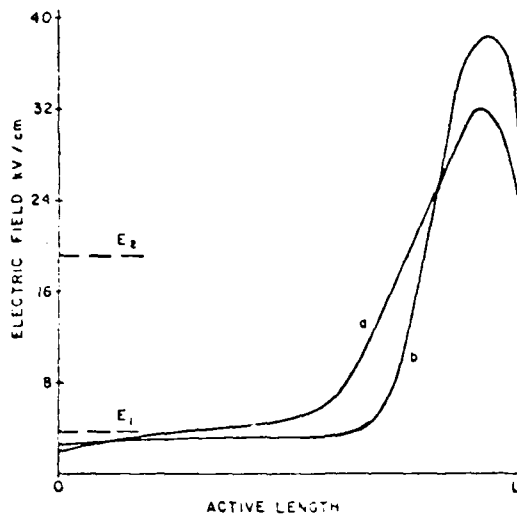


Figure 145. Electric Field Distribution Across a Gunn Amplifier

a)  $n = 1.2 \times 10^{16} / \text{cm}^3$ , no radiation

b)  $n = 3 \times 10^{15} / \text{cm}^3$ , dose rate =  $3.3 \times 10^9$  rads (Si)/sec

almost to zero and that the diode ceases to act as an amplifier.<sup>238</sup>

Utilizing the data in Figure 144 for excess carrier concentration as a function of dose rate, the gain of the diode was computed versus dose rate. This calculation was compared with the experimental results in Figure 143. The results of this comparison are shown in Figure 146. <sup>238</sup> The results are in

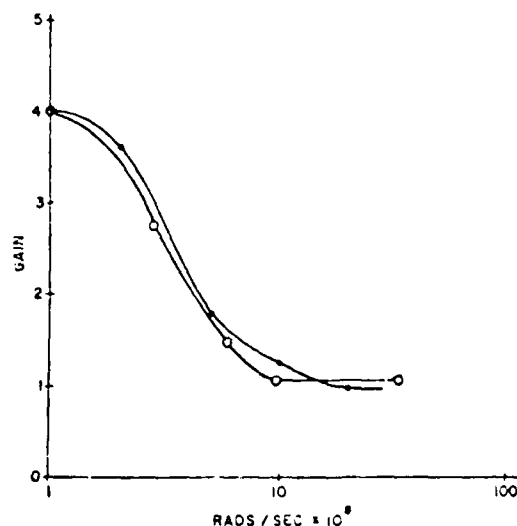


Figure 146. Gunn Amplifier Gain versus Dose Rate  
o Calculated; • Experimental



excellent agreement with one another which is a good indication that the transient failure mode is the result of radiation-induced excess carrier concentration.

The second mode of failure is a permanent destruction of the device. This destruction has only been observed at dose rates of  $6 \times 10^{10}$  rads (Si)/sec or greater for diodes operated at 12.5 volts or more.<sup>238</sup> The failure is thought to be thermal in nature and the result of the large radiation-induced photo-currents which induce thermal runaway. This effect has already been discussed in the portion of the report on Gunn oscillators and, therefore, will not be repeated here.

Table 51 is a summary of radiation effects on Gunn devices. This data should be taken as indications of the radiation levels where problems can occur. They should not be taken as damage or failure thresholds. There is not enough reported data to justify a threshold. The data simply are order of magnitude estimates of where problems can occur. However, given all of that, it is apparent Gunn diodes will experience some difficulty in the scenarios facing BMDATC-radars.

Table 51. Summary of Radiation Effects on Gunn Devices

Malfunction	Radiation
Power Failure	$10^{13} - 10^{14}$ n/cm <sup>2</sup>
Temporary Interruption	
Oscillators	
CW	$10^3$ rad(Si)/sec
Pulsed	$10^3$ rad(Si)/sec
Amplifiers	$10^3$ rad(Si)/sec
Avalanche Breakdown	
Oscillators	
CW	$> 5 \times 10^{13}$ rad(Si)/sec
Pulsed	$10^{13}$ rad(Si)/sec
Amplifiers	$6 \times 10^{13}$ rad(Si/sec)



### 6.3 PIN Diodes

Pin diodes are another class of device which may have a vulnerability problem. The devices are attractive alternatives to the customary garnet and ferrite phase shifters due to their lower cost, less weight, less volume, and ease of incorporation in or interfacing with integrated circuits. One of the most obvious applications is in a phased array radar system. A phased array is, of course, a steered electronic antenna. Its pencil beam or multibeams are focused by the phase shifters behind each radiating element. A phased-array radar system can have many thousands of elements with a phase shifter for each; therefore, it would seem that PIN diodes are promising candidates for phase shifters in any phased-array radar system.

A PIN diode is composed of a lightly doped n-type region bounded by a heavily doped p<sup>+</sup> type layer on one side and a heavily doped n<sup>+</sup> type layer on the other (i.e., p<sup>+</sup>nn<sup>+</sup>). The lightly doped n layer is generally referred to as the i layer since under normal forward biasing the injected charge density far exceeds the background impurity density.

The most lightly doped region (the i layer) of a PIN diode will be affected by neutrons first while damage in the p<sup>+</sup> and the n<sup>+</sup> regions will require much higher fluences.<sup>240</sup> In the i region, changes in mobility, lifetime, and thermal equilibrium carrier concentrations are expected. At room temperature and low doping levels, the primary scattering mechanism is interactions with lattice vibrations. Defect concentrations of approximately  $2 \times 10^{15}$  cm<sup>-3</sup> are required before defect scattering becomes important. Assuming two defects per n/cm<sup>2</sup>, a fluence of  $10^{15}$  n/cm<sup>2</sup> is required to significantly affect mobility.<sup>240</sup> In addition, reduction of thermal equilibrium carrier densities by carrier removal in the i region is not significant since the conductivity of the i region is due to injected excess carriers. The most sensitive parameter of PIN diodes to neutron irradiation is the lifetime of injected carriers. In fact, all the observed changes in the diodes are due to changes in carrier lifetimes.<sup>240</sup> The carrier lifetime as a function of neutron fluence can be expressed as<sup>241</sup>



$$\frac{1}{\tau} = \frac{1}{\tau_0} + K; \quad (34)$$

where  $\tau_0$  = initial lifetime

$\phi$  = neutron fluence

K = damage constant

The reader is reminded that this is the same equation that appeared in the section on RF devices. The value of K apparently depends on the neutron spectrum. For 14 MeV neutrons, K has a value of  $3.8 \times 10^{-7} \text{ cm}^2/\text{n-sec}^{242}$  and for 1 MeV neutrons, the value of K has been determined to be either  $1.9 \times 10^{-7} \text{ cm}^2/\text{n-sec}^{242}$  or  $1.75 \times 10^{-7} \text{ cm}^2/\text{n sec.}^{241}$

The degradation of lifetime due to 14 MeV neutron irradiation is plotted in Figure 147<sup>242</sup>. There were 56 experimental diodes in this figure of various intrinsic widths and lifetimes. The initial lifetimes ranged from 2.5 to 20  $\mu\text{sec}$  and the widths varied from 25 to 152  $\mu\text{m}$ . There were also 6 commercial devices in this figure. Manufacturer's data on these devices was not given in

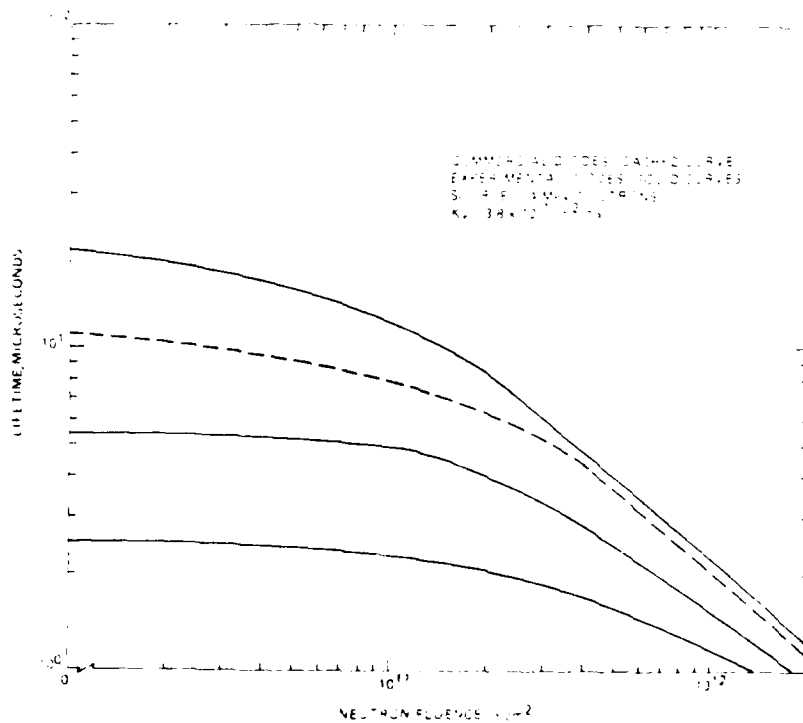


Figure 147. Degradation of PIN Diode Lifetime After Exposure to 14 MeV Neutrons

SAC

the literature. However, the intrinsic width was measured and found to be 152  $\mu\text{m}$ . As indicated in this figure, the same damage constant of  $3.9 \times 10^{-7} \text{ cm}^2/\text{n-sec}$  gave a reasonable fit (error spread of 3 to 18%) for all four curves using the lifetime equations. The three separate curves for the experimental diodes resulted from samples with three different initial lifetimes (25  $\mu\text{sec}$ , 55  $\mu\text{sec}$ , and 125  $\mu\text{sec}$ ). It should be noted that the curves converge as the neutron fluence increases regardless of the initial lifetime.

In contrast to Figure 147, lifetime degradation due to exposure to 1 MeV neutrons is depicted in Figure 148.<sup>243</sup> The nine samples were of the same type as those depicted in Figure 147. At the last fluence point, approximately  $4.5 \times 10^{13} \text{ n/cm}^2$ , the lifetime had decreased to a value of 175 nsec. In Figure 147 the exposure to 14 MeV neutrons degraded the lifetime to approximately 1  $\mu\text{sec}$ . However, continuation of the 14 MeV irradiations to the same fluence level as that in Figure 148 would have reduced the lifetime to values similar to that exhibited in Figure 147.

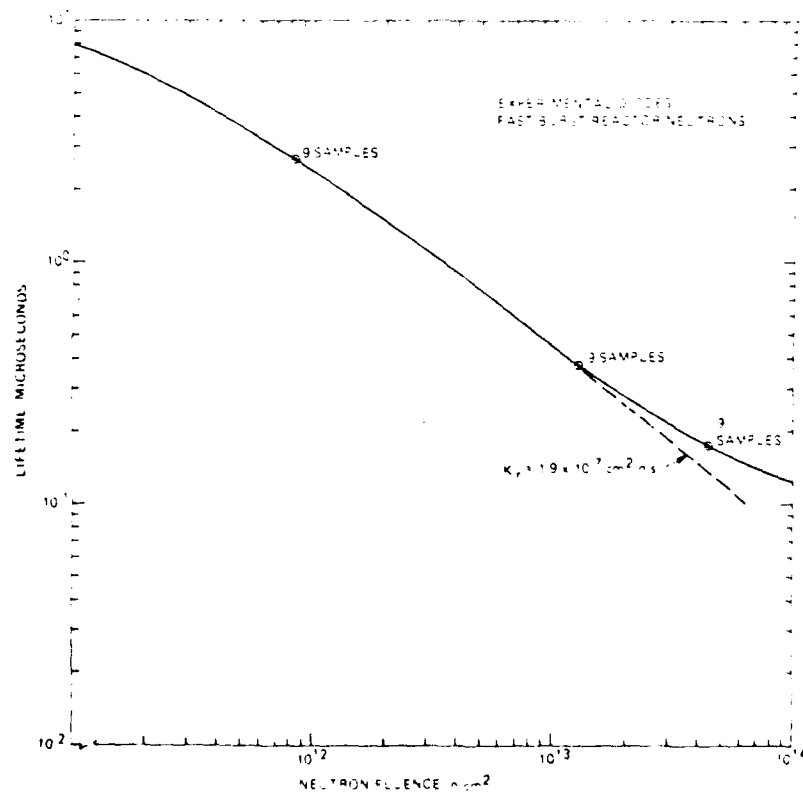


Figure 148. Lifetime Degradation of PIN Diodes Versus 1 MeV Neutron Fluence



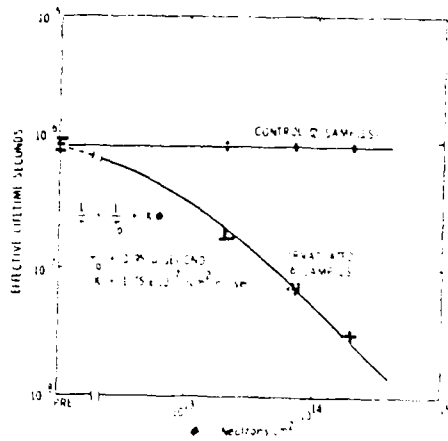


Figure 149. Lifetime Versus Neutron Fluence For PIN Diodes Irradiated with 1 MeV Neutrons

Additional lifetime degradation for 1 MeV neutron irradiation is depicted in Figure 149. The damage constant was  $1.75 \times 10^{-7} \text{ cm}^2/\text{n-sec}$  given by the data in Figure 148.

The forward resistance of the intrinsic region,  $R_i$ , depends strongly on the lifetime. The effects of neutron irradiation on low frequency PIN power rectifiers have been examined with the conclusion that there will be an increase in the forward voltage drop due to the decrease in lifetime.<sup>244</sup> Typical forward voltage-current characteristics of the diodes are shown in Figure 150<sup>240</sup>. In this

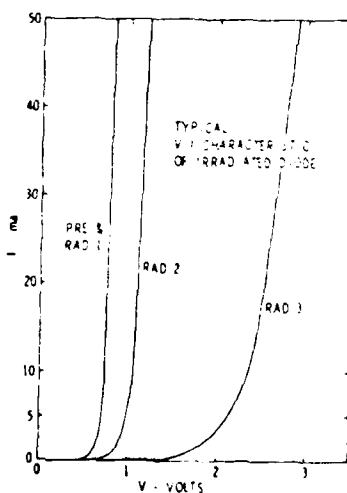


Figure 150. Typical V-I Characteristics of a PIN Diode for the Following 1 MeV Fluences:

figure the following definitions have been used:

$$\text{RAD 1} = 2 \times 10^{13} \text{n/cm}^2$$

$$\text{RAD 2} = 7 \times 10^{13} \text{n/cm}^2$$

$$\text{RAD 3} = 2 \times 10^{14} \text{n/cm}^2$$

This figure indicates that at a particular current the forward voltage drop across the diode increases with fluence. This is due primarily to an increase in  $R_i$ . An expression for  $R_i$  is given by<sup>240</sup>

$$R_i = \frac{2 \left( \frac{kT}{q} \right)}{I_0} \sinh \left( \frac{W}{2L} \right) \tan^{-1} \left[ \sinh \left( \frac{W}{2L} \right) \right]$$

where    W = width of the i region

L = diffusion length =  $\sqrt{Dt}$

D = diffusion constant

$I_0$  = bias current

k = Boltzman's constant

T = Temperature in  $^{\circ}\text{K}$

q = charge on an electron

Figure 151<sup>240</sup> compares the result from this equation with empirical data. The value of  $\tau$  was determined using equation 33. The value of  $I_0$  was held constant at 50 mA. As is obvious from the figure, the agreement is good between theory and empirical data.

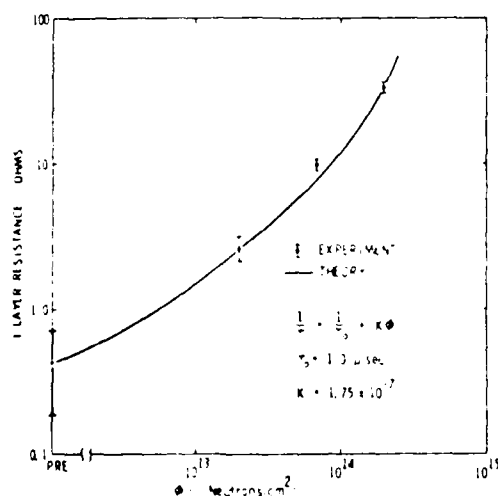


Figure 151.  $R_i$  Versus Neutron Fluence



An increase in  $R_j$ , of course, means an increase in the insertion loss. The microwave insertion losses at various 14 MeV neutron fluence levels have been reported for three phase shifters designed to produce phase shifts of  $45^\circ$ ,  $90^\circ$  and  $180^\circ$  respectively. The results are listed in Table 52.<sup>243</sup> The phase shifter designed to produce a phase shift of  $45^\circ$  was the least sensitive to neutron irradiation.

Table 52  
Increase in Insertion Loss of Microwave Circuits  
Versus 14 MeV Neutron Fluences

$\phi$ ( $n/cm^2$ )	$45^\circ$ (dB)	$90^\circ$ (dB)	$180^\circ$ (dB)
$6.43 \times 10^{10}$	0	0	.05
$4.64 \times 10^{11}$	.05	.14	.15
$8.95 \times 10^{11}$	.11	.32	.28
$1.46 \times 10^{12}$	.125	.59	.6

Table 52 was only for three phase shifters. In addition, the data on 56 discrete diodes, themselves, have been reported and is listed in Table 53.<sup>243</sup> The comparison between the effects of 1 MeV and 14 MeV seems to the

Table 53  
Average Insertion Losses for Mesa PIN Diodes  
Exposed to Neutrons

Intrinsic Width ( $\mu m$ )	Unirradiated Loss (dB)	$\phi$ ( $n/cm^2$ )	Irradiated Loss (dB)	Increase Loss (dB)
56	.38	$1.39 \times 10^{12}$ (14 MeV)	.39	Not Detectable
56	.38	$1.26 \times 10^{13}$ (1 MeV)	1.0	.66
56	.38	$4.4 \times 10^{13}$ (1 MeV)	1.6	1.2
112	.55	$1.39 \times 10^{12}$ (14 MeV)	.6	.06*

\* Approximately within the accuracy of the measurement.



authors to be inconclusive as does the effect of increasing the intrinsic width. It would appear that the only conclusion that can be drawn is that increasing the fluence above  $10^{13}$  n/cm<sup>2</sup> results in a large percentage increase of insertion loss.

Figure 151 indicates that  $R_i$  and, thus, the insertion loss does increase with neutron fluence. Failure is, of course, a system rather than a device concept. Reference 240 has determined the fluence required to increase  $R_i$  to 1Ω for a damage constant of  $1.75 \times 10^{-7}$  cm<sup>2</sup>/n-sec and  $I_0 = 50\text{mA}$ . The results are depicted in Figure 152. This figure does demonstrate that hardness increases with decreasing width of the i region. However, the width of the i region can only be decreased so far since the avalanche breakdown voltage decreases with i region width.<sup>187</sup> However, reference 242 does indicate that devices with an intrinsic region width of 56 μm and lifetimes of 6 usec can be built with acceptable breakdown characteristics. The general practice is to use the minimum i region width without going into avalanche breakdown.

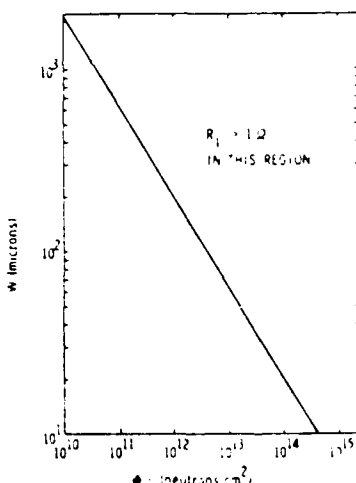


Figure 152. 1 MeV Neutron Fluence Required to Increase  $R_i$  to 1Ω versus Width of the Intrinsic Region

In the discussion two slightly different damage constants have been determined: one for 14 MeV neutrons with a value of  $3.8 \times 10^{-7}$  cm<sup>2</sup>/n-sec and one for 1 MeV neutrons with a value of  $1.9 \times 10^{-7}$  cm<sup>2</sup>/n-sec. This just means that 14 MeV neutrons are twice as effective in producing damage as 1 MeV neutrons.



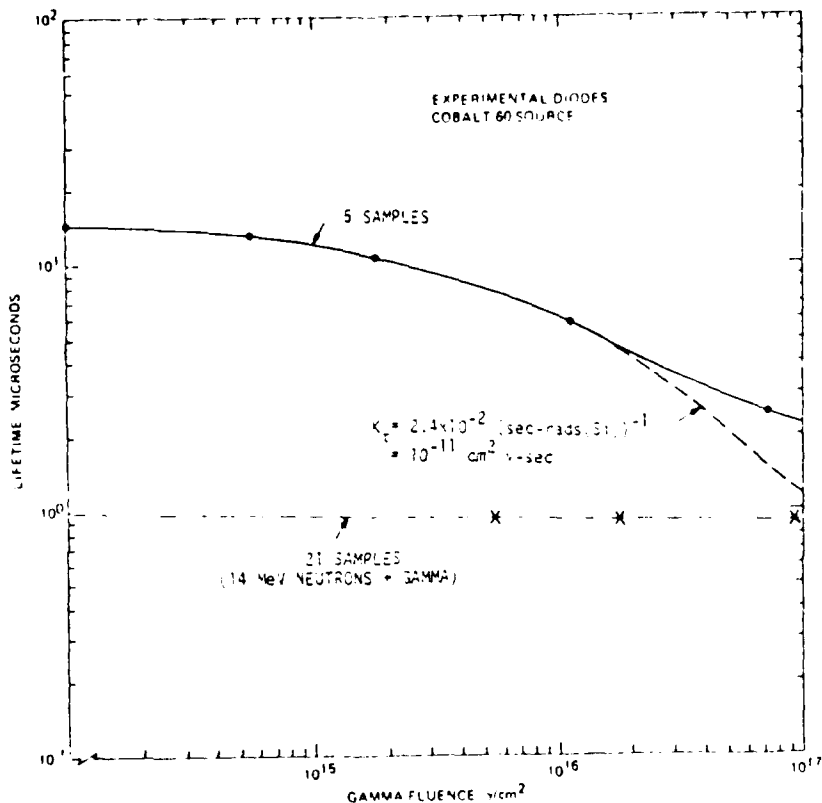


Figure 153. Decrease of PIN Diode Lifetime After Exposure to  $^{60}\text{Co}$  Gamma Rays.

This would also be expected for gamma ray exposure. Gamma rays should be much less effective in introducing defects than neutrons. Figure 153<sup>243</sup> illustrates the effect of gamma-rays on the lifetime of PIN diodes. It should be noted that the conversion factor that was used to convert  $\text{cm}^2/\text{r-sec}$  to  $\text{cm}^2/\text{rads(Si)-sec}$  was  $2.4 \times 10^9$  photons/ $\text{cm}^2\text{-rad(Si)}$  (see Table 1 in section 2.0). The factor that was used in reference 243 was  $1.8 \times 10^9$  photons/ $\text{cm}^2\text{-rad(Si)}$ .

In addition to the diodes that were exposed on  $\gamma$  to gamma-rays, Figure 153 also contains data on diodes that were used to generate Figure 147. The diodes were exposed to a cumulative 14 MeV fluence of  $1.39 \times 10^{12} \text{ n/cm}^2$  and then given the gamma-ray exposure shown in Figure 153. It should be noted that the gamma-irradiated or 14 MeV neutrons plus gamma-irradiated diodes clearly exhibit the same practical limit of 1  $\mu\text{sec}$ . This means that an exposure of approximately  $10^8 \text{ rads(Si)}$  was not sufficient to appreciably degrade the neutron

SAC

exposed samples beyond the 1  $\mu$ sec value which had already been attained due to neutron exposure.

As discussed in section 2.0, gamma-ray exposure introduces point defects involving a few atoms. Neutron exposure, however, introduces cluster defects involving hundreds of atoms. The curves in Figure 153 indicate the distinct difference in the cluster type of defect damage as compared to point defect damage. The limiting lifetime for gamma-ray irradiation from Figure 143 is 1  $\mu$ sec. For neutron irradiation from Figure 148, the limiting lifetime is 175 nsec. Thus, the limiting lifetime for gamma-ray exposure is considerably greater than that for neutron exposure. The difference, of course, results from the fact that clusters are more efficient in reducing the lifetime than are point defects. A comparison of the damage constants ( $10^{-11} \text{ cm}^2/\gamma\text{-sec}$  and  $1.9 \times 10^{-7} \text{ cm}^2/\text{n-sec}$ ) indicates that neutrons are  $10^4$  more effective than gammas in reducing the lifetime.

Figure 148 also indicates that the degradation of lifetime is saturating. This simply means that the lifetime will continue to degrade with continuing exposure but in a practical sense the degradation is not significant.<sup>243</sup>

Table 54

Damage Constants for PIN Diodes  
Exposed to Neutrons and Gammas

LIFETIME DAMAGE CONSTANTS	REFERENCE
K (14-MeV neutrons) $\text{cm}^2/\text{n-sec}$ $3.8 \times 10^{-7}$	242,243
K (1-MeV neutrons) $\text{cm}^2/\text{n-sec}$ $1.9 \times 10^{-7}$	242,243
	$1.75 \times 10^{-7}$ 240
K ( $^{60}\text{Co}$ gammas) $\text{cm}^2/\gamma\text{-sec}$ $1 \times 10^{-11}$	242,243

Table 54 contains a summary of the damage constants for all types of radiation. However, it must be remembered that these constants were determined from the linear portion of the damage curve. Therefore, because of the saturation effects evident in Figures 148 and 153, the use of these



constants in predicting damage for the higher fluences will overestimate the lifetime decreases and insertion loss increases. It is felt that the 14 MeV damage constant has higher fidelity than the others. This stems from the fact that it was determined on 62 diodes with intrinsic regions ranging from 25  $\mu$ m to 152  $\mu$ m and lifetime from 2.5  $\mu$ sec to 20  $\mu$ sec. The 1 MeV neutron and gamma were not measured on as many samples and, thus, may not have the same universality.

The above discussion indicates that PIN diodes are able to withstand at least  $10^{13}$  n/cm<sup>2</sup> and  $10^8$  rads(Si). Reduction in the intrinsic region width will lead to increased hardness but peak power handling capability will be reduced. In addition the radiation hardness of stacked diodes (i.e., two diodes in series) will be greater than the level of a single diode with the same total intrinsic width.



## 6.4 Ferrites

As mentioned in the previous section, ferrites and garnets are possible candidates for phase shifters in phased-array radars. As alluded to in that section, they have certain disadvantages when compared to PIN diodes: higher cost, weight, and volume. But, nevertheless, they are candidates for phase shifters and as such, merit some discussion.

Ferrites are ceramic ferromagnetic materials with the general chemical composition  $M_2\text{O}\cdot\text{Fe}_2\text{O}_3$  where M is a divalent metal such as iron, manganese, magnesium, nickel, zinc, cadmium, cobalt, copper, or a combination of these. It is interesting to note that lodestone is an iron ferrite or magnetite ( $\text{FeO}\cdot\text{Fe}_2\text{O}_3$  or  $\text{Fe}_3\text{O}_4$ ). Work in the field of microwave ferrites did not begin until 1949 when Polder first derived the permeability tensor which laid the foundation for understanding ferrite behavior at microwave frequencies.<sup>245</sup>

Ferrites are cubic and have the spinel structure shown in Figure 154<sup>256</sup>, after the mineral spinel ( $\text{MgAl}_2\text{O}_4$ ). In this structure, the  $\text{Mg}^{2+}$  ion occupies a tetrahedral site since each is surrounded by four oxygen ions. The  $\text{Al}^{3+}$  ion occupies an octahedral site since each is surrounded by six oxygen ions. This is a normal spinel arrangement with the divalent ion ( $\text{Mg}^{2+}$ ) occupying a tetrahedral site. There is an inverse spinel arrangement in which the octahedral sites are

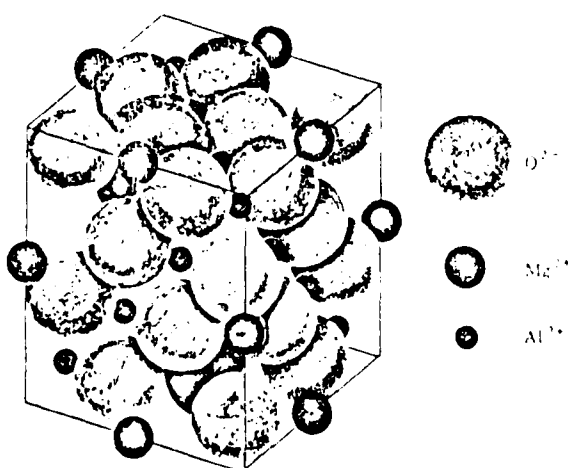


Figure 154. Crystal structure of the Mineral Spinel  
 $\text{MgAl}_2\text{O}_4$



occupied half by divalent and half by trivalent metal ions.<sup>246</sup>

Rare earth garnets are of the general chemical formula  $5\text{Fe}_2\text{O}_3 \cdot 3\text{M}_2\text{O}_3$  where M represents yttrium or some other rare earth ion ranging from samarium to lutecium. The garnet structure differs from the spinel lattice in several respects. One of the chief differences being that the garnet has three types of lattice sites available to metallic ions as compared to the two types of sites in the spinel structure.<sup>247</sup>

Before discussing the susceptibility of these materials to radiation, it is necessary to define some standard terms. Figure 155 is useful for this purpose. The coercive force is the point on the curve labeled  $-H_c$  and is the reverse H field necessary to bring the induction B to zero. The remanence  $B_r$  is the value of B at H=0. The saturation induction  $B_s$  is the limiting value of (B-H) for large H.

Magnetic ferrites including both garnet and spinel structures are susceptible to neutron radiation. The damage threshold<sup>2</sup> of these materials is  $10^{12} \text{ n/cm}^2$ . The remanence and permeability,  $\mu$ , of these materials will be reduced along with an increase in coercive force.

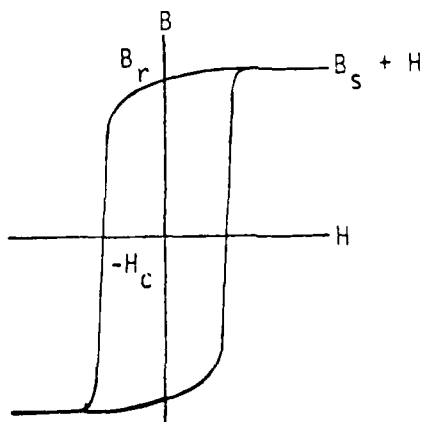


Figure 155. The Magnetization Curve or Hysterisis Loop.  
 $H_c$  is the Coercive Force.  $B_r$  is the  
Reamanence.  $B_s$  is the Saturation Inductance.

However, this is a very large class of materials with properties that vary widely. As would be expected within the ferrite class, there are examples whose damage thresholds are several orders of magnitude larger than  $10^{12} \text{ n/cm}^2$ . Ferrites with rectangular hysteresis are not appreciably affected by fluences up to  $10^{18} \text{ n/cm}^2$ . However, at this fluence ferrites with high initial permeability may suffer a 20 to 30% decrease in low field permeability.<sup>248</sup> The hysteresis properties of yttrium- and samarium-iron garnets are not affected by neutron fluence below  $10^{18} \text{ n/cm}^2$ . However, at  $10^{18} \text{ n/cm}^2$  these materials experience a 30% increase in  $H_c$  and the remanence.<sup>249</sup>

Thus, as with so many other materials, ferrites have a wide range of responses and the survivability of the system will depend to a great extent on the proper choice of materials. The literature does indicate that ferrites can be found that will be able to survive neutron fluences at the threat level. In addition, the magnetic properties of ferrites are insensitive to dose and dose-rate.<sup>250</sup>

Thermal vulnerability of ferrites deserves some mention even though it was not an area of concern for the project. However, before discussing the possible thermal vulnerability, it is necessary to briefly digress and give some background. A substance is ferromagnetic if it possesses a spontaneous magnetic moment, that is, a magnetic moment even in the absence of an applied magnetic field. The saturation magnetization,  $M_s$ , is defined as the spontaneous magnetic moment per unit volume. In the literature, the saturation flux density  $B_s = 4\pi M_s$  or even  $4\pi M_s$  is often used. The Curie point  $T_c$  is the temperature above which the spontaneous moment vanishes. The magnetic susceptibility,  $\chi$ , is given by

$$\chi = \frac{M}{H} = \frac{C}{T}$$

where C is the Curie constant. The  $\frac{1}{T}$  temperature dependence is known as the Curie law. The susceptibility above the Curie point is found by assuming that the Curie law holds provided the magnetic field is taken to be the sum of the applied field, H, and the Weiss field  $H_E$ . The Weiss field is the equivalent of an effective magnetic field,  $H_E$ , which acts on the electron spins and tends to make the ionic and atomic magnetic moments line up giving rise to a spontaneous magnetic moment and resulting in a ferromagnetic material. This



results in the Curie-Weiss law

$$X = \frac{C}{T - T_c}$$

To apply or carry this over to ferrites would require incorporating quantum mechanics, domain theory, and spin interaction and that is certainly beyond the scope of this work. However, the above discussion does indicate the magnetic properties of ferrites should be dependent on temperature, should deteriorate with increasing temperature, and should be dependent on the Curie point of the material.

For latching ferrite phase shifters, the stability of the hysteresis loop is of major importance. The remanence should be insensitive to slight variations in both temperature and stress. The Curie temperature is often used as a rough guide to temperature sensitivity. Figure 156 indicates the variation

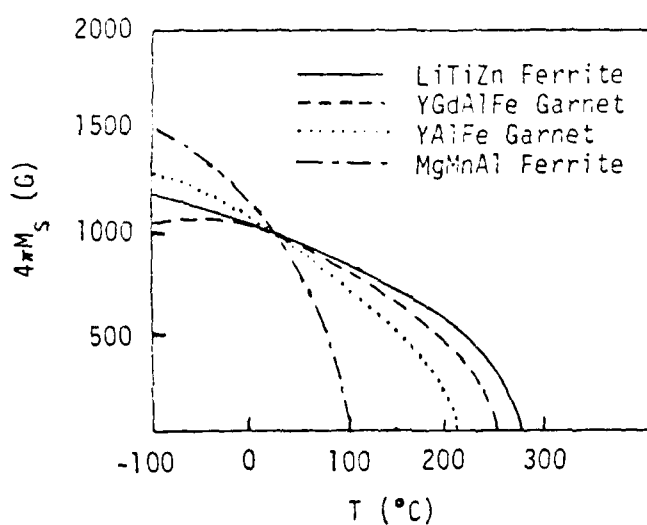


Figure 156. Magnetization Versus Temperature of Microwave Ferrites

of  $M_s$  with temperature for a number of ferrites and garnets.<sup>151</sup> The  $\text{MgMnAl}$  ferrite has the lowest Curie point of the materials shown and is quite sensitive to variations in temperature. The addition of Gd to YAlFe garnets flattens the



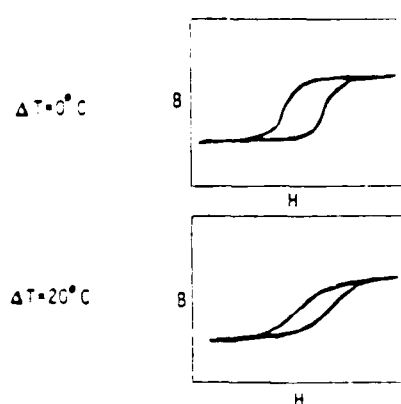


Figure 157 Effect of a Thermal Gradient on the Hysteresis Loop of a Microwave Garnet Toroid. The Outer Wall is 20°C Colder than the Inner Wall

magnetization-temperature curve. The LiTiZn ferrite has the highest Curie point of the materials shown and has the best temperature characteristics.

The effects of stress resulting from a temperature gradient between the inner and outer walls of a square loop garnet toroid can greatly deteriorate the hysteresis curve. Figure 157 taken from reference 251 indicates this effect for a temperature gradient of 20°C. It should be noted that the effect is dependent on the temperature gradient and not on the magnitude of the temperature. As mentioned before, this project is not concerned with thermal effects but it was thought that this information could be of use. In addition, it should not be inferred that all ferrites and garnets have such severe temperature problems but only that such problems associated with temperature and the rate of temperature rise can exist.

#### 6.5 Microwave Transistors

The discussion on the nuclear vulnerability of classes of devices that may appear in BMDATC-radars would be incomplete if it did not include a section on microwave transistors. Due to its inherently high speed, GaAs is being used to fabricate more and more device types in this area.<sup>252,253</sup> Nevertheless, GaAs technology is still considered embryonic and it may be difficult to produce devices in quantity.<sup>254</sup> There seems to be an oxide problem - certainly connected with



AD-A102 747

SCIENCE APPLICATIONS INC HUNTSVILLE AL  
NUCLEAR ANALYSIS AND TECHNOLOGY ASSESSMENT OF RADAR CONCEPTS. V--ETC(U)  
MAY 81 J P SWIRCZYNSKI, C S CHEEK

F/G 17/9

DASG60-78-C-0029

NL

UNCLASSIFIED

SAI-82-604-HU

4 of 4

AOA

02747

END  
DATE  
FILED  
9-18-81  
DTIC

producing ICs. However, there is some indication that the problem is in the process of being overcome with the introduction in 1980 of a 1000 gate GaAs IC by Rockwell International.<sup>255</sup> In addition, Rockwell has made a commitment to produce a 10,000 gate GaAs IC by 1983.<sup>255</sup> Hence, despite its immaturity the promise of this technology is worth investigating since gigabit GaAs logic is feasible.<sup>256</sup>

Present day GaAs microwave FET's are characterized by higher gain and lower noise than any other device in the 4 to 20 GHz frequency range and, at frequencies above about 6 GHz, are capable of greater power output than Si bipolar transistors.<sup>257</sup> Perhaps of even more importance than the high speed and low power of GaAs is their excellent radiation characteristics. Studies have found that radiation effects on GaAs FET's were negligible at total doses of  $10^6$  rads(GaAs) and neutron fluences of  $5 \times 10^{13}$  n/cm<sup>2</sup> 148,253,258,259 or higher. As discussed in section 5.2, the neutron level and total dose level, depending on device parameters (such as channel doping level) can be as high as  $10^{15}$  n/cm<sup>2</sup> and  $10^7$  rads(GaAs). In fact, this is the only technology that has the potential of being inherently survivable at the neutron and total dose levels mentioned in Volume I.

However, a significant transient response problem has been reported for GaAs metal-semiconductor field effect transistors (MESFET) that have been exposed to low total dose levels (approximately 100 rads(GaAs)) of ionizing radiation pulses.<sup>260</sup> The dose rate was roughly  $3 \times 10^{10}$  rads(GaAs)/sec.

This effect involves the generation of long-term source-drain current ( $I_{DS}$ ) transients. The transient recovery times are a strong function of temperature. At room temperature they ranged from 1 to 70 sec while at 200°C they were approximately 100  $\mu$ sec. Figure 158 depicts a typical response of a depleted mode MESFET following exposure at 25°C.<sup>260</sup> The device was initially biased at 550  $\mu$ A and was driven into cutoff by the radiation pulse. Recovery to the pre-irradiation level required more than 50 seconds.

A FET with a high density of deep level electron traps within the depletion region might be expected to exhibit a negative-going  $I_{DS}$  transient response (similar to that depicted in Figure 158) if subjected to a positive gate voltage pulse when biased in a conducting state. During the voltage pulse, traps within the depletion region are filled with electrons which tends to bias the FET closer to cutoff after the pulse. As the trapped electron population returns to



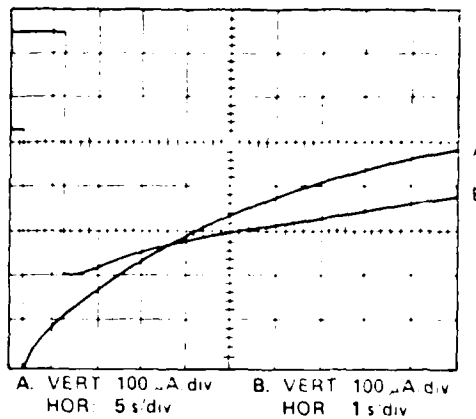


Figure 158. Radiation-Induced Transient  $I_{DS}$  Response of GaAs MESFET

equilibrium,  $I_{DS}$  decays to its quiescent level.<sup>260</sup> This simply means that behavior such as that depicted in Figure 158 can also occur in a benign environment.

GaAs MESFET's are currently fabricated by two basic techniques. The first involves the formation of the MESFET structure within an n-type surface layer implanted within the semi-insulating GaAs substrate. In the second technique, devices are formed within a thin epitaxial layer either directly on the substrate or over a semi-insulating GaAs buffer layer. These configurations are illustrated in Figure 159.<sup>260</sup> Radiation data exists for both these structures.

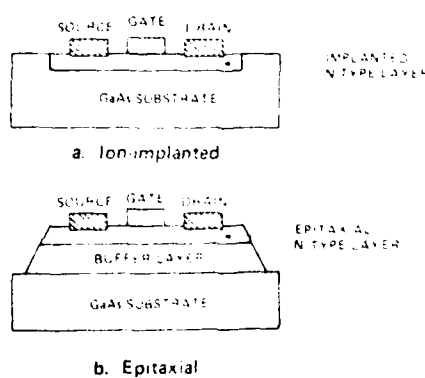


Figure 159. Two Basic GaAs FET Configurations

Typical radiation response characteristics for an implanted MESFET



operating at various quiescent current levels are shown in Figure 160.<sup>260</sup> The

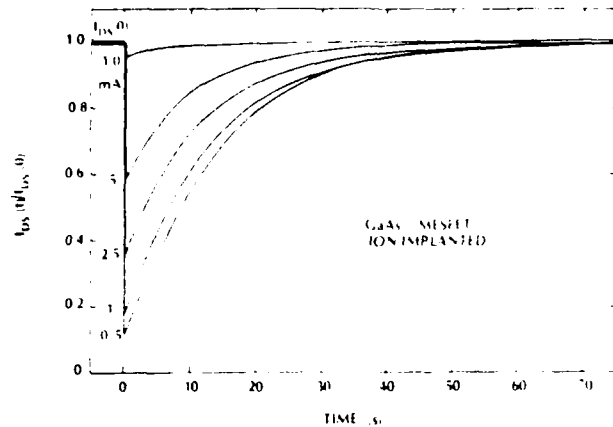


Figure 160. Pulsed Radiation Response Characteristics of GaAs MESFET's at Various  $I_{DS}$  Levels

curves were generated by an exposure to a dose level of 100 rads(GaAs). The pulse width of the exposure was 3 nsec. Thus, the dose rate was  $3.3 \times 10^{10}$  rads(GaAs)/sec.

As indicated in this figure the amplitudes of the  $I_{DS}$  transients varied from 90% of  $I_{DS}(0)$  at a quiescent current of .5 mA to less than 5% of  $I_{DS}(0)$  at a quiescent current of 10 mA. It should be noted that other samples biased at .5 mA were driven into cutoff at these exposure levels.<sup>260</sup>

The recovery time can be defined as the time for a 63% decay (down  $1/e$ ) of the transient. Using this definition the recovery times in Figure 160 are between 10 and 14 sec. It should be noted that the temperature in Figure 160 was 25 - 27°C.

Table 55<sup>260</sup> lists the results of radiation testing of epi-layer power MESFET's at 22°C. The pulse width for each of the 9 exposures was 60 nsec. Shots 1 through 5 show the increase in peak transient amplitude as the dose level of each shot was increased from 70 to 730 rads(GaAs) and the dose rate was increased from 1.2 to  $12.2 \times 10^9$  rads(GaAs)/sec. Shots 5 through 9 illustrate the progressive reduction in the relative significance of this effect as the quiescent current is increased from .5 to 100 mA. The applied gate bias,  $V_G$ , was adjusted to reduce the quiescent current to the levels shown in Table 55.

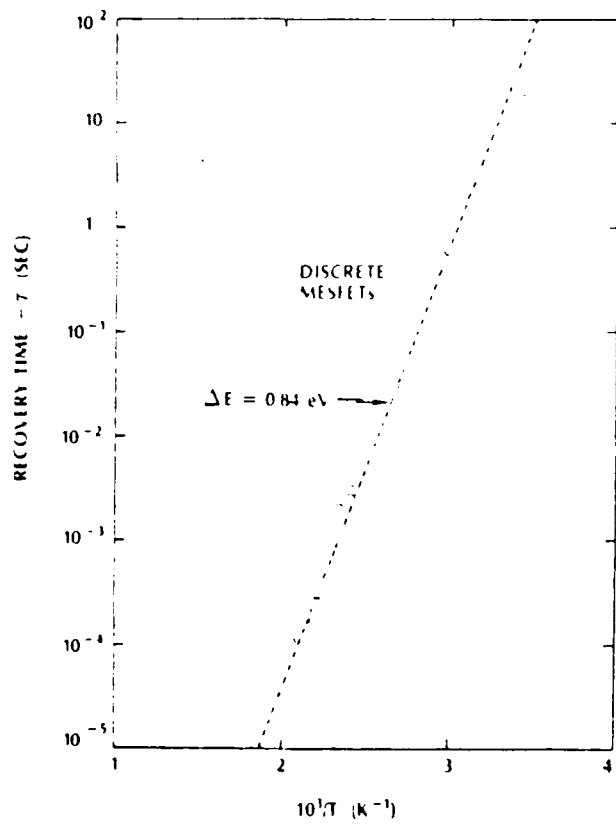
The recovery time is a strong function of temperature ranging from tens of seconds at room temperature down to roughly 100  $\mu$ sec at 200°C. Figure 161<sup>260</sup>



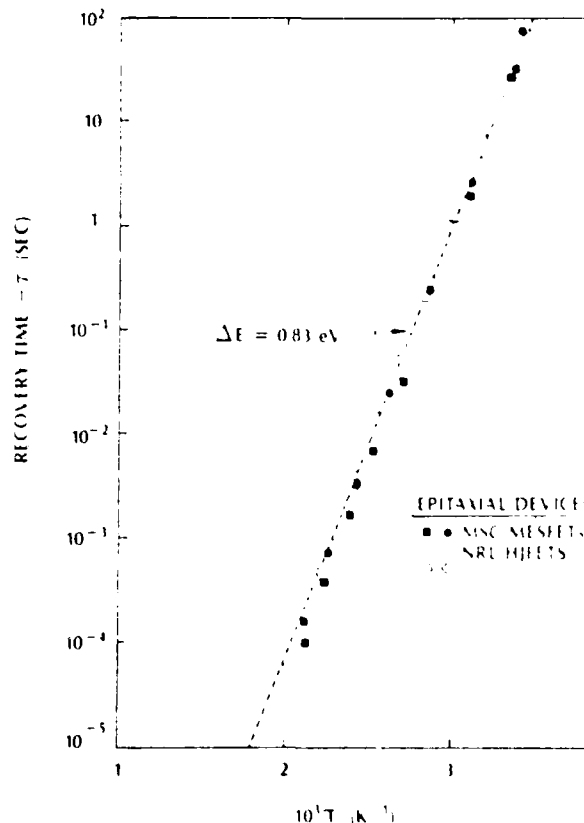
Table 55. Radiation Test Data on Epi-Layer Power MESFET'S

Shot No.	Dose* Rate	Dose (rads(GaAs))	$V_G$ (volts)	$I_{DS}$ (mA)	$\Delta I_{DS}$ (peak) (mA)	$\frac{\Delta I_{DS}}{I_{DS}}$ (%)
1	1.2	70	-6.7	0.5	0.16	32
2	2.5	147	-6.7	0.5	0.18	36
3	5.0	300	-6.7	0.5	0.21	42
4	10.8	648	-6.7	0.5	0.23	46
5	12.2	730	-6.7	0.5	0.25	50
6	7.2	434	-6.35	1.0	0.39	39
7	18.0	1080	-5.1	5.0	1.35	27
8	14.5	869	-4.0	50.0	3.0	6
9	16.8	1005	-2.0	100.0	2.2	2

\*Units are  $10^9$  rads(GaAs)/sec.



a.) Ion Implantation Devices



b.) Epitaxial Devices

Figure 161. Recovery Time Constant Versus Reciprocal Temperature for GaAs FET's

depicts the recovery time constants plotted as a function of reciprocal temperature for implanted and epi-layer devices. The data in Figure 161b labeled MSC MESFET's is for commercial power MESFET's. As mentioned previously the data labeled HJFET's is for some experimental heterojunction gate FET's.  $\Delta E$  is the activation energy or the difference in energy between the trap and the conduction band.

The response of the devices is attributed to negative charge trapping near the FET channel region during irradiation. The trapped charge, which anneals with a time constant that is characteristic of the trapping levels involved, acts like an additional negative voltage in series with the applied gate bias which tends to further pinch off the channel.<sup>260</sup>

The FET response was usually dominated by a single trapping level having an activation energy in the 0.73 to 0.80 eV range and a capture cross section of approximately  $10^{-14}$  cm<sup>2</sup>. Chromium, a known acceptor in GaAs, has been reported<sup>261</sup> to span an activation energy range of 0.56 to 0.90 eV. Activation energies of 0.57 to 0.90 eV have been reported<sup>262</sup> for oxygen in GaAs but this center typically acts like a donor. The trap parameters for the FET compare very favorably with those reported<sup>263</sup> for Cr-doped bulk material. Thus, there is a strong possibility that the acceptor level and, hence, the transient response is associated with the Cr center in GaAs. This would suggest that higher material quality would resolve to a great extent the transient response problem of the GaAs FET's.

One thing the above discussion does indicate is the importance of the processing techniques used in fabricating GaAs. These devices were fabricated on a Cr-doped GaAs substrate. There was a deeper level trap (0.87 eV) that was found to dominate the long-term response of GaAs NOR gate samples that could have been introduced during the ion-implantation sequence.<sup>260</sup> Thus, there is still a need to more closely characterize the samples that were used.

This ends the discussion on microwave transistors. Since these are fabricated from what must be considered a very immature technology no attempt has to determine techniques that could be used to mitigate the effects that were mentioned. However, it is obvious that these devices will experience transient upset at the threat levels which have been proposed for BMDATC-radars.



## 7.0 CONCLUDING REMARKS

One of the most difficult requirements that any system that is deployed by BMD will have to meet is to survive the nuclear environments that the system will be exposed to. It is not completely clear that the task can be done. It certainly can not be done unless the nuclear vulnerability issue is addressed. This does not mean simply generating the levels of the environments that the equipment will be exposed to. In fact, this is the easy part of the problem. The difficult part is designing and building a system that can survive and function in this environment. The problem is further complicated by the fact that the operational requirements necessitates the use of some state-of-the-art components. In any case, the proper choice of the technology and the class of a device within that technology is crucial and must be considered the first step toward survivability. Some technologies such as NMOS simply can not survive the environment.

The object of this project was to identify the vulnerability of state-of-art radar systems. The design of the system was not fixed nor was the parts list. Thus, a statement concerning the survivability of the system could not be made. Instead the assessment was based on technologies, materials, and components that are found in most radars. This identified those device classes that should be avoided (e.g., SCR's) and device or material classes that appeared suspect (e.g., quartz crystals, Teflon, Gunn devices). Hopefully, this will aid in identifying those technology areas which need and would profit by a development effort to provide survivable componentry when they are required (e.g., higher material quality in GaAs FET's).

This project has attempted to describe to the reader the impact of nuclear radiation on BMDATC-radars. This report is not intended to be a recipe book on how to satisfy the system's nuclear survivability requirements. No single document could achieve this for all the classes of devices that could appear in a radar system. Instead, the emphasis was placed on presenting as much of the total picture as possible with the realization that the study would be incomplete.

Design guidelines have been presented where they exist. It must be remembered that most components will exhibit some response to nuclear radiation. However, this does not mean failure. The nuclear-induced degradation can be accounted for in the design margins. The guidelines should be used to help miti-



gate the effects of nuclear radiation.

As a final note, the reader is advised that a summary of this volume is contained in the Executive Summary. A deliberate effort has been made to keep this volume and the summary unclassified to facilitate its distribution. It is hoped that this volume will serve as a source or reference book. Because of this the reference list was purposely made as extensive as possible. The topics which have been discussed are, of course, more completely discussed in the appropriate references. As a final comment, the reader who has persevered to the end of this tome is to be praised for his steadfastness of purpose.

## REFERENCES

- 1.) Principles and Techniques of Radiation Hardening; Interaction of Radiation with Matter and Material Effects; N.J. Rudie; Vol II, Western Periodicals Company, (1976).
- 2.) Fundamentals of Nuclear Hardening of Electronic Equipment; L.W. Ricketts, Wiley-Interscience, (1972).
- 3.) "Nuclear Weapon Effects on Army Tactical Systems, Vol. I, Overview"; J.J. Halpin, J.P. Swirczynski, G. Teele, E. Quigley, and M. Campi; HDL-TR-1882-1, (1979).
- 4.) The Effects of Nuclear Weapons; Samuel Gladstone and Philip J. Iolan; Department of the Army Pamphlet No. 50-3, (1977)
- 5.) "Designers Guide to Radiation Effects on Materials for Use on Jupiter Fly-Bys and Orbiters"; F.L. Bouquet, W.E. Price, and C.M. Newill; IEEE Transactions on Nuclear Science, Vol. NS-26, No. 4, (August, 1979)
- 6.) Principles and Techniques of Radiation Hardening, Interaction of Radiation with Matter and Material Effects, Vol. I; N.J. Rudie; Western Periodicals Co., (1976)
- 7.) Radiation Effects Handbook ; J.R. Bilinski and W.R. Langdon, Editors; The Institute of Electrical and Electronics Engineers, Inc., (1963)
- 8.) "The Effects of Nuclear Radiation on Elastomers and Plastic Materials"; N.J. Broadway, M.A. Youtz, M.L. Zaring, and S. Palinchak; REIC Report No. 3, The Radiation Effects Information Center, Battelle Memorial Institute, Columbus, Ohio, (May, 1958).
- 9.) Space Materials Handbook; J.B. Rittenhouse and J.B. Singletary; NASA SP-3051, 3rd Edition, (1969).
- 10.) "The Effects of Radiation on Electrical Insulating Materials"; C.L. Hanks and D.J. Hanman; REIC No. 46, Battelle Memorial Institute, Columbus (June, 1969).
- 11.) "The Effects of Nuclear Radiation on Elastomeric and Plastic Components and Materials"; N.J. Broadway and S. Palinchak; REIC Report No. 21 (Addendum), Radiation Effects Information Center, Battelle Memorial Institute, (August 31, 1964).
- 12.) "Measured Effects of the Various Combinations of Nuclear Radiation, Vac., and Cryo-temperatures on Engineering Materials"; Report No. FZK-172, General Dynamics, Fort Worth, Texas, (September 30, 1963), and Report No. FZK-290, (July 1, 1966).



- 13.) Radiation Effects on Organic Material, R. O. Bolt and J. G. Carroll, Editors; Academic Press, 1963.
- 14.) "How Radiation Changes Polymer Mechanical Properties;" C. D. Bopp and O. Sisman; Nucleonics; 13(10): 52: Oct, 1955.
- 15.) "Regularity of the Degradation of Textile Fibers with High Energy Radiations and Heat;" A. Sippel; Melland Texilber; 38:898; August 1957.
- 16.) "The Effects of Gamma Radiation on Cotton. Part I: Some of the Properties of Purified Cotton Irradiated in Oxygen and Nitrogen Atmospheres"; F.A. Blovin and J.C. Arthur, Jr.; Textile Research Journal, 28(3): 193; March, 1958.
- 17.) "Radiation Effects on Encapsulating, Potting, and Structural Plastics", L.M. Epstein, editor; Radiation Effects Handbook; IEEE; June, 1963.
- 18.) "Effects of Nuclear Radiation on the Strength of Yarns"; E.S. Gilfillan and L. Linden; Textile Research Journal; 25(9): 773: Sept, 1955.
- 19.) "Some Effects of Nuclear Irradiations on Cotton Yarn"; E.S. Gilfillan and L. Linden; Textile Research Journal; 27(2): 87; Feb, 1957.
- 20.) "Effects of Cobalt-60 Gamma Radiation on the Physical Properties of Textile Cords"; D.J. Harmon; Textile Research Journal; 27(4): 318; April, 1957.
- 21.) "The Effect of Nuclear Radiation on Fibrous Material. Part III: Relative Order of Stability of Cellulosic Fibers"; O. Tezler, L.H. Kiser, P.W. Campbell, H.A. Rutherford; Textile Research Journal; 28(5): 456; June, 1958.
- 22.) "Changing the Tensile Strength and Degree of Polymerization of Artificial Fibers by Irradiation and the Relation of These Phenomena to the Molecular Fine Structure, Especially of Cellulose"; A. Sippel; Kolloid - Z.; 112:80; Feb-Mar., 1945.
- 23.) "Effect of Gamma Radiation on Epoxy Plastics"; Colichman and Strong; Modern Plastics, 35; Oct., 1957.
- 24.) "Effects of Radiation on Polyethylene"; V.L. Lanza; Modern Plastics, 34(10): 129: July, 1957.
- 25.) "Stress-Strain Curves for Reactors-Irradiated Plastics;" C. D. Bopp and O. Sisman; Nucleonics, 14(3): 52; March, 1956.
- 26.) "Behavior of Plastics in Space Environments"; A.F. Ringwood; Modern Plastics; 41, Jan, 1964.



- 27.) "Effect of Gamma Radiation on Epoxy Plastics"; Collichman and Strong; Modern Plastics, 35; Oct., 1957.
- 28.) "Effects of Radiation on Polyethylene"; V.L. Lanza; Modern Plastics, 34(10): 129; July, 1957.
- 29.) "Effects of Nuclear Radiation and Cryogenic Temperatures on Nonmetallic Engineering Materials"; E.C. McKannan and R.L. Gause; Journal of Spacecraft, Vol 2, No. 4; 1965.
- 30.) "Gamma Irradiation in Semirigid Epoxies"; F.F. Stuchi and C.M. Newell; IEEE Transactions on Nuclear Science; Vol. NS-12, No. 2; April, 1965.
- 31.) Private communication-K. Dent; Science Application Inc.; Huntsville, AL.
- 32.) "Skipping the Hard Part of Radiation Hardening," J. T. Finnell, Jr. and F. W. Karpowich, Electronics (March 4, 1968) p. 124
- 33.) "Nuclear Radiation Effects on Resistive Elements"; Radiation Effects Information Center, REIC Report No. 31, (July 15, 1966) Battelle Memorial Institute.
- 34.) "TREE (Transient Radiation Effects on Electronics) Handbook," D. C. Jones, Editor, DASA1420, Battelle Memorial Institute
- 35.) "Rapid Annealing of Frequency Change in Crystal Resonators Following Pulsed X-Ray Irradiation"; J.C. King and H.H. Sanders; IEEE Transactions on Nuclear Science, Vol. NS-19, No. 6, (December 1972).
- 36.) "Hardness Assurance in Quartz Crystal Resonators"; T.M. Flanagan, IEEE Transactions on Nuclear Science, Vol. NS-21, No. 6, (December 1974).
- 37.) "Steady-State and Transient Radiation Effects in Precision Quartz Oscillators"; P. Pellegrini, F. Euler, A. Kahan, T.M. Flanagan, and T.F. Wrobel, IEEE Transactions on Nuclear Science, Vol. NS-25, No. 6, (December 1978).
- 38.) "Effects of Pulsed Ionizing Radiation on Some Selected Quartz Oscillator Crystals"; R.A. Poll and S.L. Ridgeway, IEEE Transactions on Nuclear Science, Vol. NS-13, No. 6, (December 1966)
- 39.) "Radiation Effects in Swept Synthetic Quartz"; T.M. Flanagan and T.F. Wrobel, IEEE Transactions on Nuclear Science, Vol. NS-16, No. 6, (December 1969).
- 40.) "Quartz Crystal Radiation Effects"; B.R. Capone, A. Kahan, R.N. Brown and J.R. Buckmelter, IEEE Transactions on Nuclear Science, Vol. NS-17, No. 6, (December 1970).



41.) "Transient Change in Q and Frequency of AT-Cut Quartz Resonators Following Exposure to Pulse X-Rays"; J.C. King and H.H. Sanders, IEEE Transactions on Nuclear Science, Vol. NS-20, No. 6, (December 1973).

42.) "Radiation Effects in Synthetic Quartz: The Role of Electrodiffusion and Radiation-Induced Mobility of Interstitial Ions"; L.E. Malin Martin, M. Markes, J.J. Martin, S.P. Doherty, N. Koumvalalis, W.A. Sibley, A.F. Armington, and R.N. Brown, IEEE Transactions on Nuclear Science, Vol. NS-20, No. 6, (December 1973).

43.) "The Aluminum Centers in  $\alpha$ -Quartz"; John A. Weil; Proceedings of the 25th Symposium in Frequency Control, 1971.

44.) "Rapid Annealing of Frequency Change in High Frequency Crystal Resonators Following Pulsed X-Irradiation at Room Temperature," J. King and H. H. Sanders, 27th Annual Symposium on Frequency Control, (1973)

45.) "Permanent Radiation Effects in Swept and Unswept Optical Grade Synthetic Quartz AT-Resonators"; E.P. EerNisse, IEEE Transactions on Nuclear Science, Vol. NS-18, No. 2, (1971).

46.) "Radiation Effects in Quartz Crystals Part 1.- [ Phenomenological Summary]"; T.M. Flanagan and R.A. Poll; Topical Report, DASA01-71-C-0092, DNA3518T-1; (December, 1974)

47.) "Steady State Radiation Effects in Precision Quartz Resonators," F. Euler, P. Ligor, A. Kahan, P. Pellegrini, T. M. Flanagan, and T. F. Wrobel, 32nd Annual Symposium on Frequency Control, (1978)

48.) "Radiation Induced Frequency and Resistance Changes in Electrolyzed High Purity Quartz Resonators," T. J. Young, D. R. Kochler, and R. A. Adams, 32nd Annual Symposium on Frequency Control, (1978)

49.) "Radiation-Stable Quartz Oscillators"; T.M. Flanagan and T.F. Wrobel; Final Report on Contract DASA01-71-C-0151, DNA2960F, (November, 1973)

50.) "The Kinetics of Atom Diffusing in One Dimension: Hydrogen in Quartz"; A. Sosin; Proceedings of the 27th Annual Frequency Control Symposium, (June, 1973)

51.) "Transient X-Ray Induced Conductivity in Single Crystal Quartz"; R.C. Hughes; Proceedings of the 27th Annual Frequency Control Symposium, (June, 1973)

52.) "Effects of  $^{60}\text{Co}$  Gamma Ray Irradiation on the Optical Properties of Natural and Synthetic Quartz from 85° to 300°K"; P.L. Mattern, K. Lenzenweiler, and P.W. Levy; Proceedings of the 27th Annual Frequency Control Symposium, (June, 1973)



53.) "Electronic Spin Resonance of Irradiated Quartz: Atoms of Hydrogen"; R.A. Weeks and M. Abraham; Journal of Chemical Physics, Vol. 42, (1965).

54.) "The Aluminum Centers in  $\alpha$ -Quartz"; J.A. Weil; Radiation Effects, Vol. 26, (1975).

55.) R. Schnadt and J. Schneider: Phys. Kondens. Materie, 11, 19, (1970).

56.) Electron Spin Resonance: Elementary Theory and Practical Applications; J.E. Wertz and J.R. Bolton; McGraw-Hill Inc., (1972).

57.) W.A. Sibley, J.J. Martin, M.C. Wintersgill, and C.C. Brown; Journal of Applied Physics, Vol. 50, (1979).

58.) "Effects of Reactor Irradiation on Thicknesses of Thin Crystal Quartz"; J.C. King and D. Fraser; Proceedings of the 16th Annual Frequency and Control Symposium, (1962).

59.) "Radiation-Stable Quartz Oscillators"; T.M. Flanagan and T.F. Wrobel; Final Report, DASA01-71-C-0151, DNA 2960F, (November, 1972).

60.) Electronic Circuits; E.J. Angelo Jr.; McGraw-Hill Inc., (1964).

61.) Electrons and Holes in Semiconductors; W. Shockley; D. Van Nostrand Co. Inc., (1950).

62.) Electronic Devices and Circuits; J. Millman and C.C. Halkins; McGraw-Hill Inc., (1967).

63.) Physical Models for Semiconductor Devices; J.E. Carroll; Crane, Russak, and Company, Inc., (1974).

64.) "Radiation Effects on Semiconductor Devices, Summary of Data"; E. Sibley, C. Wenger, and W.S. King; HDL-DS-77-1, Harry Diamond Laboratories, Adelphi, Md. 20783, (May, 1977). This is a data survey. Raw data, histograms, current inventory, complete survey, and referenced data survey can be obtained by any DOD agency or approved contractor without charge by contacting: Commander, Harry Diamond Laboratories, Attn: DELHQ-N-RS4, H. Eisen, (202) 394-3070, 2800 Powder Mill Road, Adelphi, Md 20783.

65.) "Hardening Options for Neutron Effects"; D.L. Durgin, D.R. Alexander, and R.N. Randall; Final Report, DAAG630-75-C-0052, HDL-CR-75-052-1, (November, 1975).

66.) "A Survey of the Vulnerability of Contemporary Semiconductor Components to Nuclear Radiation"; R.P. Donovan, J.R. Hauser, and M. Simons; AFWL-TR-74-61, (June, 1974).



67.) "Neutron Hardness Assurance Considerations for Temperature Compensated Reference Diodes"; D.G. Millward; IEEE Transactions on Nuclear Science, Vol. NS-25, No. 6, (December, 1978).

68.) "Fast Neutron Bombardment of Germanium and Silicon Esaki Diodes"; J.W. Easley and F.R. Blair; Journal of Applied Physics; Vol. 31, No. 10, (October, 1960)

69.) "Analysis of Steady-State Nuclear Radiation Damage of Tunnel Diodes"; J.E. Conly and C.M. Travis; IEEE Transactions on Nuclear Science, Vol. NS-11, No. 5, (November, 1964)

70.) "Radiation Induced Hump Structure in the I-V Characteristics of Esaki Diodes"; C.B. Pierce, H.H. Sander, and A.D. Kantz; Journal of Applied Physics, Vol. 33, No. 10; (October, 1962).

71.) "Low-bias Non-Esaki Current in Tunneling P-N Junction Diodes with Large Excess Currents"; M.M. Cohen and F.D. Bedard; Communications, p. 904, (1966).

72.) "Handbook of Modeling for Circuit Analysis including Radiation Effects"; D.P. Alexander, R.J. Antinone, P.A. Young, and R. Simon; Final Report; F29601-77-C-0026; AFWL-TR-79-86; (May, 1979)

73.) "The Transient Response of Transistors and Diodes to Ionizing Radiation"; J.L. Wirth and S.C. Rogers; IEEE Transactions on Nuclear Science, Vol. NS-11, (November, 1964)

74.) "Transient Radiation Effects in Silicon Diodes near and in Avalanche Break-down"; W. Sneddon, B. Buchanan, and R. Dolan; IEEE Transactions on Nuclear Science, NS-19; December, 1971.

75.) "Nuclear Damage on Avalanche Transistors and Diodes"; H.T. Gates et.al; AFWL-TR-67-95, Vol II, April 1969.

76.) Motorola Zener Diode Handbook.

77.) "Analysis of the Effects of Nuclear Radiation on Transistors," J. Lofenski, Journal of Applied Physics, 29:35 (1958)

78.) "The Effects of Neutron Irradiation on Germanium and Silicon," G. C. Messenger and J. Spratt, Proceedings of the IRE, (June 1958)

79.) "On the Variation of Junction-Transistor Current Amplification Factor with Emitter Current"; W.M. Wilson; Proceedings of IRE, (June 1954)

80.) "Statistics of the Recombination of Holes and Electrons," W. Shockley and W. Read, Physics Review, Vol. 87, No. 5

81.) Radiation Effects in Semiconductor Devices, F. Larin, John Wiley and Sons, Inc.; 1968.



82.) "Selecting Transistors for Radiation Environments," J. R. Bilinski, *Electronics*, (December 1959)

83.) "Transient-Radiation Effects on Electronics Handbook," R. K. Thatcher, Editor, DASA 1420, Battelle Memorial Institute, Columbus, Ohio, (August 1967)

84.) "Radiation Effects on Electronic Systems," H. L. Olesen, Plenum Press, New York, (1968)

85.) "Hardening Options for Neutron Effects--An Approach for Tactical Systems," D. R. Alexander, D. L. Durgin, R. N. Randall, and J. J. Haibin, IEEE Transactions on Nuclear Science, Vol. NS-23, No. 6, (December, 1976)

86.) Private Communications with P. Trimmer; Harry Diamond Laboratories.

87.) "Nuclear Hardness Assessment of the TSEC/KY-38 Tactical Communication Subsystem"; (U), J.P. Swirczynski and C.T. Self; HDL-TM-80-6, (February, 1980), SECRET

88.) The Structure of Probability Theory with Applications; A.J. Thomasian; McGraw-Hill Book Co.; 1969.

89.) "Comparison of Equations Used to Predict Circuit Probability of Failure from Neutron Damage"; P.A. Trimmer; HDL-R-210-78-1, (June, 1978).

90.) "Prediction Variations of Neutron-Induced Probability of Failure Models"; A. Leach and J.P. Swirczynski; HDL technical report to be published.

91.) "Hardness Assurance Considerations for the Neutron Environment"; G.C. Messenger; IEEE Transactions on Nuclear Science, Vol. NS-22, No. 6, (December 1975)

92.) "Statistical Analysis of the 2N697 Transistor Response to Neutron Irradiation"; C.T. Self; HDL-TM-78-7; (June, 1978).

93.) "Extension of Models for Transistor Failure Probability Due to Neutron Fluence"; J.V. Michalowicz and G.A. Ausman, Jr., IEEE Transactions on Nuclear Science; Vol. NS-24, No. 6, (December 1977).

94.) "Large-Signal Behavior of Junction Transistors"; J.J. Ebers and J.L. Moll; Proceedings of I.R.E., 1761, Dec. 1954.

95.) "Radiation or Reliability: Which Comes First"; G. Schmitz; The Electronic Engineer; April, 1969.

96.) "Development of a Nondestructive Radiation Effects Predictive Technique"; M. Frank and R. J. Sweet; AFWL-TR-67-109; January, 1968.



97.) Handbook for Predicting Semiconductor Device Performance in Neutron Radiation; M. Frank and C.D. Taulbee; AFWL-TR-67-54; April, 1968.

98.) Radiation Effects and System Hardening Short Course Notes: System Hardening Methodology, N.J. Rudie; IEEE 1980 Annual Conference on Nuclear and Space

99.) "Approaches to System Hardening," R. A. Poll, IEEE Transactions on Nuclear Science, Vol. NS-17, No. 6, (December 1970).

100.) "Electronic System Hardening Approaches," R. A. Poll, IEEE Transactions on Nuclear Science, Vol. NS-18, No. 5, (November, 1971).

101.) "Mechanisms of Ionizing Radiation Surface Effects on Transistors," O. L. Nelson and R. J. Sweet, IEEE Transactions on Nuclear Science, Volume NS-13, (December 1966)

102.) "A Model for Radiation Damage in Metal-Oxide-Semiconductor Structures," A. S. Grove and E. H. Snow, Proceedings of IEEE, Volume 54, (June 1966)

103.) "Evaluation of Combined Radiation Effects to Transistors," B. D. Shaffer and R. A. Burghard, IEEE Transactions on Nuclear Science, Volume NS-18, No. 6, (December 1971)

104.) "Radiation Test Program"; W.M. Peffley et al; SAMSO-TR-73-261; August, 1973.

105.) Radiation Effects and System Hardening Short Course: Radiation Effects on Components and Circuit Hardening; A. Johnson; IEEE Transactions on Nuclear and Space Radiation Effects, (July 1980).

106.) "Effects of Shadows on Photocurrent Compensated Integrated Circuits"; R.H. Vandre; IEEE Transactions on Nuclear Science, Vol. NS-20, No. 6, (December, 1973).

107.) "Simplified Techniques for Predicting TREE Response"; E.A. Carr; IEEE Transactions on Nuclear Science, Vol. NS-12, No. 4, (October, 1965).

108.) "Simplified Engineering Techniques for Predicting Diode TREE Response"; J.F. Bell, E.A. Carr, W.V. Handley, and K.R. Walker; AFWL-TR-65-205, (March, 1966).

109.) "Methods for Measuring and Characterizing Transistor and Diode Large Signal Parameters for Use in Automatic Circuit Analysis Programs"; W.H. Sullivan and J.L. Wirth; IEEE Transactions on Nuclear Science, Vol. NS-12, No. 4, (October 1965).

110.) "Technique for Estimating Primary Photocurrents in Silicon Bipolar Transistors"; J.K. Notthoff; IEEE Transactions on Nuclear Science, Vol. NS-16, No. 6, (December, 1969).

111.) "Microcircuit Hardening Study"; D.C. Sowen, K.E. Kells, H.W. Wicklein, and T.L. Hunter; IEEE Transactions on Nuclear Science, Vol. NS-13, No. 6, (December, 1966)

112.) "Analytical Methods and Fundamental Parameters for Predicting Response of Electronic Circuits to Transient Nuclear Radiation, with Application to Hardened Circuit Design"; The Boeing Company; AFWL-TR-65-105, (July, 1965)

113.) "Anomalous Photocurrent Generation in Transistor Structures"; D.H. Habing and J.L. Wirth; IEEE Transactions on Nuclear Science, Vol. NS-13, No. 6, (December, 1966).

114.) "Anomalous Behavior of Primary Photocurrents"; C. Rosenberg and R.S. Caldwell; Presented at the 1965 Radiation Effects Conference, University of Michigan, (July, 1965).

115.) "Pulse Power Failure Modes in Semiconductors"; D.M. Tasca; IEEE Transactions on Nuclear Science; NS-17, Dec. 1970.

116.) "Second Breakdown- A Comprehensive Review", H.A. Schafft; Proceedings of IEEE, Vol. 55, No. 8, August 1967.

117.) "The Response of Bipolar Transistors to Combined EMP and Ionization Environments", D.H. Habing; IEEE Transactions on Nuclear Science; NS-17, Dec. 1970.

118.) "Determination of Threshold Failure Levels of Semiconductor Diodes and Transistors Due to Pulse Voltages"; D.C. Wunsch and R.R. Bell; IEEE Transactions on Nuclear Science, Vol. NS-15, No. 6, (December, 1968).

119.) "Semiconductor Device Degradation by High Amplitude Current Pulses", W.D. Brown, IEEE Transactions on Nuclear Science, NS-19, Dec. 1972

120.) "A New High Current Mode of Transistor Operation", C.G. Thornton and C.O. Simmons; IRE Transactions on Electronic Devices, ED-5,6-10, January, 1958.

121.) EMP Radiation and Protective Techniques; L.W. Ricketts, J.E. Bridges, and J. Miletta, John Wiley and Sons; 1976.

122.) "Radiation-Induced Integrated Circuit Latchup", J.F. Leavy and R.A. Poll; IEEE Transactions on Nuclear Science; NS-15, Dec. 1969.

123.) "Non-Destructive Screening for Thermal Second Breakdown", C. Tasca, J. Peden, and J. Miletta, IEEE Transactions on Nuclear Science; NS-19, No. 6, Dec. 1972.

124.) "Second Breakdown in Transistors"; H.A. Schafft and J.C. French; IRE Transactions on Electronic Devices; 129-136.



125.) "Radiation-Induced Second Breakdown in Transistors"; E.A. Carr and D. Binder; IEEE Transactions on Nuclear Science, NS-15, Dec. 1969.

126.) "Transient Radiation Effects in Transistors"; E.A. Carr; IEEE Transactions on Nuclear Science; Vol. NS-12, No. 5, (November, 1964).

127.) "Charge Control Equivalent Circuit for Predicting Transient Radiation Effects in Transistors"; C. Rosenberg, D.S. Gage, R.S. Caldwell, and G.H. Hanson; IEEE Transactions on Nuclear Science, Vol. NS-10, No. 5, (November, 1963)

128.) "Generalized Model Analysis of Ionizing Radiation Effects in Semiconductor Devices"; J.P. Raymond and J.P. Willis; IEEE Transactions on Nuclear Science, Vol. NS-12, No. 5, (October, 1965).

129.) Private Communications with J.J. Halpin and H. Eisen of Harry Diamond Laboratories

130.) Radiation Effects and System Hardening Short Course Notes; System Effects and System Validation; J.J. Halpin; IEEE 1980 Annual Conference on Nuclear and Space Radiation Effects, (July, 1980).

131.) "Nuclear Hardness Guidelines for Systems with Moderate Requirements"; AFWL-TR-76-147, (September, 1976).

132.) "Nuclear Weapon Effects on Army Tactical Systems", Volume I, Overview; J.J. Halpin, J.P. Swirczynski, G. Teele, E. Quigley, and M. Campi; HDL-TR-1882-I, (April, 1979)

133.) "Nuclear Weapon Effects on Army Tactical Systems", Volume II, Management; J.J. Halpin and J.P. Swirczynski; HDL-TR-1882-II, (May, 1979)

134.) Microelectronics; Jacob Millman; McGraw-Hill Book Co., 1979.

135.) Digital Integrated Electronics; H. Taub and D. Schilling; McGraw-Hill Book Co., 1977.

136.) "State-of-the-Art Review, Hardness of MOS and Bipolar Technologies"; David M. Long; IEEE Transactions on Nuclear Science, Vol. NS-27, No. 6, (December 1980).

137.) "Radiation Response Study of New Radiation-Hardened Low Power, TTL Series"; R.J. Olson, D.R. Alexander, and R.J. Antinone; IEEE Transactions on Nuclear Science, Vol. NS-18, No. 6, (December, 1971).

138.) "CRIC, Nuclear Radiation Effects on Large Scale Integrated Circuits"; R. Polimadei, H. Eisen, and K. Pinero; HDL-DS-80-1, (July, 1980)

139.) "MSI/LSI Radiation Response, Characterization, and Testing"; Jim Raymond; IEEE Transactions on Nuclear Science, Vol. NS-21, No. 6, (December, 1974).

140.) "Development of a Hard Microcontroller"; P.R. Measel, L.L. Sivo, W.E. Quilitz, and T.K. Davidson; IEEE Transactions on Nuclear Science, Vol. NS-23, No. 6, (December, 1976).



141.) "Radiation-Induced Integrated Circuit Latchup"; J.F. Leavy and R.L. Poll; IEEE Transactions on Nuclear Science, Vol. NS-15, No. 6, (December, 1969).

142.) "High Temperature Schottky Latchup"; M.S. Cooper, G.C. Messenger, and J.P. Retzler; IEEE Transactions on Nuclear Science, Vol. NS-25, No. 6, (December, 1978).

143.) Private Communications with Charles Hill; Science Applications; Huntsville, Alabama.

144.) "A Survey of Radiation-Hardened Microelectronic Memory Technology"; Patrick Vail; IEEE Transactions on Nuclear Science, Vol. NS-25, No. 6, (December, 1978).

145.) "Upset Testing of LSI Devices"; L.L. Sivo, J.L. Andrews, and H.W. Mathers; IEEE Transactions on Nuclear Science, Vol. NS-26, No. 6, (December, 1979).

146.) "What Happens to Semiconductors in a Nuclear Environment?"; David K. Myers; Electronics, March 16, 1978.

147.) "Radiation Response of Several Memory Device Types"; P.R. Measel, R.B. Gregor, and K.L. Wahlin; IEEE Annual Conference on Nuclear and Space Radiation Effects, (July, 1980).

148.) "Transient Response of GaAs IC's to Ionizing Radiation"; R. Zuleeg and J.K. Notthoff; IEE Annual Conference on Nuclear and Space Radiation Effects, (July, 1979).

149.) "VLSI Advances Rad-Hard Technology"; Electronic Warfare/Defense Electronics, (September, 1978).

150.) "A Proposed High-Frequency Negative Resistance Diode"; W.T. Read, Jr.; Bell System Technical Journal; 37, (March, 1958).

151.) "Generalized Small-Signal Analysis of Avalanche Transit-Time Diodes"; B. Hoefflinger; IEEE Transactions on Electron Devices, Vol. ED-14, No. 9, (September 1967).

152.) "High Frequency Oscillations of  $p^{++}$ - $n^+$ - $n$ - $n^{++}$  Avalanche Diodes below the Transit-Time Cutoff"; B. Hoefflinger; IEEE Transactions on Electron Devices, Vol. ED-13, No. 1, (January, 1966).

153.) Semiconductors for Engineers; D.F. Dunster; Business Books Limited, 1969

154.) "Avalanche Breakdown in Silicon"; K.G. McKay; Physics Review, Vol. 94, 877, (May, 1954).



- 155.) "Small-Signal Impedance of Avalanche Junctions with Unequal Electron and Hole Ionization Rates and Drift Velocities"; S.T. Fisher; IEEE Transactions on Electron Devices, Vol. ED-14, No. 6, (June, 1967).
- 156.) "Ionizing Radiation Effects in Microwave Cavities"; R.J. Chaffin; IEEE Transactions on Nuclear Science, Vol. NS-18, No. 6, (December, 1971).
- 157.) "Microwave Diagnosis of a Plasma Generated in a Reactor and its Use as a Reactor Power Monitor"; M. Voth and E. Kenny; Nuclear Instruments and Methods, Vol. 63, (1968).
- 158.) "Microwave Investigation of Plasmas Produced in a Reactor"; A. Bhattacharya et al; Journal of Applied Physics, Vol. 38, (1967).
- 159.) "In-Core Thermal Neutron Sensors"; D. Brown, T. Billeter, and W. Spear; IEEE Transactions on Nuclear Science, Vol. NS-17, No. 1, (February, 1971).
- 160.) "Transient Ionizing Radiation Effects on IMPATT Diode Oscillators"; J.M. Borrego, R.J. Gutmann, P.E. Cottrell, and S.K. Ghandi; IEEE Transactions on Nuclear Science, Vol. NS-19, No. 6, (December, 1972).
- 161.) "Radiation Effects on Silicon Avalanche (IMPATT) Diodes"; D.K. Wilson, H.S. Lee, and H. Noffke; IEEE Transactions on Nuclear Science, Vol. NS-15, No. 6, (December, 1968).
- 162.) "The Effect of Neutron Radiation on an IMPATT diode"; R.J. Chaffin; IEEE Transactions on Microwave Theory and Technique, Vol. MTT-17, No. 2, (February, 1969).
- 163.) "Carrier Trapping and Recombination in Avalanche Diodes"; E.P. Eernisse and R.J. Chaffin; IEEE Transactions on Electron Devices, Vol. ED-17, No. 7, (July, 1970).
- 164.) "Saturation Current and Large Signal Operation of a Read Diode"; T. Misawa; Solid State Electronics, Vol. 13, (1970).
- 165.) "IMPATT Oscillators with Enhanced Leakage Current"; P.E. Cottrell, J.M. Borrego, and R.J. Gutmann; Solid State Electronics, Vol. 18, (1975).
- 166.) "Electron Beam Control of IMPATT Diodes"; A.C. Sanderson and A.G. Jordan; Solid State Electronics, Vol. 15, (1972).
- 167.) "A Radiation Pulse Interrupts IMPATT Diode Oscillation"; W.A. Anderson; Proceedings of the IEEE, Vol. 57, (May, 1969).



168.) "The Performance of IMPATT Diodes Under the Influence of Gamma Radiation"; W.A. Anderson; Proceedings of the IEEE, Vol. 57, (May, 1969).

169.) "The Performance of IMPATT Diodes Under the Influence of High-Intensity Gamma and Neutron Radiation"; W.A. Anderson; Proceedings of the IEEE, Vol. 57, (August, 1969).

170.) "Transient and Permanent Radiation Effects in Gunn and IMPATT Oscillators"; R.J. Chaffin; Sandia Report SC-RR-710378, (June, 1971).

171.) "Transient Radiation Effects in GaAs IMPATT Diodes"; P.T. Greiling and J. Clark; Proceedings of the IEEE, Vol. 60, (June, 1972).

172.) "Aftereffects in IMPATT Oscillators with Transient Ionizing Radiation"; J.M. Borrego, R.J. Gutmann, P.E. Cottrell, and S.K. Ghandi; Proceedings of the IEEE, Vol. 61, (May, 1973).

173.) "The Performance of Injection Locked IMPATT Oscillators Under Transient Ionizing Radiation"; R.J. Gutmann, J.M. Borrego, P.E. Cottrell, and S.K. Ghandi; IEEE Transactions on Nuclear Science, Vol. NS-20, No. 6, (December, 1973).

174.) "Evaluation of Aftereffects in IMPATT Oscillators with Transient Ionizing Radiation"; R.J. Gutmann and J.M. Borrego; IEEE Transactions on Nuclear Science, Vol. NS-23, No. 6, (December, 1976).

175.) "The Elimination of Tuning-Induced Burnout and Bias Circuit Oscillations in IMPATT Oscillators"; C.A. Brackett; Bell System Technical Journal, Vol. 52, (1973).

176.) "Design of Neutron Radiation Tolerant High Efficiency Microwave Avalanche Diode Sources (TRAPATT Oscillators)"; E.P. EerNisse and R.J. Chaffin; IEEE Transactions on Nuclear Science, Vol. NS-17, No. 6, (December, 1970).

177.) "The Effect of Neutron Irradiation on the TRAPATT Diode"; R.J. Chaffin, E.P. EerNisse, and J.A. Hood; Proceedings of the IEEE, Vol. 57, (November, 1969).

178.) "Temperature Coefficients of Avalanche  $p^{+}nn^{+}$  Junctions with Carrier Trapping"; E.P. EerNisse; Applied Physics Letters, Vol. 16, (June 15, 1970).

179.) "A Theory for the High-Efficiency Mode of Oscillation in Avalanche Diodes"; A.S. Clorfeine, R.J. Ikola, and L.S. Napoli; RCA Review, Vol. 30, (September, 1969).

180.) "Device Physics of TRAPATT Oscillators"; B.C. DeLoach, Jr. and D.L. Scharfetter; IEEE Transactions on Electron Devices, Vol. ED-17, (1970).



181.) "Operation of TRAPATT Oscillators under Transient Ionizing Radiation Conditions"; J.M. Borrego, R.J. Gutmann, H.J. Geipel, and S.K. Ghandi; IEEE Transactions on Nuclear Science, Vol. NS-20, NO. 6, (December, 1973).

182.) "Circuits for High-Efficiency Avalanche-Diode Oscillators"; W.J. Evans; IEEE Transactions on Microwave Theory and Techniques, Vol. MTT-17, (1959).

183.) "A Low-Noise Metal-Semiconductor-Metal (MSM) Microwave Oscillator"; D.J. Coleman and S.M. Sze; Bell System Technical Journal, Vol. 50, (1971).

184.) "Permanent and Transient Radiation Effects in Baritt Microwave Oscillators"; R.J. Chaffin; IEEE Transactions on Nuclear Science, Vol. NS-19, No. 6, (December, 1972).

185.) "Transit-Time Oscillations in BARITT Diodes"; D. Coleman, Jr.; Journal of Applied Physics, Vol. 20, (April, 1972).

186.) "Small-Signal Negative Conductance in BARITT Diodes"; E. EerNisse; Applied Physics Letters, Vol. 43, (April, 1972).

187.) Physics of Semiconductors; S.M. Sze; Wiley-Interscience, (1969).

188.) Microwave Semiconductor Devices: Fundamentals and Radiation Effects; R.J. Chaffin; John Wiley and Sons, (1973).

189.) "Transient Ionizing Radiation Effects on Baritt Diode Oscillators"; J.M. Borrego, R.J. Gutmann, and J. Narain; IEEE Transactions on Nuclear Science, Vol. NS-22, No. 6, (December, 1975).

190.) "Small-Signal Noise Behavior of Companion P<sup>+</sup>NP<sup>+</sup> and P<sup>+</sup>NvP<sup>+</sup> Punch-Through Microwave Devices"; G. Bjorkman and C.P. Snapp; Electronic Letters, Vol. 11, (1975).

191.) "The Effect of Chrome Thickness on the Barrier Height of Chrome-Gold Silicon Schottky Diodes"; J. Narain, J.M. Borrego, and R.J. Gutmann; Electronic Letters, Vol. 11, (1975).

192.) "Microwave Oscillations of Current in III-V Semiconductors"; J.B. Gunn; Solid-State Communications, Vol. 1, (September, 1963).

193.) Gunn-effect Electronics; B.G. Bosch and R.W.H. Engelmann; John Wiley and Sons, (1975).

194.) "Instabilities of Current in III-V Semiconductors"; J.B. Gunn; IBM Journal of Research and Development, Vol. 8, (1964).



195.) "The Possibility of Negative Resistance Effects in Semiconductors"; B.K. Ridley and T.B. Watkins; Proceedings of the Physical Society of London, Vol. 78, (1961).

196.) "Transferred Electron Amplifiers and Oscillators"; C. Hilsom; Proceedings of the Institute of Radio Engineers, Vol. 50, (1962).

197.) The Gunn Effect; G.S. Hobson; Clarendon Press, (1974).

198.) The Gunn-Hilsom Effect; M.P. Shaw, H.L. Grubin, and P.R. Solomon; Academic Press, (1979).

199.) "Measurement of the Velocity-Field Characteristic of Gallium Arsenide"; J.G. Ruch and G.S. Kino; Applied Physics Letters, Vol. 9, (1966).

200.) "Calculation of the Velocity-Field Characteristic for Gallium Arsenide"; P.N. Butcher and W. Fawcett; Physics Letters, Vol. 21, (1966).

201.) "The Low Temperature Velocity-Field Characteristic of n-Type GaAs"; G.A. Acket, H.T. Lam, and W. Heinle; Japanese Journal of Applied Physics, Vol. 7, (1968).

202.) "Indirect Electron Drift Velocity versus Electric Field Measurement in GaAs"; E.M. Bastida, G. Fabri, V. Svelto, and F. Vaghi; Applied Physics Letters, Vol. 18, (1971).

203.) "Monte Carlo Determination of Electron Transport Properties in Gallium Arsenide"; W. Fawcett, A.D. Boardman, and S. Swain; Journal of Physics and Chemistry of Solids, Vol. 31, (1970).

204.) "Displaced Maxwellian Calculation of Transport in n-Type GaAs"; W. Heinle; Physics Review, Vol. 178, (1969).

205.) "Cyclotron Resonance and Hall Experiments with High-Purity Epitaxial GaAs"; Q.H.F. Vrehen; Journal of Physics and Chemistry of Solids, Vol. 29, (1968).

206.) "Interband Magneto-Optical Absorption in Gallium Arsenide"; J.M. Chamberlain and R.A. Stradling; Solid-State Communications, Vol. 7, (1969).

207.) "Electrical Properties of the  $\text{GaAs}_{1-x}$  Minima at Low Electric Fields From High-Pressure Experiment"; G.D. Pitt and J. Lees; Physics Review, Vol. B2, (1970)

208.) "The  $\text{X}_{1C}$  Conduction Band Minimum in High-Purity Epitaxial n-Type GaAs"; G.D. Pitt and J. Lees; Solid-State Communications, Vol. 8, (1970).

209.) Transferred Electron Devices; P.J. Bulman, G.S. Hobson, and B.C. Taylor; Academic Press, (1972).

210.) "On the Form and Stability of Electric-Field Profiles Within a Negative Differential Mobility Semiconductor"; H.L. Grubin, M.P. Shaw, and P.R. Solomon, IEEE Transactions on Electron Devices, Vol. ED-20, (1973).

211.) "Some Properties of Gunn-Effect Oscillations in a Biconical Cavity"; G.S. Hobson, IEEE Transactions on Electron Devices, Vol. ED-14, (1967).

212.) "Extension of the Gunn-Effect Theory Given by Robson and Mahrous"; F.L. Warner, Electronics Letters, Vol. 2, (1966).

213.) "Oscillations Covering 4 Gc/s to 31 Gc/s from a Single Gunn Diode"; Electronics Letters, Vol. 2, (1966).

214.) "A New Mode of Operation for Bulk Negative Resistance Oscillators"; J.A. Copeland, Proceedings of IEE, Vol. 54, (1966).

215.) "LSA Oscillator Diode Theory"; J.A. Copeland, Journal of Applied Physics, Vol. 38, (1967).

216.) "Theory of the Gunn Effect"; H. Droemer, Proceedings of IEE, Vol. 52, (1964).

217.) "Mechanism of the Gunn Effect from a Pressure Experiment"; A.R. Hutson, A. Jayaraman, A.G. Chynoweth, A.S. Coriell, and W.L. Feldman, Physics Review Letters, Vol. 14, (1965).

218.) "Microwave Oscillations in  $\text{Ga}(\text{As}_x\text{P}_{1-x})$  Alloys"; J.W. Allen, M. Shyam, Y.S. Chen, and G.L. Pearson; Applied Physics Letters, Vol. 7, (1965).

219.) "Transferred Electron Devices;" B.E. Berson, European Microwave Conference, Stockholm, (1971).

220.) "Neutron Displacement Effects in Epitaxial Gunn Diodes;" N. Berg and H. Dropkin, IEE Transactions on Nuclear Science, Vol NS-18, (December 1971).

221.) "Radiation Damage in GaAs Gunn Diodes;" G.H. Marcus and H.P. Bruemmer, IEEE Transactions on Nuclear Science, Vol NS-17, (December 1970).

222.) "Predicted Effects of Neutron Irradiation GaAs Junction Field Effect Transistors," J.L. McNichols and W.S. Ginell; IEEE Transactions on Nuclear Science, Vol NS-17, (April 1970).

223.) "Radiation-Produced Energy Levels in Compound Semiconductors;" L.W. Aukerman, Journal of Applied Physics, Vol 30, (1959).

224.) "Transport Properties in Silicon and Gallium Arsenide, "R.K. Willardson, Journal of Applied Physics, Vol 30, (1959).

225.) International Conference on Semiconductor Physics, 1950; L.W. Aukerman, Academic Press, Inc.



226.) "Comparing Radiation Effects in Gunn and Impatt Diodes"; W.A. Anderson, IEEE Transactions of Nuclear Science, Vol. NS-18, (August, 1971).

227.) "Neutron Damage in Gunn Effect Devices"; H.P. Bruemer, Technical Report No. ECOM-3238, Electronic Components Laboratory, U.S. Army Electronics Command, Fort Monmouth, N.J., (1970).

228.) Vol. II, Air Force Weapons Laboratory Report, AFWL TR-68-31; R.H. Schnurr and H.D. Southward, (August, 1968).

229.) "Radiation Effects in GaAs"; L.W. Aukerman, P.W. Davis, R.D. Graft, and T.S. Shilliday, Journal of Applied Physics, Vol. 34, (1963).

230.) "Theoretical Study of a Gunn Diode in a Resonant Circuit;" J.A. Copeland, IEEE Transactions on Electron Devices, Vol ED-14, No. 1, (September 1967).

231.) "Characterization of Bulk Negative - Resistance Diode Behavior;" J.A. Copeland, IEEE Transactions on Electron Devices, Vol. ED-14, No. 9, (September 1967).

232.) "High-Efficiency Operation of a Gunn Oscillator in the Domain Mode;" G.S. Kino and I. Kuru, IEEE Transactions on Electron Devices, Vol ED-16, (1969).

233.) "Effects of Gamma Radiation on Gunn Diodes;" G.E. Brehm and G.L. Pearson, IEEE Transactions on Electron Devices, Vol ED-17, (1970).

234.) "Radiation Effects Upon Gallium Arsenide Devices;" R.H. Schnurr and H.D. Southward, IEEE Transactions on Nuclear Science, Vol. NS-15, No. 6, (December 1968).

235.) "Non-Linear Theory of Electrical Domains in the Presence of Trapping"; B.K. Ridley and P.H. Wisbey, British Journal of Applied Physics, Vol. 18, (1967)

236.) "The Effects of Ionizing Radiation on Gunn Diode Oscillators;" N. Berg and H. Dropkin, IEEE Transactions on Nuclear Science, Vol NS-18, No. 6, (December 1971).

237.) "Temperature Dependence of the Transport Properties of Gallium Arsenide Determined by a Monte Carlo Method;" J.G. Ruch and W. Fawcett, Journal of Applied Physics, Vol 41, (1970).

238.) "Effect of Ionizing Radiation on Gunn Diode Amplifiers;" H. Dropkin and N. Berg, IEEE Transactions on Nuclear Science, Vol NS-19, No. 6, (December 1972).

239.) "The Performance of IMPATT Diodes Under the Influence of High-Intensity Gamma and Neutron Radiation"; W. Anderson, Proceedings of IEEE, Vol. 57, (1969).

240.) "Permanent Neutron Damage in PIN Microwave Diode Switches"; R.J. Chaffin, IEEE Transactions on Nuclear Science, Vol. NS-18, No. 6, (December, 1971).



241.) "Minority Carrier Recombination in Neutron Irradiated Silicon;" B.L. Gregory, IEEE Transactions on Nuclear Science, Vol NS-16, No. 6, (December 1969).

242.) "Neutron Damage in PIN Diode Phase Shifters for Radar Arrays;" G.J. Brucker, A. Rosen, and A. Schwarzmann, IEEE Transactions on Nuclear Science, Vol NS-25, No. 6, (December 1978).

243.) "High-Power Low-Loss PIN Diodes for Phased-Array Radar;" A. Poser, R.U. Martinelli, A. Schwarzmann, G.J. Brucker, and G.A. Swartz, RCA Review, Vol 40, No. 1, (March 1979).

244.) "Analysis of the Effect of Fast Neutron Bombardment on the Current Voltage Characteristic of a Conductivity Modulated PIN Diode;" J. Swartz, and M. Thurston, Journal of Applied Physics, Vol 37, (1966).

245.) "On the Theory of Ferromagnetic Resonance;" D. Polder, Philosophical Magazine, Vol 40, (January 1949).

246.) Introduction to Solid State Physics; C. Kittel, John Wiley and Sons, Inc., Second Edition (1961), 4th Edition (1971).

247.) "Microwave Ferrite Materials and Devices;" R.F. Sochoo, IEEE Transactions on Magnetics, Vol MAG-4, No. 2, (June 1968).

248.) "Effects of Charged Particles and Neutrons on Magnetic Materials;" D.I. Gordon and R.S. Sery, IEEE Transactions on Communications and Electronics, Vol CE-83, (July 1964).

249.) "The Effects of Radiation on Ferrities;" S.I. Taimuty and J.S. Mills, IEEE Transactions on Communications and Electronics, Vol CE-82, (May 1963).

250.) "Radiation Effects in Magnetic Materials;" D.I. Gordon, R.S. Sery, and R.E. Fischell, Nucleonics, Vol 16, No. 6, (June 1958).

251.) "Temperature and Stress Sensitivities of Microwave Ferrites;" G.F. Dionni, IEEE Transactions on Magnetics, Vol-MAG-8, (September 1972).

252.) "Neutron Radiation Effects in Gold and Aluminum GaAs Schottky Diodes;" J.M. Borrego, R.J. Gutmann, G. Ashok, IEEE Transactions on Nuclear Science, Vol NS-23, No. 6 (December 1976).

253.) "Radiation Effects in GaAs MESFETs;" J.M. Borrego, R.J. Gutmann, S.B. Maghe, and M.J. Chudzicki, IEEE Transactions on Nuclear Science, Vol. NS-24, No. 6, (December 1978).

254.) Private communications with E. Boesch, Harry Diamond Laboratories.

255.) "GaAs - The Device Technology of Next Generation Electronics Systems;" A. Firstenberg, R.C. Eden, S.I. Lang, F.S. Lee, and B.M. Welch, Digest of Papers, 1980 Government Microcircuit Applications Conference (GOMAC).



256.) "Gigabit Electronics - A Review;" B.G. Bosch, Proceedings of IEEE, Vol 67, No. 3, (March 1979).

257.) "Compound Semiconductor;" N. Holonyak, Jr., G.E. Stillman, and C.M. Wolfe, Journal of Electrochemical Society, Vol 125, No. 12, (December 1978).

258.) "Radiation Effects in Enhancement Mode GaAs Junction Field Effect Transistors;" R. Zuleeg, J.K. Notthoff, and K. Lehovec, IEEE Transactions on Nuclear Science, Vol NS-24, No. 6, (December 1977).

259.) "Neutron Degradation of Ion-Implanted and Uniformly Doped Enhancement Mode GaAs JFET's;" R. Zuleeg and K. Lehovec, IEEE Transactions on Nuclear Science, Vol NS-25, No. 6 (December 1978).

260.) "Long-Term Radiation Transients in GaAs FETs;" M. Simons and E.E. King, IEEE Transaction of Nuclear Science, Vol NS-26, No. 6, (December 1979).

261). "Photocapacitance of Deep Levels in GaAs: Cr and GaAs: O;" P.K. Vasudev, and R.H. Bubi, Solid State Electronics, Vol 21, (1978).

262.) "Analysis of Transient Capacitance Experiments for Au-GaAs Schottky Barrier Diodes in the Presence of Deep Impurities and the Interfacial Layer;" C.I. Huang and SS Li, Solid State Electronics, Vol 16 (1973).

263.) "Electron Traps in Bulk and Epitaxial GaAs Crystals;" G.M. Martin, A. Mitonneau, and A. Mircea, Electronics Letters, Vol 13, No. 7, (March 1977).

264.) "Response of Integrated Circuits to a Simulated IEMP Environment"; William L. Vault; HDL-TR-1649, (October, 1973).

265.) "I-V Characteristics of Enhancement Mode GaAs JFET's"; K. Lehovec and R. Zuleeg; Institute of Physics Conference Ser. 33a, (1977).

266.) "Transient Response of Epitaxial GaAs JFET Structures to Ionizing Radiation"; W.S. Ginell, R. Zuleeg, J.L. McNichols, J.K. Notthoff, and K. Lehovec; IEEE Transactions on Nuclear Science, Vol. NS-20, (1973).

267.) "GaAs Integrated Circuits: MSI Status and VLSI Prospects"; R.C. Eden; IEDM Technical Digest, (1978).



## Appendix A: Recommendations and Design Guidelines

A variety of recommendations and design guidelines have been presented in this volume. It was felt that it would be useful to restate these in an outline form according to the section in which they appear. No attempt has been made to rank order these guidelines but rather list these as they appeared in this volume. Where necessary a brief introduction has been included. In addition, mention has been made of those guidelines which require obvious trade-offs.

### A.1 Materials

It was not possible to cover all types and applications of materials that could occur in a radar system. Instead, materials were divided, as in Volume II, into classes according to their application or use in the system. The division that seemed to be most appropriate was: (1) insulators, (2) adhesives, (3) seals, (4) laminates, and (5) encapsulants.

The recommendations in this section involve the use or avoidance of specific types of materials. As such, the three-level classification scheme of organic materials appropriate for each broad application category that was developed in Volume II was employed. The first level was the preferred class. This is the first choice and consists of the most radiation resistant materials. The second level was the recommended class. This consists of materials that should be used only if all members of the preferred class have been found to be unsuitable for nonradiation considerations. The third and last level was the not recommended class. This is composed of materials that should be avoided if possible. These materials should never be used unless test data on that specific material indicates an acceptable radiation response. The range of damage thresholds for each of these classes has been included as well as the page number of Volume II where these recommendations have been made.

The exception to this is laminates. These materials consist of combinations of fillers and binders and the list that classifies laminates would be extensive. Instead a set of guidelines were formulated and are listed in this appendix.



Two general guidelines exist that apply to all categories of materials. These are:

- Maximize the use of inorganic rather than organic materials.
- Avoid the use of halogenated materials.

The compilation of recommendations and guidelines will now proceed with specifics for each category of materials.

#### A.1.1 Insulators

Insulators are composed of either organic or inorganic materials. The general recommendation of using inorganic materials wherever possible applies here. When this is not possible, the following is a ranking of organic insulators.

Preferred Class:	Polyester with mineral filler (Plaskon Alkyd), preirradiated Kynar, preirradiated polyolefin, glass filled polyester, polyvinyl fluoride (Tedlar)
Recommended Class:	Bakelite, polyethylelen, polyvinyl formal (Formvar) some forms of nylon, polymethyl metharylates, polystyrene no filler
Not Recommended	
Class:	Teflon, polyvinyl chloride, Lucite, polyester with no filler, Kel-F, polystyrene with black pigment (Styron 475), butyl rubber, Neoprene

The damage thresholds are as follows:

Preferred Class: D.T.  $> 10^8$  rad(C)

Recommended Class:  $10^6$  rad(C)  $\leq$  D.T.  $\leq 10^8$  rad(C)

Not Recommended Class: D.T.  $< 10^6$  rad(C)

where D.T. is the damage threshold. This same notation will be used for the rest of the material portion of the appendix. This category of materials is discussed on pages 9 through 16.



### A.1.2 Adhesives

This category consists of organic polymers. The ranking of adhesives is

Preferred Class:	General class of phenolics, epoxy-phenolics, and epoxies excluding those epoxies using dicyandiamide
Recommended Class:	Neoprene <sup>R</sup> -phenolics
Not Recommended Class:	Neoprene <sup>R</sup> -Nylon <sup>R</sup> -phenolics, cellulose adhesives and epoxies using dicyandiamide

The damage thresholds are as follows:

Preferred Class:  $5 \times 10^8 \text{ rad(C)} \leq \text{D.T.} < 10^9 \text{ rad(C)}$

Recommended Class:  $10^7 \text{ rad(C)} \leq \text{D.T.} < 5 \times 10^8 \text{ rad(C)}$

Not Recommended Class:  $10^4 \text{ rad(C)} \leq \text{D.T.} < 10^7 \text{ rad(C)}$

This category of materials is discussed on pages 16 through 22. It should be mentioned that there is very little distinction between the preferred and recommended category in that both will easily survive the threat level environment in any scenario. However, it is good engineering practice to use the most radiation resistant material possible and, thus, it is still advisable to use the preferred class whenever possible.

### A.1.3 Seals

Seals are fabricated from plastics, elastomers, metals or a combination of metals and plastics or elastomers. Metals are invulnerable to radiation. However, their use in seals is limited due to their relatively poor compressibility and elasticity. More seals are made out of elastomers than any other class of material. Elastomers are rubber-like organic polymers and, as such, are affected by radiation. The ranking of elastomers is:



Preferred Class:	Neoprene (chloroprenes), natural rubber containing antirads, and threat sealant.
Recommended Class:	Natural rubber without antirads, silicone, and styrene-butadiene (Buna-S).
Not Recommended Class:	Butyl, fluorosilicone, fluorocarbon (Vitron), butadiene-acrylonitrile (Buna-N), and polysulfide.

The damage thresholds are as follows:

Preferred Class: D.T.  $\geq 10^7$  rad(C)  
 Recommended Class:  $10^7$  rad(C) > D.T.  $\geq 5 \times 10^6$  rad(C)  
 Not Recommended Class: D.T.  $\leq 10^6$  rad(C)

Elastomers suitable for seals are discussed on pages 22 through 24.

The other class of material that finds some application as seals either by themselves or in composite seals with metals is plastics. The ranking of plastics commonly used as seals according to radiation properties is as follows.

Preferred Class:	Kynar and Polyethylene
Recommended Class:	Nylon and Kel-F
Not Recommended Class:	Teflon (TFE and FEP), and polyvinyl chloride

The damage thresholds are as follows:

Preferred Class: D.T.  $\geq 10^7$  rad(C)  
 Recommended Class:  $10^7$  rad(C) > D.T.  $\geq 10^6$  rad(C)  
 Not Recommended Class:  $10^6$  rad(C) > D.T.

The preferred and recommended classes for both elastomers and plastics suitable for seals should survive the threat while the not recommended class should be avoided. Plastics are discussed on page 25.



#### A.1.4 Laminates

As mentioned previously a ranking of all the common laminates was not feasible since there are simply too many. Instead the following guidelines have been formulated.

##### For fillers

- Use inorganics
- If organics must be used, then choose synthetic materials.
- Avoid the use of cellulose materials.

##### For binders

- Avoid halogenated polymers
- Be guided by the recommended list for insulators

##### For laminated printed circuit boards

- Use a coating of either polyester or a silicone varnish

In any case, laminates in general should be able to withstand threat levels of the environment. The exception to this is copperclad Teflon glass laminate which has a damage threshold of approximately  $10^4$  rad(C). Laminates are discussed on pages 25 through 32.

#### A.1.5 Encapsulants

The last application of materials that was considered in the study was encapsulants. For this application, the mechanical properties are more important than the electrical properties. The ranking of encapsulants based on their radiation tolerance is as follows:

Preferred material: Polyurethane (Eccofoam FP and Hitco R), polystyrene, phenolic, epoxy (Epocast H2E-011, H2E-012, H2E-037; Scotchcast No. 3)

Recommended Material: Epoxy (insulating lacquer 1162; Epocast 202/9615, 202/9647, 202-11/9615A)

Not Recommended Material: Polysulfide (3C-737, Class A; 3C-747T, Class B); silicon rubber (Q-9-0031-1/2, Q-9-3C03-1/2, Q-9-005-1/2, RTV-503, PR-1930-1/2, PR-1920-1/2, PR-1910-1/2); silicon rubber primer (General Electric Co. SS-4C04; Products Research Co. 1902)



Encapsulants are discussed on pages 32 through 41.

There was one area that was discussed associated with propellants for the interceptor that deserves mention. An important ingredient in many propellants is the fuel binder which is typically an elastomer or a plastic. Radiation could lead to evolution of gas and loss of strength in the binder which can have serious consequences on the performance of the interceptor.

This finishes the listing of the recommendations and guidelines on materials. It must be mentioned that these listings on materials as well as the guidelines and recommendations for the other components discussed in this appendix should not be considered with the same degree of inflexibility as a specification but rather as simply guidelines and indicators of potential problem areas. Specific examples within a class may have radiation properties exceeding those which have been and will be listed.

## A.2 Nonsemiconductor Components

The components that were covered consisted of three classes: resistors, capacitors, and quartz crystal oscillators. These components are usually ignored in vulnerability assessments. However, at high exposure levels these components exhibit some susceptibility to radiation.

### A.2.1 Resistors and Capacitors

The neutron damage thresholds of some common types of resistors are given by the following:

Resistor Type	Damage Thresholds (n/cm <sup>2</sup> )
Carbon composition	$10^{13}$
Metal film	$3 \times 10^{16}$
Carbon film	$10^{15}$
Oxide film	$2 \times 10^{12}$
Precision wirewound	
Ceramic	$5 \times 10^{17}$
Epoxy	$10^{15}$



Besides neutron-induced degradation, resistors are subjected to dose-rate effects. The impacts are the generation of a replacement current,  $i_R$ , and a reduction of the effective resistance. This last effect is equivalent to a parallel transient shunt leakage resistance,  $R_S$ . The quantities  $i_R$  and  $R_S$  are given by

$$R_S \approx \frac{B_1}{\dot{\gamma}}$$

and

$$i_R \approx B_2 \dot{\gamma}$$

The proportionality constants are given by:

Resistor Type	Potting Compound	$B_1 \times 10^{13}$ (kohms-Rad(C)/sec)	$B_2 \times 10^{-12}$ (amps/Rad(C)/sec)
Carbon Composition (watts)			
1	Air (630 mm Hg)	2.1	0.78
1	Silastic	> 4.3	0.5
1/8	Dow-Corning 200	> 1.7	3.0
Ceramic encased	Paraffin	>170.0	0.045
Metal film 1/8 watt	Paraffin	> 40.0	0.044

A more complete discussion on the effects of radiation on resistors is given on pages 43 through 46.

Capacitors are also susceptible to radiation effects. The parameters that are impacted by radiation are the capacitance, the dissipation factor, and the leakage resistance. For neutrons it is possible to form the following ranking.

Preferred Class:	Glass, ceramic, mica.
Recommended Class:	Plastic.
Not Recommended Class:	Paper, paper/plastic, electrolytic.



The damage thresholds are as follows:

Preferred Class;  $10^{15} \text{n/cm}^2 \leq D.T. \leq 10^{16} \text{n/cm}^2$

Recommended Class:  $D.T. \approx 2 \times 10^{14} \text{n/cm}^2$

Not Recommended Class:  $5 \times 10^{13} \text{n/cm}^2 \leq D.T. \leq 10^{14} \text{n/cm}^2$

Some guidelines that will aid in the proper choice of capacitors are:

- Avoid organic dielectric materials.
- Paper dielectric units must not be impregnated with hydrocarbons.
- The preferred types of capacitors are glass, ceramic, and tantalum in that order.

A more complete discussion can be found on pages 46 through 48.

#### A.2.2 Quartz Crystals Oscillators

These components are critical since they are used as precision master clocks. Radiation will affect the frequency of these oscillators. They will suffer a transient and a permanent effect and in the extreme will cease to oscillate. There are two effects. The first effect is associated with low dose levels (between  $10^3$  to  $10^4$  rads(Si)). In this region the frequency change is small (typically 1 to 10 pp  $10^8$ ) and shows little dose dependance. Above  $10^4$  rads(Si) the change is much greater (several hundred pp  $10^8$  to cessation of oscillation) and has a strong dose dependance.

The accepted method of minimizing this effect is to use swept, synthetic quartz crystals. This method relies on removal of impurities. However, the effect is still present with a frequency change of a few parts pp  $10^8$ . Thus, one recommendation is to eliminate the need for ultrastable frequencies. In addition, a proposed solution which has been formulated as a result of this study is to control the movement of the impurities through the use of temperature. It consists of using partially swept synthetic quartz crystals grown employing a Na mineralizer and then to operate the crystal below  $200^{\circ}\text{K}$ . There is evidence based on a study performed at Oklahoma State University that Na impurities are immobilized below this temperature and the effect should disappear. However, this solution has never been verified. Therefore, it is recommended that Oklahoma State University be approached to determine if they would perform such a study. This recommendation stems from the fact that this University has reported the latest work performed in this area and it is apparent from this report that this institution has



access to quartz crystal processing equipment, an ESR apparatus, and a radiation facility - all of which would be necessary for such a study.

In addition, the effect of radiation on swept natural quartz has never been reported. There is no reported data on any attempt to optimize the sweeping process for radiation tolerance. It is, therefore, recommended that the following experimental studies be undertaken:

- The effects of temperature on the radiation response of synthetic crystals which have experienced various degrees of sweeping.
- The effects of sweeping and temperature on the radiation response of natural quartz.
- Optimization of the sweeping process for radiation.

Before leaving this subject the point should be made that quartz crystals are the most vulnerable component to radiation uncovered in this study.

### A.3. Radio Frequency Semiconductor Devices

This section of this appendix will summarize the hardening techniques and design guidelines presented in the text in section 5.0 for the reader who failed to read the body of the report or could not recall all of the many hardening suggestions made in the body of the report. This summary will be presented in an outline form, as opposed to the format that was used in the sections of this appendix on materials and nonsemiconductor components. Discrete devices (diodes, silicon controlled rectifiers(SCR's), and transistors) will be presented first followed by integrated circuits (IC's). These will be further divided according to the threat constituent which is being mitigated, i.e., neutrons, dose, and dose rate.

Some of these hardening techniques will involve trade-offs in other areas such as reliability or performance. Where appropriate these tradeoffs will be noted. The page numbers where specific hardening suggestions first appeared will also be noted.

#### A.3.1 Diodes

Neutron irradiation causes bulk damage in the semiconductor through displacement. There is little that can be done to prevent this damage from occurring; therefore, techniques used to mitigate the effects of neutrons on semiconductors tend to concentrate on minimizing the effects of the damage on device



operation.

Neutron damage in diodes manifests itself as an increase in leakage current and the forward voltage. Zener diodes experience a decrease in the breakdown voltage and a change in the reference voltage. Tunnel diodes exhibit an increase in the valley current. The following set of guidelines can be used to minimize the effects of neutron irradiation on diodes:

- For forward biased diodes, select those devices which have fast recovery times, low power, and a small junction volume.(p.83)
- Use low voltage, heavily doped Zener diodes. If this type of diode is used as a reference element then this element should be forward-biased and incorporate temperature compensation and gold doping. (p.84)
- Use GaAs tunnel diodes rather than silicon, and select devices with high peak current values. (p.86)

Total dose affects the leakage currents, breakdown voltage, and forward voltage of diodes. However, for exposures less than or equal to  $10^6$  rads(Si) the changes are generally less than 15% and can be tolerated. (p.96)

As in all semiconductors, dose causes the formation of electron-hole pairs. These electron-hole pairs will move under the influence of a applied field, indistinguishable from normal operating currents. These currents are called photocurrents and their magnitude is proportional to the dose-rate. The photocurrents can be minimized by the following:

- Employing heavily doped diodes and biasing these devices to less than half the avalanche breakdown voltage.(p.91)
- Zener diodes, which are biased into breakdown, should be chosen with a breakdown voltage as near to 7V. as possible and be operated at the highest practical bias current.(p.96)

#### A.3.2 Silicon Controlled Rectifiers (SCR's)

SCR's are very sensitive to neutrons, dose and dose-rate. As stated in the text they should be avoided completely. In situations where no other alternative is available, current limiting of the power supply can be used to reduce the possibility of device burnout. (p.99)



### A.3.3 Transistors

Neutron exposure, as mentioned in the section on diodes, causes displacement effects in the semiconductor material. In transistors this results in a decrease in the forward gain of the device, increases in the breakdown voltages (an advantageous), increases in the saturation voltages, and increases in the leakage currents. Gain degradation is the most serious of these and can be mitigated by using the following guidelines.

- Bias transistors at or near the peak current gain to lessen the effects of gain degradation.(p.107)
- Select devices with the highest possible gain-bandwidth product,  $f_T$ , since this implies a narrow base width and, thus, less neutron-induced gain degradation.(p.109)
- Select transistors with the highest possible pre-irradiation gain. This will result in a higher design margin and, hence, allow for more neutron-induced gain degradation.(p.111)
- Power transistors are susceptible to changes in the saturation voltage due to the fact that they have low doped collectors. Selecting power transistors with the heaviest possible doped collectors will minimize the increase in the bulk resistivity of the collector region and serve to minimize the increase in saturation voltage.(p.125)
- In applications where the transistor is operated in saturation only epitaxial transistors should be used and the base current should be maximized.(p.127)
- Circuits should be designed to tolerate transistors with low breakdown voltages. This, of course, involves a trade off with reliability. (p.127)
- Transistors with low values of saturation voltage should be chosen to allow for a neutron-induced increase in this parameter.
- Minimizing  $I_C$  will minimize  $V_{CEsat}$ . This involves a trade off with the effort to mitigate neutron-induced gain degradation since this involves maximizes  $I_C$  or at least operating the device at a  $I_C$  value which maximizes the gain. Thus, in these situations the importance of the gain must weigh against the saturation voltage for the particular circuit under consideration. (p.127) In cases where it may not be possible to lower  $I_C$ , such as in power supply regulators, it



may be necessary to parallel two or more series regulator transistors.

Total dose causes an increase in leakage currents which is generally insignificant compared to the normal operating currents of the transistor and also, when compared to the dose-induced gain degradation. The techniques that can be used to mitigate the effects of dose-induced gain degradation are the same as those for neutron-induced gain degradation. (pp.131-136) That is:

- Operate the transistor at or near peak current gain.

- Maximize  $I_C$ .

- Select devices with the highest possible pre-irradiation gain.

Dose rate causes the production of photocurrents, as has been mentioned earlier. The effects of these photocurrents can be minimized by observing the following recommendations.

- Use heavily doped transistors.(p.143)

- Use photocurrent compensation. (p.145)

- Use transistors with minimum geometries which, thus, have less material in which the electron-hole pairs can be produced. The use of narrow base width transistors increases the probability of punch-through and the occurrence of second breakdown. This, of course requires a trade off between nuclear survivability and reliability.

#### A.3.4 Integrated Circuits

The effects of neutron exposure on integrated circuits are the same as those on transistors, with the primary effect being gain degradation. In an IC, however, this gain degradation also affects fan-out, i.e., the ability of a logic gate to supply driving current to successive gates. The following hardening recommendations will reduce the impact of neutron-induced gain degradation on the performance of IC's.

- Design a large gain margin into the circuit. This means one should design the circuit so that a decrease in gain of, for example 50% will not cause circuit failure. (p.166)
- Reduce fan-out requirements. This will allow for more gain degradation without affecting circuit operation. (p.167)
- Use a large emitter current and operate at a high ambient temperature to aid post-irradiation annealing and, thus, reduce permanent gain degradation.



- Operate with as high an  $I_C$  as practical and with an increased reverse bias to drive the transistor harder into saturation. (p.167)
- Use an emitter resistor or low-impedance bias circuitry to prevent a change in the quiescent operating point caused by resistivity increases. (p.168)

Total dose causes an increase in leakage currents and a degradation of gain. The increase in leakage currents is generally insignificant. The effects of gain degradation can be minimized by observing the following guidelines.

- Gold dope the collector. (p.173)
- Operate at high injection levels. (p.173)
- Design a large gain margin into the circuitry. (p.173)
- Reduce fan-out requirements. (p.173)
- Increase the reverse bias to keep the transistor in saturation. (p.174)
- Pre-irradiation with neutrons has the same effect as gold-doping in that it decreases carrier lifetime. (p.174)

Dose rate effects in IC's are much more serious than those in discrete transistors. This is due to the large substrate area in which electron-hole pairs can be produced. The formation of parasitic pnpn SCR paths can lead to latchup and subsequent burnout. The following hardening techniques are useful in minimizing the effects of dose rate-induced photocurrents.

- Use photocurrent compensation. (p.175)
- Use minimum transistor geometries. (p.176)
- Gold dope the collector. (p.176)
- Use Schottky TTL with Darlington transistors. (p.177)
- Use current limiting to prevent photocurrents from reaching vulnerable circuitry. (p.178)
- Incorporate dielectric isolation in the fabrication process. (p.178)
- Use circumvention where practical. (p.182)
- Use nonvolatile memories where practical. (p.182)

The use of GaAs IC's provides an inherent dose rate hardened IC. The technology is still immature but does offer hope of solving the dose rate problem presently faced by commercial IC's. (p.194)

NMOS technology should be avoided completely since it has never been demonstrated that any NMOS device will survive the dose and/or dose rate threat imposed on the BMDATC-radar systems. (p.200) NMOS is the softest electronic tech-



nology in existence today. It is not even recommended for tactical scenarios where equipment only has to be as survivable as man. It really can not be over-emphasized that NMOS must be avoided in any scenario that has a nuclear requirement.

#### A.4 Microwave and Millimeter Wave Devices

The types of devices that were investigated were: 1.) Impatt-like devices; 2.) Gunn diodes; 3.) PIN diodes; 4.) Ferrite phase shifters; and 5.) Gigahertz GaAs field effect transistors. These are rather specialized classes and, as such, there is less radiation data on these classes than on RF devices. Similarly, recommendations and design guidelines have not been completely formulated. However, what does exist will be listed.

##### A.4.1 Impatt-like Devices

The device classes covered in this portion of the report were Impatts, Trapatts, and Baritt diodes as well as microwave cavities themselves. Radiation-induced air ionization in a microwave cavity causes a small change in the resonant frequency but a more significant change in the Q of the cavity. The change in Q can be as high as 30% for a dose rate of  $3 \times 10^9$  rads(Si)/sec. However, the effect is easily mitigated by simply evacuating the cavity. This effect is discussed on page 209.

Impatts will experience little or no degradation at the threat levels of neutron fluence. Ionizing transient radiation will impact the operation of Impatts. The ranking of Impatts according to increasing radiation vulnerability is the following: Si diffused diodes, GaAs diffused diodes, and GaAs Schottky diodes. These device types are discussed between pages 202 through 214 with specific recommendations made on page 214.

Trapatt diodes are Impatt-like devices. In order to mitigate neutron-induced effects it is recommended that high frequency devices which incorporate heavy doping in the p<sup>+</sup> and n<sup>+</sup> regions and an abrupt doping profile be used. These devices are discussed on pages 214 through 220 with recommendations made on pages 215 and 217.

Baritts are another device type that is related to Impatts. These devices are invulnerable to neutron exposure. If it is possible Baritt diodes



should be chosen that incorporate Schottky injecting contacts and have low injection efficiency. This will mitigate dose rate related effects. These devices are discussed on pages 220 through 228 with specific recommendations made on page 220.

#### A.4.2 Gunn Diodes

It is apparent that Gunn devices will experience some radiation-induced difficulties in the scenarios facing BMDATC-radars. The effects on Gunn diodes range from temporary interruption to destruction of the device. It is recommended that these devices be operated in CW mode at the lowest possible voltage. Diodes with the best thermal characteristics should be used. In addition, if possible a flat cavity should be used. These devices are discussed on pages 228 through 259 with specific recommendations being made on pages 255 and 256.

#### A.4.3 PIN Diodes

This class of devices is fairly resistant to radiation-induced degradation. The recommendation is to use devices with the smallest possible width of the intrinsic region without going into avalanche breakdown. This device class is discussed on pages 260 through 269 with specific recommendations being made on page 269.

#### A.4.4 Ferrite Phase Shifters

Phase shifters can be made out of ferrite devices. Ferrites are not as attractive as PIN diodes for this application but, nevertheless, they are potential candidates. The recommendation is to use those ferrites which have rectangular hysteresis loops. This recommendation is made on page 272.

#### A.4.5 Microwave Transistors

These are GaAs FET's and have exceptional radiation characteristics. The only problem associated with these devices is a transient upset problem that has been ascribed to Cr doping in the substrate. It is recommended that an effort be made to improve the quality of the material used in fabricating these devices. This recommendation is made on page 279.



#### A.5 General Comments

It has been stated previously but it must be reiterated that this listing should not be taken as an absolute but rather as guidelines. In addition, specific examples within a class of materials or devices may have radiation properties exceeding those which have been listed. The purpose of this study was to identify those areas where problems can arise and propose possible solutions but it was not intended to be a recipe book that would ensure survivability. No document could do that. Considering the threat levels contained in Volume I survivability constitutes one of the most difficult engineering and technology problems that any system ever faced. Survivability will not happen by accident and a broad based approach will not succeed. Survivability can only be achieved by constant attention to nuclear-related issues. This requires careful and constant examination of devices and technologies. This was the purpose of this study. Hopefully this goal has been partially met and the resulting documentation will aid in building a survivable system.



